A STUDY OF N_2O MOLECULAR HYPERFINE STRUCTURE IN EXCITED VIBRATIONAL STATES UTILIZING A STABILIZED TWIN LASER SPECTROMETER

by

JOHN EDWARD THOMAS

B.S. (Physics)
Massachusetts Institute of Technology
(1973)

SUBMITTED IN PARTIAL FULFILLMENT
OF THE REQUIREMENTS FOR THE
DEGREE OF
DOCTOR OF PHILOSOPHY

at the

MASSACHUSETTS INSTITUTE OF TECHNOLOGY

January, 1979

Signature of Author.....
Department of Physics

Certified by.....
Thesis Supervisor

Accepted by.....
Chairman, Departmental Committee on Graduate Students

Archives
MASSACHUSETTS INSTITUTE
OF TECHNOLOGY

MAR 30 1979

LIBRARIES

A STUDY OF N_2O MOLECULAR HYPERFINE STRUCTURE IN EXCITED VIBRATIONAL STATES UTILIZING A STABILIZED TWIN LASER SPECTROMETER

by

JOHN EDWARD THOMAS

Submitted to the Department of Physics on January 12, 1978, in partial fulfillment of the requirements for the degree of Doctor of Philosophy.

ABSTRACT

A stabilized twin laser spectrometer has been developed and applied to study, for the first time, N_2O hyperfine structure in excited vibrational states. Copropagating wave three level resonances, observed in the laser induced fluorescence, are utilized to resolve the hyperfine spectra for a number of ro-vibrational transitions in the (100 - 001) band. Closely spaced structure is simplified by adjusting the relative intensity of the two lasers to enhance specific weak resonances. Comparison of P- and R-branch spectra yields the important qualitative features of the vibrational changes in the N_2O nitrogen electric quadrupole couplings.

Fitting a theoretical lineshape to the experimental data, establishes the coupling constants: for the outer N nucleus $eqQ(100) = -806.3 \pm 23.7$ kHz; $eqQ(001) = -567.4 \pm 22.7$ kHz; for the central N nucleus $eqQ(100) = -118.5 \pm 35.3$ kHz; $eqQ(001) = -325.7 \pm 81.9$ kHz.

The theory required to analyze the experimental spectra is systematically developed from first principles. General forms are

derived for the electric quadrupole and magnetic dipole coupling of a single nucleus to the molecular rotation. The Hamiltonian for two coupled (to $\vec{J}$) nuclei is diagonalized and eigenfunctions are given in terms of a suitable basis. Calculation of the electric dipole matrix elements is facilitated by extensive use of the Wigner Eckart Theorem. The lineshape for a three level system (V configuration) interacting with two copropagating waves is calculated in the strong-wave-weak-wave approximation. (i.e. all orders in the strong wave intensity, lowest order for the weak wave). It is shown that the Doppler free copropagating wave resonance is generally much narrower and more intense than the corresponding counterpropagating wave resonance. Thus, a copropagating wave spectrometer is particularly suitable for resolving small hyperfine splittings. Since the resonances arise when two transitions share a common level, the upper and lower vibrational state splittings are measured independently. Enhancement of specific weak three level resonances by utilizing a strong-wave-weak-wave experimental technique is described. Selection of laser polarizations is discussed and a number of symmetries between R- and P-branch V and inverted V resonances are established. A treatment of line broadening mechanisms, including beam transit time effects for three level systems, is presented.

The spectrometer is suitable for general infrared spectroscopy in the 9 to 11 micron region. A complete description of the lasers, optics, and servo electronics is given. The advantage of the copropagating wave technique in eliminating optical feed back is discussed. For coupled transitions with similar frequencies, the resonance condition depends only on the twin laser difference frequency which is servo stabilized. Servo control of the absolute laser frequency is unnecessary, so that the system is simplified. Lock-in 'derivative' detection is utilized to enhance

the narrow but weak crossing resonances. Distortion of the lock-in 'derivative' lineshape from a true Lorentzian derivative is calculated. Use of an on-line computer for data averaging is described.

The final chapters are used to present the N_2O experimental data and to develop a least squares fitting procedure. Determination of the coupling constants and the associated uncertainties is discussed. Suggestions for further improvement of the resolution are given and a technique for studying the magnetic dipole coupling is presented.

Thesis Supervisor: Ali Javan
Title: F. W. Davis Professor of Physics

To

GILDA

I dedicate this thesis in its entirety, believing it to be of all my work the least unworthy of one without whose encouragement, sympathy and criticism I could never have become even such a physicist as I am.*

*Paraphrased from The Forsyte Saga

This thesis has been performed at the M.I.T. Optical and Infrared Laser Laboratories directed by Professor A. Javan. At its various stages the work described has received support from the following agencies: N.S.F., Air Force.

ACKNOWLEDGEMENTS

To my parents, Edward and Elizabeth Thomas, and to my sister Elizabeth, for their love and support during the many years of my formal education.

I am deeply indebted to my thesis advisor, Professor Ali Javan, for suggesting the line of research which has come to fruition as this thesis. I am grateful for his guidance and encouragement, and for his being both my teacher and my friend.

Dr. Charles F. Davis, Jr. has given freely of his time on so many occasions during the various stages of this thesis research. His friendship and contributions are especially appreciated.

For his many suggestions on curve fitting techniques and for providing access to the computer at the Bates Accelerator facility, I owe special thanks to my good friend Dr. Nicholas Paras.

I am particulary grateful to Professor Michael Feld for first introducing me to the laser group as an undergraduate. I have appreciated his advice and many suggestions as well as his friendship during these last seven years.

To Professor Norman Kurnit I am especially thankful for numerous patient discussions during our many years of collaboration.

I would like to thank Michael Burns for the loan of the mini computer system used for the data acquisition and for many useful suggestions. During the beginning stages of this thesis research, I enjoyed many helpful conversations with Dr. Keith Boyer. Dr. Charles Freed supplied important information for improvement of the stable lasers.

My collaboration with Dr. Michael James Kelly and Dr. Jean-Pierre Monchalin provided me with the foundation for much of my experimental and theoretical background. Their friend-

ship and encouragement have been greatly appreciated.

Special thanks go to Steven Fulghum for many stimulating conversations which I have thoroughly enjoyed.

This research work has been greatly facilitated due to the efforts of our technical supervisor, Bill Ryan. His assistance and his friendship have helped to make these years in the laser group pleasant ones.

Major mechanical parts of the apparatus were beautifully constructed by our machinist Axel Ericson. Numerous technical contributions were made by John Devir. I am especially grateful to both of them for many pleasant conversations over a pot of coffee.

Finally, I am thankful to the Fannie and John Hertz Foundation for supporting my graduate studies by means of a Predoctoral Fellowship.

TABLE OF CONTENTS

Appendix

LIST OF FIGURES AND TABLES

Figures

Tables

INTRODUCTION

A copropagating wave stabilized twin laser spectrometer has been developed and applied to a study of N_2O molecular hyperfine structure. Three level strong-wave-weak-wave crossing resonances, observed in fluorescence, are utilized to enhance weak hyperfine components. The difference between the P- and R- branch hyperfine spectra, observed for a number of ro-vibrational transitions, yields, for the first time, the nuclear electric quadrupole coupling constants for the (100) and (001) vibrational states of N_2O.

The methods described herein are among the outgrowths of the nonlinear Doppler free technique first predicted by Willis Lamb[1] and observed by A. Szöke and A. Javan[2] in 1963. This first technique, for which a narrow resonance was observed in absorption, is known as the Lamb dip. In 1966, Schlossberg and Javan[3] extended the theoretical formalism to describe generally the nonlinear interaction of laser fields with multilevel gases via a third order perturbation calculation. Among their new predictions was the three-level crossing resonance. This occurs when two laser fields interact with two transitions sharing a common level. Each field sees the modification of the common level population induced by the other. However, this only occurs when the frequencies of the two fields are such that they interact with the same velocity group, thus imposing a resonance condition.

A number of new features of three level Doppler free resonances were predicted by Feld and Javan[4] in 1969. Included was the lineshape for a coupled three level system interacting with one strong and one weak laser field.

The Lamb dip in fluorescence was first observed by C. Freed and A. Javan[5] in 1970. Realization of this technique meant that all the methods which were utilized in absorption could be extended to fluorescence. For excited state absorbers, such as CO_2 or N_2O, where the absorption coefficient is $\sim 10^{-6}$/cm-mtorr, the observation of fluorescence on a zero background allows large signal to noise ratios even though the absorption is very small.

The applications of nonlinear spectroscopic techniques to the measurement of spectra for entire ro-vibrational bands provides valuable information not obtainable from the spectra of a single line. Vibrational changes in the rotationally induced magnetic moments of N_2O and CO_2 have been measured utilizing this method.[6] The change in magnetic moment is of order $J \times 10^{-4}$ nuclear magneton and is easily measured by comparing P- and R- branch Zeeman spectra for large rotational quantum number J.

Borde´ et al.[7] have measured the vibrational change of the N^{14} nuclear quadrupole coupling in NH_3 for the Q(8,7) transition. Utilizing counter propagating wave crossing resonances in absorption, the various $\Delta F = 0$ ($\Delta J = \Delta K = 0$) transitions were shown to be split due to the vibrational change

in the coupling constant.

Ground state (000) coupling constants for N_2O have been measured previously via microwave techniques.[8] The methods described in this thesis extend the measurements of the nuclear electric quadrupole coupling to include two excited vibrational states.

The following chapters provide a systematic development of the theoretical background and experimental techniques utilized to study the N_2O hyperfine structure. The theoretical background required to analyze the experimental lineshapes is presented in the first two chapters. For completeness, the form of the nuclear electric quadrupole coupling interaction is derived from first principles, both classically and quantum mechanically. The general quantum mechanical result is then specialized to symmetric top and linear molecules. For a single coupled spin 1 nucleus, the splittings and electric dipole matrix elements between states of definite total angular momentum are calculated in closed form. Then, the more complicated problem of two coupled nuclei is considered. For two spin 1 nuclei, the general solution for the eigenstates and eigenvalues is presented. The dipole matrix elements for a suitable basis set are determined by utilizing a computer and the Wigner-Eckart theorem to find the basis set reduced matrix. Clebsch-Gordon coefficients then give the spatial orientation dependence in closed form. Since the electric quadrupole coupling mixes basis states of the same total

angular momentum, the reduced matrix for the eigenstates is easily determined in terms of the basis set reduced matrix. The magnetic dipole coupling of a nucleus with nonzero spin is derived from first principles and the interaction is shown to be negligible within the accuracy of the present experiment.

Enhancement of the weak $\Delta F = 0$ transitions in N_2O is crucial to the measurement of the nuclear electric quadrupole coupling constants. This is achieved by utilizing a strong-wave-weak-wave three level crossing resonance technique. The three level strong-wave-weak-wave lineshapes for copropagating beams are derived in Chapter 2. Exact solutions for the upper level populations are presented to all orders in the strong wave, and lowest order in the weak wave. The advantages of copropagating waves are discussed and the use of the strong-wave-weak-wave method as a transition selection technique is described. Lineshapes with two weak waves are utilized to determine the best choice for the laser polarizations. The polarizations are chosen to give the largest contribution for ($\Delta F = 0 - \Delta F = \Delta J$) crossing resonances while suppressing the ($\Delta F = \Delta J - \Delta F = \Delta J$) resonances.

Basic line broadening mechanisms are described in considerable detail in Chapter III. The example of a two level system interacting with a standing wave laser field is used to illustrate collision- and power-broadening of the resonance linewidth. Calculation is done in the rate equation approximation so that the lineshape may be averaged with a Gaussian laser beam profile.

This leads to interesting effects at low pressure, where the wings of the Gaussian contribute significantly to the absorption resonance, due to saturation in the central region. Since the power broadening is lower in the wings of the Gaussian beam, an anomalous narrowing of the resonance at low pressure occurs. Beam transit time effects are ignored in these calculations, which assume that the mean free path is small compared to the beam radius. The transit-time effects in three level systems are considered via a third order integral perturbation theory approach. Lineshapes for both copropagating and counterpropagating wave three level resonances (V configuration) are derived. The variation of the linewidth versus beam diameter is discussed.

Construction of the spectrometer is described in Chapters IV and V. Basically the system consists of two lasers, the beams of which are sent copropagating into an absorbing gas sample. For N_2O, the absorption is monitored via the 4.5 micron fluorescence (001-000 band) from the upper level manifold of the interacting transition. This facilitates the use of the copropagating wave technique as well as use of arbitrary laser plarizations. In Chapter IV a detailed description of the stabilized twin laser spectrometer is given. Stable CO_2 and N_2O lasers are described including the mechanical and plasma tube construction. The electrical system is designed so that the laser structure may be grounded for safety, while maintaining good enough voltage stability for high resolution applications.

Organometallic components, formed through the interaction of CO with its storage tank walls, cause a brownish deposit to form in the plasma tube of an N_2O laser. A suitable gas filtration technique is described to eliminate this problem. The best free running laser frequency jitter which is obtained is about 5 kHz.

Copropagating crossing resonance lineshapes depend only on the twin laser difference frequency as long as both lasers interact with similar frequency transitions. The difference frequency is calibrated by observing the beat note in a fast liquid He cooled CuGe detector. Fluorescence is monitored by a large area liquid He cooled slow CuGe detector with an interference filter (4 - 4.5μ) which is also at liquid He temperature. An on line computer is utilized to sweep the twin laser difference frequency and record the signal obtained via lock-in derivative detection. Since a finite frequency modulation of one of the lasers is required to obtain the derivative signal, the lock-in output is not exactly a Lorentzian derivative. The lock-in 'derivative' lineshape is calculated to obtain an understanding of the distortion.

In order to provide reproducible data for signal averaging, a servo system is utilized to stabilize the laser difference frequency to a tunable oscillator. The oscillator frequency is then controlled by the on-line computer. In Chapter V, a detailed description of the servo system and general servo

design techniques is given. First, phase locked loop and frequency locked loop systems are described, and the use of the lead-lag filter as a damping control is explained. Using these simple systems as a basis for discussion, the actual servo design is presented. The jitter in the twin laser difference frequency is reduced to about 200 Hz using the servo system. The long term drift is less than 1 kHz per hour.

Having described the lineshape theory and the general experimental apparatus in Chapters I - V, application to N_2O hyperfine structure is presented in Chapters VI and VII. The reduction of the experimental lineshapes requires the calculation of the contribution of thousands of transitions. These arise from the M degeneracy and 9 component structure of each ro-vibrational level. Fortunately, the M degeneracy sums may be done in closed form by means of an approximation procedure. Also, many of the electric dipole transitions are non allowed or very small, and may be neglected. The problem reduces to calculating only hundreds of transitions and is tractable for a reasonably fast computer. A least squares fitting technique is described in Chapter VI, which is utilized to determine the coupling constants for the various lines. As discussed in Chapter VII, in the rigid rotor-harmonic oscillator approximation, the coupling constants for a fixed vibrational level are independent of J. Thus, the coupling constants as determined for the various lines can be averaged. An anlaysis of the sources of error and

suggestions for further study are presented.

References

1. W. E. Lamb, Jr. Phys. Rev. 134A, 1429 (1964).

2. A. Szöke and A. Javan, Phys. Rev. Lett. 10, 521 (1963); R. A. McFarlane, W. R. Bennett, Jr., and W. E. Lamb, Jr., Appl. Phys. Lett. 2, 189 (1963).

3. H. R. Schlossberg and A. Javan, Phys. Rev. 150, 267 (1966).

4. M. S. Feld and A. Javan, Phys. Rev. 177, 540, (1969).

5. C. Freed and A. Javan, Appl. Phys. Lett. 17, 53 (1970).

6. M. J. Kelly, J. E. Thomas, J.-P. Monchalin, N. A. Kurnit, and A. Javan,Phys. Rev. Lett. 37, 686 (1976).

7. M. Ouhayoun, C. J. Bordé, and J. Bordé, Mol. Phys. 33, 597 (1977).

8. A. C. Smith, H. Ring, W. V. Smith, and W. Gordy, Phys. Rev. 73, 633 (1948); D. K. Coles, E. S. Elyash, and J. G. Gorman, Phys. Rev. 72, 971 (1947).

CHAPTER I

NUCLEAR ELECTRIC QUADRUPOLE AND MAGNETIC DIPOLE COUPLING IN MOLECULES

1. Nuclear Electric Quadrupole Interaction

A. Classical Description

In order to develop the Hamiltonian for the quadrupole coupling, consider first the most general interaction between two charge distributions as shown in Fig. 1.1.

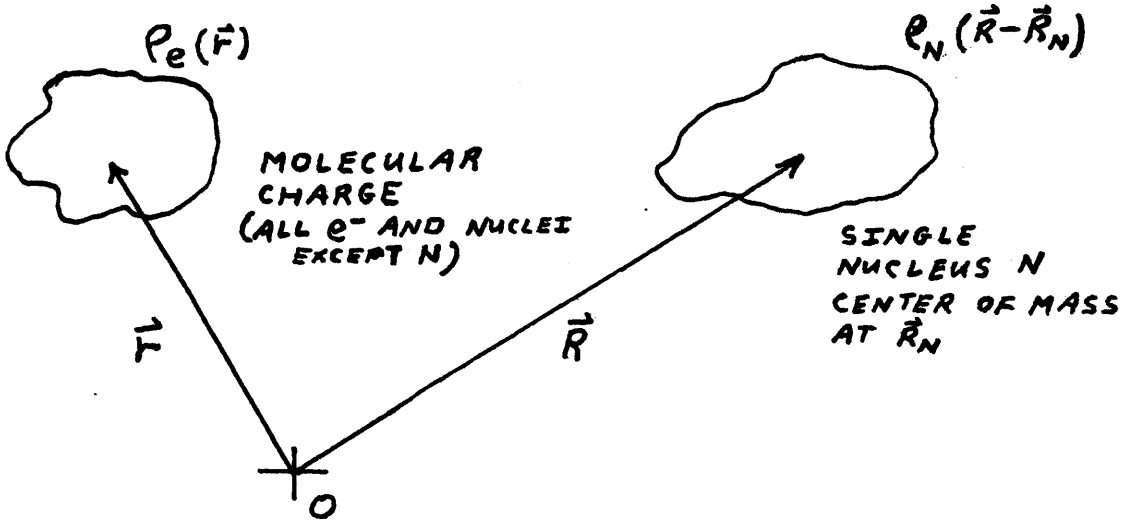

Figure 1.1

The calculation is done in the lab reference frame (inertial), but for the present the coordinate system may be left arbitrary. One simplifying assumption will be made, namely that the small

portion of ρ_e inside the region where ρ_N is nonzero will be neglected. Since the quadrupole interaction depends on the electric field gradient at the nucleus N, one can make a rough estimate of the error incurred in the following way. Consider the core electrons of the atom of nucleus N. Electrons in a relative S state are spherically symmetric, and contribute no field gradient. An electron in a p state can contribute, but the electron density varies as $\sim e r^2/a_o^5$ where $a_o \sim$ few Bohr radii. From Poisson's equation $\partial E/\partial R \sim \frac{\partial^2 \phi}{\partial R^2} \sim \rho$. Thus, the neglected field gradient varies as $\sim \left(\frac{r_N}{a_o}\right)^2 e/a_o^3$ where $r_N \sim$ nuclear dimension. The total field gradient is of order e/a_o^3, hence the fractional error is $(r_N/a_o)^2$ which is a small quantity.

The general electrostatic interaction between the charge distributions ρ_e and ρ_N may be written:

$$\text{I.1)} \quad V_N = \iint \frac{d^3\vec{r}\, d^3\vec{R}\ \rho_e(\vec{r})\, \rho_N(\vec{R}-\vec{R}_N)}{|\vec{r}-\vec{R}|}$$

Let $\vec{R}' \equiv \vec{R} - \vec{R}_N$, so that V becomes:

$$\text{I.2)} \quad V_N = \iint \frac{d^3\vec{r}\, d^3\vec{R}'\, \rho_e(\vec{r})\, \rho_N(\vec{R}')}{|\vec{r}-\vec{R}_N-\vec{R}'|}$$

Using the above assumption, that ρ_e may be taken to be zero in the vicinity where ρ_N is nonzero, one can take $|\vec{r}-\vec{R}_N| \gg |\vec{R}'|_{MAX}$

and make a Taylor expansion of $|\vec{r}-\vec{R}_N-\vec{R}'|^{-1}$. Thus,

I.3) $$\frac{1}{|\vec{r}-\vec{R}_N-\vec{R}'|} \cong \frac{1}{|\vec{r}-\vec{R}_N|} + \frac{\vec{R}'\cdot(\vec{r}-\vec{R}_N)}{|\vec{r}-\vec{R}_N|^3} +$$

$$+ \frac{R'_i R'_j}{2} \frac{3(r_i-R_{N,i})(r_j-R_{Nj}) - \delta_{ij}|\vec{r}-\vec{R}_N|^2}{|\vec{r}-\vec{R}_N|^5}$$

$$+ \cdots$$

where $R_{N,i} = \hat{e}_i \cdot \vec{R}_N$ and $r_i = \hat{e}_i \cdot \vec{r}$.

V_N may now be written:

I.4) $$V_N \cong \int d^3\vec{R}' \rho_N(\vec{R}') \int \frac{d^3\vec{r}\ \rho_e(\vec{r})}{|\vec{r}-\vec{R}_N|} +$$

$$+ \int d^3\vec{R}'\, \vec{R}' \rho_N(\vec{R}') \cdot \int \frac{d^3\vec{r}\ (\vec{r}-\vec{R}_N)\rho_e(\vec{r})}{|\vec{r}-\vec{R}_N|^3} +$$

$$+ \frac{1}{2}\int d^3\vec{R}'\, R'_i R'_j \rho_N(\vec{R}') \int \frac{d^3\vec{r}\ \rho_e(\vec{r})}{|\vec{r}-\vec{R}_N|^5}\left[3(r_i-R_{Ni})(r_j-R_{Nj}) - \delta_{ij}|\vec{r}-\vec{R}_N|^2\right]$$

$$+ \cdots$$

where a sum on repeated indices is implied in all that follows.

The first term in (I.4) is just the monopole interaction which is included in the electronic Hamiltonian. (Note that the interaction of the nucleus N with all other nuclei is also included.)

The second term is an electric dipole interaction and vanishes if the nuclear wave function has definite parity. The third term represents the nuclear electric quadrupole interaction for the nucleus N, and is the term of interest here.

$$\text{I.5)}\quad V_Q = \frac{1}{2}\int d^3\vec{R}'\, R_i' R_j' \rho_N(\vec{R}') \times \times \int d^3\vec{r}\, \rho_e(\vec{r})\, \frac{3(r_i - R_{Ni})(r_j - R_{Nj}) - \delta_{ij}|\vec{r} - \vec{R}_N|^2}{|\vec{r} - \vec{R}_N|^5}$$

Now, $$\delta_{ij}\, \frac{3(r_i - R_{Ni})(r_j - R_{Nj}) - \delta_{ij}|\vec{r} - \vec{R}_N|^2}{|\vec{r} - \vec{R}_N|^5} = 0$$

(i.e. $\vec{\nabla}\cdot\vec{E} = 0$ at $\vec{R}_N$ since we have taken $\rho_e(\vec{r}) = 0$ for $\vec{r}$ near $\vec{R}_N$)

Hence, one can subtract $\frac{1}{3}\delta_{ij}|\vec{R}'|^2$ from $R_i' R_j'$ in the first integral since this leaves V_Q unaffected. This gives:

$$\text{I.6)}\quad V_Q = \frac{1}{6}\int d^3\vec{R}' \left(3R_i' R_j' - \delta_{ij}|\vec{R}'|^2\right) \rho_N(\vec{R}') \times \times \int d^3\vec{r}\, \rho_e(\vec{r})\, \frac{3(r_i - R_{Ni})(r_j - R_{Nj}) - \delta_{ij}|\vec{r} - \vec{R}_N|^2}{|\vec{r} - \vec{R}_N|^5}$$

Written in terms of the field gradient and nuclear electric quadrupole moment V_Q becomes finally:

I.7)

a) $$V_Q = -\frac{1}{6} Q_{ij} \frac{\partial E_i}{\partial R_{Nj}}$$

b) $$\frac{\partial E_i}{\partial R_{Nj}} = -\int d^3\vec{r}\, \rho_e(\vec{r})\, \frac{3(r_i - R_{Ni})(r_j - R_{Nj}) - \delta_{ij}|\vec{r} - \vec{R}_N|^2}{|\vec{r} - \vec{R}_N|^5}$$

c) $$Q_{ij} = \int d^3\vec{R}' \left(3R_i' R_j' - \delta_{ij} R'^2\right) \rho_N(\vec{R}')$$

Note that both the field gradient and quadrupole moment are symmetric traceless tensors. This result will be used in the quantum mechanical section which follows.

In order for the quantities Q_{ij} to be dependent only on the properties of the nucleus N and not on molecular rotation, the coordinate system $(\hat{e}_i)$ must be chosen as space fixed. If one associates $\vec{I}$ with the total angular momentum of the nucleus N and $\vec{J}$ with the molecular angular momentum excluding the nuclear spins, then $\vec{I}$ and $\vec{J}$ will (for $V_Q << H_{ROT}$) 'precess' in some way about the resultant total angular momentum $\vec{F} = \vec{I} + \vec{J}$. Since V_Q is typically $<< H_{ROT}$, the 'precessional' frequency will be small compared to the molecular rotational frequency and the molecule will rotate many times during the precessional period. Thus, in the first approximation, the nucleus acts like a 'lab fixed' quadrupole interacting with the time averaged gradient of the molecular electric field. The torques tending to change $|\vec{J}|$ (also $|\vec{I}|$) average out in this approximation. For $V_Q \sim H_{ROT}$, one must consider the fact that $|\vec{J}|$ can change (since $V_Q <<< H_{NUCLEAR}$, $|\vec{I}|$ = constant). However, for most molecules V_Q is small and off diagonal matrix elements in $|\vec{J}|$ may be neglected in the quantum discription. Only diagonal elements in $|\vec{J}|$ will be considered in what follows.

B. Quantum Description

Both $\partial E_i/\partial R_{Nj}$ and Q_{ij} are symmetric traceless tensors,

characteristic of the molecule and nucleus N respectively. For fixed I, J (magnitude of angular momentum quantum numbers), the matrix elements of these quantities will transform under rotations as

I.8)

$$\text{a)}\quad (Q_{ij})_{op} = C\left[\tfrac{3}{2}(I_iI_j + I_jI_i) - \delta_{ij}I^2\right]_{op}$$

$$\text{b)}\quad (\partial E_i/\partial R_{Nj})_{op} = C'\left[\tfrac{3}{2}(J_iJ_j + J_jJ_i) - \delta_{ij}J^2\right]_{op}$$

where c, C are independent of directions i,j, and

op ≡ operator form.

The results (I.8) follow directly from the Wigner-Eckart Theorem which requires in this case that the matrix elements of all the symmetric, traceless tensors which can be associated with a given system must be proportional, having the same orientational dependence. The quantities in the square brackets in (I.8 a,b) are symmetric traceless tensors characteristic of their respective systems (nucleus and molecule) and give nonzero matrix elements for fixed I and J. [Note that the Wigner Eckart Theorem is normally given for the tensorial form of the operators rather than the Cartesian tensor form, but the above result still follows since the tensorial and Cartesian tensor forms are related by fixed linear combinations. [See Jackson: Classical Electrodynamics[1] Chapter 4, and Appendix I.1 in this work].

In order to determine c and C in terms of known quantities,

consider

I.9) a) $\langle I, M_I = I | Q_{zz} | I, M_I = I \rangle = \hbar^2 C [3I^2 - I(I+1)]$

$= C\, I(2I-1)\hbar^2$

b) $\langle J, M_J = J | \partial E_z / \partial R_{N_z} | J, M_J = J \rangle = \hbar^2 C [3J^2 - J(J+1)]$

$= C\, J(2J-1)\hbar^2$

Thus, for fixed I, J V_Q^{op} becomes

I.10) $$V_Q^{op} = -\frac{1}{6} \frac{\langle I, M_I = I | Q_{zz} | I, M_I = I \rangle \langle J, M_J = J | \partial E_z / \partial R_{N_z} | J, M_J = J \rangle}{I(2I-1)\, J(2J-1)\, \hbar^4} \times S^{op}$$

where

I.11) $$S^{op} = \left[\tfrac{3}{2}(I_i I_j + I_j I_i) - \delta_{ij} I^2\right]\left[\tfrac{3}{2}(J_i J_j + J_j J_i) - \delta_{ij} J^2\right]$$

$$= \tfrac{9}{2}\left[(\vec{I}\cdot\vec{J})^2 + I_i I_j J_j J_i\right] - 3 I^2 J^2$$

the form $I_i I_j J_j I_i$ is reduced as follows:

I.12) $$I_i I_j J_j J_i = I_j I_i J_j J_i + [I_i, I_j] J_j J_i$$

$$= (\vec{I}\cdot\vec{J})^2 + i\hbar\, \epsilon_{ijk} I_k J_j J_i$$

$$= (\vec{I}\cdot\vec{J})^2 + i\hbar\, I_k \epsilon_{ijk} [J_j, J_i] \tfrac{1}{2}$$

I.13) $$\frac{1}{2}\epsilon_{ijK} I_K [J_j, J_i] = \frac{1}{2}(-i\hbar)\epsilon_{jiK}\epsilon_{jil} J_l I_K$$
$$= -\frac{1}{2} i\hbar [\delta_{ij}\delta_{Kl} - \delta_{il}\delta_{Ki}] I_K J_l$$
$$= -i\hbar \vec{I}\cdot\vec{J}$$

Thus, f^{op} is equivalent to

I.14) $$\mathcal{F}^{op} = [q(\vec{I}\cdot\vec{J})^2 + \frac{q}{2}\hbar^2(\vec{I}\cdot\vec{J}) - 3I^2J^2]_{op}$$

Using $\vec{F} = \vec{J} + \vec{I}$, or

I.15) $$\vec{I}\cdot\vec{J} = \frac{1}{2}(F^2 - J^2 - I^2)$$

V_Q^{op} finally becomes

I.16) $$V_Q^{op} = -\frac{1}{2}\frac{\langle I, M_I = I | Q_{zz} | I, M_I = I\rangle}{I(2I-1)\hbar^2}\frac{\langle J, M_J = J | \partial E_z/\partial R_{Nz} | J, M_J = J\rangle}{J(2J-1)\hbar^2}$$
$$\times\left[\frac{3}{4}(F^2 - J^2 - I^2)(F^2 - J^2 - I^2 + \hbar^2) - I^2J^2\right]_{op}$$

for states of fixed J, I.

The nonzero matrix elements of (I.16) are

I.17)

a) $$\langle J,I;F,M_F|V_Q^{op}|J,I;F,M_F\rangle = -\frac{1}{2}\,\frac{\langle I,M_I=I|Q_{zz}|I,M_I=I\rangle}{I(2I-1)}\times$$

$$\times\,\frac{\langle J,M_J=J|\partial E_z/\partial R_{Nz}|J,M_J=J\rangle}{J(2J-1)}\times$$

$$\times\left[\frac{3}{4}P(P+1)-I(I+1)J(J+1)\right]$$

b) $$P = F(F+1)-J(J+1)-I(I+1)$$

All quantum numbers $\underline{\alpha}$ other than the F, J, and I dependence are suppressed for the present.

The result (I.17) is valid for either atoms or molecules. However, for molecules, $\langle J,M_J=J|\partial E_z/\partial R_{Nz}|J,M_J=J\rangle$ may be further reduced by writing $\partial E_z/\partial R_{Nz}$ in terms of body fixed quantities and direction cosines.

Using the notation $q_{FG} = \partial E_F/\partial R_{NG} = -\partial^2\Phi/\partial R_{NG}\partial R_{NF}$ where Φ is the electric potential, the space fixed components q_{FG} are related to body fixed components q_{fg} by the transformation law for Cartesian tensors as

I.18) $$q_{FG} = \sum_{fg} \alpha_{Ff}\alpha_{Gg}q_{fg}$$

where $\alpha_{Ff} = \hat{e}_f\cdot\hat{e}_F$ is the direction cosine of the $\underline{f}$ body fixed axis with respect to the $\underline{F}$ space fixed axis. According to I.17,

the quantity to be evaluated is $\langle J, M_J = J | q_{zz} | J, M_J = J \rangle$. This is given by

$$\text{I.19)}\quad \langle \alpha, J, M_J = J | q_{zz} | \alpha, J, M_J = J \rangle = \sum_{s,g}{}' \langle \alpha'; J, M_J = J | \phi_{zs} \times \phi_{zg} | \alpha'; J, M_J = J \rangle \times \langle J, \alpha'' | q_{sg} | J, \alpha'' \rangle$$

In expression (I.19), the quantum numbers other than J, M_J are represented by α with α' being relevant to the direction cosine matrix and α'' being irrelevant to the direction cosines. Molecular rotational wavefunctions are either symmetric or antisymmetric with respect to 180° rotations about principal axis so that terms containing $\phi_{zs}\phi_{zg}$ with f ≠ g vanish,[2] analogous to the vanishing of electric dipole matrix elements for states of definite parity. (The q_{sg} depend only on relative positions within the molecule and are unaffected.) The most general form of I.19 is then

$$\text{I.20)}\quad \langle \alpha, J, M_J = J | q_{zz} | \alpha, J, M_J = J \rangle = \sum_{s}{}' \langle \alpha'; J, M_J = J | \phi^2_{zs} | \alpha'; J, M_J = J \rangle \times \langle J, \alpha'' | q_{ss} | J, \alpha'' \rangle$$

If perturbations of the electronic and vibrational states due to rotation are neglected, the last factor is independent of J. Since the electric charge near the nucleus N is neglected, $\Phi(R_N)$ satisfies Laplace's equation in both body fixed and space fixed coordinates.

I.21) $$\nabla^2 \Phi(\vec{R}_N) = 0 = \partial^2\Phi/\partial R_{NF}\,\partial R_{NF} = \partial^2\Phi/\partial R_{Ng}\,\partial R_{Ng}$$

In terms of the q_{sg}, I.21 is

I.22) $$q_{xx} + q_{yy} + q_{zz} = 0 \qquad \text{(body fixed)}$$

Explicitly writing out (I.20) and using (I.22) gives (using a bar for the quantum average):

I.23)
$$\begin{aligned}\bar{q}_{zz} &= \overline{Q^2_{zx}}\left(\frac{\bar{q}_{xx}+\bar{q}_{yy}}{2} + \frac{\bar{q}_{xx}-\bar{q}_{yy}}{2}\right) + \\ &+ \overline{Q^2_{zy}}\left(\frac{\bar{q}_{xx}+\bar{q}_{yy}}{2} + \frac{\bar{q}_{yy}-\bar{q}_{xx}}{2}\right) + \\ &+ \overline{Q^2_{zz}}\;\bar{q}_{zz} \\ &= \overline{Q^2_{zx}}\left(-\frac{\bar{q}_{zz}}{2}\right) + \overline{Q^2_{zy}}\left(-\frac{\bar{q}_{zz}}{2}\right) + \overline{Q^2_{zz}}\;\bar{q}_{zz} \\ &\quad + \overline{\Delta q}\left(\overline{Q^2_{zx}} - \overline{Q^2_{zy}}\right) \;;\; \overline{\Delta q} \equiv \frac{\bar{q}_{xx}-\bar{q}_{yy}}{2}\end{aligned}$$

Using $\Phi_{zx}^2 + \Phi_{zy}^2 + \Phi_{zz}^2 = 1$ gives:

$$\bar{q}_{zz} = (1 - \bar{\Phi}_{zz}^2)\left(-\frac{\bar{q}_{zz}}{2}\right) + \bar{\Phi}_{zz}^2\,\bar{q}_{zz} + \overline{\Delta q}\,(\bar{\Phi}_{zx}^2 - \bar{\Phi}_{zy}^2)$$

I.24) $$\bar{q}_{zz} = \frac{1}{2}\bar{q}_{zz}(3\bar{\Phi}_{zz}^2 - 1) + \overline{\Delta q}(\bar{\Phi}_{zx}^2 - \bar{\Phi}_{zy}^2)$$

Having derived the general result (I.24), consider the special case of a symmetric top. Denoting α' by K, the projection of J along the molecular symmetry axis, $\bar{\Phi}_{zz}^2$ becomes

I.25) $$\langle J, M_J = J, K | \Phi_{zz}^2 | J, M_J = J, K\rangle = \sum_{\substack{J'=J,\\ J\pm1}}' |\langle J, J, K | \Phi_{zz} | J', J, K\rangle|^2$$

where the selection rule $\Delta M = 0$, $\Delta K = 0$ has been used for Φ_{zz}.

Using the tables of direction cosine matrix elements given in Appendix I.2, one readily obtains:

I.26) a) $$\frac{3\bar{\Phi}_{zz}^2 - 1}{2} = \frac{-J}{2J+3}\left(1 - \frac{3K^2}{J(J+1)}\right)$$

b) $$\bar{\Phi}_{zx}^2 - \bar{\Phi}_{zy}^2 = 0$$

Denoting by q the quantity $-\bar{q}_{zz} = +\overline{\frac{\partial^2 \Phi}{\partial z^2}}$ (body fixed) and putting $eQ = \langle I, M_I = I | Q_{zz} | I, M_I = I\rangle$ (space fixed), $\bar{V}_Q$

becomes finally:

I.27) a) $$\langle \alpha, J, I; F, M_F | V_Q | \alpha, J, I; F, M_F \rangle = \frac{-eQq}{2I(2I-1)(2J-1)(2J+3)} \times \left(1 - \frac{3K^2}{J(J+1)}\right)\left[\frac{3}{4}P(P+1) - J(J+1)I(I+1)\right]$$

b) $$P = F(F+1) - J(J+1) - I(I+1)$$

The electronic and vibrational dependence α of $\overline{V}_Q$ is contained in q which is given by

I.28) $$q = \langle \alpha | \int d^3\vec{r}\, \rho_e(\vec{r}) \frac{3(z-z_N)^2 - |\vec{r}-\vec{R}_N|^2}{|\vec{r}-\vec{R}_N|^5} | \alpha \rangle$$

where $\vec{r}$, $\vec{R}$ are symbolic for the set of 3 body fixed components of $\vec{r}$ and $\vec{R}$ respectively. Watson[3] has shown that the rotational wave functions and direction cosine matrix for a linear molecule are those of a symmetric top, where $K\hbar$ is then the vibrational angular momentum about the symmetry axis. [This neglects K changing torques such as the Coriolis coupling perturbation.] Hence the result I.27 may be utilized unchanged for linear molecules.

C. <u>One Nucleus Coupling</u>

Having determined the F, I, and J dependence of $\overline{V}_Q$, one can

calculate the splittings of a given J level if eqQ is known. For the ground state of N_2O, the outer $\underline{N}^{14}$ nucleus coupling constant eqQ is -1020 kilohertz[4], while the inner $\underline{N}^{14}$ coupling constant is -270 kilohertz[4]. Neglecting for the present the inner nucleus coupling, and noting that for N^{14} I = 1, each J level will be split into three levels, one for each of the possible F values J − I, ..., J + I = J − 1, J, J + 1. For the ground state, where K = 0, the outer nucleus splittings are given in Table I.1, for J = 1 to 20.

Since the matrix of V_Q for fixed J, I is diagonal in F, M_F, the eigenstates for the single coupled nucleus problem are readily determined using Clebsch-Gordon coefficients. Thus, for $J \geq I$ (suppressing quantum numbers $\underline{\alpha}$)

$$\text{I.29)} \quad |J,I,F,M_F\rangle = \sum_{M_I} |J,M_F-M_I\rangle|I,M_I\rangle \times \langle J,I;M_F-M_I,M_I|J,I;F,M_F\rangle$$

The Clebsch-Gordon coefficients for I = 1 are given in Table I.2. These may be utilized to calculate the electric dipole ($\vec{\mu}$) transition matrix. In all that follows, only <u>linear</u> molecules in states with K = 0 will be considered. The matrix elements of the space fixed components of $\vec{\mu}$ on a J, M_J basis are given in Table I.3. These are easily calculated from the direction cosine matrix of Appendix I.2 with K = 0, by noting

TABLE I.1

N_2O Ground State Splittings Neglecting Central Nitrogen Nucleus Coupling (eqQ outer N = - 1020 kHz)

Q(KHZ)	=-1020	I=	1	J=	1	N=	0	HQ(KHZ)=	510.00
Q(KHZ)	=-1020	I=	1	J=	1	N=	1	HQ(KHZ)=-	255.00
Q(KHZ)	=-1020	I=	1	J=	1	N=	2	HQ(KHZ)=	51.00
Q(KHZ)	=-1020	I=	1	J=	2	N=	1	HQ(KHZ)=	255.00
Q(KHZ)	=-1020	I=	1	J=	2	N=	2	HQ(KHZ)=-	255.00
Q(KHZ)	=-1020	I=	1	J=	2	N=	3	HQ(KHZ)=	72.86
Q(KHZ)	=-1020	I=	1	J=	3	N=	2	HQ(KHZ)=	204.00
Q(KHZ)	=-1020	I=	1	J=	3	N=	3	HQ(KHZ)=-	255.00
Q(KHZ)	=-1020	I=	1	J=	3	N=	4	HQ(KHZ)=	85.00
Q(KHZ)	=-1020	I=	1	J=	4	N=	3	HQ(KHZ)=	182.14
Q(KHZ)	=-1020	I=	1	J=	4	N=	4	HQ(KHZ)=-	255.00
Q(KHZ)	=-1020	I=	1	J=	4	N=	5	HQ(KHZ)=	92.73
Q(KHZ)	=-1020	I=	1	J=	5	N=	4	HQ(KHZ)=	170.00
Q(KHZ)	=-1020	I=	1	J=	5	N=	5	HQ(KHZ)=-	255.00
Q(KHZ)	=-1020	I=	1	J=	5	N=	6	HQ(KHZ)=	93.08
Q(KHZ)	=-1020	I=	1	J=	6	N=	5	HQ(KHZ)=	162.27
Q(KHZ)	=-1020	I=	1	J=	6	N=	6	HQ(KHZ)=-	255.00
Q(KHZ)	=-1020	I=	1	J=	6	N=	7	HQ(KHZ)=	102.00
Q(KHZ)	=-1020	I=	1	J=	7	N=	6	HQ(KHZ)=	156.92
Q(KHZ)	=-1020	I=	1	J=	7	N=	7	HQ(KHZ)=-	255.00
Q(KHZ)	=-1020	I=	1	J=	7	N=	8	HQ(KHZ)=	105.00
Q(KHZ)	=-1020	I=	1	J=	8	N=	7	HQ(KHZ)=	153.00
Q(KHZ)	=-1020	I=	1	J=	8	N=	8	HQ(KHZ)=-	255.00
Q(KHZ)	=-1020	I=	1	J=	8	N=	9	HQ(KHZ)=	107.37
Q(KHZ)	=-1020	I=	1	J=	9	N=	8	HQ(KHZ)=	150.00
Q(KHZ)	=-1020	I=	1	J=	9	N=	9	HQ(KHZ)=-	255.00
Q(KHZ)	=-1020	I=	1	J=	9	N=	10	HQ(KHZ)=	109.29
Q(KHZ)	=-1020	I=	1	J=	10	N=	9	HQ(KHZ)=	147.63
Q(KHZ)	=-1020	I=	1	J=	10	N=	10	HQ(KHZ)=-	255.00
Q(KHZ)	=-1020	I=	1	J=	10	N=	11	HQ(KHZ)=	110.37

TABLE I.1 (continued)

```
Q(KHZ) =-1020 I=   1 J=  11 N=  10 HQ(KHZ)=   145.72
Q(KHZ) =-1020 I=   1 J=  11 N=  11 HQ(KHZ)=-  255.00
Q(KHZ) =-1020 I=   1 J=  11 N=  12 HQ(KHZ)=   112.20

Q(KHZ) =-1020 I=   1 J=  12 N=  11 HQ(KHZ)=   144.13
Q(KHZ) =-1020 I=   1 J=  12 N=  12 HQ(KHZ)=-  255.00
Q(KHZ) =-1020 I=   1 J=  12 N=  13 HQ(KHZ)=   113.33

Q(KHZ) =-1020 I=   1 J=  13 N=  12 HQ(KHZ)=   142.80
Q(KHZ) =-1020 I=   1 J=  13 N=  13 HQ(KHZ)=-  255.00
Q(KHZ) =-1020 I=   1 J=  13 N=  14 HQ(KHZ)=   114.31

Q(KHZ) =-1020 I=   1 J=  14 N=  13 HQ(KHZ)=   141.67
Q(KHZ) =-1020 I=   1 J=  14 N=  14 HQ(KHZ)=-  255.00
Q(KHZ) =-1020 I=   1 J=  14 N=  15 HQ(KHZ)=   115.16

Q(KHZ) =-1020 I=   1 J=  15 N=  14 HQ(KHZ)=   140.69
Q(KHZ) =-1020 I=   1 J=  15 N=  15 HQ(KHZ)=-  255.00
Q(KHZ) =-1020 I=   1 J=  15 N=  16 HQ(KHZ)=   115.91

Q(KHZ) =-1020 I=   1 J=  16 N=  15 HQ(KHZ)=   139.84
Q(KHZ) =-1020 I=   1 J=  16 N=  16 HQ(KHZ)=-  255.00
Q(KHZ) =-1020 I=   1 J=  16 N=  17 HQ(KHZ)=   116.57

Q(KHZ) =-1020 I=   1 J=  17 N=  16 HQ(KHZ)=   139.09
Q(KHZ) =-1020 I=   1 J=  17 N=  17 HQ(KHZ)=-  255.00
Q(KHZ) =-1020 I=   1 J=  17 N=  18 HQ(KHZ)=   117.16

Q(KHZ) =-1020 I=   1 J=  18 N=  17 HQ(KHZ)=   138.43
Q(KHZ) =-1020 I=   1 J=  18 N=  18 HQ(KHZ)=-  255.00
Q(KHZ) =-1020 I=   1 J=  18 N=  19 HQ(KHZ)=   117.69

Q(KHZ) =-1020 I=   1 J=  19 N=  18 HQ(KHZ)=   137.84
Q(KHZ) =-1020 I=   1 J=  19 N=  19 HQ(KHZ)=-  255.00
Q(KHZ) =-1020 I=   1 J=  19 N=  20 HQ(KHZ)=   118.17

Q(KHZ) =-1020 I=   1 J=  20 N=  19 HQ(KHZ)=   137.31
Q(KHZ) =-1020 I=   1 J=  20 N=  20 HQ(KHZ)=-  255.00
Q(KHZ) =-1020 I=   1 J=  20 N=  21 HQ(KHZ)=   118.61
*
```

TABLE I.2

Clebsch-Gordon Coefficients for Addition of J to I = 1

$F = J+1$

$$\langle M,0 | J+1, M\rangle = \sqrt{\frac{(J+1)^2 - M^2}{(2J+1)(J+1)}}$$

$$\langle M-1,1 | J+1, M\rangle = \sqrt{\frac{(J+M)(J+M+1)}{2(2J+1)(J+1)}}$$

$$\langle M+1,-1 | J+1, M\rangle = \sqrt{\frac{(J-M)(J-M+1)}{2(2J+1)(J+1)}}$$

$F = J$

$$\langle M,0 | J, M\rangle = \frac{M}{\sqrt{J(J+1)}}$$

$$\langle M-1,1 | J, M\rangle = -\sqrt{\frac{(J+M)(J-M+1)}{2J(J+1)}}$$

$$\langle M+1,-1 | J, M\rangle = \sqrt{\frac{(J-M)(J+M+1)}{2J(J+1)}}$$

$F = J-1$

$$\langle M,0 | J-1, M\rangle = -\sqrt{\frac{J^2 - M^2}{J(2J+1)}}$$

$$\langle M-1,1 | J-1, M\rangle = \sqrt{\frac{(J-M)(J-M+1)}{2J(2J+1)}}$$

$$\langle M+1,-1 | J-1, M\rangle = \sqrt{\frac{(J+M)(J+M+1)}{2J(2J+1)}}$$

TABLE I.3

Linear Molecule Electric Dipole Matrix Elements (k = 0)

$$\mu_0 = \mu_z \; ; \; \mu_\pm = \mp \frac{1}{\sqrt{2}} (\mu_x \pm i\mu_y)$$

$$\langle J-1, M | \mu_z | J, M \rangle = \mu \sqrt{\frac{J^2 - M^2}{4J^2 - 1}}$$

$$\langle J-1, M \pm 1 | \mu_\pm | J, M \rangle = -\mu \sqrt{\frac{(J \mp M)(J \mp M - 1)}{2(4J^2 - 1)}}$$

$$\langle J+1, M | \mu_z | J, M \rangle = \mu \sqrt{\frac{(J+1)^2 - M^2}{(2J+1)(2J+3)}}$$

$$\langle J+1, M \pm 1 | \mu_\pm | J, M \rangle = \mu \sqrt{\frac{(J \pm M + 1)(J \pm M + 2)}{2(2J+1)(2J+3)}}$$

that the only non-vanishing component of $\vec{\mu}$ in the body fixed coordinate system is μ_z. Here μ_z is the transition matrix element between two electronic-vibrational states. The electric dipole transition elements for the F, M_F basis may be written as

$$\text{I.30)}\quad \langle J',I';F',M_F'|\vec{\mu}|J,I;F,M_F\rangle = \sum_{M_I} \langle J',I';F',M_F'|J',I';M_F'-M_I,M_I\rangle \times \langle J',M_F'-M_I|\vec{\mu}|J,M_F-M_I\rangle \times \langle J,I;M_F-M_I,M_I|J,I;F,M_F\rangle$$

In I.30 use has been made of the fact the M_I is conserved for electric dipole transitions between molecular states.

The Wigner-Eckart Theorem may be utilized to reduce the work required to evaluate I.30. To do this, use the tensorial form of the dipole operator given by:

$$\text{I.31)}\quad \text{a)}\quad \mu_\pm = \mp\frac{1}{\sqrt{2}}(\mu_x \pm i\mu_y)$$

$$\text{b)}\quad \mu_0 = \mu_z$$

The signs and multiplicative constants in (I.31) are chosen so that the dipole operators have the correct commutators with $F_\pm$ and F_z as given in Appendix I.1. The Wigner-Erkart Theorem then states:

I.32) $\langle J', I; F', M_F' | \mu_q | J, I; F, M_F \rangle =$

$$= \langle F, 1; M_F, q | F, 1; F', M_F' \rangle \times$$

$$\times \langle J', I; F' \| \mu \| J, I; F \rangle$$

Quantum numbers other than those pertaining to angular momentum are suppressed in the reduced matrix element $\langle \cdots \| \mu \| \cdots \rangle$. To use the Theorem, one calculates all the possible matrix elements for fixed q, say (+). In addition one may fix J' = J + 1 and later calculate the results for J' = J - 1 by complex conjugation and (I.31). The properties of the Clebsch-Gordon coefficients require $M_F' = M_F + q$ and $F' = F, F \pm 1$. Dividing the above results by the appropriate Clebsch-Gordon coefficients then yields the reduced matrix $\langle \cdots \| \mu \| \cdots \rangle$, and (I.32) gives the matrix elements for all q. The algebra required to calculate the matrix elements will not be reproduced here as it is straightforward. The results for the P-branch (J' = J - 1) are given in Table I.4. In the limit that the molecule contains only one strongly coupled nucleus, the results in Table I.4 may be utilized to calculate the intensities of the various transitions.

D. Two Coupled Nuclei

Having treated the single nucleus coupling, the more

TABLE I.4

P-Branch Electric Dipole Matrix Elements for States of Definite Total Angular Momentum $\vec{F} = \vec{J} + \vec{I}$ (I = 1; K = 0)

$\langle J', 1; F', M_F' | \mu_q | J, 1; F, M_F \rangle$

$$\langle J-1, 1; J, M_F \mp 1 | \mu_\mp | J, 1; J+1, M_F \rangle = \frac{-\mu}{2J+1} \sqrt{\frac{J(J \pm M_F)(J \pm M_F + 1)}{2(J+1)}}$$

$$\langle J-1, 1; J, M_F | \mu_z | J, 1; J+1, M_F \rangle = \frac{\mu}{2J+1} \sqrt{\frac{J[(J+1)^2 - M_F^2]}{J+1}}$$

$$\langle J-1, 1; J, M_F \mp 1 | \mu_\mp | J, 1; J, M_F \rangle = \mp \frac{\mu}{J} \sqrt{\frac{(J \pm M_F)(J \mp M_F + 1)}{2(J+1)(2J+1)}}$$

$$\langle J-1, 1; J, M_F | \mu_z | J, 1; J, M_F \rangle = -\frac{\mu}{J} \frac{M_F}{\sqrt{(J+1)(2J+1)}}$$

$$\langle J-1, 1; J-1, M_F \mp 1 | \mu_\mp | J, 1; J, M_F \rangle = -\frac{\mu}{J} \sqrt{\frac{(J^2-1)(J \pm M_F - 1)(J \pm M_F)}{2(4J^2-1)}}$$

$$\langle J-1, 1; J-1, M_F | \mu_z | J, 1; J, M_F \rangle = -\frac{\mu}{J} \sqrt{\frac{(J^2-1)(J^2 - M_F^2)}{4J^2-1}}$$

$$\langle J-1, 1; J-1, M_F \mp 1 | \mu_\mp | J, 1; J-1, M_F \rangle = \mp \frac{\mu}{J} \sqrt{\frac{(J \pm M_F - 1)(J \mp M_F)}{2(J-1)(2J-1)}}$$

$$\langle J-1, 1; J-1, M_F | \mu_z | J, 1; J-1, M_F \rangle = -\frac{\mu}{J} \frac{M_F}{\sqrt{(J-1)(2J-1)}}$$

TABLE I.4 (continued)

$$\langle J-1,1;J-2,M_F\mp1|\mu_\mp|J,1;J-1,M_F\rangle = \frac{-\mu}{2J-1}\sqrt{\frac{J(J\pm M_F-2)(J\pm M_F-1)}{2(J-1)}}$$

$$\langle J-1,1;J-2,M_F|\mu_z|J,1;J-1,M_F\rangle = \frac{-\mu}{2J-1}\sqrt{\frac{J[(J-1)^2-M_F^2]}{J-1}}$$

$$\langle J-1,1;J,M_F\mp1|\mu_\mp|J,1;J-1,M_F\rangle = \frac{-\mu\sqrt{(J\mp M_F)(J\mp M_F+1)}}{J(4J^2-1)\sqrt{2}}$$

$$\langle J-1,1;J,M_F|\mu_z|J,1;J-1,M_F\rangle = \frac{-\mu\sqrt{J^2-M_F^2}}{J(4J^2-1)}$$

difficult case of two coupled nuclei will now be considered, as this is necessary for evaluation of the theoretical lineshape required to fit the N_2O data. The general theory will be considered first and then the results will be specialized to the N_2O case. The treatment is by Bardeen and Townes.[5]

Consider a Hamiltonian consisting of two terms:

I.33) $$H = H_1(\vec{I}_1 \cdot \vec{J}) + H_2(\vec{I}_2 \cdot \vec{J})$$

where it is assumed that J is constant and $\vec{I}_i$ is the spin of nucleus i.

Since there are no external torques, the total angular momentum $\vec{F}$ is conserved, where $\vec{F}$ is given by

I.34) $$\vec{F} = \vec{J} + \vec{I}_1 + \vec{I}_2$$

Let

I.35

a) $$\vec{F}_1 = \vec{J} + \vec{I}_1$$

b) $$\vec{F}_2 = \vec{J} + \vec{I}_2$$

In constructing the states of total $\vec{F}$, one can add $\vec{I}_1$ to $\vec{J}$ to obtain $\vec{F}_1$ and then add $\vec{I}_2$ to $\vec{F}_1$ to obtain $\vec{F}$. Similarly, one can form $\vec{F}_2$ first and then add $\vec{I}_1$ to obtain $\vec{F}$.

The states of definite $|\vec{F}_1|$ diagonalize H_1 while the states of definite $|\vec{F}_2|$ diagonalize H_2. This fact allows considerable

simplification of the problem.

The states of definite F_1, F, M = M_F are given by: (suppressing unnecessary quantum numbers)

$$\text{I.36)}\quad |F_1;F,M\rangle = \sum_{M_2} |F_1, M-M_2\rangle |I_2,M_2\rangle \times \times \langle F_1, I_2; M-M_2, M_2 | F_1, I_2; F, M\rangle$$

$$= \sum_{M_1,M_2} |J, M-M_1-M_2\rangle |I_1,M_1\rangle |I_2,M_2\rangle \times \langle J,I_1; M-M_1-M_2, M_1 | J,I_1; F_1, M-M_2\rangle \times \times \langle F_1,I_2; M-M_2, M_2 | F_1,I_2; F,M\rangle$$

Similarly, states of definite F_2, F, M are given by:

$$\text{I.37)}\quad |F_2;F,M\rangle = \sum_{M_2',M_1'} |J, M-M_1'-M_2'\rangle |I_1,M_1'\rangle |I_2,M_2'\rangle \times \times \langle J,I_2; M-M_1'-M_2', M_2' | J, I_2; F_2, M-M_1'\rangle \times \times \langle F_2,I_1; M-M_1', M_1' | F_2,I_1; F,M\rangle$$

The states in both I.36 and I.37 form complete sets equivalent to the set $|J, M_J\rangle |I_1, M_1\rangle |I_2, M_2\rangle$. Thus, there must exist transformation coefficients between the basis I.36 and I.37 <u>i.e.</u>

$$\text{I.38)}\quad |F_1;F,M\rangle = \sum_{F_2} C_F(F_1,F_2) |F_2;F,M\rangle$$

Since F, M are definite for both sets, only the states of the given F, M are required in the expansion. Also $|F_1;\ F,\ M\rangle$ and $|F_2;\ F,\ M\rangle$ transform in the same way under rotations, so the C_F's must be independent of M. To see this note that

I.39) $$C_F(F_1, F_2) = \langle F_2; F, M | F_1; F, M\rangle$$

Clearly (I.39) is independent of M which is defined by an arbitrary axis. Using (I.36) and (I.37), and the orthonormality of the states which gives $M_i = M_i'$, the C_F's are given by

I.40) $$C_F(F_1, F_2) = \sum_{M_1, M_2} \langle J, I_1; M-M_1-M_2, M_1 | J, I_1; F_1, M-M_2\rangle \times$$
$$\times \langle F_1, I_2; M-M_2, M_2 | F_1, I_2; F, M\rangle \times$$
$$\times \langle J, I_2; M-M_1-M_2, M_2 | J, I_2; F_2, M-M_1\rangle$$
$$\times \langle F_2, I_1; M-M_1, M_2 | F_2, I_1; F, M\rangle$$

Since the Clebsch Gordon coefficients are real $C^*(F_1, F_2) = C(F_1, F_2)$. The result (I.40) is impractical and does not make use of the fact that the C_F's are independent of M. Instead, a result due to Racah allows a much more compact statement of the C_F's. For the case where $I_1 = I_2 = 1$, the C_F's are given in Table I.5 taken from Townes and Schawlow.[2]

Proceeding to the solution of the problem, let the correct

TABLE I.5

Transformation Coefficients of Equation (I.39) for $I_1 = I_2 = 1$

$C_F(F_1, F_2)$; $I_1 = I_2 = 1$; $\Sigma' \equiv F + J + 2$

F_2	$F_1 = F-1$
$J-1$	$\left[\frac{(\Sigma'-2F-1)(\Sigma'-2F)(\Sigma'-2J-1)(\Sigma'-2J)}{2J(2J+1)2F(2F+1)}\right]^{\frac{1}{2}}$
J	$\left[\frac{2(\Sigma'-2F)(\Sigma'-3)\Sigma'(\Sigma'-2J-1)}{2J(2J+2)2F(2F+1)}\right]^{\frac{1}{2}}$
$J+1$	$\left[\frac{(\Sigma'-3)(\Sigma'-2)\Sigma'(\Sigma'+1)}{(2J+1)(2J+2)2F(2F+1)}\right]^{\frac{1}{2}}$

F_2	$F_1 = F$
$J-1$	$\left[\frac{2(\Sigma'-2F-1)(\Sigma'-3)\Sigma'(\Sigma'-2J)}{2J(2J+1)2F(2F+2)}\right]^{\frac{1}{2}}$
J	$\frac{2F(F+1)+2J(J+1)-4}{[2J(2J+2)2F(2F+2)]^{1/2}}$
$J+1$	$-\left[\frac{2(\Sigma'-2J-1)(\Sigma'-2F)(\Sigma'-2)(\Sigma'+1)}{(2J+1)(2J+2)2F(2F+2)}\right]^{\frac{1}{2}}$

F_2	$F_1 = F+1$
$J-1$	$\left[\frac{(\Sigma'-3)(\Sigma'-2)\Sigma'(\Sigma'+1)}{2J(2J+1)(2F+1)(2F+2)}\right]^{\frac{1}{2}}$
J	$-\left[\frac{2(\Sigma'-2F-1)(\Sigma'-2)(\Sigma'-2J)(\Sigma'+1)}{2J(2J+2)(2F+1)(2F+2)}\right]^{\frac{1}{2}}$
$J+1$	$\left[\frac{(\Sigma'-2J-1)(\Sigma'-2J)(\Sigma'-2F-1)(\Sigma'-2F)}{(2J+1)(2J+2)(2F+1)(2F+2)}\right]^{\frac{1}{2}}$

wave function be given by

I.41) $$\Psi(F) = \sum_{F_1}' a(F_1)\,\Psi_1(F_1, F)$$

Only states of the same F are mixed since $\vec{F}$ is conserved. $\Psi_1(F_1, F)$ is $|F_1; F, M\rangle$ where the M's are suppressed.

The J quantum number is fixed and definite so that the states $\Psi_1(F_1, F)$ automatically diagonalize the rotational Hamiltonian. Thus, we need only diagonalize the Hamiltonian H of (I.33).

I.42) $$H\Psi(F) = W\Psi(F)$$

Now, we have

I.43) a) $$H_1\Psi_1(F_1, F) = W_1(F_1)\Psi_1(F_1, F)$$

b) $$H_2\Psi_2(F_2, F) = W_2(F_2)\Psi_2(F_2, F)$$

Using (I.43) and (I.38), (I.42) becomes

I.44) $$\sum_{F_1}' H_1 a(F_1)\Psi_1(F_1, F) + \sum_{F_1'}' H_2 a(F_1') \sum_{F_2}' C_F(F_1', F_2)\Psi_2(F_2, F)$$
$$= W \sum_{F_1}' a(F_1)\Psi_1(F_1, F)$$

or using (I.43)

I.45) $$\sum_{F_1} a(F_1) W_1(F_1) \Psi_1(F_1, F) + \sum_{F_1'} a(F_1') \sum_{F_2'} C_F(F_1', F_2) W_2(F_2) \Psi_2(F_2, F) = W \sum_{F_1} a(F_1) \Psi_1(F_1, F)$$

Since $\Psi_2(F_2, F) = \sum_{F_1} C_F(F_1, F_2) \Psi_1(F_1, F)$, (I.45) may be written as

I.46) $$\sum_{F_1} \Psi(F_1, F) \sum_{F_1'} a(F_1') \left\{ \delta_{F_1, F_1'} (W(F_1) - W) + \sum_{F_2} C_F(F_1, F_2) C_F(F_1', F_2) W_2(F_2) \right\} = 0$$

Using the orthonomality of the $\Psi_1(F_1, F)$ then gives

I.47) $$\sum_{F_1'} \left\{ \delta_{F_1, F_1'} (W_1(F_1) - W) + A_F(F_1, F_1') \right\} a(F_1') = 0$$

where

I.48) $$A_F(F_1, F_1') = \sum_{F_2} C_F(F_1, F_2) C_F(F_1', F_2) W_2(F_2)$$

which is merely the matrix of H_2 on the $\Psi_1(F_1, F)$ basis.

Specializing to the case where $I_1 = I_2 = 1$, one can easily determine which states are mixed for the various possible F's. The simplest case is for F = J + 2 which requires that

$F_1 = F_2 = J + 1 = F - 1$. Thus (I.47) reduces to a 1 x 1 problem. From Table I.5, $C_F(F_1 = F - 1, F_2 = J + 1) = 1$. The eigenvalue is

I.49) $W = W_1(J+1) + W_2(J+1) \quad ; \quad F = J+2$

and the eigenstate is $|J+2, M\rangle_{F_1 = J+1} \equiv |J+1; J+2, M\rangle$

For the case where $F = J + 1$, one may have $F_1 = J, J + 1$ which when adding $I_2 = 1$ gives $F = J + 1$. Hence $F_2 = J, J + 1$ also. Thus, in this case there are two $\Psi_1(F_1, F)$ states mixed and (I.47) amounts to a 2 x 2 problem. In this case, the C_F's depend on J, hence the A_F's depend on J both through the C_F's and W_2's. The results for the various cases are summarized in Appendix I.3. As can be seen from the appendix, the original 9 x 9 matrix of H ($F \times F'$) factors into 2 (1 x 1) matrices, 2 (2 x 2) matrices, and 1 (3 x 3) matrix, as a result of the angular momentum addition rules.

Instead of using the results as they appear in Appendix I.3, one may substitute the explicit form of $W_2(F_2)$ into the A_F's to significantly reduce the algebra required for numerical evaluation. The form of W_2 is taken to be that of I.17. The J dependence of this form is completely general, allowing J dependent perturbations to affect the J dependence of the $(\partial E_Z / \partial R_{NZ})$ factor. Defining a quantity a by

I.50) $$a = -\frac{1}{2}\,\frac{\langle I, M_I = I \mid Q_{zz} \mid I, M_I = I\rangle}{I(2I-1)} \times$$

$$\times \langle J, M_J = J \mid \partial E_z / \partial R_{Nz} \mid J, M_J = J\rangle$$

one can write (I.17) as

I.51) a) $$W_i(F_i) = \frac{a_i}{J(2J-1)}\left[\frac{3}{4}P(P+1) - I_i(I_i+1)J(J+1)\right]$$

b) $$P = F_i(F_i+1) - J(J+1) - I_i(I_i+1)$$

where i = 1, 2 for nucleus 1 or 2. The explicit J dependence of $\underline{a}$ will be suppressed for the present. For the N_2O molecule $I_1 = I_2 = 1$ so $F_i = J, J \pm 1$. Evaluating (I.51) for the various F_i gives

I.52)

a) $$W_i(J-1) = \frac{a_i}{2}\,\frac{(J+1)(2J+3)}{J(2J-1)}$$

b) $$W_i(J) = -\frac{a_i}{2}\,\frac{(2J+3)}{J}$$

c) $$W_i(J+1) = \frac{a_i}{2}$$

Comparing (I.51) with (I.27), one may write a_i for the linear molecule neglecting perturbations as

I.53) $$a_i = -\frac{(eQq)_i}{2}\,\frac{J}{2J+3}\left(1 - \frac{3K^2}{J(J+1)}\right)$$

where $K\hbar$ is the vibrational angular momentum about the symmetry axis. By substituting (I.52) into the results of Appendix I.3, the simplified forms given in Table I.6 emerge. Referring to Table I.6, equation (I.) gives the form of the single spin 1 nucleus coupling energy valid for either nucleus. Equations (II.) give the eigenvalue equations for the various total F. By solving for the expansion coefficients of the $\Psi_W(F)$ in terms of the $\Psi(F_1, F)$, one obtains the eigenfunctions as well. The eigenfunctions may then be used to compute electric dipole transition elements between the various states (9 levels for each value of J).

The eigenfunctions Ψ_W may be expanded as in (I.41):

$$|W; J, F, M\rangle = \sum_{F_1} a(W; J, F_1, F)\,|J, F_1; F, M\rangle \tag{I.54}$$

In (I.54), the J dependence is displayed since this will be of importance in the electric dipole transition matrix. The transition matrix is then given by:

$$\langle W'; J', F', M'|\mu_q|W; J, F, M\rangle = \sum_{F_1, F_1'} a^*(W'; J', F_1', F')\langle J', F_1'; F', M'|\mu_q|J, F_1; F, M\rangle \times a(W; J, F_1, F) \tag{I.55}$$

where q = ± 1, 0

TABLE I.6

EXACT SPLITTINGS FOR TWO QUADRUPOLE COUPLED SPIN 1 NUCLEI : RESULTS

I. 1) $H_Q(J-1) = \frac{q}{2}\frac{(J+1)(2J+3)}{J(2J-1)}$; 2) $H_Q(J) = -\frac{q}{2}\frac{2J+3}{J}$; 3) $H_Q(J+1) = \frac{q}{2}$ (GENERAL MOLECULE)

$q = \frac{-eqQ}{2}\frac{J}{2J+3}$; $(I=1)$ (RIGID LINEAR MOLECULE)

II. A.) $\underline{F = J+2}$; $F_1 = J+1$; $|F=J+2, M_F\rangle_{F_1=J+1} = |J+1; J+2, M\rangle$; $W_{J+1,J+2} = W_1(J+1) + W_2(J+1) = \frac{q_1+q_2}{2}$

B.) $\underline{F = J-2}$; $F_1 = J-1$; $|F=J-2, M_F\rangle_{F_1=J-1} = |J-1; J-2, M\rangle$; $W_{J-1,J-2} = W_1(J-1) + W_2(J-1) = \frac{q_1+q_2}{2}\frac{(J+1)(2J+3)}{J(2J-1)}$

C.) $\underline{F = J+1}$; $F_1 = J, J+1$

1) $A_{J+1}(J,J) = \frac{q_2}{2}\frac{J^2+J-3}{J(J+1)}$; 2) $A_{J+1}(J,J+1) = -\frac{q_2}{2}\frac{3\sqrt{J(J+2)}}{J(J+1)}$; 3) $A_{J+1}(J+1,J+1) = -\frac{q_2}{2}\frac{2J+5}{J+1}$

$$\begin{pmatrix} W_1(J) + A(J,J) - W & A(J,J+1) \\ A(J,J+1) & W_1(J+1) + A(J+1,J+1) - W \end{pmatrix}\begin{pmatrix}\alpha\\ \beta\end{pmatrix} = 0$$

D.) $\underline{F = J-1}$; $F_1 = J, J-1$

1) $A_{J-1}(J,J) = \frac{q_2}{2}\frac{(2J+3)(J^2+J-3)}{(2J-1)J^2}$; 2) $A_{J-1}(J,J-1) = \frac{q_2}{2}\frac{3\sqrt{J^2-1}\,(2J+3)}{J^2(2J-1)}$; 3) $A_{J-1}(J-1,J-1) = -\frac{q_2}{2}\frac{(J+1)(4J^2-9)}{J^2(2J-1)}$

$$\begin{pmatrix} W_1(J) + A(J,J) - W & A(J,J-1) \\ A(J,J-1) & W_1(J-1) + A(J-1,J-1) - W \end{pmatrix}\begin{pmatrix}\alpha\\ \beta\end{pmatrix} = 0$$

TABLE I.6 (continued)

E.) $F = J$; $F_1 = J-1, J, J+1$

1) $A_J(J-1, J-1) = \frac{q_2}{2} \frac{(J^2-1)(4J^2-9)}{J^2(4J^2-1)}$; 2) $A_J(J-1, J) = -\frac{q_2}{2}\sqrt{\frac{2J-1}{2J+1}} \frac{3(J-1)(2J+3)}{J^2(2J-1)}$

3) $A_J(J-1, J+1) = \frac{q_2}{2} \frac{6\sqrt{(2J-1)(2J+3)}}{J(4J^2-1)}$; 4) $A_J(J, J) = -\frac{q_2}{2} \frac{(2J+3)(J^2+J-3)}{J^2(J+1)}$

5) $A_J(J, J+1) = \frac{q_2}{2}\sqrt{\frac{2J+3}{2J+1}} \frac{3(J+2)}{J(J+1)}$; 6) $A_J(J+1, J+1) = \frac{q_2}{2} \frac{(J+2)(2J+5)}{(J+1)(2J+1)}$

$$\begin{pmatrix} W_1(J-1) + A(J-1, J-1) - W & A(J-1, J) & A(J-1, J+1) \\ A(J-1, J) & W_1(J) + A(J, J) - W & A(J, J+1) \\ A(J-1, J+1) & A(J, J+1) & W_1(J+1) + A(J+1, J+1) - W \end{pmatrix} \begin{pmatrix} \alpha \\ \beta \\ \gamma \end{pmatrix} = 0$$

Thus, if the matrix of $\vec{\mu}$ with respect to the basis $|J, F_1; F, M\rangle$ is known, the matrix of $\vec{\mu}$ with respect to the eigenstates is also known. Rather than calculate the result (I.55) for each M, M' using the Clebsch-Gordon coefficients and a computer, it is easier again to exploit the Wigner-Eckart Theorem and calculate only the reduced matrix by computer. This approach is particularly fruitful since the eigenfunctions of total angular momentum F are expanded in terms of basis functions of total angular momentum F. Thus,

I.56) a) $$\langle W'; J', F', M+q|\mu_q|W; J, F, M\rangle = \langle F, 1; M, q|F, 1; F', M+q\rangle \times \times \langle W'; J', F'||\mu||W; J, F\rangle$$

b) $$\langle J', F_1'; F', M+q|\mu_q|J, F_1; F, M\rangle = \langle F, 1; M, q|F, 1; F', M+q\rangle \times \times \langle J', F_1'; F'||\mu||J, F_1; F\rangle$$

Substituting (I.56 a,b) into (I.55), one obtains (choosing any nonzero C. G. coefficient)

I.57) $$\langle W'; J', F'||\mu||W; J, F\rangle = \sum_{F_1, F_1'} a^*(W'; J', F_1', F)\langle J', F_1'; F'||\mu||J, F_1; F\rangle \times \times a(W; J, F_1, F)$$

In order to evaluate the reduced matrix of μ with respect to the basis $|J, F_1; F, M>$, equation (I.36) is used, remembering that the M_I are conserved for electric dipole transitions. Only the reduced matrix is desired, so one may take the matrix of $\mu_z(q = 0)$, which requires M' = M. This gives:

I.58) $$\langle J', F_1'; F', M|\mu_z|J, F_1; F, M\rangle =$$

$$= \sum_{M_1, M_2} \langle J'; M-M_2-M_1|\mu_z|J, M-M_2-M_1\rangle \times$$
$$\times \langle J, I_1; M-M_2-M_1, M_1|J, I_1; F_1, M-M_2\rangle \times$$
$$\times \langle F_1, I_2; M-M_2, M_2|F_1, I_2; F, M\rangle \times$$
$$\times \langle J', I_1; M-M_2-M_1, M_1|J', I_1; F_1', M-M_2\rangle \times$$
$$\times \langle F_1', I_2; M-M_2, M_2|F_1', I_2; F', M\rangle$$

where $I_1 = I_2 = 1$ for N_2O,
and I_1, I_2 are suppressed on the left side of (I.58) for convenience.

Using (I.56b), one may write:

$$\langle J', F_1'; F, M|\mu_z|J, F_1; F, M\rangle =$$
$$= \langle F, 1; M, 0|F, 1; F', M\rangle \times$$
$$\times \langle J', F_1'; F'||\mu||J, F_1; F\rangle$$

or

$$\text{I.59)}\quad \langle J;F_1';F'\|\mu\|J,F_1,F\rangle = \frac{\langle J;F_1';F',M|\mu_z|J,F_1;F,M\rangle}{\langle F,1;M,0|F,1;F',M\rangle}$$

provided that the Clebsch-Gordon coefficient is nonzero.

In order to ensure that the C.G. coefficient is nonzero, the value of M is chosen which maximizes the C.G. coefficient for a particular F', F. Table I.2 shows that for $\Delta F = F' - F = \pm 1$, the maximum value of the C.G. coefficient occurs for M = 0, while for $\Delta F = F' - F = 0$ transitions, the maximum value occurs for M = F. In addition, the angular momentum addition rules require for nonvanishing matrix elements that $\Delta F_1 = \pm 1, 0$ as well as $\Delta F = \pm 1, 0$. Furthermore, the linear molecule dipole selection rules for K = 0 (which will be the case of interest) require that $\Delta J = \pm 1$.

For actual evaluation of the reduced matrix, a simple computer program was written which takes into account the various selection rules and evaluates (I.58). Prior to using (I.59) to find the reduced matrix elements, (I.58) was evaluated for a number of different M's holding ΔF, ΔF_1, and J fixed, to be sure that the results scaled as the appropriate C.G. coefficients. The program was then modified to calculate the reduced matrix according to (I.59). The M value was chosen to maximize the C.G. coefficient and hence the matrix element of μ_Z, to reduce round-off error.

The results of the calculation for the P-branch ($\Delta J = -1$) are given for P(3), P(4), P(5), and P(20) in Appendix I.4, where the vibrational transition matrix element $\equiv \mu_o$ has been set equal to 1. The corresponding R-branch ($\Delta J = \pm 1$) results will be obtained as explained below (see Chapter II).

Using the ground state inner and outer nucleus coupling constants as given above, the results of a calculation of the eigenvalues and eigenfunctions for J = 2 and J = 3 and the transition matrix for P(3) is given in Appendix I.5. The calculations are done utilizing computer programs which will be described later. Energy level diagrams are shown in Fig. 1.2 for J = 3 and J = 2.

2. Magnetic Dipole Interactions

In order to complete the discussion of the relevant hyperfine interactions in molecules, it will be interesting to evaluate the form and estimate the size of the magnetic dipole interaction in $^1\Sigma$ molecules (which includes N_2O).

The basic interaction is of the form

I.60) $$W = -\vec{\mu}_I \cdot \vec{B}'(\vec{R}_N)$$

where $\vec{\mu}_I$ is the magnetic moment of the nucleus in question which is given by

I.61) $$\vec{\mu}_I = g_N \mu_N \frac{\vec{I}}{\hbar}$$

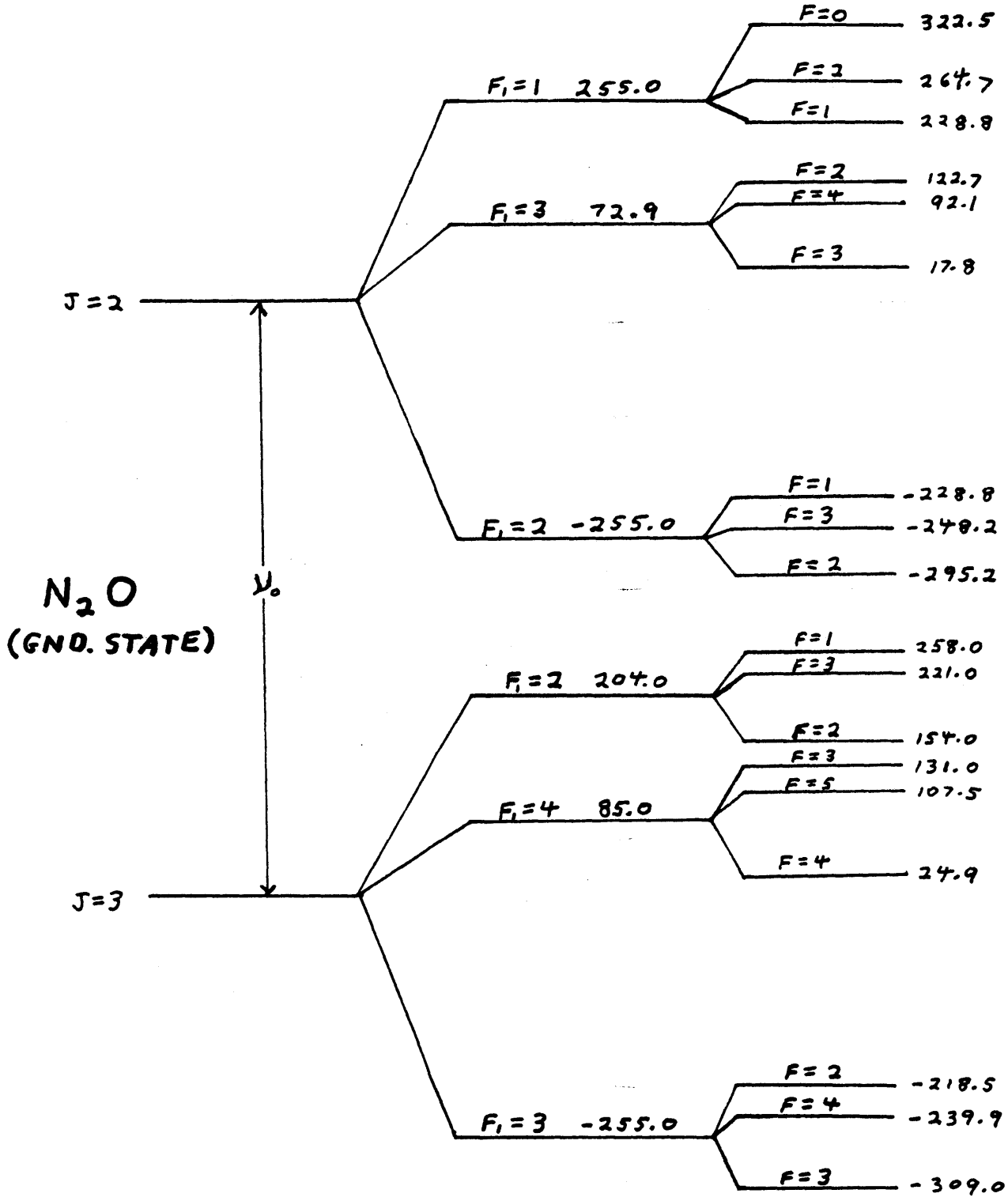

Figure 1.2 Energy Level Diagram Determined from Ground State Coupling Constants (Splittings in kHz)

The magnetic field $\vec{B}'$ is the total magnetic field as observed at the moving nucleus and is the quantity to be determined. In terms of quantities calculated in the lab reference frame, the field $\vec{B}'$ is generally given by (to lowest order in V/C)

$$\text{I.62)} \quad \vec{B}'(\vec{R}_N) = \vec{B}(\vec{R}_N) - \frac{\vec{V}_N}{c} \times \vec{E}(\vec{R}_N) + \vec{B}_T(\vec{R}_N)$$

The notation should be obvious, except for $\vec{B}_T(\vec{R}_N)$ which is the effective applied field due to Thomas precession of the accelerating nucleus. For a molecule at rest the electric field (and hence the net force) must vanish at any nucleus in order to achieve equilibrium. A nucleus in a rotating molecule, however, undergoes centripetal acceleration which must be supplied by some net applied electric field. The Thomas field $\vec{B}_T$ is easily shown to be similar in magnitude to the electric field term. Using these ideas, one can then show that the last two terms are of order $J^2\frac{m_e}{M_N}$ compared to the first, assuming that the typical bond length is of angstrom dimensions. These terms can be neglected except for exceedingly large J.

The magnetic field at the nucleus $\vec{R}_N$ is then shown by an elementary calculation to be

$$\text{I.63)} \quad \vec{B}'(\vec{R}_N) \cong \vec{B}(\vec{R}_N) = \frac{1}{c} \sum_{i \neq N} e_i \frac{(\vec{r}_i - \vec{R}_N) \times \vec{v}_i}{|\vec{r}_i - \vec{R}_N|^3}$$

The sum on $\underline{i}$ is over all particles (electrons and nuclei)

excluding the nucleus N. Note that in the quantum mechanical form, the numerator and denominator commute. The nuclear contribution to the sum (I.63) is given for a rigid rotor by

$$\text{I.64)}\quad \vec{B}^{NUC}(\vec{R}_N) = \frac{1}{c}\sum_{j\neq N} e_j \frac{(\vec{R}_j-\vec{R}_N)\times(\vec{\omega}\times\vec{R}_j)}{|\vec{R}_j-\vec{R}_N|^3}$$

since $\vec{v}_j = \vec{\omega} \times \vec{R}_j$.

Taking components of (I.64) along body fixed axes and evaluating the triple product yields

$$\text{I.65)}\quad B_g^{NUC}(\vec{R}_N) = B_{g\mathcal{F}}^{NUC} J_{\mathcal{F}}$$

$$\text{I.66)}\quad B_{g\mathcal{F}}^{NUC} = \frac{1}{c}\sum_{j\neq N} \frac{e_j[(\vec{R}_j-\vec{R}_N)\cdot\vec{R}_j\,\delta_{g\mathcal{F}} - (R_j)_g(R_j-R_N)_{\mathcal{F}}]}{|\vec{R}_j-\vec{R}_N|^3 I_{\mathcal{F}\mathcal{F}}}$$

where $\vec{\omega}_f = J_f/I_{ff}$ has been used, and I_{fg} is the moment of inertia tensor.

The electronic contribution to (I.63) is easily shown to be

$$\text{I.67)}\quad B_g^{el}(\vec{R}_N) = \frac{-e}{mc}\sum_i \frac{(L'_i)_g}{|\vec{r}_i-\vec{R}_N|^3} \equiv -\frac{e}{mc}\sum_i a_i (L'_i)_g$$

where

$$\text{I.68)}\quad (L'_i)_g \equiv \epsilon_{g\mathcal{F}h}(r_i-R_N)_{\mathcal{F}}(p_i)_h \;;\; a_i = \frac{1}{|\vec{r}_i-\vec{R}_N|^3}$$

and P_{ig} is the electron momentum in the lab reference frame referred to body fixed axes.

For a $^1\Sigma$ molecule, one expects that $\langle \psi_{el}^{(0)} | B_g^{el} | \psi_{el}^{(0)} \rangle = 0$, neglecting molecular rotation. This follows since electrons are

paired off such that there is no total average electronic angular momentum, and $\langle i|a_i|i\rangle$ would be the same for paired electrons. Indeed, the electronic contribution to the magnetic field would be a factor $\frac{M}{m}$ larger were this not the case. Experimentally, the spin-rotation coupling in $^1\Sigma$ molecules is found to be consistent with the molecular rotational g-factor. Hence, the rotational perturbation of the electron distribution, of order $\frac{m}{M}$, induces the entire electronic contribution to B_g.

The calculation of the rotationally perturbed electronic states proceeds as given by Eshbach and Strandberg.[6] The rigid-rotor-electronic Hamiltonian is expressed in terms of the total (electronic plus nuclear framework) angular momentum $\vec{J}$ as

I.69) $$H = H_R + H_{el} + H'$$

where

I.70) a) $$H_R = \sum_g \frac{J_g^2}{2I_{gg}}$$

b) $$H_{el} = \sum_{i,g} \frac{p_{ig}^2}{2m} + V(a,b,c)$$

The rotational perturbation of interest, H' is given by

I.71) $$H' = -\sum_g \frac{J_g L_g}{I_{gg}}$$

where $\vec{L}$ is the total electronic angular momentum. All quantities are calculated in the lab reference frame and projected onto body fixed axes.

The effect of H' on the heavy nuclear framework is unimportant, and the rotational wavefunctions may be taken in lowest order. Using first order perturbation theory to calculate the perturbed electronic wavefunction, one obtains

I.72) $$\psi_{el}^{(1)} = \psi_{el}^{(0)} - \sum_{n,g}{}' \psi_n^{(0)} \frac{\langle n|L_g|0\rangle}{E_0 - E_n} \frac{J_g}{I_{gg}}$$

In order to proceed with the calculation, the interaction (I.60) must be expressed in operator form. A lab coordinate system is chosen so that the components of $\vec{I}$ commute those of the molecular operator $\vec{B}$. This gives

I.73) $$W = -g_N \mu_N I_F (B_F^{el} + B_F^{Nuc})$$

The electronic and nuclear B_F field components can be expressed in terms of body fixed components by the hermitian forms:

I.74)

a) $$B_F^{el} = \sum_{g'}{}' \Phi_{Fg'} B_{g'}^{el}$$

b) $$B_F^{Nuc} = \frac{1}{2} \sum_{g'}{}' (\Phi_{Fg'} B_{g'}^{Nuc} + B_{g'}^{Nuc} \Phi_{Fg'})$$

Note that the direction cosines Φ_{Fg}, commute with the electronic operator B^{el}, but that the operator B^{nuc} contains J_g, which does not commute with Φ_{Fg}.

The electronic contribution to B_F may now be written down using (I.74) and (I.72) as

$$\text{I.75)} \quad \langle \Psi_{el}^{(1)} | B_F | \Psi_{el}^{(1)} \rangle = \sum_{s,g} \left(B_{sg}^{el} \Phi_{Fs} J_g + B_{sg}^{*el} J_g \Phi_{Fs} \right)$$

where

$$\text{I.76)} \quad B_{sg}^{el} = -\frac{e}{mc} \sum_{i,n} \frac{\langle o | a_i L_{is} | n \rangle \langle n | L_g | o \rangle}{(E_n - E_o) I_{gg}}$$

From (I.65) and (I.74), the nuclear contribution to B_F may be expressed by

$$\text{I.77)} \quad B_F^{Nuc} = \sum_{s,g} \frac{B_{sg}^{Nuc}}{2} \left[\Phi_{Fs} J_g + J_g \Phi_{Fs} \right]$$

The total field B_F can then be written as

$$\text{I.78)} \quad B_F = \sum_{s,g} \left(B_{sg} \Phi_{Fs} J_g + B_{sg}^{*} J_g \Phi_{Fs} \right)$$

where

$$\text{I.79)} \quad B_{sg} = B_{sg}^{el} + \frac{B_{sg}^{Nuc}}{2}$$

using the fact that B_{fg}^{nuc} is real.

In (I.78) the rotational wavefunction matrix elements of B_F remain to be determined. The equation (I.78) is in exactly the

same form as the magnetic moment results of Ref. 6. To utilize these results, note that B_F is a vector operator with respect to $J_{F'}$. This follows immediately from the commutation relations.

I.80)

a) $$[J_{F'}, \Phi_{Fg}] = i\hbar\, \epsilon_{F'FG}\, \Phi_{Gg}$$

b) $$[J_{F'}, J_g] = 0$$

where B_{fg} is angle independent. The commutators (I.80) are valid for the nonlinear molecule and using Watson's techniques[3], for the linear molecule also. Thus, between states of fixed J, one has

I.81) $$B_F = \frac{\langle J, M=J | B_z | J, M=J \rangle}{J\hbar} J_F$$

Using (I.73) for W, this gives

I.82) $$W = -g_N \mu_N \vec{I}\cdot\vec{J}\, \frac{\langle J, M=J | B_z | J, M=J \rangle}{J\hbar}$$

where all other quantum numbers besides J, M are suppressed. Since the coupling is very small generally, the off diagonal matrix in J is unnecessary.

By direct analogy to the results for the magnetic moment, Ref. 6, the diagonal matrix element of B_Z in (I.82) on a symmetric top basis $|JKM>$ gives

I.83) $$W = -g_N \mu_N \vec{I}\cdot\vec{J}\; 2\left\{\frac{B_{xx}+B_{yy}}{2} + \frac{K^2}{J(J+1)}\left[B_{zz} - \frac{B_{xx}+B_{yy}}{2}\right] + \frac{iK}{J(J+1)}\left[\frac{B_{yx}-B_{yx}^*}{2} - \frac{B_{xy}-B_{xy}^*}{2}\right]\right\}$$

For a nucleus on the axis of a symmetric top, by symmetry $B_{xx} = B_{yy}$ and $B_{yx} = B_{xy} = 0$ and (I.83) reduces to the result given in Townes and Schawlow.[7] The off diagonal elements in $\underline{K}$, required to evaluate W for an assymmetric top, may be obtained from Ref. 6 in a manner analogous to (I.83).

One may write (I.83) as

I.84) $$W = C(J,K)\,\vec{I}\cdot\vec{J} = \frac{\hbar^2}{2} C(J,K)\left[F(F+1) - J(J+1) - I(I+1)\right]$$

with $\vec{F} = \vec{J} + \vec{I}$.

The tables in Townes and Schawlow[7] show that C for an N^{14} nucleus in a typical molecule is only a few kHz and will unobservable within the resolution of the present experiment. However, with some improvement, magnetic hyperfine structure in N_2O should be observable for moderate J. The only modification required in the above quadrupole-coupling theory is the replacement of $H_Q(F_i)$ by $H_Q(F_i) + W(F_i)$. The spin-spin interaction $(\vec{I}_1, \vec{I}_2)$ is also a few kHz, but it does not increase with J and will not be considered here.

References

1. J. D. Jackson, Classical Electrodynamics, John Wiley & Sons, Inc., New York (1962).

2. C. H. Townes and A. L. Schawlow, Microwave Spectroscopy, Dover Publications, Inc., New York (1975).

3. J. K. G. Watson, Mol. Phys., 19, 465 (1970).

4. A. G. Smith, H. Ring, W. V. Smith, and W. Gordy, Phys. Rev. 73, 633 (1948); D. K. Coles, E. S. Elyash, and J. G. Gorman, Phys. Rev. 72, 971 (1947).

5. J. Bardeen, and C. H. Townes, Phys. Rev. 73, 97 (1948).

6. J. R. Eshbach and M. W. P. Strandberg, Phys. Rev. 85, 24 (1952).

7. Townes and Schawlow, Microwave Spectroscopy, p. 217.

CHAPTER II

STRONG-WAVE-WEAK-WAVE THEORY OF COPROPAGATING WAVE CROSSING RESONANCES

1. Three-Level Lineshape

The theoretical lineshape required to reduce the experimental data will be calculated in this chapter. Following the derivation of the general result, a discussion of the advantages of the experimental technique will be given. Expressions for the relative intensities of the various transitions will be calculated for the lowest order lineshape and the approximations required to utilize the more general lineshape will be discussed.

The level diagram of Fig. (2.1) will form the basis of this discussion.

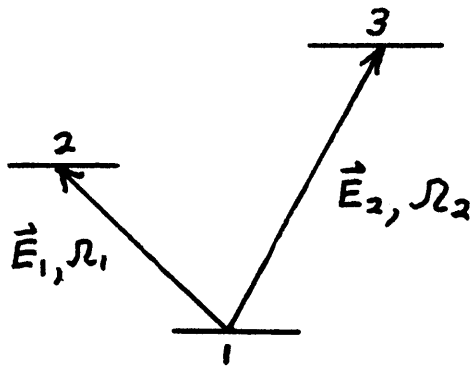

Figure 2.1

It is assumed the fields interact only with the levels as shown.

(Experimentally, crossed linear polarizations are used. This will be discussed below.)

The starting point of the calculation will be the ensemble-averaged density matrix[1] equations for an arbitrary system interacting with a potential V. Denoting the convective derivative by a (•), the equation of motion may be written:

II.1) $$\dot{\rho} = -\frac{i}{\hbar}[H_0+V, \rho] - \Gamma(\rho-\rho_0)\,;\ \Gamma \text{ defined below}$$

The interaction potential V is given by:

II.2) $$V = -\vec{\mu}\cdot\frac{\vec{E}_1}{2}e^{-i(kz-\omega_1 t)} - \vec{\mu}\cdot\frac{\vec{E}_2}{2}e^{-i(kz-\omega_2 t)} + c.c.$$

where the dipole approximation has been made (Z = center of mass of system) and the wave vectors may be taken equal assuming that the differential doppler shift $(K_1 - K_2)V$ is << (the homogeneous linewidth), where V is the velocity along the direction of propagation = $\hat{e}_z$.

Approximating the laser field by a plane wave implies that the density matrix elements are independent of x and y and that the convective derivative may be written:

II.3) $$\bullet = \frac{\partial}{\partial t} + v\frac{\partial}{\partial z}$$

where V is the velocity along the wave vector $\vec{K} = K\hat{e}_z$.

Taking matrix elements of V gives

II.4)

a) $V_{12} = -\vec{\mu}_{12} \cdot \frac{\vec{E}_1}{2} e^{-i(Kz - \Omega_1 t)}$

b) $V_{13} = -\vec{\mu}_{13} \cdot \frac{\vec{E}_2}{2} e^{-i(Kz - \Omega_2 t)}$

c) $V_{23} = 0$ (by assumption)

where the rotating wave approximation has been made (i.e. the c.c. results would contribute anti-resonant terms to the ρ_{12} and ρ_{13} equations; see below)

μ_{12} and μ_{13} will be taken as real by a suitable phase choice for the H_o eigenfunctions.

Taking matrix elements of eq. (II.1) and explicitly indicating the action of Γ gives:

II.5)

a) $\dot{\rho}_{11} = -\frac{i}{\hbar}(V_{12}\rho_{21} - \rho_{12}V_{21}) - \frac{i}{\hbar}(V_{13}\rho_{31} - \rho_{13}V_{31}) - \gamma_1(\rho_{11} - \rho_{11}^o)$

b) $\dot{\rho}_{22} = -\frac{i}{\hbar}(V_{21}\rho_{12} - \rho_{21}V_{12}) - \gamma_2(\rho_{22} - \rho_{22}^o)$

c) $\dot{\rho}_{33} = -\frac{i}{\hbar}(V_{31}\rho_{13} - \rho_{31}V_{13}) - \gamma_3(\rho_{33} - \rho_{33}^o)$

d) $\dot{\rho}_{12} = i\omega_{21}\rho_{12} - \frac{i}{\hbar}V_{12}(\rho_{22} - \rho_{11}) - \frac{i}{\hbar}V_{13}\rho_{32} - \gamma_{12}\rho_{12}$

e) $\dot{\rho}_{13} = i\omega_{31}\rho_{13} - \frac{i}{\hbar}V_{13}(\rho_{33} - \rho_{11}) - \frac{i}{\hbar}V_{12}\rho_{23} - \gamma_{13}\rho_{13}$

f) $\dot{\rho}_{23} = i\omega_{32}\rho_{23} - \frac{i}{\hbar}(V_{21}\rho_{13} - \rho_{21}V_{13}) - \gamma_{23}\rho_{23}$

g) $\rho_{ji} = \rho_{ij}^*$

The matrix of the zero order density matrix ρ^o has been chosen so that in the absence of V, the phase coherences (off diagonal elements of ρ) decay to zero, while the populations (diagonal elements of ρ) decay to the thermal populations.

The system of partial differential equations in (II.5) may be reduced to algebraic equations with the following assumptions for the steady state solutions:

II.6)

a) $\dot{\rho}_{11} = \dot{\rho}_{22} = \dot{\rho}_{33} = 0$

b) $\rho_{12} = \lambda_{12} e^{-i(kz - \Omega_1 t)}$; $\dot{\lambda}_{12} = 0$

c) $\rho_{13} = \lambda_{13} e^{-i(kz - \Omega_2 t)}$; $\dot{\lambda}_{13} = 0$

d) $\partial \rho_{23} / \partial z = 0$

e) $\rho_{23} = \lambda_{23} e^{-i(\Omega_1 - \Omega_2)t}$; $\dot{\lambda}_{23} = 0$

Eq.(II.6a) results from the fact that the two travelling waves E_1, E_2 interact only with their respective transitions and also requires the rotating wave approximation. Equations (II.6b, c) simply require that the induced polarizations be in phase with their respective fields. Equations (II.6 d, e) are valid for the case where $K_1 \cong K_2 = K$ ($(K_1 - K_2)$ V << γ's). In the steady state one expects all amplitudes to be constant in space (travelling waves) and time. The slowly varying envelope

approximation $\frac{\lambda}{E_0}\frac{\partial E_0}{\partial z} << 1$ (λ = mean free path) is of course assumed in obtaining $\dot{\lambda}_{ij}=0$. To show that there do exist exact solutions of (II.5) within the above stated approximations, one may substitute (II.6) into (II.5) to obtain:

II.7)

a) $$\lambda_{23} = \frac{i\left(\frac{\vec{\mu}_{12}\cdot\vec{E}_1}{2\hbar}\lambda_{13} - \frac{\vec{\mu}_{13}\cdot\vec{E}_2}{2\hbar}\lambda_{12}^*\right)}{i\left(\Omega_2-\Omega_1-\omega_{32}\right)+\gamma_{23}}$$

b) $$\lambda_{12} = \frac{i\left(\frac{\vec{\mu}_{12}\cdot\vec{E}_1}{2\hbar}(\rho_{22}-\rho_{11}) + \frac{\vec{\mu}_{13}\cdot\vec{E}_2}{2\hbar}\lambda_{23}^*\right)}{i\left(\Omega_1-\omega_{21}-Kv\right)+\gamma_{12}}$$

c) $$\lambda_{13} = \frac{i\left(\frac{\vec{\mu}_{13}\cdot\vec{E}_2}{2\hbar}(\rho_{33}-\rho_{11}) + \frac{\vec{\mu}_{12}\cdot\vec{E}_1}{2\hbar}\lambda_{23}\right)}{i\left(\Omega_2-\omega_{31}-Kv\right)+\gamma_{13}}$$

where $\hbar\omega_{ij} = E_i - E_j$.

The population equations will be given below after the notation of (II.7) is modified as follows. Let

II.8)

a) $$\lambda_{12} \equiv i\frac{\vec{\mu}_{12}\cdot\vec{E}_1}{2\hbar}\pi_{12}$$

b) $$\lambda_{13} \equiv i\frac{\vec{\mu}_{13}\cdot\vec{E}_2}{2\hbar}\pi_{13}$$

Then λ_{23} may be written:

II.9) $$\lambda_{23} = -\frac{\vec{\mu}_{13}\cdot\vec{E}_2}{2\hbar}\,\frac{\vec{\mu}_{12}\cdot\vec{E}_1}{2\hbar}\,\frac{\pi_{13}+\pi_{12}^*}{i(\Omega_2-\Omega_1-\omega_{32})+\gamma_{23}}$$

substituting (II.8, II.9) into (II.7 b,c) gives

II.10)

a) $$\pi_{12} = \frac{(\rho_{22}-\rho_{11}) - \left(\frac{\vec{\mu}_{13}\cdot\vec{E}_2}{2\hbar}\right)^2 \frac{\pi_{13}^*+\pi_{12}}{-i(\Omega_2-\Omega_1-\omega_{32})+\gamma_{23}}}{i(\Omega_1-\omega_{21}-Kv)+\gamma_{12}}$$

b) $$\pi_{13} = \frac{(\rho_{33}-\rho_{11}) - \left(\frac{\vec{\mu}_{12}\cdot\vec{E}_1}{2\hbar}\right)^2 \frac{\pi_{13}+\pi_{12}^*}{i(\Omega_2-\Omega_1-\omega_{32})+\gamma_{23}}}{i(\Omega_2-\omega_{31}-Kv)+\gamma_{13}}$$

The population equations then take the simple forms:

II.11)

a) $$\gamma_1(\rho_{11}-\rho_{11}^\circ) = \left(\frac{\vec{\mu}_{12}\cdot\vec{E}_1}{2\hbar}\right)^2(\pi_{12}+\pi_{12}^*) + \left(\frac{\vec{\mu}_{13}\cdot\vec{E}_2}{2\hbar}\right)^2(\pi_{13}+\pi_{13}^*)$$

b) $$\gamma_2(\rho_{22}-\rho_{11}^\circ) = -\left(\frac{\vec{\mu}_{12}\cdot\vec{E}_1}{2\hbar}\right)^2(\pi_{12}+\pi_{12}^*)$$

c) $$\gamma_3(\rho_{33}-\rho_{33}^\circ) = -\left(\frac{\vec{\mu}_{13}\cdot\vec{E}_2}{2\hbar}\right)^2(\pi_{13}+\pi_{13}^*)$$

The systems of equations (II.10, II.11) are still exact to the extent stated above, and while the 7 equations (π_{ij} , π_{ij}^*) may be solved algebraically, the velocity integration over V (see below) cannot be done. Instead, a perturbation theory will be developed assuming that one wave E_2 is weak. To simplify the notation, let

II.12)

a) $L_{12} \equiv i(\Omega_1 - \omega_{21} - Kv) + \gamma_{12}$

b) $L_{13} \equiv i(\Omega_2 - \omega_{31} - Kv) + \gamma_{13}$

c) $L_{23} \equiv i(\Omega_2 - \Omega_1 - \omega_{32}) + \gamma_{23} \equiv i\Delta + \gamma_{23}$

d) $\beta^2 \equiv \left|\frac{\vec{\mu}_{12}\cdot\vec{E}_1}{2\hbar}\right|^2 = \left(\frac{\vec{\mu}_{12}\cdot\vec{E}_1}{2\hbar}\right)^2$; μ_{ij} real

e) $\alpha^2 \equiv \left(\frac{\vec{\mu}_{13}\cdot\vec{E}_2}{2\hbar}\right)^2$

Then (II.10 and II.11) take on the form:

II.13)

a) $\gamma_1(\rho_{11} - \rho_{11}^0) = \beta^2(\pi_{12} + \pi_{12}^*) + \alpha^2(\pi_{13} + \pi_{13}^*)$

b) $\gamma_2(\rho_{22} - \rho_{22}^0) = -\beta^2(\pi_{12} + \pi_{12}^*)$

c) $\gamma_3(\rho_{33} - \rho_{33}^0) = -\alpha^2(\pi_{13} + \pi_{13}^*)$

d) $\pi_{13} = \frac{(\rho_{33} - \rho_{11})}{L_{13}} - \frac{\beta^2}{L_{13}L_{23}}(\pi_{13} + \pi_{12}^*)$

e) $\pi_{12} = \frac{(\rho_{22} - \rho_{11})}{L_{12}} - \frac{\alpha^2}{L_{12}L_{23}^*}(\pi_{12} + \pi_{13}^*)$

One may now develop a perturbation theory assuming that $\alpha^2/\gamma^2 << 1$ where $\gamma \sim \gamma_{ij}$, and β^2/γ^2 is arbitrary. Let

II.14) $$\rho_{ij} = \rho_{ij}^{(0)} + \rho_{ij}^{(1)} + \cdots$$

where $\rho_{ij}^{(1)}$ is $\propto \alpha^2/\gamma^2$, etc. Substituting (II.14) into (II.13) and equating terms of the same order gives:

II.15)

a) $$\gamma_1 (\rho_{11}^{(0)} - \rho_{11}^{0}) = \beta^2 (\pi_{12}^{(0)} + \pi_{12}^{(0)*})$$

b) $$\gamma_2 (\rho_{22}^{(0)} - \rho_{22}^{0}) = -\beta^2 (\pi_{12}^{(0)} + \pi_{12}^{(0)*})$$

c) $$\gamma_3 (\rho_{33}^{(0)} - \rho_{33}^{0}) = 0$$

d) $$\pi_{13}^{(0)} = \frac{\rho_{33}^{(0)} - \rho_{11}^{(0)}}{L_{13}} - \frac{\beta^2}{L_{23} L_{13}} (\pi_{13}^{(0)} + \pi_{12}^{(0)*})$$

e) $$\pi_{12}^{(0)} = \frac{\rho_{22}^{(0)} - \rho_{11}^{(0)}}{L_{12}}$$

II.16)

a) $$\gamma_1 \rho_{11}^{(1)} = \beta^2 (\pi_{12}^{(1)} + \pi_{12}^{(1)*}) + \alpha^2 (\pi_{13}^{(0)} + \pi_{13}^{(0)*})$$

b) $$\gamma_2 \rho_{22}^{(1)} = -\beta^2 (\pi_{12}^{(1)} + \pi_{12}^{(1)*})$$

c) $$\gamma_3 \rho_{33}^{(1)} = -\alpha^2 (\pi_{13}^{(0)} + \pi_{13}^{(0)*})$$

d) $$\pi_{12}^{(1)} = \frac{\rho_{22}^{(1)} - \rho_{11}^{(1)}}{L_{12}} - \frac{\alpha^2}{L_{23}^{*} L_{12}} (\pi_{12}^{(0)} + \pi_{13}^{(0)*})$$

Since β^2 is arbitary, (II.15d) is solved for $\pi_{13}^{(o)}$ with the result

II.15d') $$\pi_{13}^{(o)} = \frac{\rho_{33}^{(o)} - \rho_{11}^{(o)}}{L_{13} + \beta^2/L_{23}} - \frac{\beta^2 \pi_{12}^{(o)*}}{L_{23}(L_{13} + \beta^2/L_{23})}$$

In N_2O, all levels are excited vibrational states, and collisions are the dominant population decay and dephasing mechanism. For simplicity, it is reasonable to assume under these circumstances that:

II.17) $$\gamma_1 = \gamma_2 = \gamma_3 = \gamma \; ; \; \gamma_{12} = \gamma_{13} = \gamma' \; ; \; \gamma_{23} \quad \text{arbitrary}$$

Furthermore, the Boltzmann factor for the thermal populations allows one to take

II.18) $$\rho_{11}^{o} \neq 0 \; ; \; \rho_{22}^{o} = \rho_{33}^{o} \cong 0$$

Some simple algebra then yields the lowest order solutions of (II.15) as:

(II.19)

a) $$\rho_{22}^{(o)} - \rho_{11}^{(o)} = -\frac{\rho_{11}^{o}}{D}$$

b) $$D \equiv 1 + \frac{2\beta^2}{\gamma}\left(\frac{1}{L_{12}^{*}} + \frac{1}{L_{12}}\right)$$

c) $$\pi_{12}^{(o)} = -\frac{\rho_{11}^{o}}{D L_{12}}$$

d) $$\rho_{11}^{(o)} = \rho_{11}^{o} - \rho_{11}^{o}\frac{\beta^2}{\gamma D}\left(\frac{1}{L_{12}} + \frac{1}{L_{12}^{*}}\right)$$

e) $\rho_{33}^{(0)} = 0$

f) $\pi_{13}^{(0)} = \frac{-\rho_{11}^{0}}{L_{13}+\beta^2/L_{23}} + \frac{\rho_{11}^{0}}{L_{13}+\beta^2/L_{23}} \frac{\beta^2}{D}\left[\frac{1}{\gamma}\left(\frac{1}{L_{12}}+\frac{1}{L_{12}^{*}}\right)+\frac{1}{L_{23}L_{12}^{*}}\right]$

The first order solutions will give the resonant results of interest. For N_2O, fluorescence (to the ground state) from the upper levels is used as the monitor of absorption. Hence, both $\rho_{22}^{(1)}$ and $\rho_{33}^{(1)}$ must be calculated. The zero order terms act as the driving terms for the first order equations. Calculation of $\rho_{33}^{(1)}$ is trivial since (II.16c) is (using (II.17))

II.20) a) $\rho_{33}^{(1)} = -\frac{\alpha^2}{\gamma}\pi_{13}^{(0)} + c.c.$

Calculation of $\rho_{22}^{(1)}$ is complicated by the generally strong coupling (β^2 arbitrary) of equations (II.16 a, b, and d), which must be solved explicitly for $\rho_{22}^{(1)}$. Solving for $\rho_{22}^{(1)} - \rho_{11}^{(1)}$ from (II.16 a, b and d) and then substituting this result into (II.16d) gives:

II.21) $\pi_{12}^{(1)} = \frac{-\alpha^2}{\gamma D L_{12}}\left[\pi_{13}^{(0)} - \frac{2\beta^2}{L_{23}L_{12}^{*}}\left(\pi_{13}^{(0)}+\pi_{12}^{(0)*}\right) + c.c.\right]$

$$- \frac{\alpha^2}{L_{23}^{*}L_{12}}\left(\pi_{12}^{(0)} + \pi_{13}^{(0)*}\right)$$

Eq. (II.16b) becomes

$$\text{II.22)}\quad \rho_{22}^{(1)} = -\frac{\beta^2}{\gamma}\left(\pi_{12}^{(1)} + \pi_{12}^{(1)*}\right)$$

The zero order results (II.19 c and f), substituted into (II.21), (II.22) and (II.20) give after somewhat tedious algebra, the following results:

$$\text{II.23)}\quad \text{a)}\ \rho_{22}^{(1)} = -\frac{\rho_{11}^{0}\beta^2\alpha^2}{\gamma D^2 (L_{12}^{*})^2 L_{23}} - \frac{\rho_{11}^{0}\beta^2\alpha^2\left(\frac{1}{\gamma}\left(\frac{1}{L_{12}}+\frac{1}{L_{12}^{*}}\right)+\frac{1}{L_{23}L_{12}^{*}}\right)}{\gamma D\left(L_{13}+\beta^2/L_{23}\right)}$$

$$+\frac{\rho_{11}^{0}\beta^{*}\alpha^2\left(\frac{1}{\gamma}\left(\frac{1}{L_{12}}+\frac{1}{L_{12}^{*}}\right)+\frac{1}{L_{23}L_{12}^{*}}\right)^2}{\gamma D^2\left(L_{13}+\beta^2/L_{23}\right)} + \text{c.c.}$$

$$\text{b)}\ \rho_{33}^{(1)} = \frac{\rho_{11}^{0}\alpha^2}{\gamma\left(L_{13}+\beta^2/L_{23}\right)} - \frac{\rho_{11}^{0}\beta^2\alpha^2\left(\frac{1}{\gamma}\left(\frac{1}{L_{12}}+\frac{1}{L_{12}^{*}}\right)+\frac{1}{L_{23}L_{12}^{*}}\right)}{\gamma D\left(L_{13}+\beta^2/L_{23}\right)}$$

$$+\ \text{c.c.}$$

The results in Eq.'s (II.23 a, b) are for an ensemble of atoms moving with velocity $\underline{V}$. Using

II.24) $$\rho^{0}_{11}(v)dv = N^{(0)} e^{-v^2/u^2} \frac{dv}{u\sqrt{\pi}} \; ; \; u^2 = 2KT/m$$

which is the number of atoms moving with velocity V, the total contribution to N_{22}, and N_{33} from atoms of all velocities is:

II.25) $$N^{(1)}_{ii} = N^{(0)} \int_{-\infty}^{\infty} e^{-v^2/u^2} \frac{dv}{u\sqrt{\pi}} \rho^{(1)}_{ii}$$

The first term of Eq. (II.23b) is the Doppler broadened background of the travelling wave E_2, and will be eliminated. (Note that the form of the denominator is $i(\varepsilon - kv) + \delta$, which on adding the complex conjugate and integrating over $\underline{V}$ gives a constant independent of ε and δ.) The various terms in (II.23) are all sharply peaked in velocity space, so that the Maxwellian factor may be taken outside the integral. Assuming that both lasers are tuned near their respective atom fixed transition frequencies and that $\omega_{32} << Ku$, (Ku = Doppler width), the Maxwellian factor may be simply put equal to one. With the definitions :

II.26)

a) $$\chi = KV - \Delta_1 \; ; \; \Delta_1 = \Omega_1 - \omega_{21}$$

b) $$S = 4\beta^2/\gamma\gamma'$$

The resonant part of N_{33} (from the 2nd term of (II.23b) is given by

$$\text{II.27)}\quad N_{33}^{(1)} = 2\,Re\,\frac{-\beta^2\alpha^2}{\gamma K u\sqrt{\pi}}\,N^{(0)}\int_{-\infty}^{\infty} dx\,\frac{\frac{2\gamma'}{\delta}+\frac{-ix+\gamma'}{L_{23}}}{[x^2+\gamma'^2(1+S)][-i(x-a)+\gamma'+\beta^2/L_{23}]}$$

where Eq. (II.19b) has been used, and the numerator and denomenator have been multiplied by suitable factors of the L_{ij} (Eq. II.12). Note that the 2nd term in Eq. (II.23a) will give exactly the same result as (II.27). The other two terms of (II.23a) contain 2nd order poles and must be evaluated separately.

The integrals are most easily done using Residue Calculus. The poles in the integrand of Eq. (II.27) occur at

$$\text{II.28)}\quad x = \pm i\gamma'(1+S)^{\frac{1}{2}} \equiv \pm ia \;;\; x = a\left(1-\frac{\beta^2}{a^2+\gamma_{23}^2}\right) - i\left(\gamma'+\frac{\gamma_{23}\beta^2}{a^2+\gamma_{23}^2}\right)$$

Since there are two poles in the lower half plane and only one (at ia) in the upper half plane, the upper contour will be used. (see Fig. 2.2)

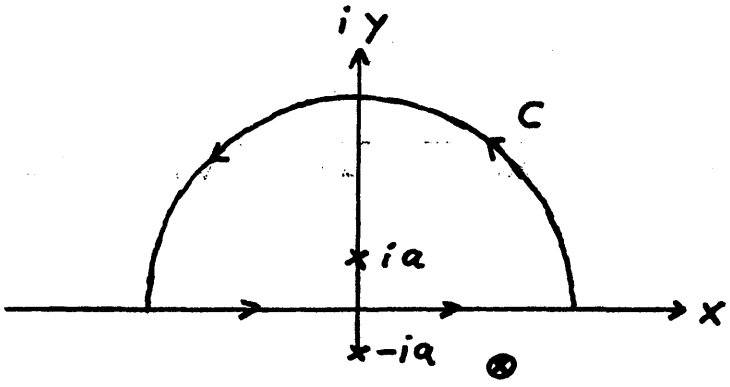

Figure 2.2

The integrand tends to zero for $|x| \to \infty$ as $1/|x|^2$, so the contribution on C vanishes giving

II.29) $$N_{33}^{(1)} = 2\,Re\,\frac{-\beta^2\alpha^2}{\gamma K u\sqrt{\pi}}\,N^{(0)}\,2\pi i\,Res(ia)$$

where

II.30) $$2\pi i\,Res(ia) = = \frac{\pi\left(\frac{2\gamma'}{\gamma} + \frac{\gamma'+\gamma'(1+S')^{\frac{1}{2}}}{i\Delta+\gamma_{23}}\right)}{\gamma'(1+S')^{1/2}\left(\gamma'+\gamma'(1+S')^{1/2}+\frac{\beta^2}{i\Delta+\gamma_{23}}+i\Delta\right)}$$

The other integrals appearing in (II.23a) are done analagously, except for the 2nd order poles at ia. Only the integrals and results will be given here.

Equation (II.23a) may be written as

II.31) $$N_{22}^{(1)} = N_{33}^{(1)} + I_1 + I_2$$

where

II.32) a) $$I_1 = 2\,Re\,\frac{-\beta^2\alpha^2}{\gamma K u\sqrt{\pi}}\,\frac{N^{(0)}}{L_{23}}\int_{-\infty}^{\infty} dx\,\frac{(-ix+\gamma')^2}{[x^2+\gamma'^2(1+S')]}$$

b) $$I_2 = 2\,Re\,\frac{\beta^4\alpha^2}{\gamma K u\sqrt{\pi}}\,N^{(0)}\int_{-\infty}^{\infty} dx\,\frac{\left[\frac{2\gamma'}{\gamma}+\frac{-ix+\gamma'}{L_{23}}\right]^2}{[x^2+\gamma'^2(1+S')]^2\left[-i(x-\Delta)+\gamma'+\beta^2/L_{23}\right]}$$

Evaluating I_1 and I_2 and adding gives

$$\text{II.33)}\quad I_1+I_2 = 2\,Re\,\frac{\beta^4\alpha^2}{\gamma' K u\sqrt{\pi}}\,N^{(0)}\left\{\frac{2\pi}{a^3}\frac{\gamma'}{\gamma}\,\frac{\frac{\gamma'}{\gamma}+\frac{\gamma'+i\Delta}{L_{23}}+\frac{a+\gamma'}{L_{23}}}{a+\gamma'+\beta^2/L_{23}+i\Delta}+\right.$$

$$\left.+\frac{\pi\left(\frac{2\gamma'}{\gamma}+\frac{a+\gamma'}{L_{23}}\right)^2}{2a^2\left[a+\gamma'+\beta^2/L_{23}+i\Delta\right]^2}\right\}$$

where $\underline{a}$ is given by Eq. (II.28) as $\gamma'(1+S')^{\frac{1}{2}}$.

The final general result for $N_{33}^{(1)}$ using (II.29) and (II.30) may be written as:

$$\text{II.34)}\quad N_{33}^{(1)} = \frac{-2\beta^2\alpha^2\sqrt{\pi}}{\gamma' K u}N^{(0)}\,Re\,\frac{\left(\frac{2\gamma'}{\gamma}+\frac{\gamma'+\gamma'\sqrt{1+S'}}{i\Delta+\gamma_{23}}\right.}{\gamma'\sqrt{1+S'}\left(\gamma'+\gamma'\sqrt{1+S'}+\frac{\beta^2}{i\Delta+\gamma_{23}}+i\Delta\right)}$$

This will be evaluated for two limits, that rate equation approximation $\gamma_{23}\to\infty$, and for the case where $\gamma_{23}=\gamma'=\gamma$. The former gives:

$$\text{II.35)}\quad N_{33}^{(1)\,REA} = -\frac{\alpha^2\sqrt{\pi}}{\gamma' K u}N^{(0)}\frac{S'}{\sqrt{1+S'}}\,\frac{1+\sqrt{1+S'}}{\left(1+\sqrt{1+S'}\right)^2+(\Delta/\gamma')^2}$$

For the latter case one obtains

$$\text{II.36)}\quad N_{33}^{(1)} = -\frac{\alpha^2\sqrt{\pi}}{\gamma K u} N^{(0)} \frac{S'}{\sqrt{1+S'}} \frac{\frac{1+\sqrt{1+S'}}{2}}{\left(\frac{1+\sqrt{1+S'}}{2}\right)^2 + (\Delta/\gamma)^2}$$

after factoring $[\Delta'^2 + (Q+2)^2/4]$ from the numerator and denominator, where $Q = 1+\sqrt{1+S'}$ and $\Delta' = \Delta/\gamma$. If, in the rate equation approximation, γ' is taken equal to γ so that (II.35) and (II.36) may be properly compared, one immediately sees that the area under the two curves is identical but that the result (II.36) is narrower and larger in size by a factor of 2. It can be shown that for counter propagating travelling waves, the effect of γ_{23} is reduced yielding a result similar to (II.35) where $\Delta \rightarrow (\Omega_1+\Omega_2)-(\omega_{12}+\omega_{13})$. Thus, the copropagating travelling waves result in a generally narrower and larger resonance than the counter propagating case. This is very useful for studying the spectra of molecules or atoms which exhibit hyperfine structure with small splittings.

After considerable algebra, the contributions of I_1 and I_2 of Eq. (II.33) may be evaluated in the limit $\gamma_{23} = \gamma' = \gamma$. By factoring the numerators and denominators as was done to obtain Eq. (II.36), one obtains for the sum of $N_{33}^{(1)}$ and $N_{22}^{(1)}$:

II.37) $$\left(N_{33}^{(1)}+N_{22}^{(1)}\right)_{RES} =$$

$$= \frac{\alpha^2 S}{\gamma K u}\sqrt{\pi}\,N^{(o)}\left\{\left(\frac{1}{2}+\frac{S}{4(1+S)}\right)\frac{1}{\sqrt{1+S}}\;\frac{Q}{\left(\frac{\Delta}{\gamma}\right)^2+\frac{Q^2}{4}}\right.$$

$$\left. - \frac{S}{16(1+S)}\;\frac{Q^2-(\Delta/2\gamma)^2}{\left[\left(\frac{\Delta}{\gamma}\right)^2+\frac{Q^2}{4}\right]^2}\right\}$$

where

II.38) $$Q = 1+\sqrt{1+S}$$

The $\frac{1}{2}$ in the first term comes from $N_{33}^{(1)}$ and the equivalent result in $N_{22}^{(1)}$. The rest of (II.37) is due to the contributions of Eq. (II.33) to $N_{22}^{(1)}$. The rate equation results ($\gamma_{23} \to \infty$) are not of special interest here and will not be given.

In fitting the data, the lineshape for both the $\underline{V}$ (given above) and inverted $\underline{V}$ configurations are required. The inverted $\underline{V}$ results will now be derived using the symmetry of the equations (II.15) and (II.16). (See Fig. 2.3.) The population ρ_{11} which fluoresces to the ground state (not shown) must be calculated to first order in the weak wave E_2. In this case $\rho_{11}^{o} = 0$ and $\rho_{33}^{o} = \rho_{22}^{o} = N^{(o)}(V)$, where $\hbar\omega_{32}$

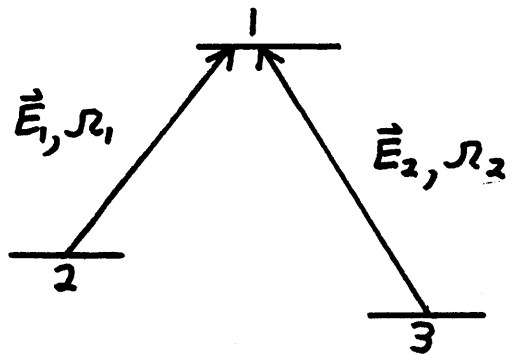

Figure 2.3

is assumed very small compared to KT. A number of minor changes are required in Eqs. (II.15) and (II.16) for the inverted V. Since ω_{21}, ω_{31}, and ω_{32} are all negative, the complex conjugate terms of the potential give the resonant contributions to ρ_{12}, ρ_{13} (the rotating wave approximation). This has the effect of replacing $(\Omega_i - KV)$ by $-(\Omega_i - KV)$, $(i = 1, 2)$ in all equations. The result is that

II.39) $$L_{ij} \rightarrow L^*_{ji}$$

where $\omega_{ij} \rightarrow \omega_{ji}$ as indicated in (II.39), and the L_{ij} are given by Eq. (II.12). All other algebra is unchanged, so that Eqs. (II.15) and (II.16) yield the correct results, except for the substitution (II.39). For the case at hand, all the levels 1,2 and 3 represent excited vibrational states, where collisions cause the primary depopulating and dephasing rates (except at pressures << 1 m Torr). Hence the assumption that $\gamma_1 \cong \gamma_2 \cong \gamma_3 = \gamma$ and $\gamma_{12} \cong \gamma_{13} = \gamma'$ is very reasonable and will be made here.

Using the above assumptions on the unperturbed populations, it is then easily shown that $\pi_{12}^{(o)}$ and $\pi_{13}^{(o)}$ change sign. The form of Eqs. (II.16) is unchanged except for the substitutions (II.39) so that the result (II.21) for the form of $\pi_{12}^{(1)}$ is also unchanged. However the fact that $\pi_{12}^{(o)}$ and $\pi_{13}^{(o)}$ have changed sign then implies via (II.21) that $\pi_{12}^{(1)}$ has also changed sign. Noting from (II.16 a, b, c) that $\rho_{11}^{(1)}$ contains $\pi_{12}^{(1)}$ and $\pi_{13}^{(o)}$ with the opposite sign of $(\rho_{22}^{(1)} + \rho_{33}^{(1)})$, the result for $\rho_{11}^{(1)}$ in the inverted $\underline{V}$ configuration will yield identical results to that for $(\rho_{22}^{(1)} + \rho_{33}^{(1)})$ in the $\underline{V}$ configuration. The fact that the real part of π_{ij} appears means that the only relevant change in the former result Eq. (II.37) is that ω_{32} in Δ must be changed to ω_{23} according to (II.39).

II.40) $$\Delta = \mathcal{R}_2 - \mathcal{R}_1 - \omega_{32} \longrightarrow \mathcal{R}_2 - \mathcal{R}_1 - \omega_{23}$$

(for the inverted V configuration Fig. 2.2).

2. Intensities of the Three Level Resonances

An examination of Eq. (II.37) shows that for a high intensity strong wave i.e. $S >> 1$, the intensity at resonance ($\Delta = 0$) is proportional to

II.41) $$I \propto \alpha^2 S'/Q^2 \sim \alpha^2$$

since $Q^2 \sim S$ when $S >> 1$.

Consider a 3 level system where μ_{13} is very small and μ_{12} is large. If the two laser fields are tuned so that the weak field E_2 interacts with the transition μ_{13} and the strong field E_1 with μ_{12} (i.e. $\mathcal{R}_2 - \mathcal{R}_1 > 0$ and $\omega_{32} > 0$ for noninverted V), then (II.41) shows that $I \propto (\mu_{13}E_2)^2$ which is very small. In addition, (II.37) shows that the resonance is severely broadened since $S \propto (\mu_{12}E_1)^2$.

Now consider the situation when μ_{13} is large and μ_{12} is very small. Assuming that E_1 is still large enough so that S is greater than 1, Eq. (II.14) gives $I \propto (\mu_{13}E_2)^2$ where μ_{13} is now assumed large (but $\alpha^2/\gamma\gamma' << 1$). The resonance intensity is thus larger by a factor of the ratio of the strong to weak matrix element squared. In addition, S is smaller by the same factor so that resonance is both narrower and larger than in the previous situation. Hence, all resonances for which the strong field interacts with a weak transition when the weak field interacts with a strong transition are enhanced tremendously compared to the resonances for which the strong field and strong transition interact and the weak field and weak transition interact. One immediately sees that the lineshape for $\mathcal{R}_3 - \mathcal{R}_1 > 0$ will then be different from that for which $\mathcal{R}_2 - \mathcal{R}_1 < 0$ when hyperfine structure is present, because different transitions are enhanced in each case. Thus, by using unequal intensities E_2^2 and E_1^2, a complicated

hyperfine spectrum may be considerably simplified. This will be discussed at length in the experimental part of this work.

In order to make practical use of Eq. (II.37), the contributions from the various 3 level resonances forming the total lineshape must be summed. For the case of N_2O where each rotational-vibrational level is split into 9 components each of which contains M degeneracy, this is a non trivial exercise. The details of the curve fitting will be discussed below, but the M degeneracy problem will be addressed here.

Note that the fluorescence intensity is proportional to the total population of the upper levels. This is due to the fact that the fluorescence lifetime is long compared to the collision time, so that fluorescence is observed from the entire upper J manifold.[2] Consider the case where $\omega_{32} >$ (total linewidth), and where $\vec{E}_1$, $\vec{E}_2$ are perpendicular linearly polarized laser fields. Then, taking $\vec{E}_1 = E_1 \hat{e}_Z$ and $\vec{E}_2 = E_2 \hat{e}_x$, there will be only $\Delta M = 0$ transitions for the strong wave E_1 and only $\Delta M = \pm 1$ transitions for the weak wave E_2, where $M = \vec{F} \cdot \hat{e}_Z$, and $|F|$ is conserved.

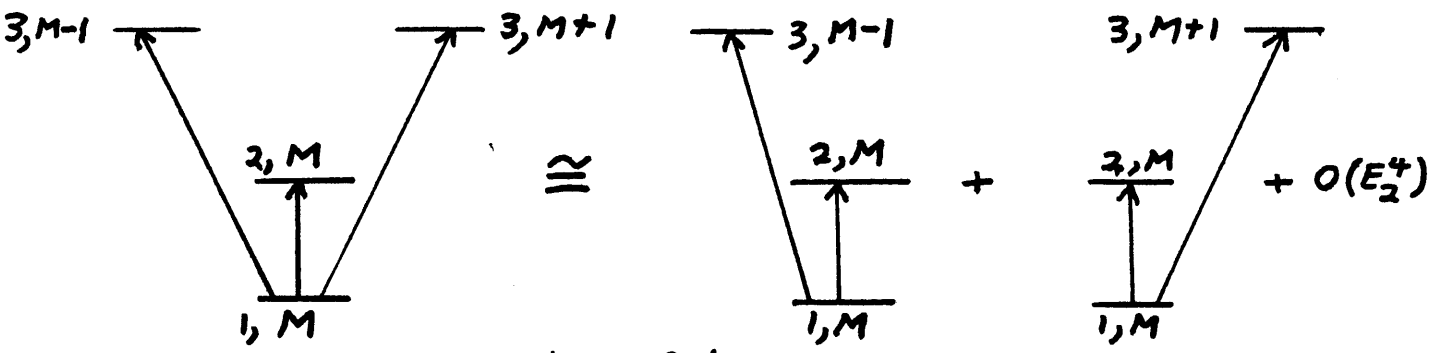

Figure 2.4

If M changing collisions are neglected, the resonant contributions from the various M degenerate terms can then be added to lowest order in the weak wave intensity as shown in Fig. 2.4. For parallel polarizations, both waves induce only $\Delta M = 0$ transitions, if the M quantization axis is taken along the polarization direction. The uncoupling is then obvious. When $\omega_{32} = 0$, the strongly coupled wave leads to some 4-level resonances which will not uncouple in the simple way shown in Fig. 2.4 for either the parallel or perpendicular polarizations. These will not be considered here.

M-Sums When E_1 and E_2 are Weak

When both E_1 and E_2 are weakly saturating, the resonant contribution to the lineshape from the various M transitions can be uncoupled to lowest order in E_1 and E_2 for any ω_{32}. (in a manner similar to that shown in Fig. 2.4). Equation (II.37) shows that in this case ($S \ll 1$) the resonance intensity is $\propto \alpha^2 S \propto \mu_{12}^2 \mu_{13}^2$. The total intensity from all the M degenerate components of a particular set of energy levels 1, 2 and 3 is then proportional to

II.42) $$I_{TOT} \propto \sum_M \mu_{12}^2(M)\mu_{13}^2(M)$$

where M is that of the common level.

In order to determine the best choice of laser polarizations,

one can study the polarization dependence of (II.42) by utilizing the Wigner-Eckart Theorem result given in Eq.(I.56a)

II.43) $$\langle W'; J'; F'; M' | \mu_q | W; J, F, M \rangle =$$

$$= \langle F, 1; M, q | F, 1; F', M+q \rangle \times$$

$$\times \langle W'; J'; F' || \mu || W, J, F \rangle$$

where $q = \pm 1, 0$

and

II.44)

a) $$\mu_{\pm} = \mp \frac{1}{\sqrt{2}} (\mu_x \pm i \mu_y)$$

b) $$\mu_0 = \mu_z$$

Polarization dependence is then determined by some simple sums of products of squares of Clebsch-Gordon coefficients, since the reduced matrix elements factor out and are independent of laser polarizations. The best choice of laser polarizations is the one which suppresses the strong crossing resonances where μ_{12} and μ_{13} both have $\Delta F = \Delta F_1 = \Delta J$, since these all occur when $\Delta \tilde{=} 0$ as can be seen from the energy level diagram (Fig. 1.2). From Fig. 1.2 one can see that crossing resonances with large ω_{32} require $\Delta F = -1$ in combination with $\Delta F = 0$. These resonances should be enhanced as much as possible. From Table I.7, note that $\Delta F = 0$ transitions are much weaker than $\Delta F = \Delta J$ ($= -1$ for P Branch) transitions. $\Delta F = -\Delta J$ transitions

are even weaker and need not be considered in the polarization optimization.

The results of Equation (II.42) are given in Table (II.1) for various polarizations. It is clear that perpendicular polarizations represent the best choice.

Clebsch-Gordon Sums Eq. (II.42) are given in Appendix II.1 for all of the important types of 3-level resonances (inverted V and V configurations) for the P-Branch. ($\perp$ polarizations).

Instead of calculating the Clebsch-Gordon Sums Eq. (II.42) again for the R-Branch, using some simple symmetries between the R and P branch transitions will allow the R branch results to be expressed in the same form as for the P branch (except for a different reduced matrix). This is accomplished in the following way.

Suppose the matrix required for the R branch ($J = J' + 1$) is given as:

$$\text{II.45)}\quad \langle \alpha'; \tilde{w}'; J, F, M | \mu_q | \alpha, \tilde{w}; J', F', M' \rangle =$$
$$= \sum_{F_1, F_1'} \tilde{a}^*(\alpha'; \tilde{w}'; J, F_1, F) \langle J, F_1; F, M | \mu_q | J', F_1'; F', M' \rangle \times \tilde{a}(\alpha, \tilde{w}; J', F_1'; F')$$

by analogy to Eq. (I.55) where F_1, F_1' are dummy summation variables. The quantum number α' is added to represent say, the vibrational state. The problem is then to evaluate the matrix of μ_q with

TABLE II.1

Weighting Functions (Eq. II.42) For Various Polarizations

A. Right and Left Circular Polarizations

$$\vec{E}_\pm = \mp \frac{1}{\sqrt{2}} (\hat{e}_x \pm i \hat{e}_y) E_0 e^{-i(Kz - \omega_\pm t)} \; ; \; \frac{1}{2} \vec{E}_\pm \cdot \vec{E}_\pm^* = \frac{1}{2} E_0^2$$

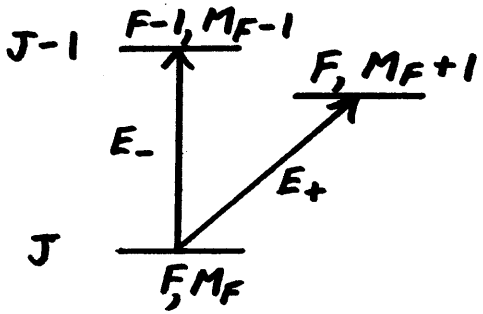

$$I^{+,-}_{F;F-1,F} = |\langle J-1,1;\, F-1 \| \mu \| J,1;\, F\rangle|^2 \times$$
$$\times |\langle J-1,1;\, F \| \mu \| J,1;\, F\rangle|^2 \frac{(F-1)(2F-1)}{10F}$$

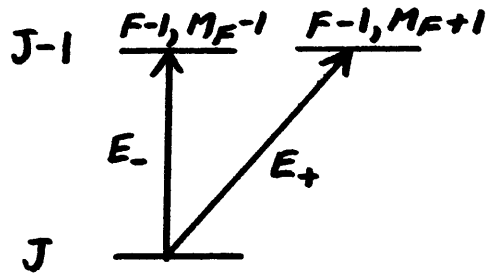

$$I^{+,-}_{F;F-1,F-1} = |\langle J-1,1;\, F-1 \| \mu \| J,1;\, F\rangle|^4 \frac{(2F-3)(2F-1)(F-1)}{30F(2F+1)}$$

TABLE II.1 (continued)

B. Parallel Linear Polarizations

$$\vec{E}_z^{(1,2)} = \hat{e}_z E_0 e^{-i(kz-\omega_{1,2}t)} \quad ; \quad \frac{\vec{E}\cdot\vec{E}^*}{2} = \frac{E_0^2}{2}$$

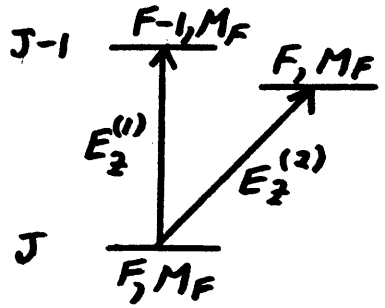

$$I^{z,z}_{F;F-1,F} = |\langle J-1,1;F-1\|\mu\|J,1;F\rangle|^2 \times$$
$$\times |\langle J-1,1;F\|\mu\|J,1;F\rangle|^2 \frac{2(F-1)(2F-1)}{30F}$$

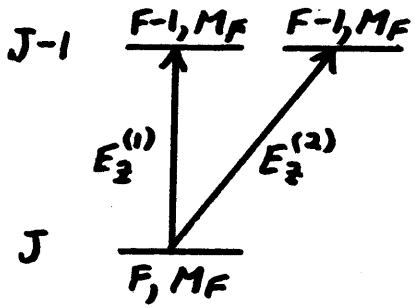

$$I^{z,z}_{F;F-1,F-1} = |\langle J-1,1;F-1\|\mu\|J,1;F\rangle|^4 \frac{2(2F-1)(4F^2+1)}{30F(2F+1)}$$

(INVERTED V CONTRIBUTES EQUALLY)

TABLE II.1 (continued)

C. Perpendicular Linear Polarizations

$$\vec{E}_x = \hat{e}_x E_0 e^{-i(kz-\omega_x t)} \; ; \; \vec{E}_z = \hat{e}_z E_0 e^{-i(kz-\omega_z t)} \; ; \; \tfrac{1}{2}\vec{E}\cdot\vec{E}^* = \tfrac{1}{2}E_0^2$$

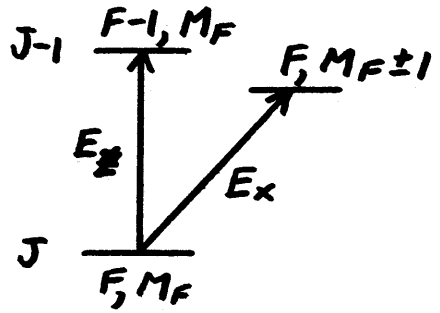

$$I^{z,x}_{F;F-1,F} = |\langle J-1,1;F-1\|M\|J,1;F\rangle|^2 \times \langle J-1,1;F\|M\|J,1;F\rangle|^2 \frac{(2F-1)(4F+1)}{30F}$$

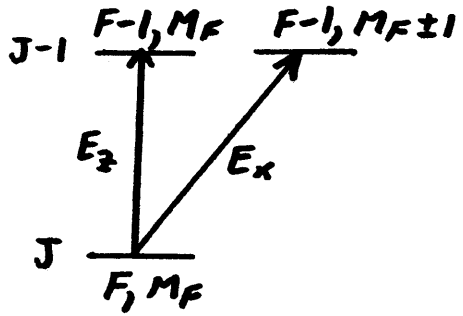

$$I^{z,x}_{F;F-1,F-1} = |\langle J-1,1;F-1\|M\|J,1;F\rangle|^4 \frac{(F-1)(2F-1)(6F+1)}{30F(2F+1)}$$

respect to the basis $|J, F_1; F, M>$. This can be done using the Wigner-Erkart Theorem, but the resulting expression would require a recalculation of sums Eq. (II.42) for the R branch ($J = J' + 1$) even though the P branch ($J' = J - 1$) results are known. Instead, the matrix of μ_q with respect to the basis set for the R-branch will be related to that of the P branch. Consider

II.46) $$\langle J, F_1; F, M|\mu_q|J', F_1'; F', M'\rangle^* =$$

a) $$= \langle J', F_1'; F', M'|\mu_q^*|J, F_1; F, M\rangle$$

b) $$= (-1)^{|q|}\langle F, 1; M, -q|F, 1; F', M'\rangle \times$$
$$\times \langle J', F_1'; F'||\mu||J, F_1, F\rangle$$

c) $$= \langle J, F_1; F, M|\mu_q|J', F_1'; F', M'\rangle$$

Step b) follows from Eq. (II.44) (i.e. $\mu_q^* = (-1)^{|q|}\mu_{-q}$ since (μ_x, μ_y, μ_z) is hermitian.) Step c) results from the fact that everything on the right hand side of b) is real (see Table I.7). Now, define the matrix element in Step c) as

II.47) $$\langle J, F_1; F, M|\mu_q|J', F_1'; F', M'\rangle \equiv$$
$$\equiv (-1)^{|q|}\langle F, 1; M, -q|F, 1; F', M\rangle \times$$
$$\times \langle J, F_1; F||\alpha||J', F_1'; F'\rangle$$

Using Step b), this requires

II.48) $$\langle J, F_1; F \| \tilde{\mu} \| J', F_1'; F' \rangle \equiv \langle J', F_1'; F' \| \mu \| J, F_1, F \rangle$$

Letting J = J' + 1, the R branch reduced matrix $\langle\|\tilde{\mu}\|\rangle$ is then merely the transpose of the P branch reduced matrix $\langle\|\mu\|\rangle$, which is given in Appendix I.4.

Eq. (II.45) may now be written as:

II.49) $$\langle \alpha', \tilde{w}'; J, F, M | \mu_q | \alpha, \tilde{w}; J', F', M' \rangle =$$
$$= (-1)^{|q|} \langle F, 1; M, -q | F, 1; F', M' \rangle \times$$
$$\times \langle \alpha, \tilde{w}'; J, F \| \tilde{\mu} \| \alpha, \tilde{w}; J', F' \rangle ; M' = M - q$$

where

II.50) $$\langle \alpha', \tilde{w}'; J, F \| \tilde{\mu} \| \alpha, \tilde{w}; J', F' \rangle =$$
$$= \sum_{F_1, F_1'} \tilde{a}^*(\alpha', \tilde{w}'; J, F_1, F) \langle J, F_1; F \| \tilde{\mu} \| J', F_1'; F' \rangle \times$$
$$\times \tilde{a}(\alpha, \tilde{w}; J', F_1', F')$$

As in Chapter I, the eigenvalue problem for each (α, J) is solved to give the $\tilde{a}$ coefficients which are then used in

Eq. (II.50) along with the matrix of $\tilde{\mu}$ (II.48).

A comparison of (II.49) and (I.56) shows that the results have an identical dependence on F and F' inside the Clebsch-Gordon coefficient. For q = o <u>i.e.</u> μ_Z, the M dependence of (II.49) and (I.56) is obviously identical.

From Eqs. (II.49, I.56) it is obvious that a symmetry for the (F,M) contributions to the R and P branch weighting functions (II.42) is shown in Fig. 2.5. The reason for using this particular symmetry is that $\Delta F = \Delta J$ transitions are strong, but $\Delta J = -1$ for P and $+1$ for R.

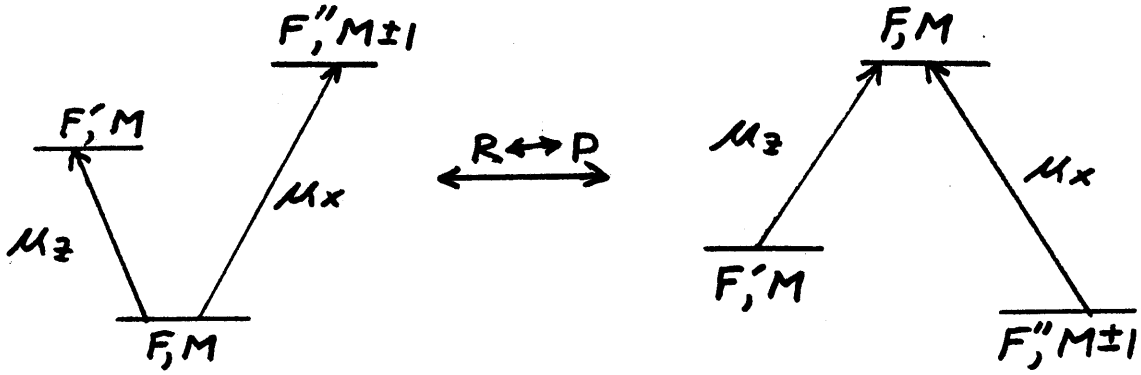

Figure 2.5

From (II.44), one has

II.51) $$|\langle M\pm1|\mu_x|M\rangle|^2 = \tfrac{1}{2}|\langle M\pm1|\mu_\pm|M\rangle|^2$$

For an R branch transition, $M \rightarrow M + 1$ gives the same M dependence as $M + 1 \rightarrow M$ for the P branch since then $q_R = - q_P$. In intensity calculations, only the square of the matrix element is used, so that the $(-1)^{|q|}$ factor in (II.49) is irrelevant. Thus, the weighting functions (Clebsch-Gordon Sums as required by Eq.(II.42)) for the R branch are determined from those of the P branch by interchanging V and inverted V configurations. Note that the results are always given in terms of the common level total angular momentum F.

By the above procedure, the calculations of both the weighting functions and the basis set reduced matrix have been eliminated for the R branch. In addition the P and R branch have been treated symmetrically with respect to the strong and weak transitions. This will prove useful in the computer evaluation of the lineshape.

References

1. B. J. Feldman and M. S. Feld, Phys. Rev. A1, 1375 (1970).

2. A study of the Zeeman spectra shows that M changing collisions may be neglected. See M. J. Kelly, Ph.D. Thesis, M.I.T., 1976, (unpublished).

CHAPTER III

LINE BROADENING MECHANISMS

In any spectroscopic measurement, there always exist effects which tend to broaden the lineshape, and hence limit the resolution. Formerly, Doppler broadening determined the primary limit on resolution. Current molecular (also atomic) beam and nonlinear techniques eliminate the Doppler broadening so that the limiting resolution is determined by the natural linewidth, collisions, power broadening and more recently, by beam transit-time effects.

A discussion of basic broadening mechanisms pertinent to nonlinear techniques (applied to gases) will be given first, neglecting transit-time effects. Then, a derivation of the three level lineshape (V configuration) including transit-time effects will be given via a perturbation calculation.

1. Rate Equation Lineshape for a Two Level Standing Wave Saturation Resonance

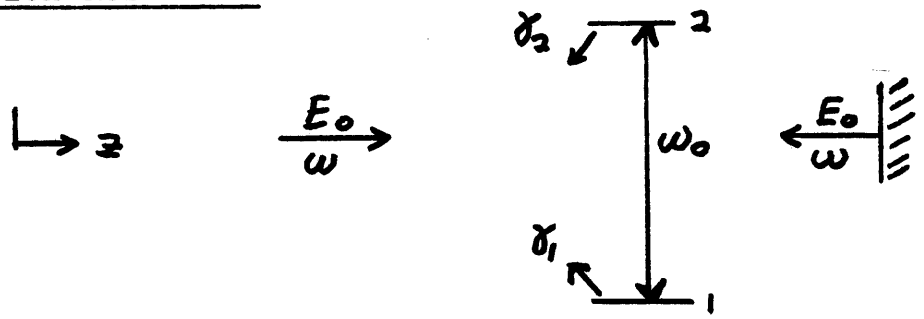

Figure 3.1

The two level standing wave saturation resonance (SWSR) provides a relatively simple example for which the basic line-broadening mechanisms may be studied. Fig. 3.1 shows the experimental situation, where the total absorption of the standing wave is monitored via, for example, fluorescence from the upper level.

The starting point of the calculation is the density matrix formalism. For the two level system, the equations of motion are written as,[1]

III.1) $$\left(\frac{\partial}{\partial t} + v\frac{\partial}{\partial z}\right)\rho_{22} = -\gamma_2(\rho_{22} - \rho_{22}^0) + \frac{i}{\hbar}V_{12}(\rho_{21} - \rho_{12})$$

III.2) $$\left(\frac{\partial}{\partial t} + v\frac{\partial}{\partial z}\right)\rho_{11} = -\gamma_1(\rho_{11} - \rho_{11}^0) - \frac{i}{\hbar}V_{12}(\rho_{21} - \rho_{12})$$

III.3) $$\left[\left(\frac{\partial}{\partial t} + v\frac{\partial}{\partial z}\right) + i\omega_0 + \gamma_{12}\right]\rho_{12} = -\frac{i}{\hbar}(\rho_{22} - \rho_{11})V_{12}$$

III.4) $$\rho_{21} = \rho_{12}^*$$

III.5) $$V_{12} = -\mu_{12}E(z,t)$$

where $h\omega_o = \varepsilon_2 - \varepsilon_1$ and μ_{12} is real by a suitable choice of phase for the wavefunctions. Also, $V = \vec{V} \cdot \hat{e}_Z$ is the velocity along the laser beam. For the standing wave, the electric field E(Z, t)

is given by

III.6) $$E(z,t) = 2E_0 \sin kz \cos\omega t$$
$$= E_0[\sin(kz+\omega t) + \sin(kz-\omega t)]$$
$$\equiv E_+ + E_-$$

In the steady state,

III.7) $$\frac{\partial \rho_{aa}}{\partial t} = \frac{\partial \rho_{bb}}{\partial t} = 0$$

Neglecting spatial harmonic terms[2] which do not alter the basic effects which are to be studied, one may take

III.8) $$\frac{\partial \rho_{aa}}{\partial z} = \frac{\partial \rho_{bb}}{\partial z} \cong 0$$

Consistent with the above approximations, only the polarization proportional to the first spatial harmonic of the applied field is considered

III.9) $$\rho_{12} \cong e^{-i\omega t}[\lambda^+(v)e^{ikz} + \lambda^-(v)e^{-ikz}]$$

where the rotating wave approximation is made. ρ_{11} and ρ_{22} depend only on V according to (III.7) and (III.8).

Substituting (III.9) and (III.6) into Eqs. (III.1 - III.5) reduces the problem to algebra, provided that spatial and temporal harmonics are neglected as stated above.

This gives

III.10) $$\left[(\rho_{22}-\rho_{11})-(\rho^{\circ}_{22}-\rho^{\circ}_{11})\right] = \frac{\mu_{12}E_0}{2\hbar}\left(\frac{1}{\gamma_2}+\frac{1}{\gamma_1}\right)\left(\lambda^{+}-\lambda^{-}+c.c.\right)$$

III.11) $$\gamma_2(\rho_{22}-\rho^{\circ}_{22})+\gamma_1(\rho_{11}-\rho^{\circ}_{11}) = 0$$

III.12) $$\lambda_{\pm} = \frac{\pm\frac{\mu_{12}E_0}{2\hbar}(\rho_{11}-\rho_{22})}{i(\Delta\pm Kv)+\gamma_{12}} \; ; \; \Delta \equiv \omega_0-\omega$$

Substituting (III.12) into (III.10) yields

III.13) $$(\rho_{22}-\rho_{11})-(\rho^{\circ}_{22}-\rho^{\circ}_{11}) = -S\left[\frac{\gamma_{12}^2}{(\Delta+Kv)^2+\gamma_{12}^2}+\right.$$

$$\left.+\frac{\gamma_{12}^2}{(\Delta-Kv)^2+\gamma_{12}^2}\right](\rho_{22}-\rho_{11})$$

where

III.14) $$S \equiv \left(\frac{\mu_{12}E_0}{\hbar}\right)^2\frac{1}{2\gamma_{12}}\left(\frac{1}{\gamma_1}+\frac{1}{\gamma_2}\right)$$

is defined to be the saturation parameter. Solving for $(\rho_{22} - \rho_{11})$

in (III.13), one obtains

III.15) $$\rho_{22} - \rho_{11} = \frac{\rho_{22}^{o} - \rho_{11}^{o}}{1 + S\left[\frac{\gamma_{12}^2}{(\Delta+Kv)^2+\gamma_{12}^2} + \frac{\gamma_{12}^2}{(\Delta-Kv)^2+\gamma_{12}^2}\right]}$$

For an optical or infrared transition, the thermal population of the lower level is much larger than that of the upper level, so that $\rho_{22}^{o} \equiv 0$, and $\rho_{11}^{o} \equiv N(V)$, where

III.16) $$N(v)dv = N_o \frac{e^{-v^2/u^2}}{u\sqrt{\pi}} dv \; ; \; u^2 \equiv 2K_B T/m$$

is the number of atoms with velocity V. With the above assumptions, Eqs. (III.15) and (III.11) may be solved for ρ_{22} to yield

III.17) $$\rho_{22} = \left[\gamma_2\left(\frac{1}{\gamma_1} + \frac{1}{\gamma_2}\right)\right]^{-1} N(v) \frac{S\left[\frac{\gamma_{12}^2}{(\Delta+Kv)^2+\gamma_{12}^2} + \frac{\gamma_{12}^2}{(\Delta-Kv)^2+\gamma_{12}^2}\right]}{1 + S\left[\frac{\gamma_{12}^2}{(\Delta+Kv)^2+\gamma_{12}^2} + \frac{\gamma_{12}^2}{(\Delta-Kv)^2+\gamma_{12}^2}\right]}$$

Since the fluorescence from the upper level is proportional to ρ_{22}, (III.17) yields the desired contribution for atoms of velocity V. Unnecessary proportionality constants will be eliminated in what follows.

The contribution from atoms of all possible velocities V is found by integrating (III.17). The resulting integral is

III.18) $$I(\Delta) = \frac{N_0 S}{u\sqrt{\pi}} \int_{-\infty}^{\infty} dV \frac{\left[\frac{\gamma_{12}^2}{(\Delta+KV)^2+\gamma_{12}^2} + \frac{\gamma_{12}^2}{(\Delta-KV)^2+\gamma_{12}^2}\right]}{1+\left[\frac{\gamma_{12}^2}{(\Delta+KV)^2+\gamma_{12}^2} + \frac{\gamma_{12}^2}{(\Delta-KV)^2+\gamma_{12}^2}\right]S} e^{-\frac{V^2}{u^2}}$$

The Lorentzians peak sharply in velocity space compared to u so long as $\gamma_{12}/Ku \ll 1$. Thus, the Maxwellian factor may be removed from under the integral and evaluated at $V = \pm \frac{\Delta}{K}$ for the corresponding Lorentzians. With the substitution X = KV, (III.18) then becomes

III.19) $$I(\Delta) = \frac{N_0 S}{Ku\sqrt{\pi}} e^{-\left(\frac{\Delta}{Ku}\right)^2} \int_{-\infty}^{\infty} dx \frac{\left[\frac{\gamma_{12}^2}{(\Delta+x)^2+\gamma_{12}^2} + \frac{\gamma_{12}^2}{(\Delta-x)^2+\gamma_{12}^2}\right]}{1+S\left[\frac{\gamma_{12}^2}{(\Delta+x)^2+\gamma_{12}^2} + \frac{\gamma_{12}^2}{(\Delta-x)^2+\gamma_{12}^2}\right]}$$

Multiplying through by the Lorentzian denominators yields

III.20) $$I(\Delta) = \frac{2\gamma_{12}^2 N_0 S}{Ku\sqrt{\pi}} e^{-\left(\frac{\Delta}{Ku}\right)^2} \int_{-\infty}^{\infty} \frac{dx\,[\Delta^2+\gamma_{12}^2+x^2]}{x^4+2Bx^2+q}$$

where

III.21)

a) $$B = \gamma_{12}^2(1+S) - \Delta^2$$

b) $$q = \Delta^4 + 2\gamma_{12}^2\Delta^2(1+S) + \gamma_{12}^4(1+2S)$$

The integration is done using residue calculus, where the poles of the denominator occur at

III.22) $$x^2 = -B \pm \sqrt{B^2 - q}$$

For sufficiently large Δ, (III.21) shows that $B^2 - q$ is negative. With Δ in this region, let

III.23) $$x^2 \equiv a \pm ib$$

where

III.24)

a) $$a = \Delta^2 - \gamma_{12}^2(1+S)$$

b) $$b = \gamma_{12}^2\sqrt{4(1+S)\frac{\Delta^2}{\gamma_{12}^2} - S^2}$$

The roots of (III.23) are then defined as

III.25)

a) $$x = \pm(C_1 + iC_2) \quad \text{for } a+ib$$

b) $$x = \pm(C_1 - iC_2) \quad \text{for } a-ib$$

where C_1 and C_2 are <u>real.</u>

Values of C_1 and C_2 are easily defined in terms of <u>a</u> and <u>b</u> with the reality requirement. Choosing the upper half plane for the integration contour, one obtains after some algebra:

III.26) $$I(\Delta) = \frac{2\gamma_{12}^2 N_0 S'}{Ku\sqrt{\pi}} e^{-\left(\frac{\Delta}{Ku}\right)^2} \frac{\pi}{C_2} \left\{ \frac{\Delta^2 + \gamma_{12}^2}{C_1^2 + C_2^2} + 1 \right\}$$

where

III.27)

a) $$C_1 = \frac{b}{2C_2}$$

b) $$C_2 = \sqrt{-\frac{a}{2} + \frac{1}{2}\sqrt{a^2 + b^2}}$$

c) $$C_1^2 + C_2^2 = \sqrt{a^2 + b^2}$$

Substituting (III.27) and the results for a, b (Eq. III.24) into (III.26) gives the following lineshape:

III.28) $$I(\Delta) = \frac{2\sqrt{\pi}\,\gamma_{12}^2 N_0 S' e^{-\left(\frac{\Delta}{Ku}\right)^2}}{Ku\sqrt{\Delta^2 + \gamma_{12}^2(1+2S')}} \times$$

$$\times \quad \frac{\sqrt{\Delta^2 + (1+S')\gamma_{12}^2 + \sqrt{(\Delta^2+\gamma_{12}^2)[\Delta^2 + \gamma_{12}^2(1+2S')]}}}{\sqrt{-\Delta^2 + (1+S')\gamma_{12}^2 + \sqrt{(\Delta^2+\gamma_{12}^2)[\Delta^2 + \gamma_{12}^2(1+2S')]}}}$$

Equation (III.28) has been derived assuming that Δ is large. However, the lineshape must be continuous and well behaved for

all Δ, so that (III.28) is generally valid. It is easy to show that $I(\Delta = 0)$ is, in fact, correctly given in (III.28) by taking $\Delta = 0$ in (III.19) and directly performing the integration using elementary techniques.

2. Lineshape for a Gaussian Beam

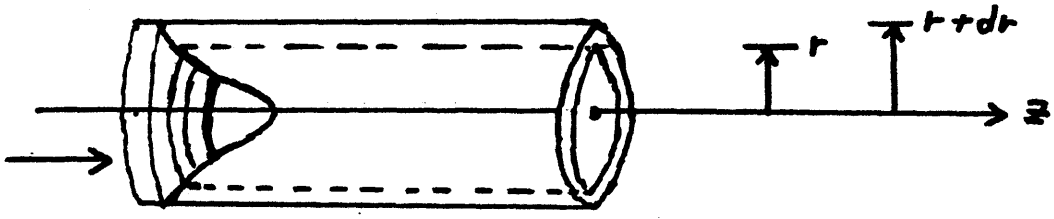

Figure 3.2

For a Gaussian beam,

III.29) $$S = S_0 e^{-r^2/R^2}$$

where R is the intensity $\frac{1}{e}$ radius.

With the assumption that R >> mean free path, the contribution to the fluorescence per unit length from atoms in the annulus at $\underline{r}$ is given as $I(\Delta, S(r))\ 2\pi r dr$. ($\underline{i.e.}$ The beam is treated as a local plane wave (beam waist) with a Gaussian intensity distribution.)

Transit time effects are neglected in this approximation.

The total fluorescence per unti length is then

III.30) $$F_L(\Delta) \propto \int_0^\infty I(\Delta, S'(r))\, 2\pi r\, dr$$

where the absorption cell diameter is assumed large compared to R.

Using (III.28) for I and the substitution

III.31) $$x = S' = S_0' e^{-r^2/R^2} \; ; \; 2r\,dr\, S_0' e^{-r^2/R^2} = -R^2 dx$$

F_L becomes

III.32) $$F_L(\Delta) \propto N_0 \frac{2\sqrt{\pi}}{ku} e^{-\left(\frac{\Delta}{ku}\right)^2} \pi R^2 I'(\Delta)$$

III.33) $$I'(\Delta) \equiv \int_0^{S_0'} \frac{dx\, \gamma_{12}^2}{\sqrt{\Delta^2+\gamma_{12}^2(1+2x)}} \frac{\sqrt{\Delta^2+(1+x)\gamma_{12}^2+\sqrt{(\Delta^2+\gamma_{12}^2)[\Delta^2+\gamma_{12}^2(1+2x)]}}}{\sqrt{-\Delta^2+(1+x)\gamma_{12}^2+\sqrt{(\Delta^2+\gamma_{12}^2)[\Delta^2+\gamma_{12}^2(1+2x)]}}}$$

The integral (III.33) may be done by elementary techniques as follows. Let

III.34) $$v = \sqrt{\Delta^2+\gamma_{12}^2(1+2x)} \; ; \; \frac{\gamma_{12}^2\, dx}{\sqrt{\Delta^2+\gamma_{12}^2(1+2x)}} = dv$$

Then

III.35) $$\Delta^2 + (1+x)\gamma_{12}^2 + \sqrt{(\Delta^2+\gamma_{12}^2)[\Delta^2+\gamma_{12}^2(1+2x)]} = \tfrac{1}{2}\left[V + (\Delta^2+\gamma_{12}^2)^{\frac{1}{2}}\right]^2$$

Using (III.34) and (III.35), I' becomes

III.36) $$I'(\Delta) = \int_{(\Delta^2+\gamma_{12}^2)^{1/2}}^{[\Delta^2+\gamma_{12}^2(1+2S_0')]^{1/2}} dV \sqrt{\frac{\frac{1}{2}\left[V+(\Delta^2+\gamma_{12}^2)^{\frac{1}{2}}\right]^2}{\frac{1}{2}\left[V+(\Delta^2+\gamma_{12}^2)^{\frac{1}{2}}\right]^2 - 2\Delta^2}}$$

With the substitution

III.37) $$y = V + (\Delta^2+\gamma_{12}^2)^{\frac{1}{2}}$$

the integral in (III.36) is easily done and yields

III.38) $$F_L(\Delta) \propto \frac{\pi R^2 N_0}{Ku}\left[\sqrt{2\gamma_{12}^2(1+S_0') + 2(\Delta^2+\gamma_{12}^2)\left(1+\frac{2\gamma_{12}^2 S_0'}{\Delta^2+\gamma_{12}^2}\right)^{\frac{1}{2}} - 2\Delta^2} - 2\gamma_{12}\right]$$

The Maxwellian in Δ has been dropped assuming that Δ is $<<$ Ku always. In addition, unimportant constants have been eliminated.

3. Linewidth of the SWSR

The function $F_L(\Delta)$ of (III.38) is considerably simpler than that of the unintegrated result (III.33). This allows a closed form expression for the halfwidth of half maximum to be derived.

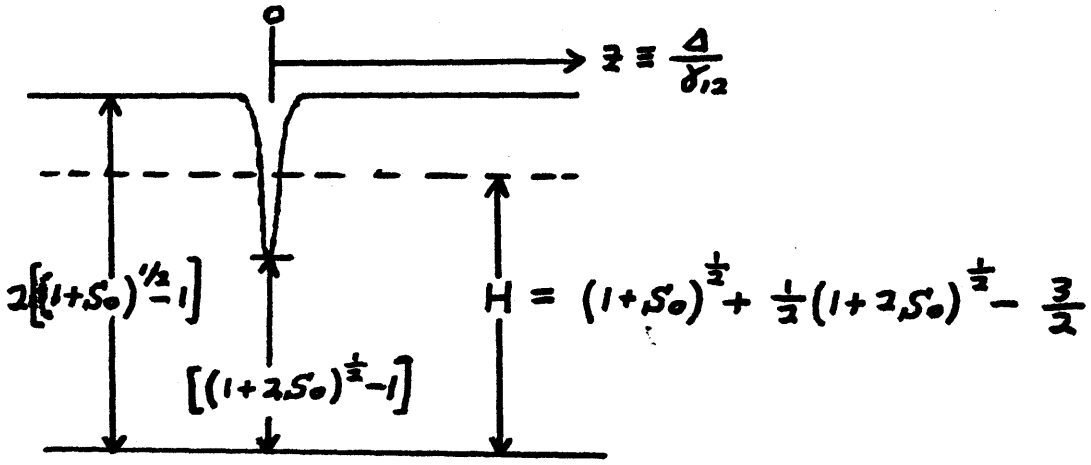

Figure 3.3

By determining the limiting behavior of $F_L(Z)$ at $Z = 0$ and $Z \to \infty$ (but $Z << \omega_u/\gamma_{12}$) as shown in Fig. 3.3, the half width at half maximum $\underline{X}$ may be calculated from

$$H = \left[\sqrt{2(1+S_0) + 2(x^2+1)\left(1+\frac{2S_0}{x^2+1}\right)^{\frac{1}{2}} - 2x^2} - 2\right] \tag{III.39}$$

Note that all unnecessary factors have been dropped from (III.38).

The result $\underline{X}$ for the half width is given by

III.40) a) $$x^2_{HWHM} = \frac{1}{4}\left[\frac{4S_o^2 - 4(1+S_o)(H+2)^2 + (H+2)^4}{4(1+S_o) - (H+2)^2}\right]$$

b) $$(H+2) = (1+S_o)^{1/2} + \frac{1}{2}(1+2S_o)^{1/2} + \frac{1}{2}$$

c) $$W_{HWHM} = \gamma_{12}\, x_{HWHM}$$

For the limit $S_o >> 1$, the width becomes

III.41) $$W_{HWHM}(S_o \to \infty) \cong 0.438\,\gamma_{12}\, S_o^{1/2}$$

For $S_o \to 0$, (III.40) is approximately given by

III.42) $$W_{HWHM}(S_o \to 0) \cong \gamma_{12}(1+S_o)^{1/2}$$

Equation (III.42) is the same as the standard power broadened formula which is often used (incorrectly) to describe the SWSR width.

For a molecular transition where pressure broadening dominates the decay rates (γ_{ij}), one has

III.43) $$\gamma_{ij} \propto P \; ; \; S \propto 1/P^2$$

As the pressure is lowered, the width will tend to the limit given in (III.41) ($\gamma_{12}\, S_o^{1/2}$ is pressure independent). This limit

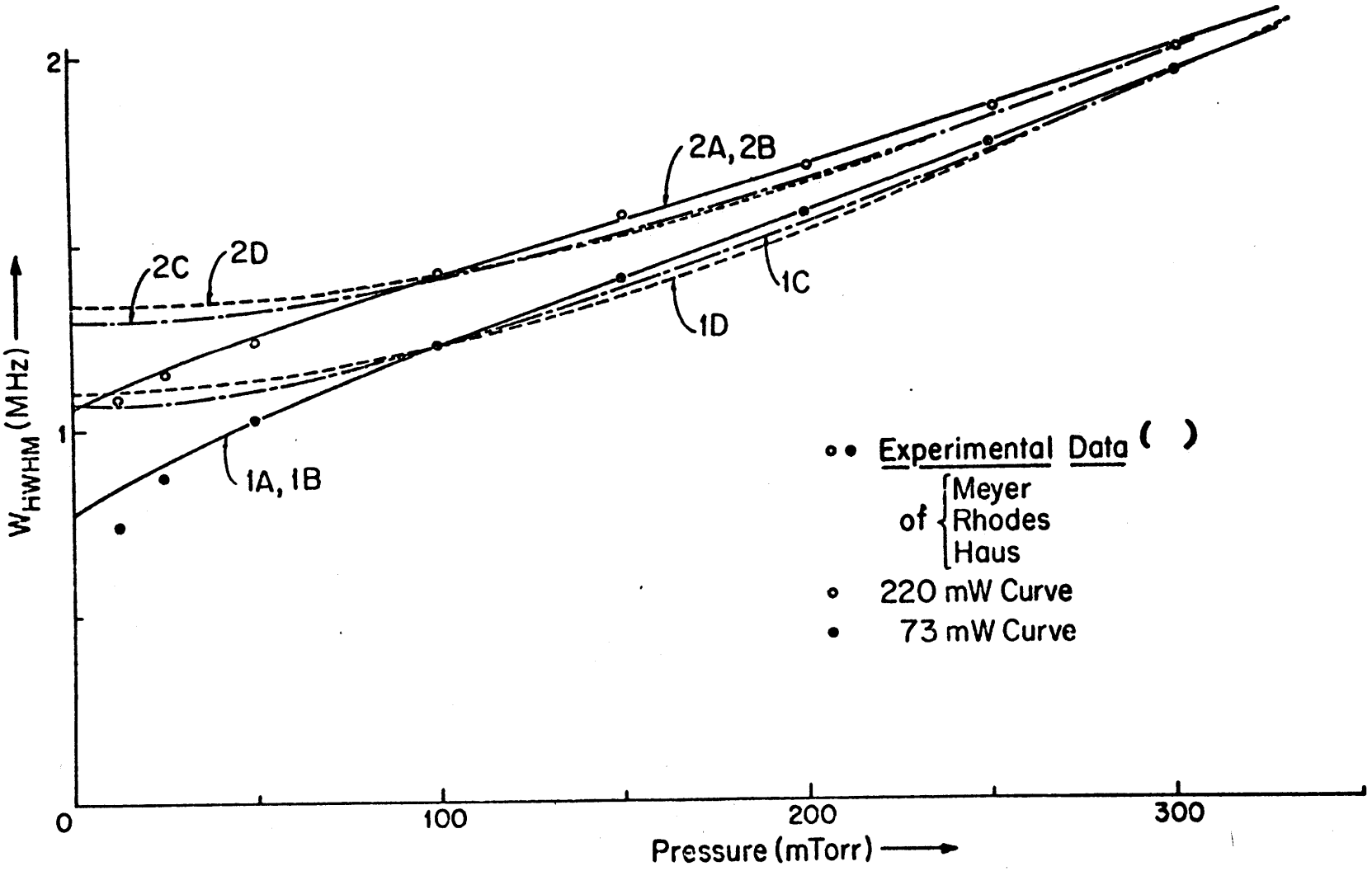

Figure 3.4. See Captions on next page

Figure 3.4 Captions

1, 2 D Fit of Eq. (III.42) to Data

1, 2 C Fit of Eq. (III.28) to Data (width determined numerically)

1, 2 B Fit of Eqs.(III.40, 43) to Data (Gaussian Beam Average)

1, 2 A Fit of Matrix Element Average of Eqs. (III.40, 43) to Data

Note: For a more complete discussion, see M. Kelly, Ph.D. thesis, Feb. 1976 (unpublished)

is smaller than would be predicted by the (incorrect) use of (III.42). Thus, a plot of width squared versus pressure squared will show a down turn at low pressures.

Figure 3.4 shows a plot of width versus pressure for the plane wave lineshape (III.28) (calculated numerically) and for the Gaussian averaged result (III.40). The behavior of the two curves is very different at low pressure. Physically, at low pressure, the wings of the Gaussian intensity distribution produce a large fraction of the fluorescence. The power broadening is low in this region however, so a narrowing of the overall width occurs.

A similar effect occurs due to M degeneracy of the rotational states where the weaker transitions contribute more heavily at low pressures. This effect is not so dramatic as that of the Gaussian beam since the weakest transition has finite strength. The M degeneracy will not be considered here.[3]

4. Transit-Time Effects in Three-Level Systems

Consider the 3-level system shown in Fig. 3.5.

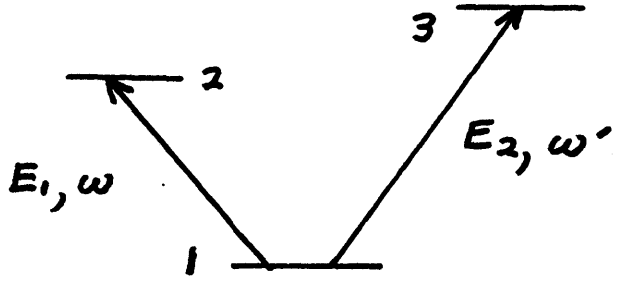

Figure 3.5

It is assumed that $\mu_{23} = 0$ and that E_1 and E_2 interact only with the transitions as shown due to, perhaps, orthogonal polarizations. Transit-time effects will manifest themselves in the Gaussian radial dependence assumed for the fields E_1 and E_2. The calculation will be done to third order in the fields E_1 and E_2 (weak saturation) using integral perturbation theory. The differential perturbation theory which is so useful for plane waves leads to radial differential equations which are not easily solved, and hence cannot be used efficiently.

The starting point for the calculation will be the density matrix equations for a single atom which are given by

III.44)

a) $\dot{\rho}_{11} = -\frac{i}{\hbar}(V_{12}\rho_{21} - \rho_{12}V_{21}) - \frac{i}{\hbar}(V_{13}\rho_{31} - \rho_{13}V_{31}) - \gamma_1\rho_{11}$

b) $\dot{\rho}_{22} = -\frac{i}{\hbar}(V_{21}\rho_{12} - \rho_{21}V_{12}) - \gamma_2\rho_{22}$

c) $\dot{\rho}_{33} = -\frac{i}{\hbar}(V_{31}\rho_{13} - \rho_{31}V_{13}) - \gamma_3\rho_{33}$

d) $\dot{\rho}_{12} = +i\omega_{21}\rho_{12} - \frac{i}{\hbar}V_{12}(\rho_{22} - \rho_{11}) - \frac{i}{\hbar}V_{13}\rho_{32} - \gamma_{12}\rho_{12}$

e) $\dot{\rho}_{13} = +i\omega_{31}\rho_{13} - \frac{i}{\hbar}V_{13}(\rho_{33} - \rho_{11}) - \frac{i}{\hbar}V_{12}\rho_{23} - \gamma_{13}\rho_{13}$

f) $\dot{\rho}_{23} = +i\omega_{32}\rho_{23} - \frac{i}{\hbar}(V_{21}\rho_{13} - \rho_{21}V_{13}) - \gamma_{23}\rho_{23}$

g) $\rho_{ij} = \rho_{ji}^*$

where $V_{23} = 0$, and $\dot{} = \frac{d}{dt}$ (time dependence as seen by atom). For

the interaction V, the following form is taken (near the Gaussian beam waist):

III.45) a) $V = -\vec{\mu}\cdot\vec{E}_1(x,y)\cos(kz-\omega t) - \vec{\mu}\cdot\vec{E}_2(x,y)\cos(kz+\omega' t)$

where

b) $\vec{E}_1(x,y) = \hat{e}_1 E_0 U(x) U(y)$

c) $U(x) = e^{-\alpha x^2}$; $\alpha = \frac{1}{R^2}$; R = field $\frac{1}{e}$ radius

d) $\int_0^\infty \frac{c}{8\pi} E_0^2 e^{-2\alpha r^2} 2\pi r\, dr$ = Travelling wave power in each beam

The beam radii and E_0's have been taken equal in E_1 and E_2 for simplicity. In order to obtain the results for both co-propagating and counterpropagating waves, one can allow $\omega' = \pm|\omega'|$ provided that attention is paid to the resonant contributions for both cases. The slowly varying envelope approximation $\lambda m s p \frac{1}{E_0}\frac{\partial E_0}{\partial z} \ll 1$ is assumed.

By a suitable choice of phase for the wavefunctions of levels 2 and 3, one may take μ_{12} and μ_{13} to be real, where

III.46) a) $\mu_{12} = \int \psi_1^* \vec{\mu}\cdot\hat{e}_1 \psi_2 \, d^3\vec{x}$

b) $\mu_{13} = \int \psi_1^* \vec{\mu}\cdot\hat{e}_2 \psi_3 \, d^3\vec{x}$

and the dipole approximation has been made. This gives

III.47)

a) $$V_{12} = -\mu_{12} E_0 U(x) U(y) \cos(kz - \omega t)$$

b) $$V_{13} = -\mu_{13} E_0 U(x) U(y) \cos(k'z + \omega' t)$$

where $\omega' > 0$ gives counterpropagating waves and $\omega' > 0$ gives copropagating waves. The vector (x, y, z) is the position of the atomic center of mass according to the dipole approximation in (III.46).

Due to the Boltzmann factor, the unperturbed populations of states 2 and 3 will be negligible compared to that of state 1. Hence, the initial conditions on the density matrix will be taken as:

III.48) $$\rho_{ij}^{(0)}(t = t_0; \vec{v}, \vec{r}_0, t_0; 1) = \delta_{i1}\delta_{j1}$$

This notation refers to the creation of an atom in state 1 at time t_0 at position $\vec{r}_0$ with velocity $\vec{v}$. It is assumed that the atoms move in straight lines and simply decay out of the three-level system into other levels which do not interact with the applied field. The density matrix equations may be rewritten in a form suitable for real V_{ij}.

In lowest order,

III.49) $$\dot{\rho}_{11}^{(0)} = -\gamma_1 \rho_{11}^{(0)}$$

so that using (III.5) gives

III.50) $$\rho_{11}^{(0)}(t) = e^{-\gamma_1 (t-t_0)}$$

The result (III.50) may be substituted into equations (III.44) to obtain the 1st order corrections (in V) to the density matrix elements. (The first order results are Doppler broadened and are not of interest except for calculation the higher order corrections.) Continuing in this fashion, one obtains to 3rd order in perturbation theory:

III.51) a) $$\rho_{12}^{(3)} = \left(\frac{i}{\hbar}\right)^3 \int_{t_0}^{t} dt_3 \int_{t_0}^{t_3} dt_2 \int_{t_0}^{t_2} dt_1 \, e^{-(\gamma_{12} - i\omega_{21})(t-t_3)} \times$$

$$\times \Big[V_{12}(t_3)\left(e^{-\gamma_2(t_3-t_2)} + e^{-\gamma_1(t_3-t_2)}\right) V_{12}(t_2)\left(e^{-(\gamma_{12}+i\omega_{21})(t_2-t_1)} + \text{c.c.}\right) \times$$

$$\times V_{12}(t_1) + V_{12}(t_3) e^{-\gamma_1(t_3-t_2)} V_{13}(t_2)\left(e^{-(\gamma_{13}+i\omega_{31})(t_2-t_1)} + \text{c.c.}\right) V_{13}(t_1)$$

$$+ V_{13}(t_3)\, e^{-(\gamma_{23}+i\omega_{32})(t_3-t_2)} V_{12}(t_2)\, e^{-(\gamma_{13}+i\omega_{31})(t_2-t_1)} V_{13}(t_1)$$

$$+ V_{13}(t_3)\, e^{-(\gamma_{23}+i\omega_{32})(t_3-t_2)} V_{13}(t_2)\, e^{-(\gamma_{12}-i\omega_{21})(t_2-t_1)} V_{12}(t_1) \Big]$$

$$\times e^{-\gamma_1(t_1-t_0)}$$

b) $$\rho_{13}^{(3)} = \text{same with } 2 \leftrightarrow 3$$

Equation (III.51b) follows since the labelling of levels

2 and 3 is arbitrary and they are treated symmetrically. The first term of Eq. (III.51a) of order V_{12}^3 contains only the travelling wave E_1 and is then just a correction to the Doppler broadened background. It will be eliminated from further consideration. (A similar term of $0(V_{13}^3)$ appears in $\rho_{13}^{(3)}$).

Having written the third order correction to the density matrix in terms of $V_{ij}(t_n)$, the explicit form of V(t) must now be given. For an atom moving in a straight line with velocity $\vec{V}$ which is created at time to a position $\vec{x}_o$, one has

III.52) $$\vec{x} = \vec{x}_o + \vec{v}(t-t_o)$$

Substituting this into (III.47), the matrix elements of V at $t = t_n$ are given by

III.53)

a) $$V_{12}(t_n) = -\mu_{12} E_o \, U(x_o + v_x(t_n - t_o)) \, U(y_o + v_y(t_n - t_o)) \times \cos[k(z_o + v_z(t_n - t_o)) - \omega t_n]$$

b) $$V_{13}(t_n) = -\mu_{13} E_o \, U(x_o + v_x(t_n - t_o)) \, U(y_o + v_y(t_n - t_o)) \times \cos[k'(z_o + v_z(t_n - t_o)) + \omega' t_n]$$

The polarization at $\vec{x}$ at time $\underline{t}$ will be the measured quantity, so only atoms created at time t_o and position $\vec{x}_o$

satisfying

III.54) $$\vec{x}_o = \vec{x} - \vec{v}(t-t_o)$$

will contribute to the polarization observed at $(\vec{X}, t)$.

Thus, the contribution from atoms labelled by $(\vec{X}_o, t_o)$ which affects the measurement at $(\vec{X}, t)$ is given by operating on $\rho(\vec{X}_o \cdots)$ with

III.55) $$\int d^3\vec{x}_o \; \delta\left[\vec{x} - (\vec{x}_o + \vec{v}(t-t_o))\right]$$

This is equivalent to substituting (III.54) into the $V_{12}(t_n)$ to obtain

III.56) a) $$V_{12}(t_n) \rightarrow V_{12}'(\vec{x}, t; \vec{v}, t_n) = -\mu_{12} E_o \cos\left[k(z - v_z(t-t_n)) - \omega t_n\right] U(x - v_x(t-t_n))\, U(y - v_y(t-t_n))$$

b) $$V_{13}(t_n) \rightarrow V_{13}'(\vec{x}, t; \vec{v}, t_n) = -\mu_{13} E_o \cos\left[k'(z - v_z(t-t_n)) + \omega' t_n\right] U(x - v_x(t-t_n))\, U(y - v_y(t-t_n))$$

The results (III.56) merely give the interaction experienced by an atom of velocity $\vec{v}$ in terms of its final position $(\vec{X}, t)$ instead of its initial position $(\vec{X}_o, t_o)$.

Dropping the Doppler broadened terms, one obtains for $\rho_{12}^{(3)}$:

$$\text{III.57)}\quad \rho_{12}^{(3)}(\vec{x},\vec{v},t;t_o;1) = \left(\frac{i}{\hbar}\right)^3 \int_{t_o}^{t} dt_3 \int_{t_o}^{t_3} dt_2 \int_{t_o}^{t_2} dt_1 \; e^{-(\gamma_{12}-i\omega_{21})(t-t_3)}$$
$$\times \Big[V_{12}'(t_3)\, e^{-\gamma_1(t_3-t_2)} V_{13}'(t_2) \big(e^{-(\gamma_{13}+i\omega_{31})(t_2-t_1)} + \text{c.c.} \big) V_{13}'(t_1)$$
$$+ V_{13}'(t_3)\, e^{-(\gamma_{23}+i\omega_{32})(t_3-t_2)} V_{12}'(t_2)\, e^{-(\gamma_{13}+i\omega_{31})(t_2-t_1)}$$
$$\times V_{13}'(t_1) + V_{13}'(t_3)\, e^{-(\gamma_{23}+i\omega_{32})(t_3-t_2)}\, V_{13}'(t_2)$$
$$\times\, e^{-(\gamma_{12}-i\omega_{21})(t_2-t_1)} V_{12}'(t_1) \Big] \times e^{-\gamma_1(t_1-t_o)}$$

III.58) $\rho_{13}^{(3)}$ same form as (3.14) with $2 \leftrightarrow 3$

Equations (III.57) and (III.58) give the contribution to $\rho_{12}^{(3)}$ from an atom created in level 1 in the interval $(t_o,\ t_o + dt_o)$, with velocity $\vec{v}$. In equilibrium, the number of such atoms is given by $N_1^{(0)}(\vec{v})\, d^3\vec{v}\, \gamma_1\, dt_o$ where

$$\text{III.59)}\quad N_1^{(0)}(\vec{v}) = N^{(0)} \frac{1}{(u\sqrt{\pi})^3}\, e^{-\vec{v}^2/u^2}\,; \quad u^2 = 2k_B T/m$$

Hence, the total contribution from atoms of all velocities created at all possible t_o is given by:

$$\text{III.60)}\quad \rho_{12}^{(3)}(\vec{x},t;1) = \int d^3\vec{v}\, N_1^{(0)}(\vec{v}) \int_{-\infty}^{t} dt_o\, \gamma_1\, \rho_{12}^{(3)}(\vec{x},\vec{v},t;t_o;1)$$

$$\equiv \int d^3\vec{v}\, N_1^{(0)}(\vec{v})\, \rho_{12}^{(3)}(\vec{x},\vec{v},t;1)$$

From Eqs. (III.56) the $V'(t_n)$ do not depend on t_o so that the only t_o dependence is in the factor $e^{-\gamma_1(t_1 - t_o)}$ and in the integral limits. To perform the t_o integration first, the order of integration is changed as follows:

$$\text{III.61)}\quad \int_{-\infty}^{t} dt_o \int_{t_o}^{t} dt_3 = \int_{-\infty}^{t} dt_3 \int_{-\infty}^{t_3} dt_o$$

Continuing in this fashion gives

$$\text{III.62)}\quad \int_{-\infty}^{t} dt_o \int_{t_o}^{t} dt_3 \int_{t_o}^{t_3} dt_2 \int_{t_o}^{t_2} dt_1 \longrightarrow \int_{-\infty}^{t} dt_3 \int_{-\infty}^{t_3} dt_2 \int_{-\infty}^{t_2} dt_1 \int_{-\infty}^{t_1} dt_o$$

Using $\int_{-\infty}^{t_1} dt_o\, \gamma_1\, e^{-\gamma_1(t_1 - t_o)} = 1$, the following result is obtained:

III.63) $$\rho^{(3)}_{12}(\vec{x},\vec{v},t;1) = \left(\frac{i}{\hbar}\right)^3 \int_{-\infty}^{t} dt_3 \int_{-\infty}^{t_3} dt_2 \int_{-\infty}^{t_2} dt_1 \; e^{-(\gamma_{12}-i\omega_{21})(t-t_3)}$$

$$\times \Big[V'_{12}(t_3)\, e^{-\gamma_1(t_3-t_2)} V'_{13}(t_2) \big(e^{-(\gamma_{13}+i\omega_{31})(t_2-t_1)} + \text{c.c.} \big) V'_{13}(t_1)$$

$$+ V'_{13}(t_3)\, e^{-(\gamma_{23}+i\omega_{32})(t_3-t_2)} V'_{12}(t_2)\, e^{-(\gamma_{13}+i\omega_{31})(t_2-t_1)}$$

$$\times V'_{13}(t_1) + V'_{13}(t_3)\, e^{-(\gamma_{23}+i\omega_{32})(t_3-t_2)} V'_{13}(t_2)$$

$$\times e^{-(\gamma_{12}-i\omega_{21})(t_2-t_1)} V'_{12}(t_1) \Big]$$

A change of variables will simplify the integration limits in (III.63). Let

III.64)

a) $\tau_3 = t - t_3$; t const. ; $d\tau_3 = -dt_3$

b) $\tau_2 = t_3 - t_2$; t_3 const. ; $d\tau_2 = -dt_2$

c) $\tau_1 = t_2 - t_1$; t_2 const. ; $d\tau_1 = -dt_1$

III.65)

a) $t - t_3 = \tau_3$; $t_3 = t - \tau_3$

b) $t - t_2 = \tau_3 + \tau_2$; $t_2 = t - (\tau_2 + \tau_3)$

c) $t - t_1 = \tau_3 + \tau_2 + \tau_1$; $t_1 = t - (\tau_1 + \tau_2 + \tau_3)$

Using the substitutions (III.64) and (III.65), (III.63) takes the form:

$$\text{III.66)}\quad \rho_{12}^{(3)}(\vec{x},\vec{v},t;1) = \left(\frac{i}{\hbar}\right)^3 \int_0^\infty d\tau_3 \int_0^\infty d\tau_2 \int_0^\infty d\tau_1\, e^{-(\gamma_{12}-i\omega_{21})\tau_3}$$
$$\times \Big[V_{12}'(t-\tau_3)\, e^{-\gamma_1\tau_2} V_{13}'(t-\tau_2-\tau_3)\left(e^{-(\gamma_{13}+i\omega_{31})\tau_1} + \text{c.c.}\right) *$$
$$* V_{13}'(t-\tau_1-\tau_2-\tau_3) + V_{13}'(t-\tau_3)\, e^{-(\gamma_{23}+i\omega_{32})\tau_2} *$$
$$* V_{12}'(t-\tau_2-\tau_3)\, e^{-(\gamma_{13}+i\omega_{31})\tau_1} V_{13}'(t-\tau_1-\tau_2-\tau_3)$$
$$+ V_{13}'(t-\tau_3)\, e^{-(\gamma_{23}+i\omega_{32})\tau_2} V_{13}'(t-\tau_2-\tau_3) *$$
$$* e^{-(\gamma_{12}-i\omega_{21})\tau_1} V_{12}'(t-\tau_1-\tau_2-\tau_3)\Big]$$

III.67) $\rho_{13}^{(3)}$ same form as $\rho_{12}^{(3)}$: $3 \leftrightarrow 2$

An examination of Eq. (III.66) shows that V_{12} appears linearly in each term so that the resonant part of ρ_{12} will be $\propto e^{i\omega t}$. It is assumed that $\vec{E}_2$ does not interact with the polarization $\vec{P}_{12}$ either because $\omega_{32}/\gamma >> 1$ and ω,ω' near resonance, or because

$\hat{e}_2 \cdot \vec{\mu}_{12} = 0$. When the time average of $\vec{P}_{12} \cdot \vec{E}_1$ is performed to find the absorbed power, only the first harmonic term in ω will survive. Thus, the only terms which need be retained in the integrand must be slowly varying in time t, except for the factor $e^{i\omega t}$. This will become clear below.

Substituting in the explicit potentials, the following somewhat complicated result is obtained:

III.68) $$\rho^{(3)}_{12}(\vec{x},\vec{v},t;1) = \left(\frac{-iE_2}{\hbar}\right)^3 \mu_{12}\mu_{13}^2 \int_0^\infty d\tau_3 \int_0^\infty d\tau_2 \int_0^\infty d\tau_1$$

$$\left[U(x-v_x\tau_3)U(x-v_x(\tau_2+\tau_3))U(x-v_x(\tau_1+\tau_2+\tau_3))\right] \times$$

$$\times \left[\text{same } (y,v_y)\right] e^{-(\gamma_{12}-i\omega_{21})\tau_3} \Big\{ \cos\left[\kappa(z-v_z\tau_3)\right.$$

$$\left. - \omega(t-\tau_3)\right] e^{-\gamma_1\tau_2} \cos\left[\kappa'(z-v_z(\tau_2+\tau_3))+\omega'(t-\tau_2-\tau_3)\right]$$

$$\left(e^{-(\gamma_{13}+i\omega_{31})\tau_1} + \text{c.c.}\right) \cos\left[\kappa'(z-v_z(\tau_1+\tau_2+\tau_3)) + \right.$$

$$\left. + \omega'(t-\tau_1-\tau_2-\tau_3)\right] + \cos\left[\kappa'(z-v_z\tau_3)+\omega'(t-\tau_3)\right] \times$$

$$e^{-(\gamma_{23}+i\omega_{32})\tau_2} \cos\left[\kappa(z-v_z(\tau_2+\tau_3))-\omega(t-\tau_2-\tau_3)\right] \times$$

$$e^{-(\gamma_{13}+i\omega_{31})\tau_1} \cos\left[\kappa'(z-v_z(\tau_1+\tau_2+\tau_3))\right. +$$

$$\left. + \omega'(t-\tau_1-\tau_2-\tau_3)\right] + \cos\left[\kappa'(z-v_z\tau_3)+\omega'(t-\tau_3)\right] \times$$

$$e^{-(\gamma_{23}+i\omega_{32})\tau_2} \cos\left[\kappa'(z-v_z(\tau_2+\tau_3))+\omega'(t-\tau_2-\tau_3)\right] \times$$

$$e^{-(\gamma_{12}-i\omega_{21})\tau_1} \cos\left[\kappa(z-v_z(\tau_1+\tau_2+\tau_3))-\omega(t-\tau_1-\tau_2-\tau_3)\right] \Big\}$$

By looking at the integrand in (III.68), one sees that the combination $\omega(t-\tau_3)$ appears in each term due to V'_{12}. Multiplying the bracketed { } terms is the factor $e^{i\omega_{21}\tau_3}$. Hence, the resonant results for the τ_3 integration (slowly varying in τ_3) must contain $e^{i\omega(t-\tau_3)}$. The complex conjugate will be anti-resonant and may be neglected. From each of the three products of three cosines, the following slowly varying (in τ_3) results proportional to $e^{i\omega t}$ are obtained.

III.69)

a) $$\frac{1}{8} e^{-i(K(z-v_z\tau_3)-\omega(t-\tau_3))}\left[e^{i(K'v_z\tau_1+\omega'\tau_1)} + c.c.\right]$$

$$+ 2^{nd} \text{ order in } \omega'$$

b) $$\frac{1}{8} e^{-i(K(z-v_z(\tau_2+\tau_3))-\omega(t-\tau_2-\tau_3))} \times \left[e^{i(K'v_z(\tau_1+\tau_2)+\omega'(\tau_1+\tau_2))} + c.c.\right]$$

c) $$\frac{1}{8} e^{-i(K(z-v_z(\tau_1+\tau_2+\tau_3))-\omega(t-\tau_1-\tau_2-\tau_3))} \times \left[e^{i(K'v_z\tau_2+\omega'\tau_2)} + c.c.\right]$$

The results (III.69) do not depend on the sign of ω'. All other terms give a rapidly varying integrand with respect to the τ_3 integral and vary as $\omega' t$. Substituting (III.69) for each of the three cosine products one obtains:

III.70) $$\rho_{12}^{(3)}(\vec{x},\vec{v},t;1) = \left(\frac{-iE_0}{2\hbar}\right)^3 \mu_{12}\mu_{13}^2\, e^{-i(kz-\omega t)} \times$$

$$\times \int_0^\infty d\tau_3 \int_0^\infty d\tau_2 \int_0^\infty d\tau_1 \left[U(x-v_x\tau_3)\cdots U(x-v_x(\tau_1+\tau_2+\tau_3))\right] \times$$

$$\times \left[\text{same}(y)\right] e^{-(\gamma_{12}-i\omega_{21}+i\omega)\tau_3} \Big\{ e^{-\gamma_1\tau_2}\left(e^{-(\gamma_{13}+i\omega_{31})\tau_1} + \text{c.c.}\right)$$

$$\times \left(e^{i(k'v_z\tau_1+\omega'\tau_1)} + \text{c.c.}\right) e^{ikv_z\tau_3} + e^{-(\gamma_{23}+i\omega_{32}+i\omega)\tau_3} \times$$

$$\times e^{-(\gamma_{13}+i\omega_{31})\tau_1}\left(e^{i(k'v_z(\tau_1+\tau_2)+\omega'(\tau_1+\tau_2))} + \text{c.c.}\right) e^{-ikv_z(\tau_2+\tau_3)}$$

$$+ e^{-(\gamma_{23}+i\omega_{32}+i\omega)\tau_2} e^{-(\gamma_{12}-i\omega_{21}+i\omega)\tau_1}\left(e^{i(k'v_z\tau_2+\omega'\tau_2)} + \text{c.c.}\right) \times$$

$$\times e^{ikv_z(\tau_1+\tau_2+\tau_3)} \Big\}$$

Using

III.71) $$\rho_{12}^{(3)}(\vec{x},t;1) = \int d^3\vec{v}\, N_1^{(0)}(\vec{v})\, \rho_{12}^{(3)}(\vec{x},\vec{v},t;1)$$

the V_z integration may now be done to considerably simplify (III.70). $N_1^{(0)}(\vec{v})$ is given as:

III.72) $$N_1^{(0)}(\vec{v}) = N^{(0)} \frac{e^{-(v_x^2+v_y^2+v_z^2)/u^2}}{(u\sqrt{\pi})^3}$$

Take $\Delta KV = (K' - K)V = \omega_{32} \frac{V}{c} << \gamma$, so that $K' \cong K$.

Consider an integral of the form

III.73) $$I(\tau) = \frac{1}{u\sqrt{\pi}} \int_{-\infty}^{\infty} dv_z \, e^{ikv_z\tau} e^{-v^2/u^2}$$

$$= e^{-k^2u^2\tau^2/4}$$

The terms in (III.70) will give $\tau = (\tau_3 \pm \tau_1)$, etc. These terms will be slowly varying in τ since the rapidly varying parts will be removed. Hence, the result (III.73) is sharply peaked in τ since $Ku >> \gamma$ (where γ is a typical collision or beam transit rate). Thus, one may take $I(\tau) \propto \delta(\tau)$ and integrate $I(\tau)$ to find the constant of proportionality.

III.74) $$\int_{-\infty}^{\infty} e^{-k^2u^2\tau^2/4} d\tau = \frac{2}{ku}\sqrt{\pi}$$

This gives

III.75) $$I(\tau) \cong \frac{2\sqrt{\pi}}{ku} \delta(\tau)$$

when $I(\tau)$ is used in integrals of the form $\int d\tau F(\tau) I(\tau)$, where $\frac{1}{Ku}\frac{dF}{d\tau} << F$, as in the above case. Now, a term with $\tau = \tau_3 - \tau_1$ will contribute whenever $\tau_3 = \tau_1$ while a term containing $(\tau_1 + \tau_3)$ contributes only for $\tau_1 = \tau_3 = 0$ since $\tau_i \geq 0$. Hence, contri-

butions of the latter type may be dropped by comparison to the former. The last term in the brackets { } of Eq. (III.70) may be excluded on this basis. Note that the result (III.75) does not depend on the sign of V_z due to the symmetric V_z integration. It is easily seen that in the first two terms of { } in (III.70), only the complex conjugate part of the KV_z factors need be retained, since these give $\delta(\tau_1 - \tau_3)$. Hence, one obtains

III.76) $$\rho_{12}^{(3)}(\vec{x},t;1) = N^{(0)}\left(\frac{-iE_0}{2\hbar}\right)^3 \mu_{12}\mu_{13}^2\, e^{-i(Kz-\omega t)}$$
$$\frac{2\sqrt{\pi}}{Ku}\int_{-\infty}^{\infty}dV_x\int_{-\infty}^{\infty}dV_y\ \frac{e^{-(V_x^2+V_y^2)/u^2}}{(u\sqrt{\pi})^2}\int_0^{\infty}d\tau_3\int_0^{\infty}d\tau_2\int_0^{\infty}d\tau_1$$
$$\times\left[U(x-V_x\tau_3)\cdots U(x-V_x(\tau_1+\tau_2+\tau_3)\right]\left[\text{same}(y)\right]$$
$$\times e^{-(\gamma_{12}-i\omega_{21}+i\omega)\tau_3}\Big\{e^{-\gamma_1\tau_2}\left(e^{-(\gamma_{13}+i\omega_{31})\tau_1}+\text{c.c.}\right)$$
$$\times e^{-i\omega'\tau_1}\delta(\tau_3-\tau_1) + e^{-(\gamma_{23}+i\omega_{32}+i\omega)\tau_2}\times$$
$$\times\ e^{-(\gamma_{13}+i\omega_{31})\tau_1}e^{-i\omega'(\tau_1+\tau_2)}\delta(\tau_3-\tau_1)\Big\}$$

Note that the ω' terms give some rapid variation, but these terms will be removed after the sign of ω' is chosen for co- and counter-

propagating waves. The τ_3 integral then gives $\tau_3 = \tau_1$ so that:

III.77) $$\rho_{12}^{(3)}(\vec{x},t;1) = N^{(0)}\left(\frac{-iE_0}{2\hbar}\right)^3 \mu_{12}\mu_{13}^2\, e^{-i(kz-\omega t)}$$
$$\times \frac{2\sqrt{\pi}}{ku}\int_0^\infty d\tau_2 \int_0^\infty d\tau_1\, I(x,\tau_1,\tau_2)\, I(y,\tau_1,\tau_2) \times$$
$$\times e^{-(\gamma_{12}-i(\omega_{21}-\omega))\tau_1}\Big\{e^{-\gamma_{13}\tau_2}\left(e^{-(\gamma_{13}+i\omega_{31})\tau_1} + \text{c.c.}\right)e^{-i\omega'\tau_1}$$
$$+ e^{-(\gamma_{23}+i\omega_{32}+i\omega)\tau_2} e^{-(\gamma_{13}+i\omega_{31})\tau_1} e^{-i\omega'(\tau_1+\tau_2)}\Big\}$$

where rapidly varying terms in τ are defined equal to zero.

III.78) $$I(x,\tau_1,\tau_2) = \int_{-\infty}^{\infty} \frac{dv_x}{u\sqrt{\pi}}\, e^{-v_x^2/u^2}\, U(x - v_x\tau_1) \times$$
$$\times U(x - v_x(\tau_1+\tau_2))\, U(x - v_x(\tau_2+2\tau_1))$$

and similarly for y.

Using Eq. (III.45c), the integral (III.78) is elementary and yields

III.79)

a) $$I(x,\tau_1,\tau_2) = \frac{e^{-x^2\left(3\alpha - \frac{\alpha^2 A^2}{\alpha B + 1/u^2}\right)}}{\sqrt{1+\alpha u^2 B}}$$

b) $$A = 4\tau_1 + 2\tau_2$$

c) $$B = 6\tau_1^2 + 6\tau_1\tau_2 + 2\tau_2^2$$

Eq. (III.77) may be rewritten as:

III.80)

a) $$\rho_{12}^{(3)}(\vec{x},t;1) = e^{-i(kz-\omega t)} N^{(0)} \frac{2\sqrt{\pi}}{ku}\left(\frac{-iE_0}{2\hbar}\right)^3 \mu_{13}^2 \mu_{12}$$

$$\times \int_0^\infty d\tau_2 \int_0^\infty d\tau_1 \; \frac{e^{-(x^2+y^2)\left(3\alpha - \frac{\alpha^2 A^2}{\alpha B + 1/u^2}\right)}}{1+\alpha u^2 B} F(\tau_1,\tau_2)$$

b) $$F(\tau_1,\tau_2) = e^{-(\gamma_{12}-i\omega_{21}+i\omega)\tau_1}\Big\{ e^{-\gamma_1\tau_2}\left(e^{-(\gamma_{13}+i\omega_{31})\tau_1} + c.c.\right) \times$$

$$\times e^{-i\omega'\tau_1} + e^{-(\gamma_{23}+i\omega_{32}+i\omega)\tau_2} e^{-(\gamma_{13}+i\omega_{31})\tau_1}$$

$$\times e^{-i\omega'(\tau_1+\tau_2)}\Big\}$$; (drop rapidly varying terms below)

The average power absorbed per unit length is given by

III.81) $$\bar{P}_{/L} = \frac{1}{L}\int_0^L dz \int_{-\infty}^{\infty} dx \int_{-\infty}^{\infty} dy \; \overline{\left(\dot{\vec{P}}_{0L} \cdot \vec{E}\right)}$$

where the bar over $(\dot{\vec{P}} \cdot \vec{E})$ denotes a time average and where $L >> \lambda, \lambda_{mfp}$ but $L \frac{\delta E_0}{\delta_Z} << E_0$.

The power density absorbed due to $\vec{P}_{12}$ and $\vec{E}_1$ is $\dot{\vec{P}}_{12} \cdot \vec{E}_1$

where

III.82) $$\dot{\vec{P}}_{12} = \mu_{12}\dot{\rho}_{21} + \mu_{21}\dot{\rho}_{12}$$

and

III.83) $$\vec{E}_1 = \hat{e}_1 E_0 e^{-\alpha(x^2+y^2)} \frac{1}{2}\left(e^{+i(kz-\omega t)} + c.c.\right)$$

Written explicitly this is

III.84) $$\bar{P}_{/L}^{(1,2)} = \frac{1}{L}\int_0^L dz \frac{1}{T}\int_0^T dt \; \frac{e^{i(kz-\omega t)} + c.c.}{2} E_0$$

$$\times \int_{-\infty}^{\infty} dx \int_{-\infty}^{\infty} dy \left[i\omega e^{-i(kz-\omega t)} N^{(0)} \frac{2\sqrt{\pi}}{ku} \left(\frac{-iE_0}{2\hbar}\right)^3 \right.$$

$$\left. \mu_{13}^2 \mu_{12} \int_0^{\infty} d\tau_2 \int_0^{\infty} d\tau_1 \, F(\tau_1,\tau_2) \; \frac{e^{-(x^2+y^2)\left(4\alpha - \frac{\alpha^2 A^2}{\alpha B + 1/u^2}\right)}}{1+\alpha u^2 B} + c.c. \right]$$

Using $\frac{1}{T}\int_0^T dt\, e^{-i\omega t} e^{i\omega t} = 1$; $\frac{1}{L}\int_0^L dz\, e^{-ikz} e^{ikz} = 1$,

while all other terms average to zero, the absorbed power per unit length may be written as:

III.85) $$\bar{P}_{/L}^{(1,2)} = -2\left(\frac{\mu_{12}E_0}{2\hbar}\right)^2\left(\frac{\mu_{13}E_0}{2\hbar}\right)^2 \frac{\hbar\omega\sqrt{\pi}}{ku} N^{(0)}$$

$$\times \int_0^{\infty} d\tau_2 \int_0^{\infty} d\tau_1 \int_0^{\infty} 2\pi r\, dr \; \frac{e^{-r^2\left(4\alpha - \frac{\alpha^2 A^2}{\alpha B + 1/u^2}\right)}}{1+\alpha u^2 B} F(\tau_1,\tau_2)$$

$$+ \; c.c.$$

where $r^2 = x^2 + y^2$. Since the radial dependence is contained in the exponential only, the radial integral is elementary and (III.85) becomes:

$$\text{III.86)}\quad \bar{P}_{/L}^{(1,2)} = \frac{-\pi^{3/2}}{2\alpha}\left(\frac{\mu_{12}E_0}{2\hbar}\right)^2\left(\frac{\mu_{13}E_0}{2\hbar}\right)^2 \frac{\hbar\omega}{\kappa u} N_1^{(0)} \times \int_0^\infty d\tau_1 \int_0^\infty d\tau_2 \; \frac{F(\tau_1,\tau_2)}{1+\alpha u^2(2\tau_1^2+2\tau_1\tau_2+\tau_2^2)} + c.c.$$

where $F(\tau_1, \tau_2)$ is given by (III.80b)

For counter propagating waves, $\omega' > 0$ so that the resonant terms of $F(\tau_1, \tau_2)$ are

$$\text{III.87)}\quad F(\tau_1,\tau_2) = e^{-(\gamma_{12}-i\omega_{21}+i\omega)\tau_1} e^{-\gamma_1\tau_2} e^{-(\gamma_{13}-i\omega_{31}+i\omega')\tau_1}$$

(counter propagating waves)

For copropagating waves $\omega' < 0$, so let $\omega' \equiv -|\omega'| \equiv -\omega'$. Then, the resonant part of $F(\tau_1, \tau_2)$ is

$$\text{III.88)}\quad F(\tau_1,\tau_2) = e^{-(\gamma_{12}+\gamma_{13}+i(\omega-\omega_{21}+\omega_{31}-\omega'))\tau_1} \times \left(e^{-\gamma_1\tau_2} + e^{-(\gamma_{23}+i(\omega+\omega_{32}-\omega'))\tau_2}\right)$$

(copropagating waves)

The final results for the power absorbed per unit length on the 1-2 transition are given by

III.89) $$\bar{P}_{/L}^{(1,2)} = \frac{-\pi^{3/2}}{2\alpha}\left(\frac{\mu_{12}E_0}{2\hbar}\right)^2\left(\frac{\mu_{13}E_0}{2\hbar}\right)^2\frac{\hbar\omega}{\kappa u}N_1^{(0)} \times$$
$$\times \int_0^\infty d\tau_1 \int_0^\infty d\tau_2 \left\{ \frac{e^{-(\gamma_{12}+\gamma_{13}+i(\omega+\omega_{32}-\omega'))\tau_1}}{1+\alpha u^2(2\tau_1^2+2\tau_1\tau_2+\tau_2^2)} \times \right.$$
$$\left. \times \left(e^{-\gamma_1\tau_2} + e^{-(\gamma_{23}+i(\omega+\omega_{32}-\omega'))\tau_2}\right)\right\} + c.c.$$

(copropagating)

III.90) $$\bar{P}_{/L}^{(1,2)} = \frac{-\pi^{3/2}}{2\alpha}\left(\frac{\mu_{12}E_0}{2\hbar}\right)^2\left(\frac{\mu_{13}E_0}{2\hbar}\right)^2\frac{\hbar\omega}{\kappa u}N_1^{(0)} \times$$
$$\times \int_0^\infty d\tau_1 \int_0^\infty d\tau_2 \left\{ \frac{e^{-(\gamma_{12}+\gamma_{13}+i(\omega-\omega_{21}+\omega'-\omega_{31}))\tau_1}\, e^{-\gamma_1\tau_2}}{1+\alpha u^2(2\tau_1^2+2\tau_1\tau_2+\tau_2^2)}\right\}$$
$$+ c.c.$$

(counterpropagating)

By symmetry $\bar{P}_{/L}^{(13)}$ is of the same form but $2 \leftrightarrow 3$ and $\omega' \leftrightarrow \omega$ since $V_{12} \leftrightarrow V_{13}$. The resulting contribution (including the C.C. terms) is then equal to that of (III.89) and (III.90)

III.91) $$\bar{P}_{/L}^{(1,3)} = \bar{P}_{/L}^{(1,2)} \times \frac{\omega'}{\omega} = \bar{P}_{/L}^{(1,2)} \; ; \; \omega' \cong \omega$$

Note that (III.91) occurs due to the fact that only the resonant contribution to the absorbed power has been considered. The Doppler broadened contributions are not generally identical.

The lineshapes represented by Eqs. (III.89) and (III.90) may be calculated numerically by utilizing a two dimensional analogue of Simpson's rule. For copropagating waves, the lineshape will be given by

III.92) $$I(\Delta) \propto \int_0^\infty d\tau_1 \int_0^\infty d\tau_2 \frac{e^{-(\gamma_{12}+\gamma_{13})\tau_1}\left[e^{-\gamma_{12}\tau_2}\cos\Delta\tau_1 + e^{-\gamma_{23}\tau_2}\cos\Delta(\tau_1+\tau_2)\right]}{1+\alpha u^2(2\tau_1^2+2\tau_1\tau_2+\tau_2^2)}$$

where $\Delta = \omega+\omega_{32}-\omega'$

Defining $\gamma_{12}=\gamma_{13}=\gamma'$ and letting $x_1=\gamma'\tau_1$ and $x_2=\gamma'\tau_2$ gives

III.93) $$I(\Delta') \propto \int_0^\infty dx_1 \int_0^\infty dx_2 \frac{e^{-2x_1}\left[e^{-\frac{\gamma_{12}}{\gamma'}x_2}\cos\Delta' x_1 + e^{-\frac{\gamma_{23}}{\gamma'}x_2}\cos\Delta'(x_1+x_2)\right]}{\beta^2+2x_1^2+2x_1x_2+x_2^2}$$

where $\Delta' \equiv (\omega+\omega_{32}-\omega')/\gamma'$

and

III.94) $$\beta = \gamma'/\sqrt{\alpha u^2}$$

For counterpropagating waves,

III.95) $$I(\Delta') \propto \int_0^\infty dx_1 \int_0^\infty dx_2 \frac{e^{-2x_1} e^{-\frac{\gamma_1}{\gamma} x_2} \cos \Delta' x_1}{\beta^2 + 2x_1^2 + 2x_1 x_2 + x_2^2}$$

$$\text{where} \quad \Delta' = (\omega + \omega' - \omega_{21} - \omega_{31})/\gamma$$

The integrals are done numerically, and the resulting lineshapes are shown in Figs. 3.6 - 3.8. Figure 3.9 shows a plot of width versus $1/\beta$, for the counterpropagating case where $\gamma_1 = \gamma'$. The linewidth does not broaden as rapidly as one would expect using $\gamma_t \sim u/R$.[4] This effect is due to selection of low transverse velocity atoms which interact longer with the beam, thus enhancing their contribution. However, the number of atoms with radial velocity V_r is proportional to V_r, so there is a compromise between number and interaction time. Further information on transit time effects, including the variation of the lowest order power broadening contribution to the linewidth, are given in Ref. 4.

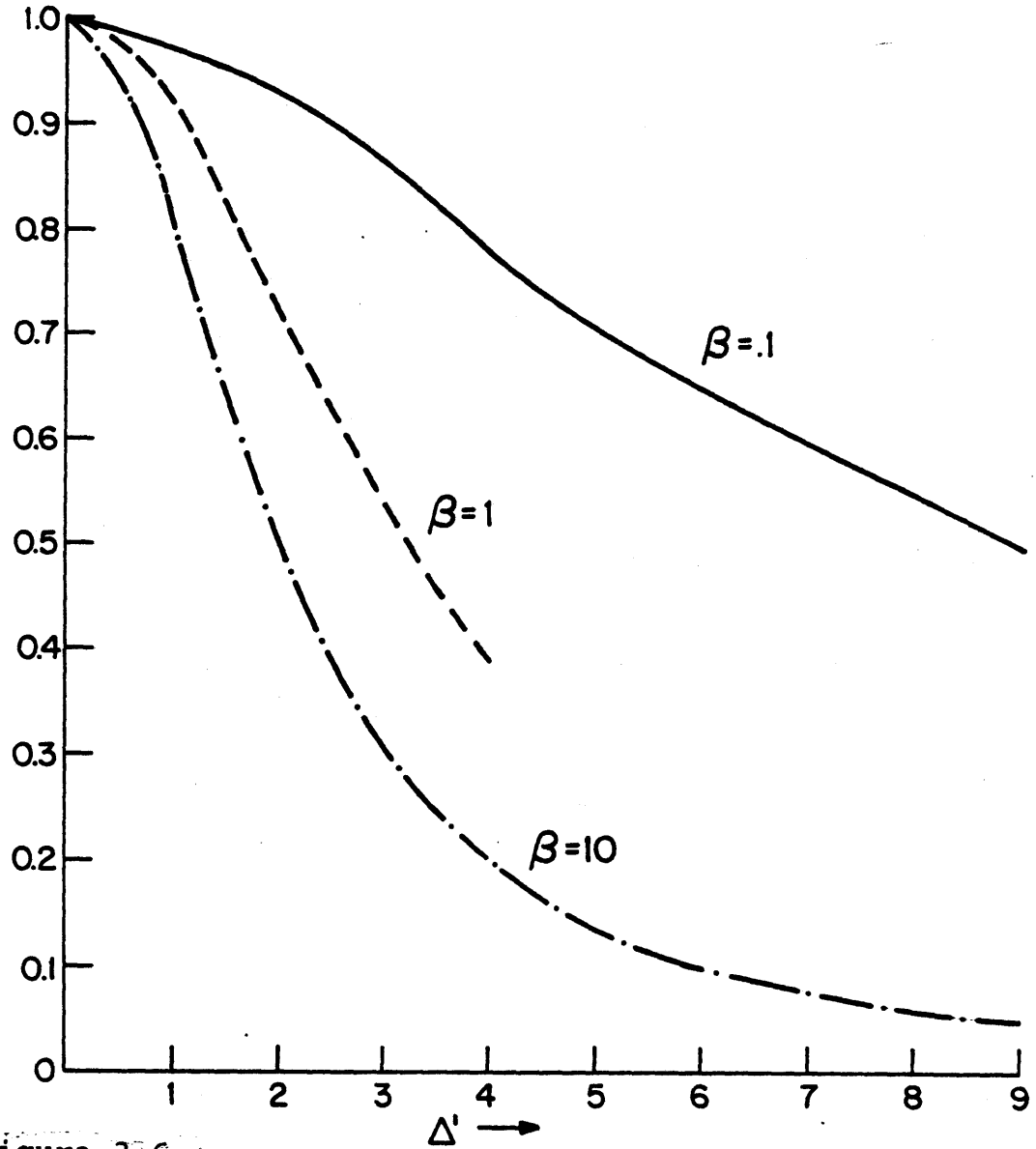

Figure 3.6 Counter Propagating Crossing Resonance Lineshape with Transit Time Broadening (Eq. III.95; $\gamma_1 = \gamma'$)

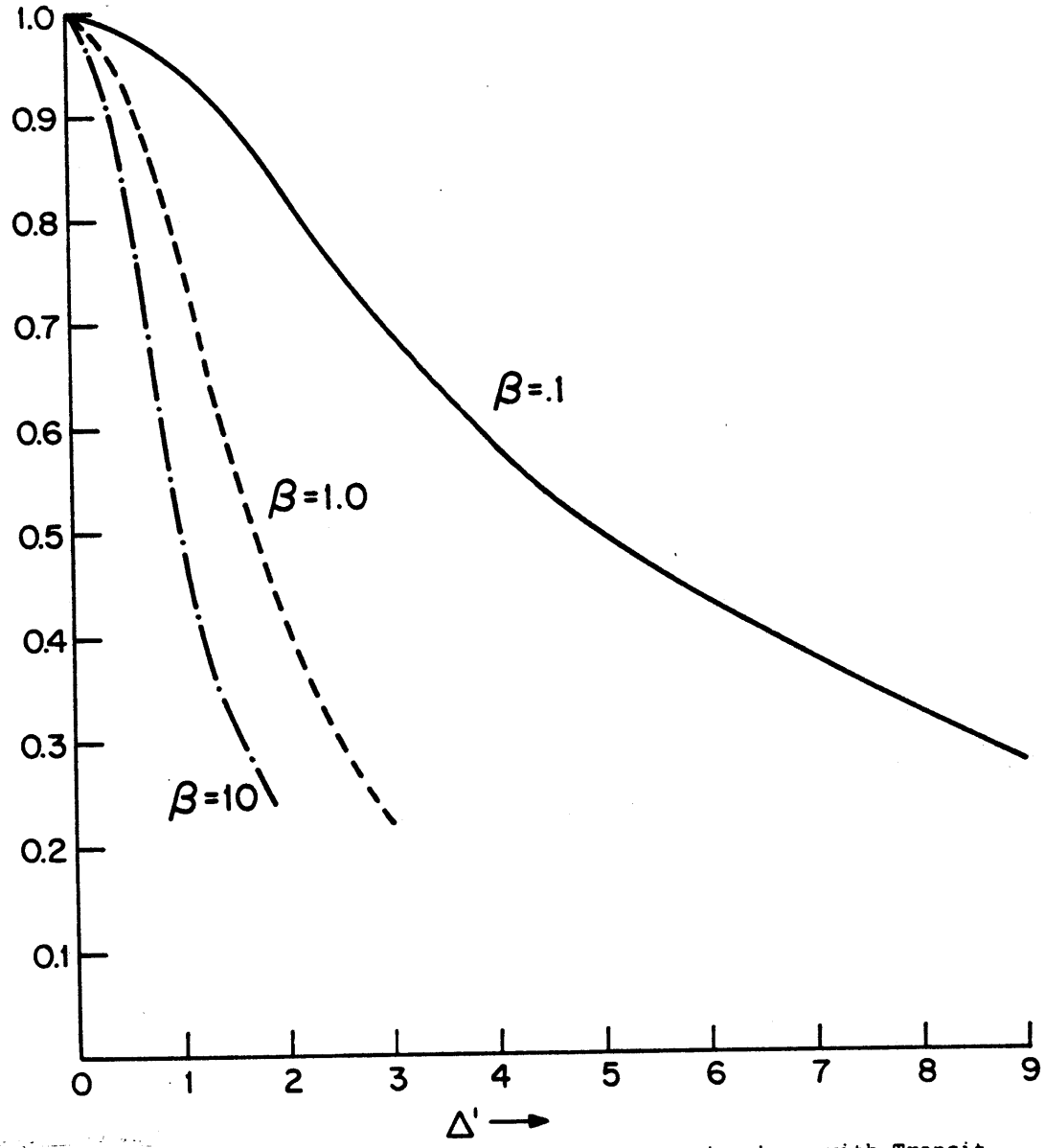

Figure 3.7 Copropagating Crossing Resonance Lineshape with Transit Time Broadening (Eq. III.93; $\gamma_1 = \gamma_{23} = \gamma'$)

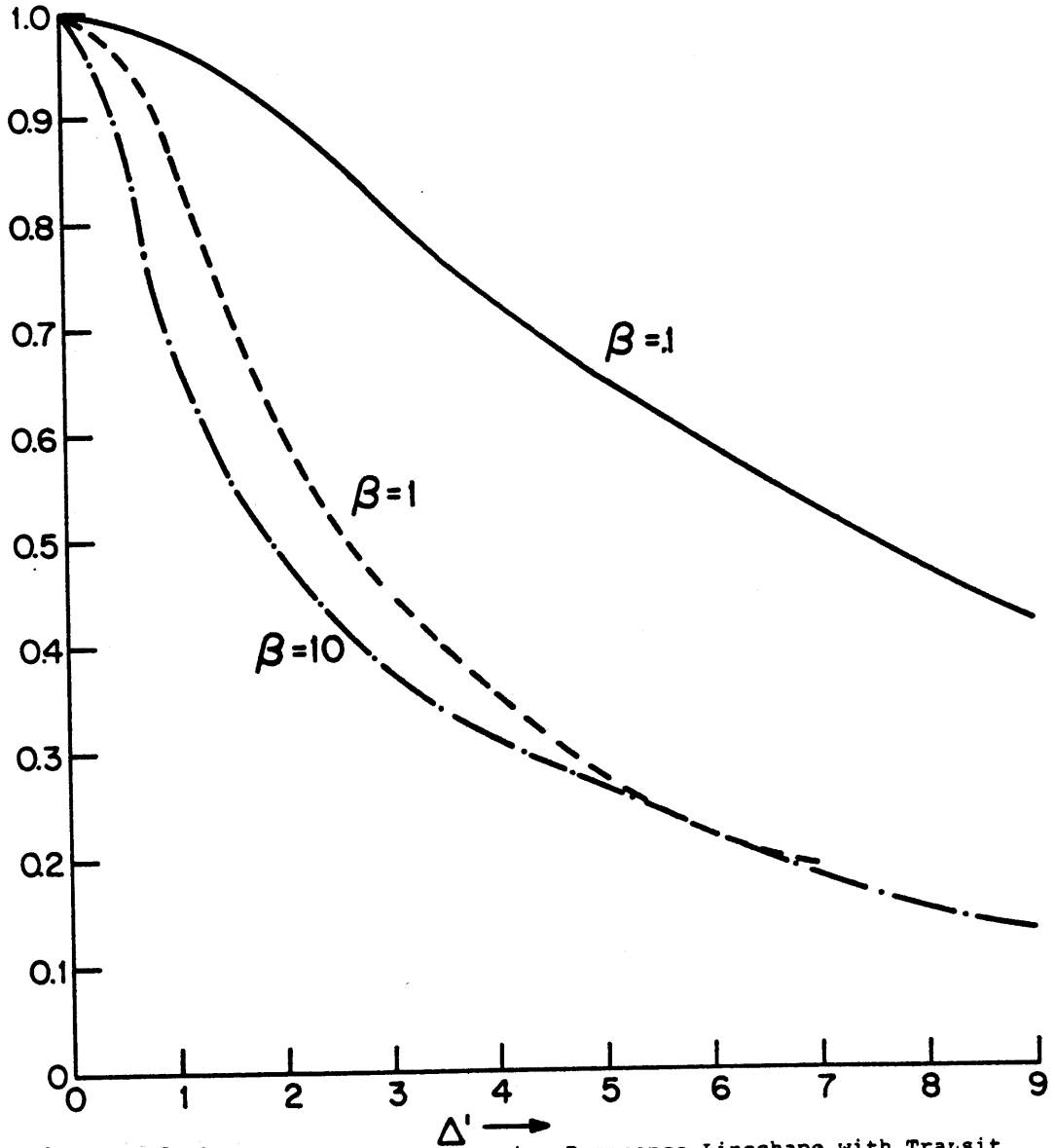

Figure 3.8 Copropagating Crossing Resonance Lineshape with Transit Time Broadening (Eq. III.92; $\gamma_1 = \gamma_{23} = \gamma'$; $\gamma_{12} = \gamma_{13} = 2\gamma'$)

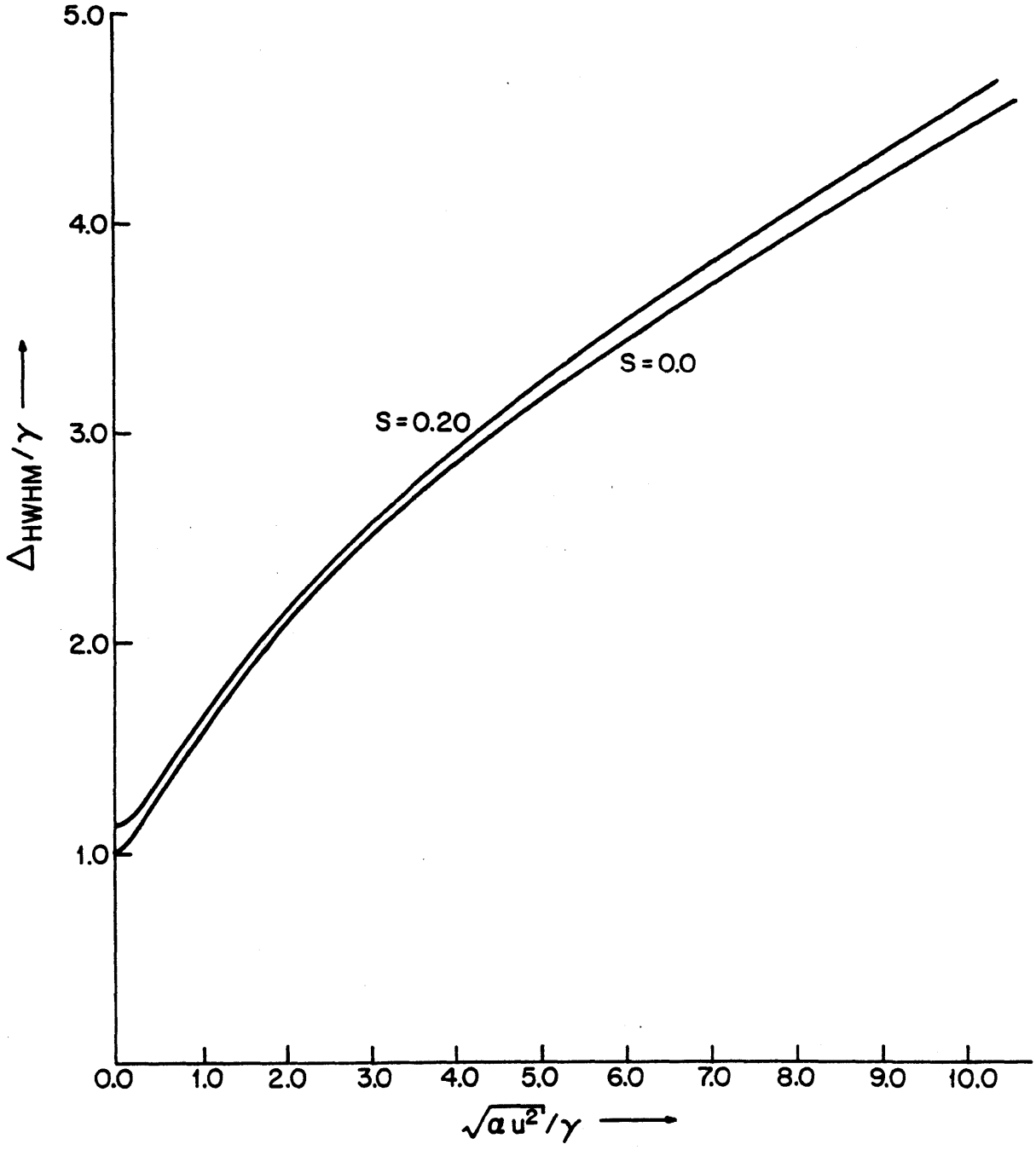

Figure 3.9 Transit Time Broadening of the Width for a Two Level System Standing Wave Saturation Resonance( )

The S = 0.0 curve is equivalent to that obtained for the counterpropagating resonance (Eq. III.95; $\gamma_1 = \gamma'$). The S = 0.2 curve shows the effect of power broadening. See Ref. ( ).

References

1. M. J. Kelly, Ph.D. Thesis, M.I.T., 1976, (unpublished).

2. Neglect of spatial harmonics is equivalent to the rate equation approximation in this case. For a complete treatment of the two level-standing wave problem, see B. J. Feldman and M. S. Feld, Phys. Rev. A1, 1375 (1970).

3. A treatment of the M degeneracy effect when M changing collisions are neglected is given in Ref. 1.

4. J. E. Thomas, M. J. Kelly, J.-P. Monchalin, N. A. Kurnit, and A. Javan, Phys. Rev. A15, 2356 (1977).

CHAPTER IV

STABILIZED TWIN LASER SPECTROMETER

A schematic of the spectrometer is shown in Fig. 4.1. Basically, the system consists of a pair of stable N_2O (or CO_2) lasers where both beams are sent copropagating into an absorbing gas sample. Crossing resonance signals may be observed either by monitoring the direct absorption of one or both of the laser fields (for ground state absorbers), or by monitoring the fluorescence emitted on a coupled transition as is useful for excited state absorbers. The fluorescence technique[1] lends itself very well to copropagating wave spectroscopy since there is no need to separate a weak probe beam from a strong pump beam as is required for signal to noise reasons in ground state absorbers. Furthermore, the fluorescence technique allows one to utilize arbitrary intensity ratios for the two laser fields as well as arbitrary polarizations with no loss in signal to noise ratio.

Copropagating wave spectroscopy has a number of advantages over counterpropagating wave spectroscopy. From a theoretical standpoint, the copropagating crossing resonance is generally larger and narrower than its counterpropagating equivalent. This is particularly suitable for observing the hyperfine spectra of molecules with small splittings. Experimentally, copropagating

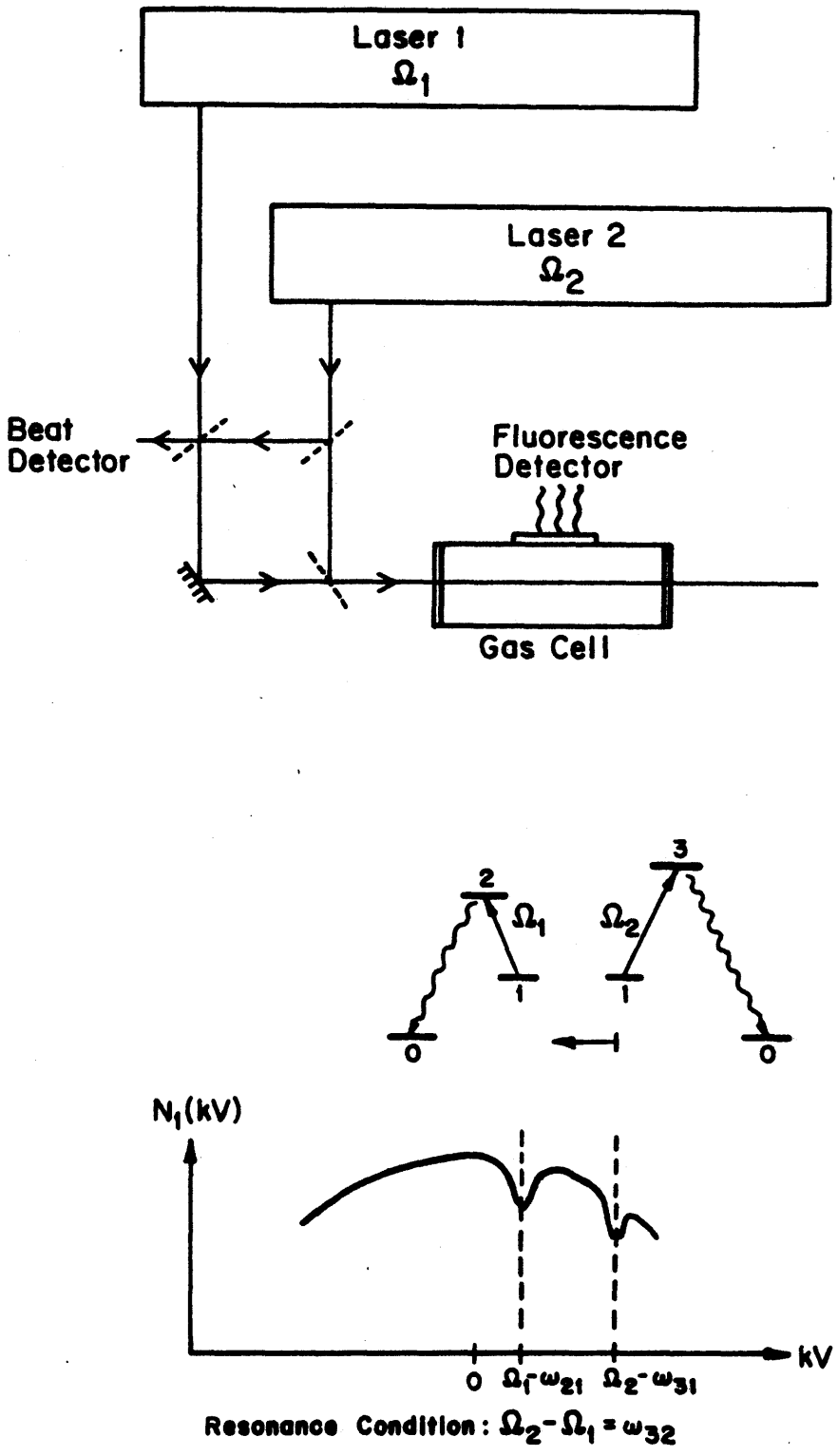

Figure 4.1. Schematic of Spectrometer and Crossing Resonance Technique. At resonance, laser 2 sees the hole bleached by laser 1 in the N_1 population and vice versa.

wave systems eliminate optical feedback entirely, regardless of the choice of laser polarizations. Thus, no beam misalignment is necessary which would broaden the resonances at a rate of $\sim$ 20kHz/mrad.[2] The frequency calibration is very simple for copropagating waves, since the crossing resonances depend only on the frequency difference between the two lasers and not on their absolute frequency (as long as $\omega_{32}\frac{v}{c} \ll \gamma$ as shown in Ch. II). Hence, the beat frequency between the two lasers provides an extremely accurate frequency scale. For stabilized operation, only one servo system is required, namely a system to control the difference frequency between the two lasers. This assumes that the absolute frequency of the lasers drifts sufficiently slowly that the power remains constant over the time required to sweep across the lineshape. In addition, the free running laser frequency jitter must be small over times comparable to the (natural linewidth)$^{-1}$ or collision time in molecules. These conditions are easily met in most cases, and in particular by the lasers utilized in the N_2O experiments.

A more detailed description of the spectrometer is shown in Fig. 4.2. Each of the laser beams is sent through an NaCl beam splitter and mixed in a fast CuGe detector to obtain a beat signal. This is used for both the frequency calibration and the servo system which stabilizes the difference frequency between the two lasers. Laser beam 1 is attenuated in a dimethyl

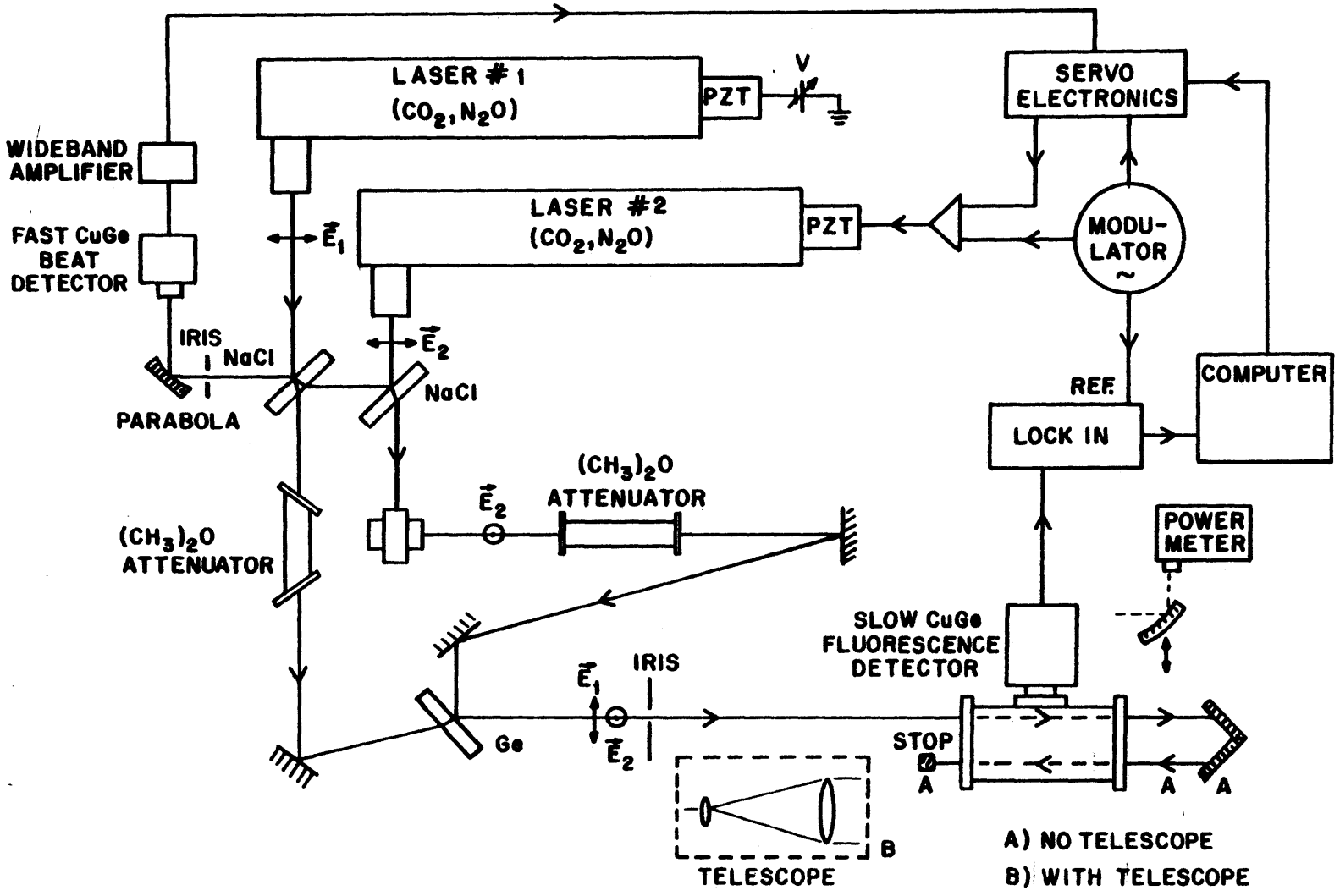

Figure 4.2. Twin Laser Spectrometer

ether absorption cell to obtain continuously adjustable intensity. The pressures are sufficiently high (10's of torr) that the response is flat over the scale of the sweep. Laser beam 2 is first flipped in polarization and then attenuated before mixing with beam 1 at the Germanium beam splitter. In order to obtain parallel propagation as well as perpendicular polarization careful attention is paid both to the beam alignment and to the methods by which the beams were raised and lowered, so as not to severely distort the linear polarizations. After mixing at the Ge beam splitter, the two copropagating beams are passed through the 3" diameter absorption cell three times (windows A.R. coated) to increase the fluorescence signal. The large cell diameter allows this to be done without any beam overlap. (The mean free path at the pressures used is small compared to the beam spacing which is $\sim$ 2.5 cm.) Fluorescence is observed via a slow CuGe detector and is sent to a PAR HR-8 lock-in amplifier for synchronous detection. A derivative detection system is chosen, both to eliminate the unwanted Doppler background and to enchance the weak but narrow hyperfine resonances with respect to the strong (and broad) zero beat resonance. Finally, the lock-in signal is sent to a minicomputer which is used to average the results of multiple sweeps to improve the signal to noise ratio.

Having given a brief description of the components of the

spectrometer, each element will now be discussed in detail. A description of the lasers will be given first.

1. Laser Design

In the following sections, a presentation of the mechanical and tube designs as well as the gas handling and electrical system designs will be given. Performance is discussed in the final section.

A. Optical

The resonator is a 1.6 m semiconfocal cavity consisting of a 3 meter radius of curvature mirror and a grating, as shown in Fig.4.3. The mirror is silver-coated and dielectrically enhanced for 10.6μ. The master grating has a groove density of 75 lines per mm and is suitable for both CO_2 (9, 10 μ) and N_2O (10 μ) operation. It is ruled on a copper substrate and is gold coated. Output coupling is via the zero order reflection and feedback is provided by the first order reflection. [See Ref. (3) for a discussion of the choice of groove density.] The grating assembly is designed to give a fixed output direction when rotated for wavelength selection as described in Ref. (3). An iris is provided at each end of the cavity to restrict the transverse modes. At the beam waist (grating) side the iris is set from 8-10 mm for an 11 mm tube diameter. The mirror end iris is adjustable and is set to give a good Gaussian beam profile.

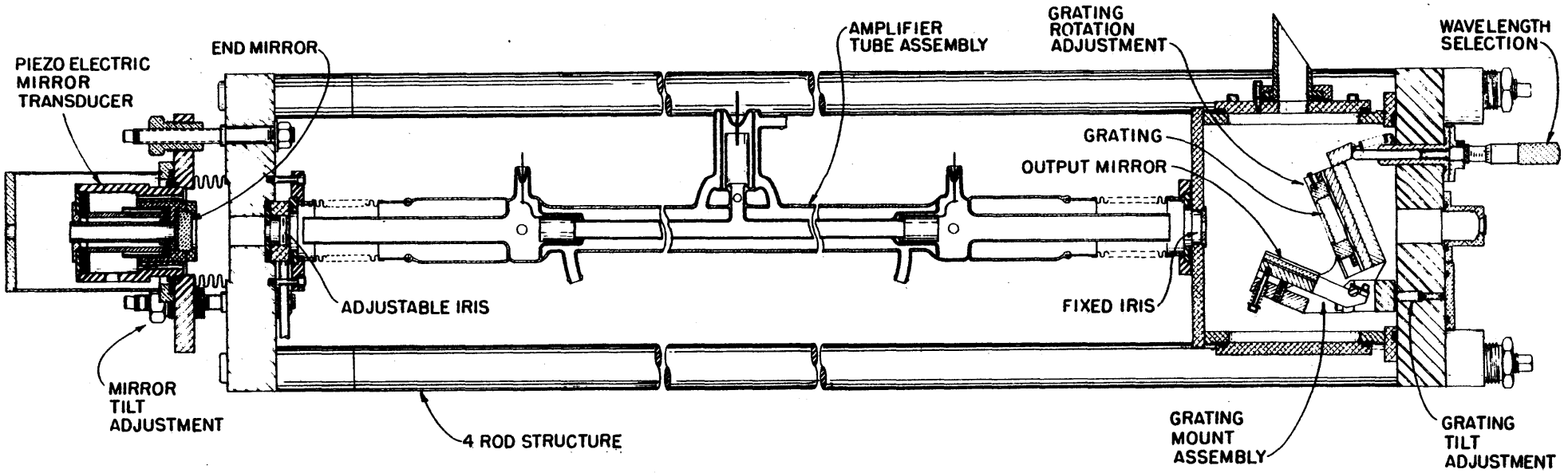

Figure 4.3. Laser Structure

B. Mechanical

A four rod structure is used to support the grating and mirror assemblies as shown in Fig.4.3. The rods are 1 1/8" diameter invar except for a short length of insulator which electrically isolates the two stainless steel endplates. Grating alignment is achieved by means of rotation and tilt provisions for the grating mount. Since crushed metal is not used in the tilt adjustments, a simple iterative procedure may be utilized to obtain accurate grating alignment with respect to the mechanical axis of the structure. Thus, this method greatly facilitates grating changes. Mirror alignment is done with the differential screw assembly.

A piezoelectrical mirror transducer (PZT) assembly is used for fine tuning of the laser, after the course tuning is done with the micrometer of the grating assembly. The PZT assembly consists of an aluminum piston-stainless steel cylinder arrangement which conducts heat away from the piezoelectric crystal to reduce thermal frequency drift. The aluminum piston retains the mirror by means of a cap and phosphor-bronze spring.

C. Tube Design

The laser amplifier tube is made of quartz and consists basically of an 11 mm inner bore and a water cooling jacket as shown in Fig.4.4. There are two platinum anodes each of which

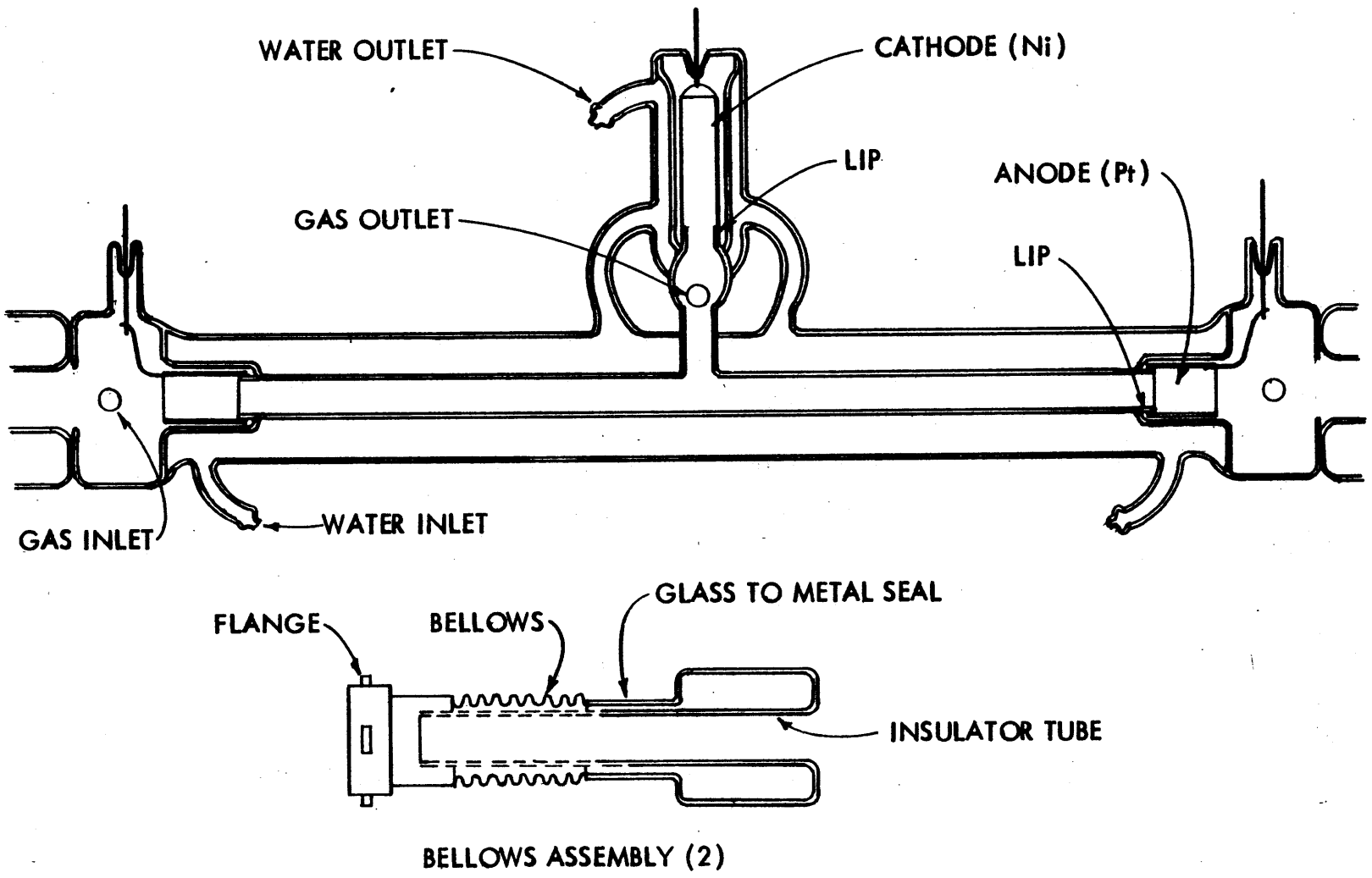

Figure 4.4. Tube Design

fits snugly around a lip protruding from the inner bore. The nickel cathode is located such that the cathode fall region and tube outlet are external to the central bore. This minimizes plasma instabilities within the amplifying region. The cathode also fits snugly around a lip so that instabilities due to the sharp ends of the cylindrical electrode are eliminated. Two gas inlets and a central outlet are provided to achieve a uniform gas flow throughout the gain region. An insulating quartz tube runs the length of each bellows assembly to prevent arcing to the laser end plates.

D. Gas Handling System

A slow flow gas handling system is utilized to obtain both CO_2 and N_2O laser capability. In addition, such a system avoids the complexities and cost inherent in sealed off operation. The system shown in Fig.4.5 allows a simple conversion between CO_2 and N_2O gas mixtures by means of the valves 1-5 and the mixture metering valves. The mixture ratios are given in Table IV.1. An N_2O laser plasma requires extreme cleanliness for good stability in contradistinction to the CO_2 plasma which is well behaved. For this reason, no grease is used in the rubber o-ring seals throughout the laser. For N_2O laser operation, a set of filters is utilized to eliminate the formation of a brownish deposit in the amplifier tube. Apparently, the deposit results from an

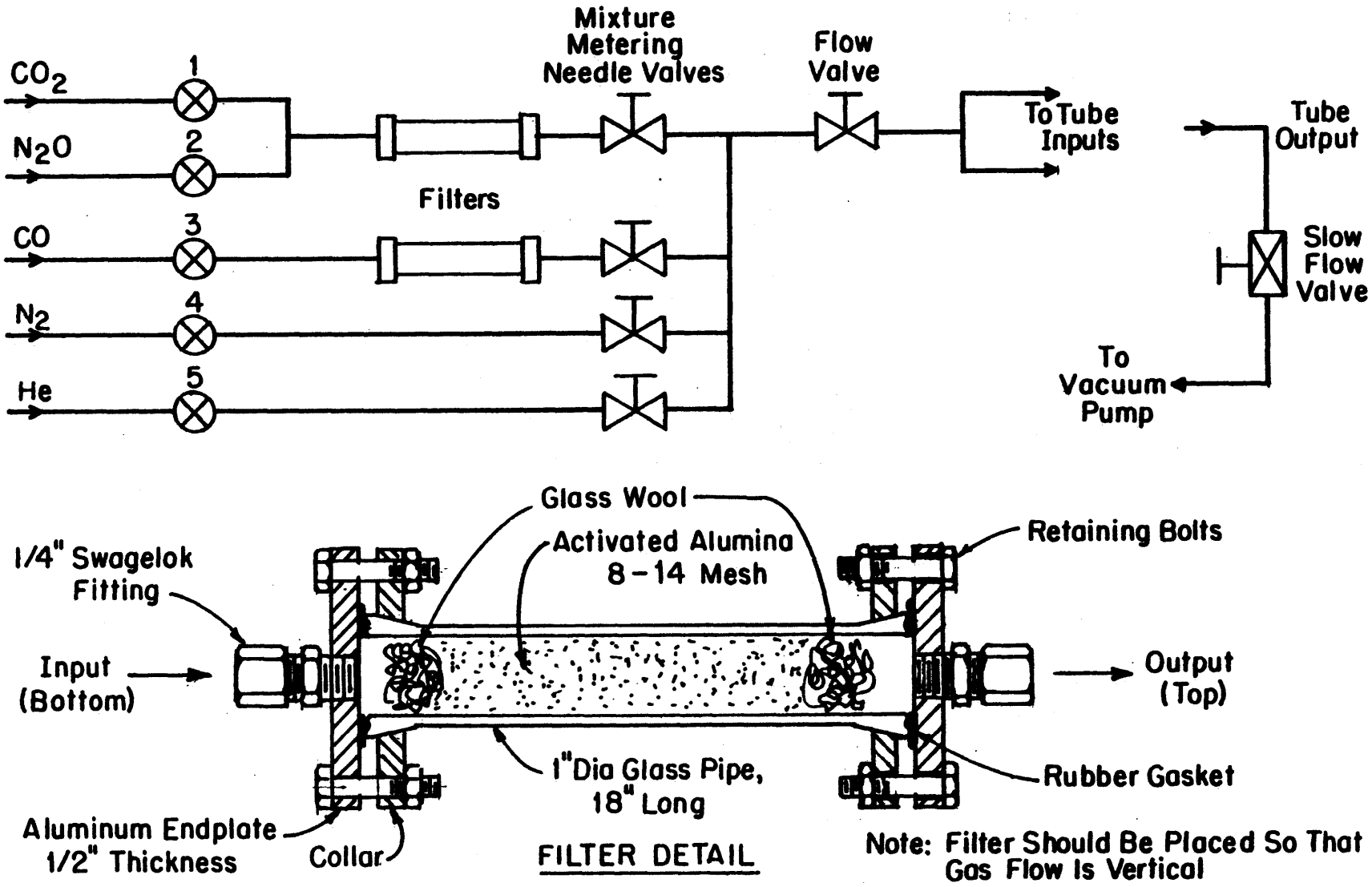

Figure 4.5. Gas Handling System

TABLE IV.1

Mixture Ratios

Partial pressures for CO_2 operation:
(set with flow valve fully open)

CO_2	: 4.0	torr
N_2	: 1.5	torr
He	: 4.5	torr
	10.0	torr

Flow pressure ∿5.5 - 6.0 torr

Partial pressures for N_2O operation:
(set with flow valve fully open)

N_2O	: 0.6	torr
CO	: 0.9	torr
N_2	: 2.9	torr
He	: 5.6	torr
	10.0	torr

Flow pressure ∿6.5 - 7.5 torr

impurity formed by the interaction of the CO with the storage gas cylinder walls over a long period of time.

During operation, the slow flow valve is opened to exhaust the amplifier tube and then the flow valve is opened until the appropriate total pressure is obtained at equilibrium.

E. Electrical System

In the interest of safety, a capacitive power supply ground and a fully grounded laser structure is utilized instead of a floating laser structure. (See Fig.4.6) (The power supply housings are grounded.) One end of the laser is permanently grounded and the other end is grounded via a knife switch after a stable discharge is established. A tesla coil is used to facilitate the starting procedure. The lower (2kv) power supply voltage is chosen to establish a virtual ground at the anodes after a stable discharge is obtained. The (A.C.) capacitive ground between the two power supplies effectively eliminates 60 cycle pickup which would otherwise cause power supply instability. This method is adequate for most purposes as discussed below (see Performance). The H.V. connectors provide a simple means of obtaining appropriate ballast resistance for either CO_2 or N_2O operation. Suitable power supplies must have low voltage drift (.01%/hour) and low ripple (2mv p-p) for best performance.

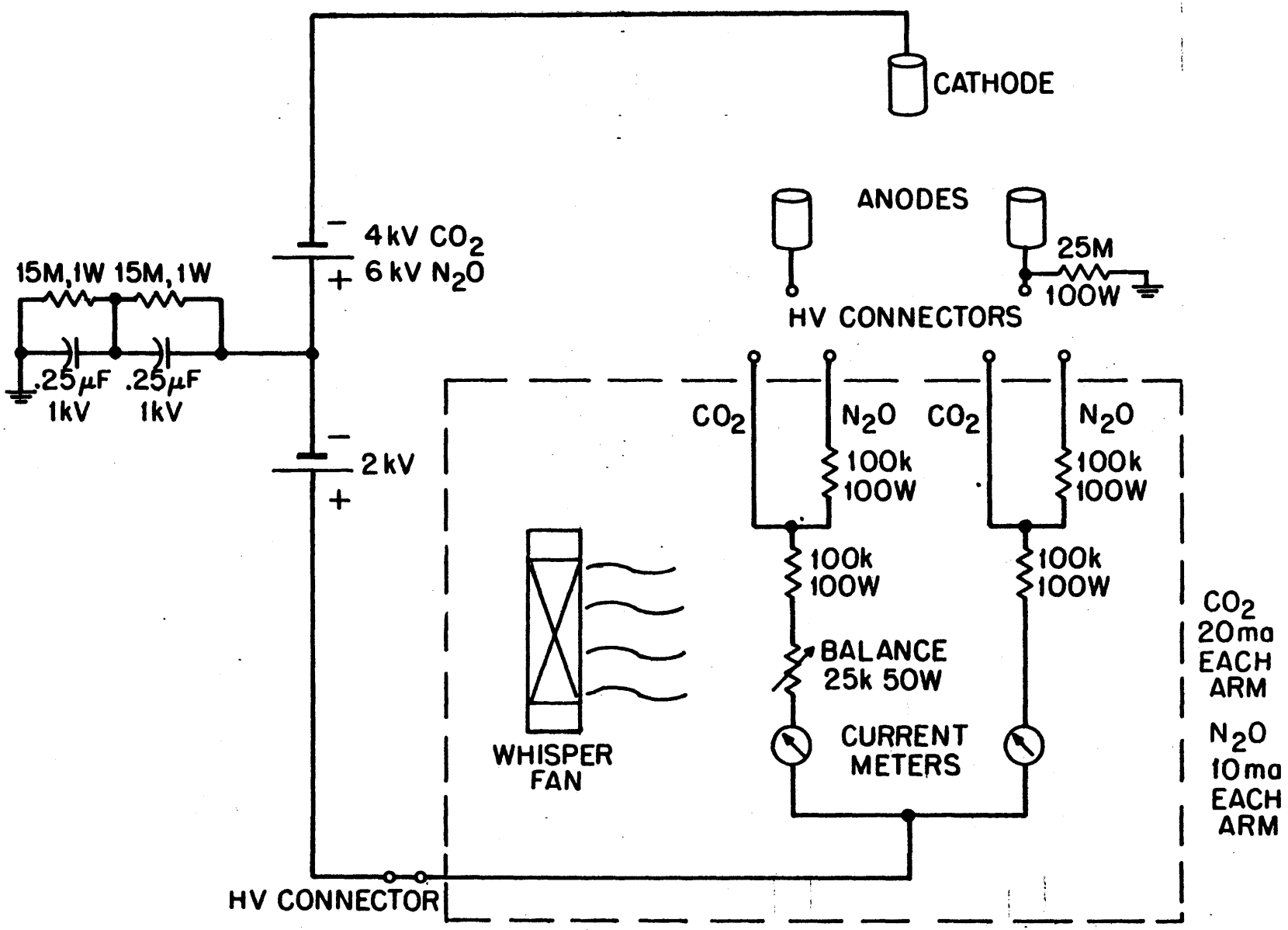

Figure 4.6. Electrical System

F. Performance

A spectrum analysis of the beat note between two free-running CO_2 lasers is shown in Fig.4.7. Typical free running jitter is 5 kHz for CO_2 and 8 kHz for N_2O. The intensity jitter is 1/100 of 1% and consists mainly of a 60 cycle signal which is primarily due to residual power supply instability resulting from the capacitive grounding (A.C.) technique. While improvement can be obtained by floating the laser structure and fully grounding (D.C.) the power supplies, the above stability is suitable for most applications. Frequency offset locking of CO_2 lasers may be achieved with a servo system. The beat note spectrum (500 kHz beat note) for two offset locked CO_2 lasers is shown in Fig.4.8 As can be seen from the figure, the jitter is less than 200 Hz. Similar results are attainable with N_2O lasers. The laser design has been oriented toward high frequency stability and wide tunability (i.e. low output coupling to obtain as many rotational vibrational transitions as possible). Nevertheless, the power output on a strong CO_2 line is $\sim$13 watts, and the output on a strong N_2O line is $\sim$4 watts.

2. Detectors

The beat detector design and circuitry is shown in Fig.4.9 This consists of a fast He-cooled 3mm x 3mm CuGe crystal which exhibits a resistance change when irradiated with the 10μ laser

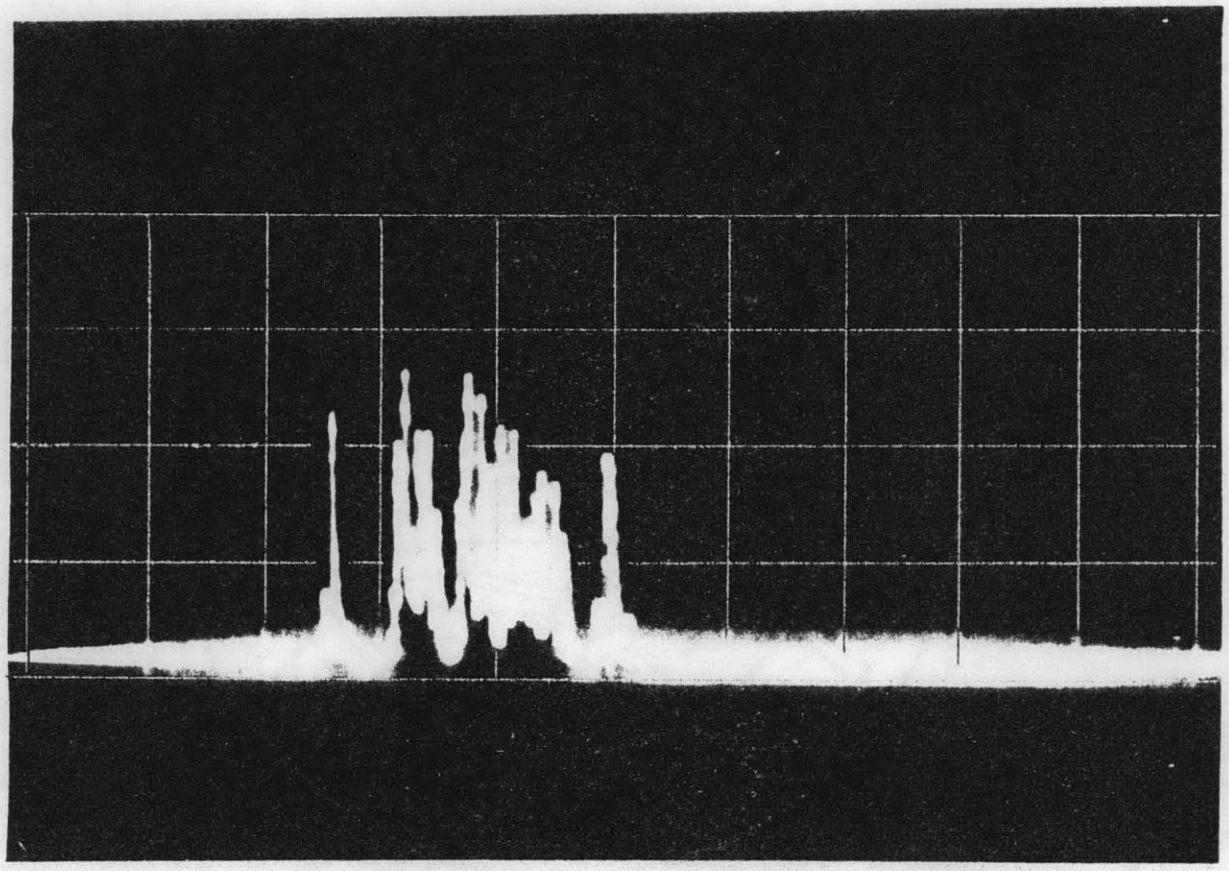

Figure 4.7 Free Running Beat Frequency Spectrum at 500 kHz (2kHz/cm; τ = 50 ms/cm)

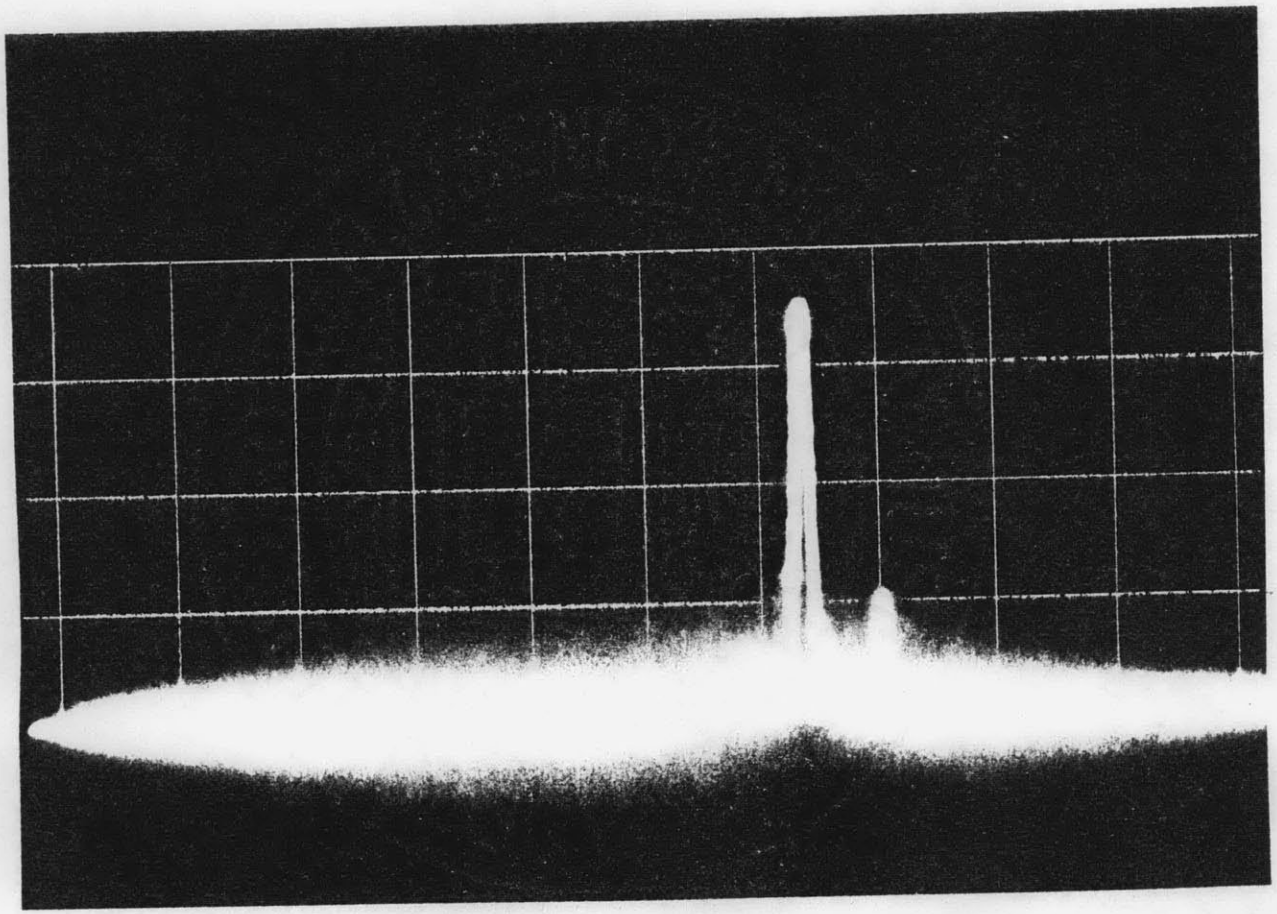

Figure 4.8. Locked Beat Frequency Spectrum at 600 kHz (1 kHz/cm; τ = .1 s/cm)
Note: Outer loop time constant = .01 sec; see Ch.V.

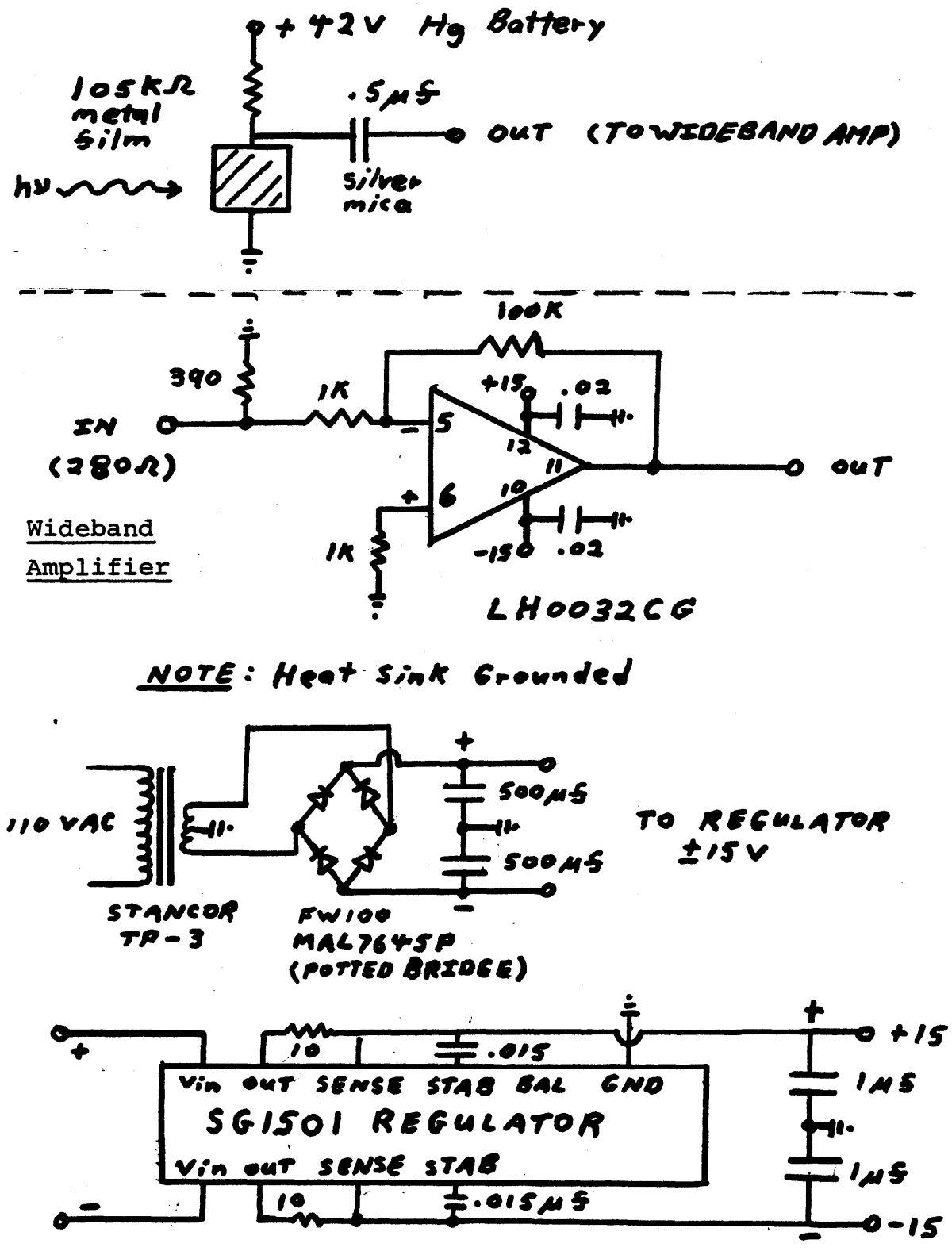

Figure 4.9. Beat Frequency Detector and Wideband Amplifier

radiation. The crystal is biased with a 105 kΩ metal film resistor and a 42 volt mercury battery. The output is the a.c. voltage across the crystal transmitted through the capacitor. If the amplitude of the output voltage is plotted versus beat frequency for a high impedence load, the resulting plot is sharply peaked at low frequencies, (so long as $\frac{1}{\omega C} << R_{load}$) and falls off rapidly at high frequencies $\gtrsim$ 500 kHz. This situation is remedied by placing a 300Ω load across the detector output and amplifying with a wideband amplifier. The amplifier is designed to give a gain of 100 and provides flat response out to ∿6 MHz where the gain rises slightly before descending near a frequency of ∿8 MHz. Since the operating range is $\lesssim$ 1 MHz, the amplifier is more than adequate. A circuit diagram is shown in Fig.4.9 It should be emphasized that the mechanical design of the amplifier requires extremely short lead lengths from the 300Ω load to the op-amp inputs as well as in the feedback circuitry. Futhermore, careful grounding of the heat sink is required to prevent oscillation. A ground plane is provided in the design. With the beat detector system as shown in Fig.4.9, typical signals range from 1.5 to 2.5 volts in amplitude for laser powers of ∿1 watt each and ∿1% coupling off of the NaCl beamsplitters. The frequency response is extremely flat over the 0-1 MHz range, and the noise is typically 5-10 mv.

The fluorescence detector and its circuitry are shown in

Fig.4.10. The biasing and output are similar to that of the beat detector, except that the crystal is not loaded down since a fixed 170 Hz modulation frequency is used for the derivative technique. The large area 20 mm x 20 mm slow CuGe crystal allows fluorescence to enter through a large solid angle. A 5 mm thick sapphire window on the cell is used to initially attenuate scattered 10μ radiation. The 4μ fluorescence passes through a 3 mm thickness of BaF_2 which forms the detector window and finally through a 4-4.5μ bandpass filter mounted directly on top of the CuGe crystal mount so that it is cooled to liquid He temperatures. The background black-body radiation is thus reduced to that of 4°K. The scattered 10μ radiation is eliminated.

3. Optics

The beam splitter assembly used to obtain the beat frequency signal is shown in Fig.4.11. The laser polarizations are parallel to the plane of incidence and the angle of incidence is ∿45°. The reflected laser intensity is then given by

IV.1) $$\frac{I_R}{I_o} = \left(\frac{\tan(i-r)}{\tan(i+r)}\right)^2$$

where

IV.2) $$\sin r = \frac{1}{N}\sin i = \frac{1}{N\sqrt{2}}$$

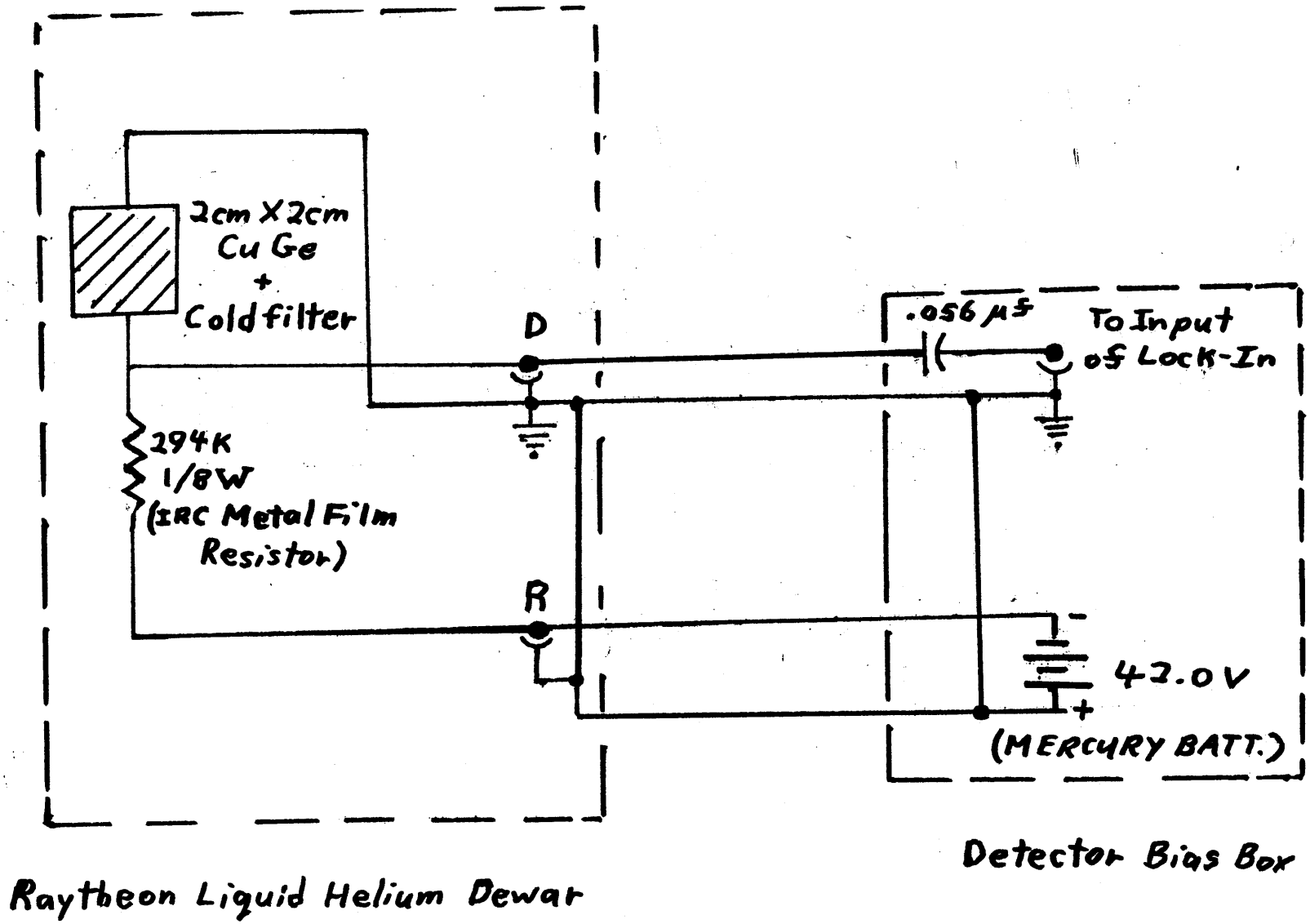

Figure 4.10. Slow CuGe Detector and Biasing Circuit

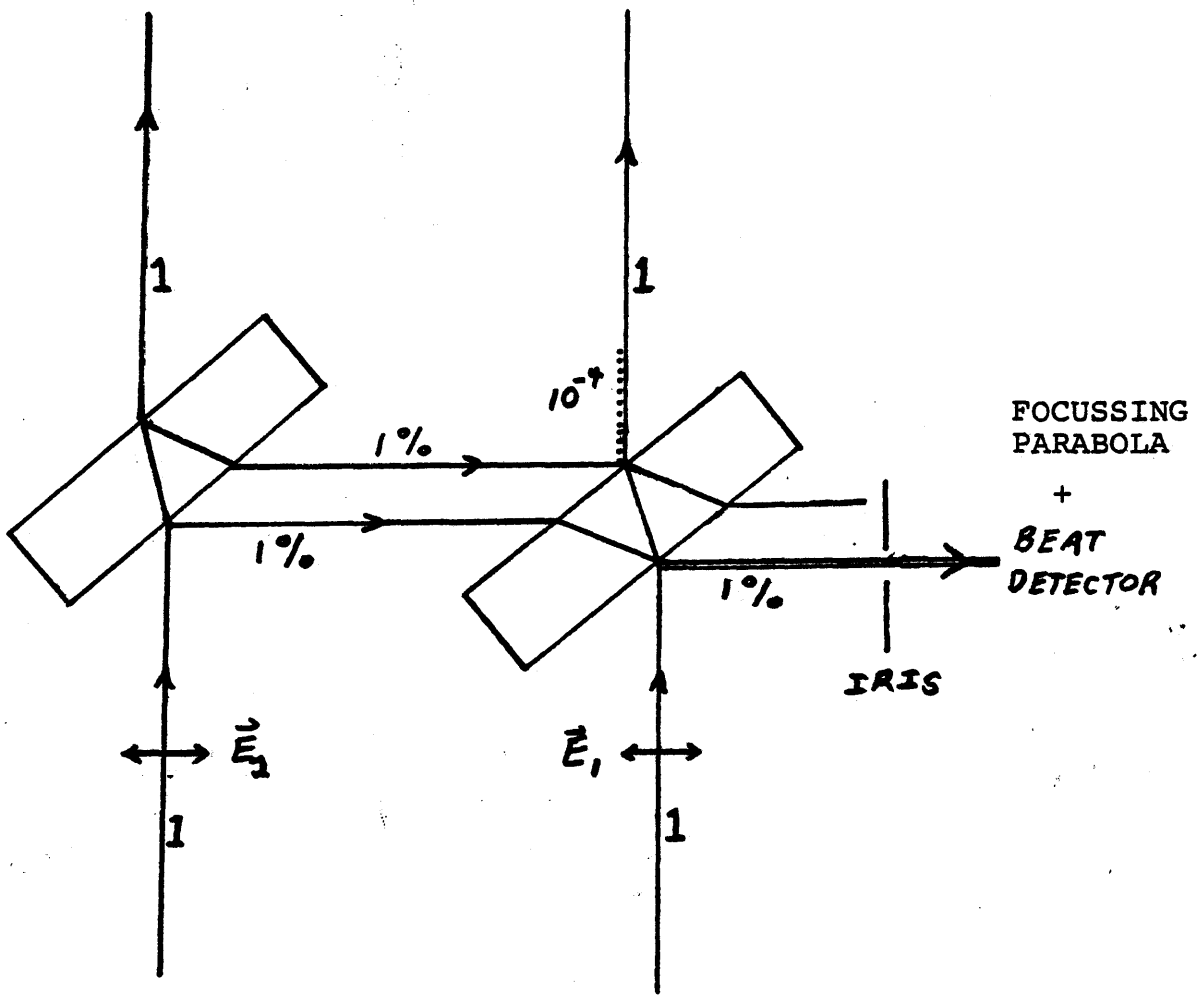

Figure 4.11. NaCl Beam Splitter Assembly for Detection of Laser Beat Frequency.

and $N \cong 1.49$ at $\lambda \cong 10\mu$ for NaCl.

Equations (IV.1) and (IV.2) yield $I_R/I_o \lesssim 1\%$, which is sufficient to obtain a good beat signal since this gives $\gtrsim 10$ mw from each laser when the laser power is $\gtrsim 1$ W. In addition, the small amount of power reflected in this polarization helps to limit optical coupling between the two lasers as a result of various reflections at the detector. The feedback will be $\sim(1\%)^2$ or $10^{-4}\ I_o$, and hence should be negligibly small. The alignment of the beat note optics is extremely critical since a small misalignment of the wave vectors will result in a phase averaging over dimensions comparable to the beam diameter. Since the CuGe crystal is an intensity detector, the detector signal is

IV.3) $$S \propto \frac{1}{2} Re\,(\vec{E}_1+\vec{E}_2)\cdot(\vec{E}_1+\vec{E}_2)^*$$

$$\propto \frac{|\vec{E}_1|^2+|\vec{E}_2|^2}{2} + \frac{\vec{E}_1\cdot\vec{E}_2^* + \vec{E}_2\cdot\vec{E}_1^*}{2}$$

where a time average has been performed over times large compared to the laser oscillation period but small compared to the detector response (beat frequency period). Using

IV.4)

a) $$\vec{E}_1 \sim Re\ \vec{E}_o\ e^{i(\vec{k}_1\cdot\vec{x}-\omega_1 t)}$$

b) $$\vec{E}_2 \sim Re\ \vec{E}_o\ e^{i(\vec{k}_2\cdot\vec{x}-\omega_2 t)}$$

The A.C. signal is then

IV.5) $S \propto I_0 \cos\left[(\vec{K}_1 - \vec{K}_2)\cdot\vec{x} - (\omega_1 - \omega_2)t\right]$

where it is assumed that each laser contributes equal intensities. For any fixed position, the signal varies in time as $(\omega_1 - \omega_2)t$. However, the phase varies as $(\vec{K}_1 - \vec{K}_2)\cdot\vec{X}$ when the position is varied. In general, $|\vec{X}|$ will vary over distances $d \sim 1$ cm, and $\vec{X}$ will not generally lie in a plane $\perp$ to $(\vec{K}_1 - \vec{K}_2)$ (<u>i.e.</u> a plane of constant phase). In order to avoid phase cancellation, it is necessary that

IV.6) $(\vec{K}_1 - \vec{K}_2)\cdot\hat{x}\, d \lesssim \pi$

Assuming that $\hat{X} \equiv \hat{e}_Z$ and taking $<K_1 X = \frac{\pi}{2} + \frac{\delta}{2}$ and $<K_2\ X = \frac{\pi}{2} - \frac{\delta}{2}$ so that both waves are nearly perpendicular to the detector plane, (IV.6) gives

IV.7) $\left(\sin\frac{\delta}{2} - \sin\frac{-\delta}{2}\right)\frac{2\pi}{\lambda}\, d \lesssim \pi$

or

IV.8) $\delta \lesssim \frac{\lambda}{2d}$

For $\lambda = 10\mu = 10^{-5}$ and $d = 10^{-2}$m, the beam alignment accuracy must be of order δ where

IV.9) $\delta \lesssim 0.5$ mrad

The Germanium beam splitter geometry is shown in Fig. 4.12. A slight wedge $\varepsilon \sim 1°$ is provided between the two surfaces of the Ge to allow elimination of unwanted reflections. Due to the limited size of the beamsplitter, it is not practical to use θ_i = Brewster's angle $\cong 76°$, for the L1 beam (polarized in the plane of incidence). Instead, $\theta_i \cong 45°$ is used. The output direction is to be along an optical rail, so the input direction with respect to the optical rail must be calculated roughly so that the input mirrors may be positioned. Once this is done, the Ge beamsplitter may be rotated slightly to obtain an output direction parallel to the optical rail. A final pair of adjustable mirrors is then used to obtain exact propagation of the beam along the optical rail as required for telescope operation.

From the geometry of Fig.4.12, the input angle with respect to the optical rail is given by

IV.10) $\alpha = \theta_o - \epsilon - \theta_i$

θ_o must be determined in terms of θ_i and ε. Using Snell's law at each boundary gives

IV.11)

a) $N \sin r = \sin \theta_i$

b) $N \sin(r+\epsilon) = \sin\theta_o \Rightarrow N\sin r + \epsilon N \cos r \cong \sin\theta_o$

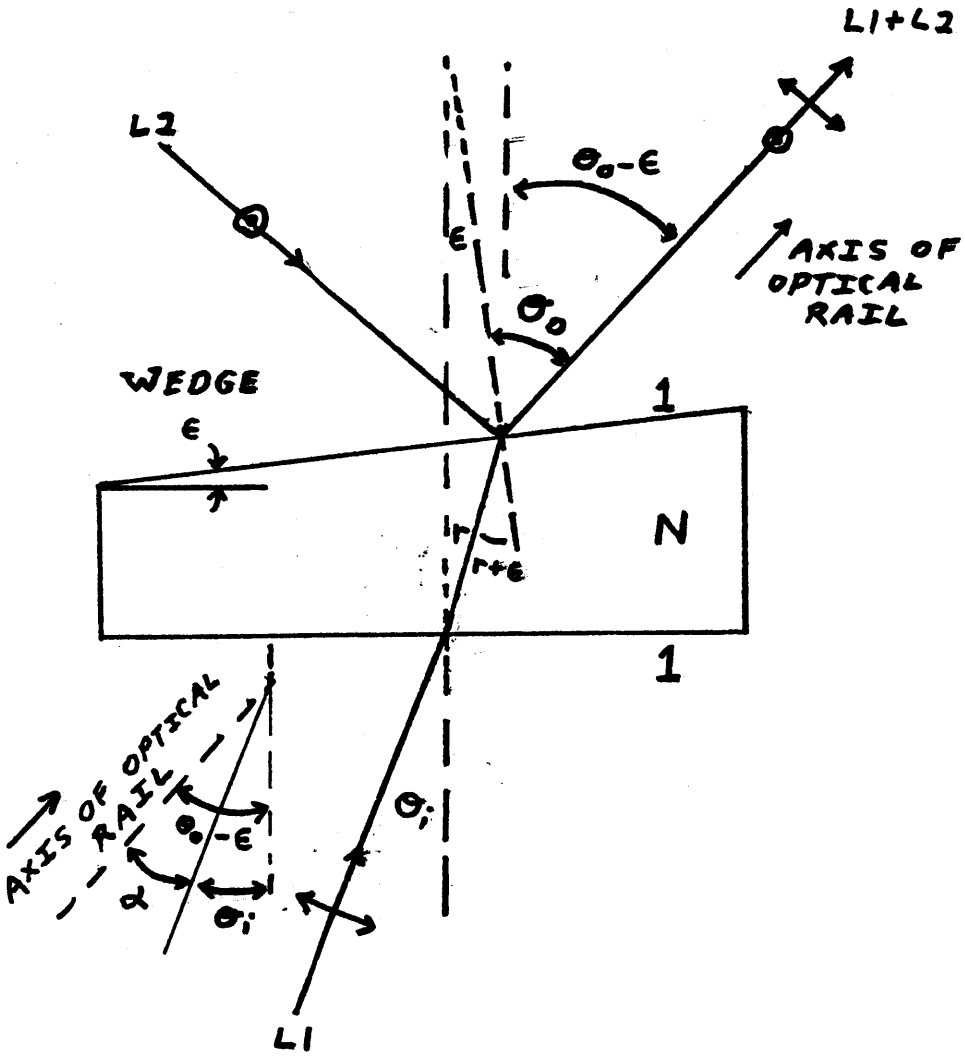

Figure 4.12. Germanium Beam Splitter Geometry

to lowest order ε. Using (IV.11a) in (IV.11b) gives

IV.12) $$\sin\theta_i + \epsilon N\sqrt{1-\left(\frac{\sin\theta_i}{N}\right)^2} \cong \sin\theta_o$$

For $N \cong 4.0$ for Ge at $\lambda = 10\mu$ and $\sin\theta_i = \frac{1}{\sqrt{2}}$ for $\theta_i \cong 45°$, so that $(\sin\theta_i/N)^2 << 1$. Hence

IV.13) $$\sin\theta_i + \epsilon N\,(1) \cong \sin\theta_o$$

Since $\epsilon N \lesssim \frac{1}{10}$ rad., one can write

IV.14) $$\theta_o \cong \sin^{-1}(\sin\theta_i) + \epsilon N \frac{d}{dx}(\sin^{-1}x)\Big|_{x=\sin\theta_i}$$

$$\cong \theta_i + \frac{\epsilon N}{\cos\theta_i}$$

this gives for α

IV.15) $$\alpha = \theta_o - \theta_i - \epsilon \cong \left(\frac{N}{\cos\theta_i} - 1\right)\epsilon$$

For $\theta_i \cong 45°$, and $N \cong 4$, $\alpha = (4\sqrt{2} - 1)1° \sim 5°$.

After placing the input mirrors at ∿5° with respect to the optical rail, only a very small change in θ_i was required to obtain a beam from L1 propagating very nearly parallel to the optical rail. The mirrors for the L2 beam are easily located and adjusted so that this beam propagates parallel to L1. This

alignment is facilitated by using a He-Ne laser beam which is introduced after the Ge beam splitter via a sliding mirror and which is aligned parallel to the L1 beam.

With the two beams L1 and L2 copropagating nearly parallel to the optical rail, a set of two adjustable mirrors is used to raise the beam vertically and to precisely align the beams with the optical rail; using a sliding iris. The iris is located so that the telescope lenses, if used, line up nearly at the iris center. All of this alignment is done with the He-Ne laser. The telescope optics are easily introduced onto the optical rail and positioned to maintain the He-Ne beam direction unchanged. The lens spacing is determined using the known focal length at 10.6μ. However, as will be shown below, the extremely weak $\Delta F = 0$ transitions are difficult to saturate when the telescope is used.

4. Servo Operation

In order to provide reproducible signals to enable signal averaging, a servo system is used to stabilize the difference frequency between lasers 1 and 2. A Tektronix voltage controlled oscillator (VCO) is used as a frequency reference and the servo system acts to maintain a zero beat frequency between the VCO and the laser beat signal. The derivative technique requires a modulation of the relative frequency of the two lasers. This is

accomplished by adding a small voltage dither into the error signal going to the PZT of laser 2. Laser 1 is free running. A synchronous modulation is applied to the VCO so that the servo system does not generate an error voltage unless the average beat frequency of lasers 1 and 2 drifts. The sweep control voltage (from the computer) is applied to the VCO so that the relative laser frequency may be swept. A detailed description of the frequency stabilization system will be given in Chapter V.

5. Frequency Calibration

The amplified beat signal from lasers 1 and 2 is used for the servo stabilization and is, in addition, used for the calibration of the frequency scale. This is easily accomplished by sending the beat signal to a Hewlett Packard Digital Frequency Counter (Model 5245M) which has been previously calibrated. The computer sweep divides the 1 MHz sweep interval into 255 parts. The beat frequency can be monitored throughout the sweep if desired. Usually, a .1 sec frequency average is used, since the time spent in each frequency bin ($\sim$4kHz wide) is $\sim$1 sec.

In addition to the magnitude of the beat frequency, the sign of the beat frequency must be determined. (i.e. Is laser 2 at higher or lower absolute frequency with respect to laser 1?) The laser cavity resonance determines the laser frequency since

the PZT tuning obviously works! To determine whether the PZT expands or contracts with increasing applied voltage, the following experiment is done. The beat frequency between the two lasers is observed both on an oscilloscope and with the digital counter. After tuning the beat frequency into the vicinity of a few MHz, the grating of laser 2 is rotated so as to shorten the cavity, hence raising the absolute frequency. If the beat frequency increases, then laser 2 is at a higher frequency than laser 1. Then the voltage to the PZT of laser 2 is increased and the beat frequency increases further. Thus, increasing the voltage applied to the PZT of laser 2 increases the absolute frequency. By tuning the beat frequency between lasers 1 and 2 through zero beat to interchange the laser relative frequencies, this result is again obtained. Once it is known that the laser 2 frequency increases with increasing PZT voltage, it is easy to tell from the behavior of the beat note which of the lasers has the higher frequency. The servo system requires that the lasers have a particular relative frequency in order to lock. (Otherwise the laser beat frequency is pushed away from, rather than toward the VCO frequency.) This guarantees that the lasers remain at known, fixed relative frequencies. Polarity switches then enable the relative frequencies of the lasers to be interchanged. This is essential since the lineshape with the weaker laser at higher frequency

is very different than the lineshape with the weaker laser at lower frequency.

The J value of the P- and R-branch N_2O rotational-vibrational transitions is determined utilizing a Bausch and Lomb monochromator. The monochromator grating has a groove density of 8 grooves/mm and is blazed at 112.5μ. Calibration of the monochromator is accomplished by using the known strong absorption of the P(13) N_2O line in ammonia. A simple counting operation is then used to obtain P(13) - P(3). By fitting a straight line to wavelength versus monochromator reading, the monochromator positions of the R branch lines are predicted. This technique avoids using the weak lines near the R(0)-P(1) gap. It is found that predicted and observed R lines agree after R(2) is properly assigned.

6. Lock-In Detection - Derivative Signal

As stated above, a lock-in derivative technique is used to enhance the weak signals corresponding to ($\Delta F = 0 - \Delta F = \Delta J$) crossing resonances. Due to the fact that the finite frequency modulation amplitude causes some distortion of the lineshape, a discussion of the form of the lock-in derivative lineshape will be given.

Fig.4.13 shows how the lock-in amplifier integrates with positive amplitude during the positive portion of its reference

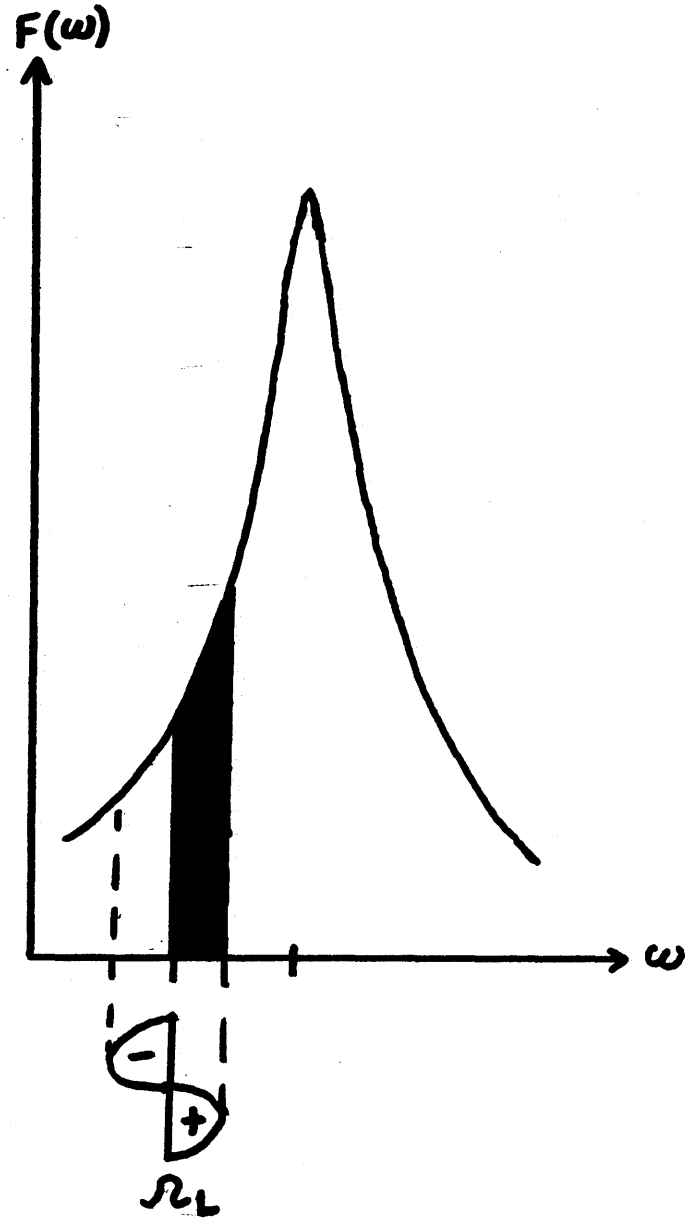

Figure 4.13. Function of Lock-in Amplifier in Lock-in Derivative Detection (Ω_L = reference frequency modulation amplitude)

signal and with negative amplitude during the negative portion of its reference to obtain a signal proportional to the difference of the unshaded and shaded areas of Fig.4.13. For small modulation amplitudes, the output is clearly proportional to the derivative $dF(\omega)/d\omega$. Experimentally, the reference signal is synchronized with the frequency modulation of one of the lasers, so that the signal moves along the curve $F(\omega)$ as shown in Fig.4.13. However, this requires that the gas molecules be in quasi equilibrium as the laser frequency is varied. The required restriction on the modulation amplitude and frequency may be determined in the following way. Assuming that the quasi equilibrium condition is fulfilled, the density matrix element ρ_{12} will be proportional to the resonant part of the potential V_{12} (provided that the fields applied to obtain the crossing resonances interact only with their respective transitions as in Chapter II). Hence,

IV.16) $$\rho_{12} = \lambda_{12} e^{-i(kz - \omega(t)t)}, \text{ etc.}$$

The condition that (IV.16) provide a good approximation to the true solution is that the frequency must change by an amount small compared to γ over times of order $1/\gamma$, where γ is an equilibrium determining rate (<u>i.e.</u> natural linewidth, collision rate, etc.). Thus,

IV.17) $$\dot{\omega} \ll \gamma^2$$

is the condition for quasi equilibrium. Using (IV.16) and treating the ω as a constant will yield the same results as in Chapter II. The lineshape will be roughly Lorentzian in shape but the signal will contain the time dependence of ω. ω is taken to be

IV.18) $$\omega(t) = \omega + \omega_1 \sin \Omega t$$

so that (IV.17) becomes

IV.19) $$\Omega \omega_1 << \gamma^2$$

For ω_1 = 50 kHz, and $\Omega = 170$ $H_z \cong .2$kHz, this requires $[\gamma(\text{kHz})]^2 >> 10$. This is easily satisfied at pressures of a few mTorr where $\gamma \gtrsim 10$ kHz so that $\gamma^2 \sim 100$ in the above units. Assuming a Lorentzian lineshape, the lock-in output signal is proportional to

IV.20) $$F(x_0, x_1) = \frac{\Omega}{2\pi}\left[\int_0^{\pi/\Omega} \frac{dt}{1+(x_0+x_1 \sin \Omega t)^2} - \int_{\pi/\Omega}^{2\pi/\Omega} \frac{dt}{1+(x_0+x_1 \sin \Omega t)^2}\right]$$

where a Lorentzian lineshape of HωHM equal to Γ is assumed and

IV.21) $$x_0 = \frac{\omega - \omega_0}{\Gamma} \; ; \; x_1 = \frac{\omega_1}{\Gamma}$$

are the detuning and modulation amplitude in dimensionless units.

Also, it is assumed that the phase between the signal and the reference is perfectly adjusted and that the lock-in integration time is large compared to the modulation period $2\pi/\Omega$.

Using $u = \Omega t$ in the first integral and $u = \Omega t - \pi$ in the second integral, F becomes

IV.22) $$F(x_0, x_1) = \frac{1}{2\pi}\int_0^{\pi} du \left[\frac{1}{1+(x_0+x_1 \sin u)^2} - \frac{1}{1+(x_0-x_1 \sin u)^2}\right]$$

By explicitly adding the terms of Eq. (IV.22) using their common denominator and letting $Z = \cos u$, F may be cast into the form

IV.23) $$F(x_0, x_1) = -\frac{4x_1 x_0}{\pi x_1^4}\int_0^1 \frac{dz}{z^4 + Bz^2 + A}$$

where

IV.24) a) $$A = \frac{1 + 2(x_0^2 + x_1^2) + (x_0^2 - x_1^2)^2}{x_1^4} \quad ; x_1 > 0$$

b) $$B = \frac{2(x_0^2 - x_1^2 - 1)}{x_1^2} \quad ; \quad x_1 > 0$$

Since $$\left(\frac{B}{2}\right)^2 - A = -\frac{4x_0^2}{x_1^4} \leq 0 ,$$

the denominator generally cannot be factored into real factors using the quadratic formula. However, the denominator can be factored into two factors of the form $(Z^2 + b_i Z + c_i)$ where $i = 1, 2$, and b_i and c_i are required to be real. The integral is then easily done by partial fractions. This gives

$$\text{IV.25)} \quad \int_0^1 \frac{dz}{z^4+Bz^2+A} = \frac{1}{2\sqrt{A}}\left\{\frac{1}{2\sqrt{2\sqrt{A}-B}}\ln\left(\frac{1+\sqrt{2\sqrt{A}-B}+\sqrt{A}}{1-\sqrt{2\sqrt{A}-B}+\sqrt{A}}\right)\right.$$

$$\left. + \frac{1}{\sqrt{2\sqrt{A}+B}}\left[\tan^{-1}\frac{2+\sqrt{2\sqrt{A}-B}}{\sqrt{2\sqrt{A}+B}} + \tan^{-1}\frac{2-\sqrt{2\sqrt{A}-B}}{\sqrt{2\sqrt{A}+B}}\right]\right\}$$

In the limit $X_i^2 << X_o^2$, 1, the function (IV.25) gives using (IV.24) and considerable algebra;

$$\text{IV.26)} \quad F(X_1^2 << X_o^2, 1) \cong \frac{-4X_1 X_o}{\pi(1+X_o^2)^2}$$

This is seen to be correct by expanding (IV.22) to lowest order in X_1 and integrating. (For $X_o^2 < X_1^2$, the higher order terms are necessary since $|X_o|X_1 < X_1^2$).

The result (IV.23) and (IV.25) has been evaluated for various values of $X_1 = \omega_1/\Gamma$. Here, Γ is the half width at half maximum of the Lorentzian response and hence includes power

broadening in an experimental situation. The distortion introduced by a modulation which fulfills the quasi static condition (IV.19) is basically the result of the convolution of the Lorentzian response of the atoms with the frequency spectrum of the modulated laser. When the modulation amplitude ω_1 is small compared to Γ, the atom sees an almost pure laser frequency yielding a Lorentzian derivative, as in (IV.26). However, for large modulation amplitudes, the atomic Lorentzian acts as a sampling function for the laser frequency distribution. For a sinusoidal modulation, the laser spends most of its time at the turning points of the sine wave. Hence, one expects the laser spectrum to peak near $\omega = \omega_o \pm \omega_1$. The atoms then sample this distorted spectrum.

In Figs. 4.14 and 4.15 the lineshape represented by the exact function $F(X_o, X_1)$ versus X_o is shown for various values of X_1. Since the function is antisymmetric in X_o as can be seen from (IV.23) and (IV.24), only one side of the derivative signal is shown. For small values $X_1 \lesssim 1$, the shape is nearly Lorentzian, and can be represented fairly well by a Lorentzian shape with an increased effective width. For values of $X_1 \gtrsim 3$, the distortion is significant. The maximum signal occurs for $X_1 \cong 2$ or $\omega_1 = 2\Gamma$ which is the Lorentzian full width.

For the experimental situation, the modulation full width is $\lesssim$70 kHz so that $\omega_1 \lesssim$ 35 kHz. The narrow resonances typically

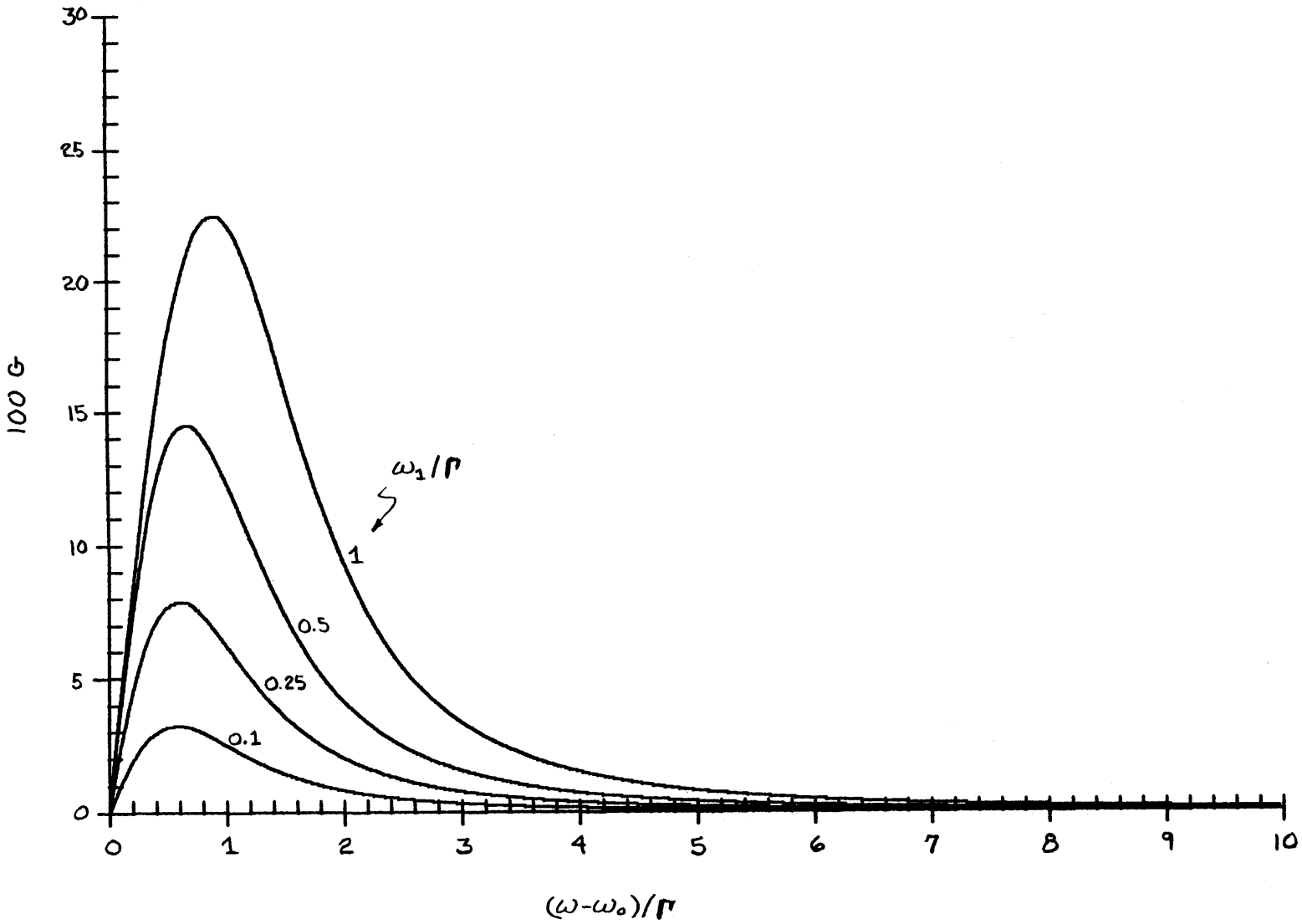

Figure 4.14. Lock-in 'Derivative' Signal for Small Frequency modulations ($2\omega_1$ = frequency modulation amplitude $p_0 - p_1$; Γ = HWHM of unmodulated Lorentzian Response ; $F \equiv \frac{-4}{\pi}$ G)

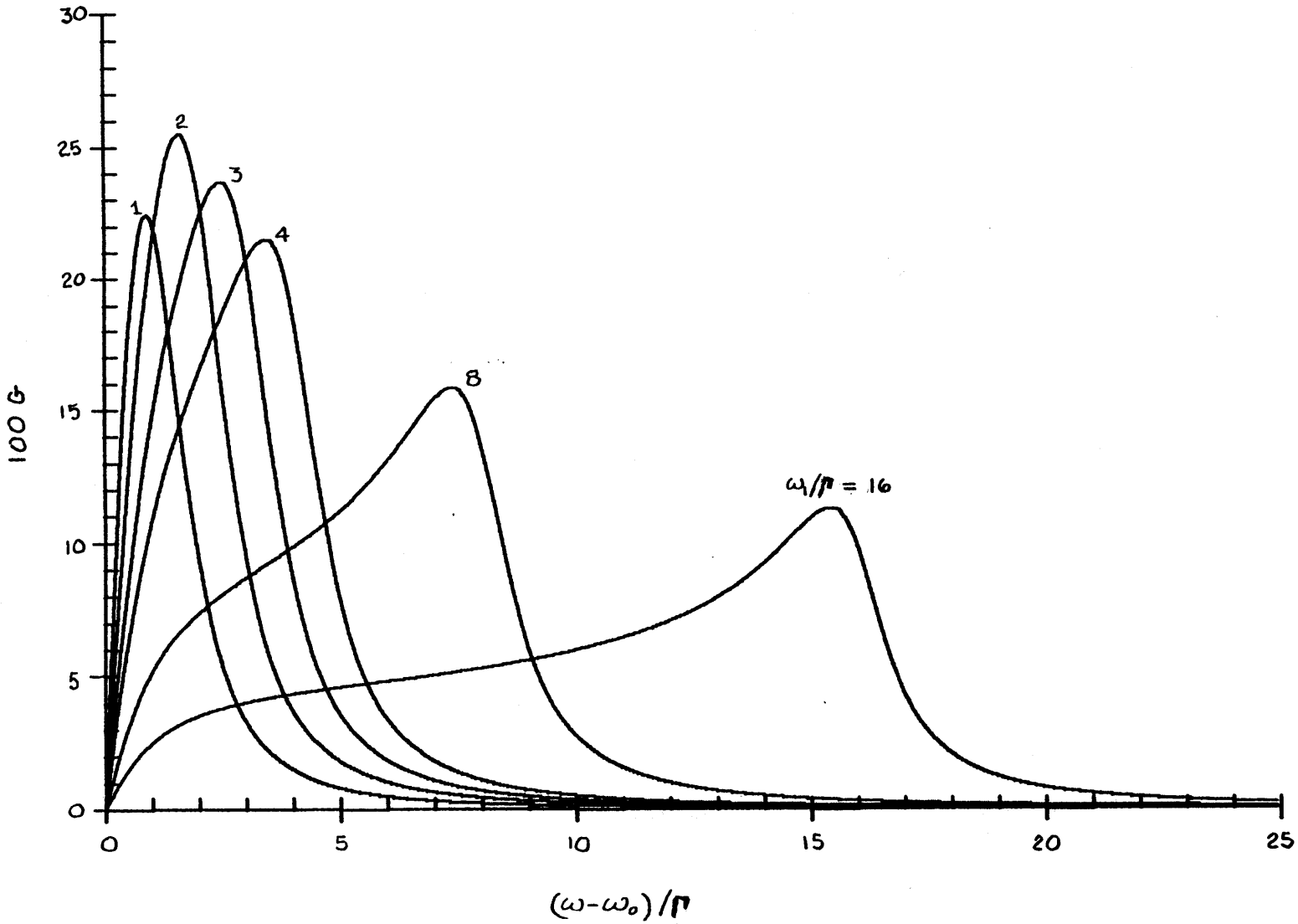

Figure 4.15. Lock-in 'Derivative' Signal for Large Frequency Modulations (Definitions as in Fig. 4.14)

have power broadening $\sim$100 kHz full width, so that $\Gamma \sim 50$ hMz. Thus $X_1 \sim .7$ and the lineshapes are nearly Lorentzian.

7. Computer Data Averaging

Significant improvement in signal to noise ratio can be obtained by signal averaging. Through the use of the frequency locking technique, a reproducible frequency sweep is obtained so that the signal averaging becomes particularly easy.

Basically, the computer produces a voltage ramp which is divided into 255 steps. This voltage is filtered slightly $RC << \tau_{bin}$ (τ_{bin} = time spent in each of the 255 steps) and fed into the voltage controlled oscillator (VCO) to sweep the frequency of the VCO and hence the laser difference frequency. The slight filtering is used to reduce the abrubtness of the voltage transitions. In this manner, the frequency sweep which starts at $\sim$1000 kHz and ends at $\sim$50 kHz is divided into 255 parts. After each voltage is outputed, the computer waits $\sim$1 sec before sampling the lock-in signal, to allow the entire system time to reach equillibrium. The lock-in time constant is set at 1 sec and a double filter (12 db/octave) is used. Since the signal varies significantly over $\sim$10 bins, the waiting time is sufficient. After an entire single sweep is finished, it is remembered as an array F(I), where I is an integer from 0 to 255. Assuming that there are no problems during the sweep, such as a loss of lock,

the lineshape F(I) is summed into an array of accumulated sweeps A(I). Typically, 20 sweeps are averaged in this fashion, corresponding to ∿1 1/2 hours integration time for each final lineshape. By comparing the total lineshape for various numbers of sweeps it is found that all peaks line up consistently and that the lineshape does not change except for the noise reduction.

In addition to the primary operation described above, the computer is programmed to perform a number of other functions, such as strong data on a disc, reading from a disc, plotting the normalized accumulated data, and writing out the digitized data A(I) in integer form.

It should be pointed out that the frequency calibration is done only at the end points of the sweep. These endpoints are reproducible within 1 kHz over hour long periods. In addition, the starting point of the sweep at 1000 kHz can be reset prior to the onset of the computer data sampling. The voltage applied to the VCO varies from +5V at 1000 kHz to -5V at ∿525 kHz. The VCO is sufficiently linear with respect to the present resolution that a direct computer sampling of the digital frequency for each bin is unnecessary.

A complete list of the computer program is given in Appendix IV.1. The minicomputer used to take the data was built around a S-100 bus type microcomputer and has a 32 Kbytes of RAM memory as well as a mini-floppy disc for storage. The analog

interface consists of 8 channels of ADC and 2 channels of DAC which are used to receive the lock-in signal and provide the sweep voltage.

References

1. C. Freed and A. Javan, Appl. Phys. Lett. 17, 53 (1970).

2. M. J. Kelly, Ph.D. Thesis, M.I.T., 1976 (unpublished).

3. T. M. Hard, App. Opt. 9, 1825 (1970).

CHAPTER V.

SERVO SYSTEM DESIGN ANALYSIS

The electronic frequency stabilization system utilized in the spectrometer evolved out of an attempt to use a phase-locked loop as the basis for the servo system. This technique proved to be impractical. Instead, a two loop system was devised which will be discussed below.

In the following sections, a phase-locked loop will be described first, followed by a frequency-locked loop. Finally, the actual servo system used in the experiments will be described. The principles explained in the first two sections will form the basis for an understanding of the two loop system.

1. Phase Locked Loop

A block diagram of the basic phase-locked loop is shown in Fig. 5.1. The purpose of the loop is to lock the phase (and hence the frequency) of the VCO output $e_2(t)$ to the input signal $e_1(t)$. The input is supplied from some oscillator which need not be specified. Let the signals have the form:

V.1) a) $e_1(t) = e_1 \sin[\theta_1(t)]$

b) $e_2(t) = e_2 \cos[\theta_2(t)]$

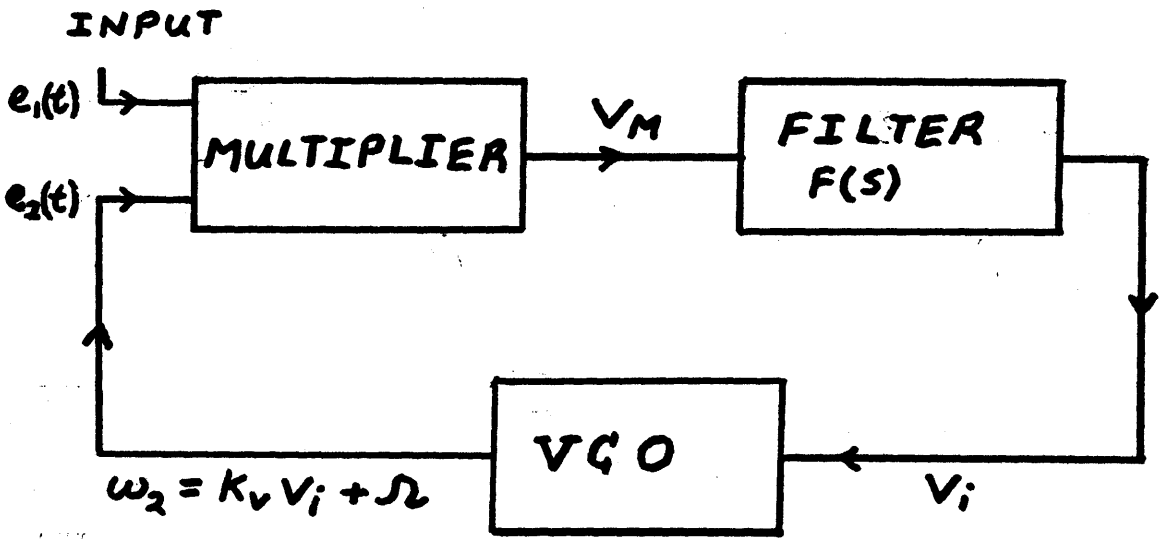

Figure 5.1. Phase-Locked Loop Block Diagram

The relative phase is arbitrary initially, but the loop will act to maintain a 90° phase shift between $e_1(t)$ and $e_2(t)$ so as to give a zero D.C. component to the multiplied signal, as shown below.

A multiplier with carrier suppression will, to a fairly high degree of perfection, give an output proportional to

V.2) $$e_1(t)e_2(t) = e_1 e_2 \sin[\theta_1(t)]\cos[\theta_2(t)]$$
$$= \frac{e_1 e_2}{2}\left[\sin(\theta_1+\theta_2) + \sin(\theta_1-\theta_2)\right]$$

By assumption, the component containing $\theta_1 + \theta_2$ will be rapidly varying and will be filtered out completely by the filter F(s) . This component will be neglected. The low frequency part of the multiplier output will be

V.3) $$V_M \cong -K_D \sin(\theta_2-\theta_1)$$

where $K_D = + ge_1e_2$ is a constant taken >0 for later convenience and a multiplier gain g has been included. (The filter gain may also be lumped into g.)

The voltage controlled oscillator (VCO) output has a frequency $\omega_2(t)$ which is described by

V.4) $$\omega_2(t) = K_V V_f(t) + \Omega(t)$$

$\Omega(t)$ is the slowly varying free running frequency of the VCO and K_V is the constant which describes how ω_2 will change as the VCO input voltage V_i is changed.

The input frequency $\omega_1(t)$ may be arbitrarily prescribed, except that it is slowly varying. Since the time derivative of the phase is the frequency, one obtains

V.5) $$\frac{d}{dt}(\theta_2-\theta_1) = \omega_2(t)-\omega_1(t) = K_V V_i + \Omega - \omega_1$$

V.6) $$\frac{d^2}{dt^2}(\theta_2-\theta_1) = K_V \dot{V}_i + \dot{\Omega} - \dot{\omega}_1$$

where $$\cdot \equiv \frac{d}{dt}$$

The differential Equations (V.5 and V.6) relate $\theta_2 - \theta_1$ and V_i. Eq. (V.3) relates V_M to $(\theta_2 - \theta_1)$. Hence, the only other relation needed to express all the variables in terms of $(\theta_2 - \theta_1)$ is the filter relation between V_i and V_M.

For an arbitrary filter described by a transfer function F(S), the output voltage is linearly related to the fourier transform of the input voltage by

V.7) $$V_i(t) = \int F(S)\, V_M(S)\, e^{jst}\, ds$$

where

V.8) $$V_M(t) = \int V_M(s)\, e^{jst}\, ds$$

and the real part is to be taken.

In order to use (V.7) to obtain an explicit relation between $V_i(t)$ and $V_M(t)$, a filter must be chosen. For simplicity, a single low pass filter will be chosen first. This is shown in Fig. (V.2a). The transfer function is given by

V.9) $$F(s) = \frac{1}{1 + jsRC}$$

where it is assumed that the filter gain has been lumped into the multiplier gain g. (Since V_i is linear in V_M, this is acceptable.) Hence, (V.2) becomes:

V.10) $$V_i(t) = \int \frac{V_M(s)\, e^{jst}\, ds}{1 + jsRC}$$

This implies that

V.11) $$RC\,\dot{V}_i(t) + V_i(t) = \int \frac{jsRC + 1}{1 + jsRC}\, V_M(s)\, e^{jst}\, ds$$
$$= V_M(t)$$

Solving Equations (V.5) and (V.6) for V_i and $\dot{V}_i$ respectively, and using equations Eq. (V.3) for V_M, Eq. (V.11) yields the equation of motion for $(\theta_2 - \theta_1)$:

V.12) $$\frac{d^2}{dt^2}(\theta_2 - \theta_1) + \frac{1}{RC}\frac{d}{dt}(\theta_2 - \theta_1) + \frac{K_V K_D}{RC}\sin(\theta_2 - \theta_1) =$$
$$= \frac{1}{RC}(\Omega - \omega_1) + (\dot{\Omega} - \dot{\omega}_1)$$

a)

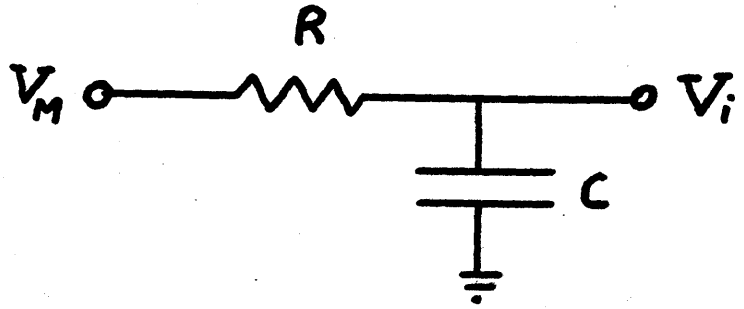

$$F(s) = \frac{1}{1 + jsRC}$$

b)

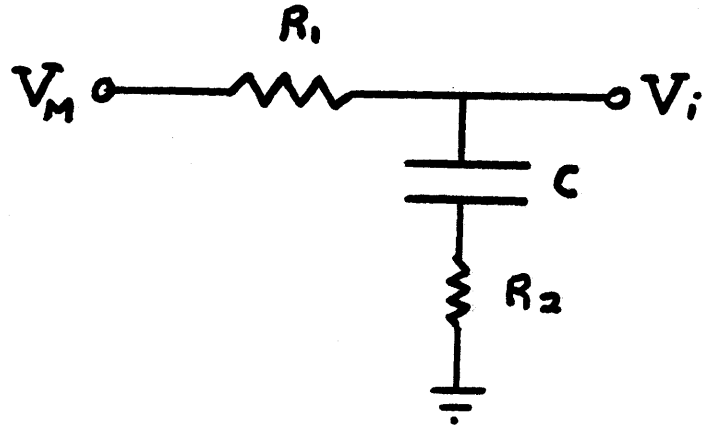

$$F(s) = \frac{1 + jsR_2C}{1 + js(R_1+R_2)C}$$

Figure 5.2 a) Simple Low Pass

b) Lead-Lag Filter

With the loop locked, the phase difference $(\theta_2 - \theta_1)$ is small, so that $\sin(\theta_2 - \theta_1) \cong \theta_2 - \theta_1$. The equation for the phase difference is then that of a driven, damped harmonic oscillator.

V.13) $$(\ddot{\theta}_2 - \ddot{\theta}_1) + \frac{1}{RC}(\dot{\theta}_2 - \dot{\theta}_1) + \frac{K_V K_D}{RC}(\theta_2 - \theta_1) = \frac{1}{RC}(\Omega - \omega_1) + (\dot{\Omega} - \dot{\omega}_1)$$

In the same approximation, the equation for V_i is:

V.14) $$\ddot{V}_i + \frac{1}{RC}\dot{V}_i + \frac{K_V K_D}{RC} V_i = \frac{K_D}{RC}(\omega_1 - \Omega)$$

From Eq. (V.12), it may be seen that the sign of K_D and the relative initial phase of e_1 and e_2 (when $\theta_2 - \theta_1 = 0$) are arbitrary. The loop will not lock until $\theta_2 - \theta_1$ is such that the sine term in (V.12) gives a restoring force. Hence if $K_D < 0$, then $\theta_2 - \theta_1 \to \pi + \theta_2' - \theta_1'$ to obtain lock. The equation for $\theta_2' - \theta_1'$ will be the same as (V.12) with $-K_D \equiv K_D' > 0$

The first result to be derived from Eq. (V.12) is the lock range. Consider the D.C. situation where all time derivatives $\to 0$. Then,

V.15) $$\sin(\theta_2 - \theta_1) = \frac{\Omega - \omega_1}{K_V K_D}$$

Note that the multiplier constant K_D has units of volts/phase = volts as seen from (V.3). The VCO constant K_V has units of angular frequency per volt as seen from (V.4). Thus $K_V K_D$ has angular frequency units as it should.

The frequency ω_2 is always the same as ω_1 as long as

(V.15) is satisfied. This may be seen from Eqs. (V.15), (V.3), and (V.11) for D.C. conditions ($V_M = V_i$). Substituting into (V.4) yields $\omega_2 = \omega_1$. To determine just how far one may tune ω_1 away from the VCO free running frequency Ω, while still maintaining $\omega_2 = \omega_1$, consider Eq. (V.15). The sine may only vary over the range ±1 for $(\theta_2 - \theta_1) = \pm \frac{\pi}{2}$ to maintain a restoring force. Thus, the maxiumum lock range is $\Omega - \omega_1 = \pm\omega_L$, where ω_L is given by

V.16) $$\omega_L = K_V K_D$$

The tracking range is proportional to the total loop gain $K_V K_D$. Hence, large gains are desired if one is to obtain large tracking ranges.

From Eqs. (V.13) and (V.14) for small phase differences, the natural frequency of the loop (undamped oscillator resonance frequency) is given by

V.17) $$\omega_o = \sqrt{\frac{K_V K_D}{RC}}$$

The damping constant is given by

V.18) $$\gamma = \frac{1}{RC}$$

For stability, the natural oscillations should damp quickly <u>i.e.</u> $\frac{1}{\gamma} < \frac{1}{\omega_o}$ or $\frac{\gamma}{\omega_o} > 1$. From (V.17) and (V.18), the damping ratio $\equiv \frac{\gamma}{\omega_o}$ is

V.19) $$\frac{\gamma}{\omega_o} = \frac{1}{\sqrt{K_D K_V RC}}$$

For large gains, $K_D K_V$, or large filters RC (for good signal to noise ratio), the damping ratio will be <1 and the system will tend to oscillate.

The problems with the loop as given above may be solved by using the lead-lag filter shown in Fig. 5.2b. The transfer function is given by

V.20) $$F(s) = \frac{1 + js R_2 C}{1 + js(R_1+R_2)C}$$

Then, $V_i(t)$ is given by

V.21) $$V_i(t) = \int \frac{1+js R_2 C}{1+js(R_1+R_2)C} V_M(s) e^{jst} ds$$

This gives

V.22) $$(R_1+R_2)C\dot{V}_i + V_i = \int (1+js R_2 C) V_M(s) e^{jst} ds$$
$$= V_M + R_2 C \dot{V}_M$$

as the result analogous to (V.11).

Using exactly the same techniques as before, the equation of motion for $(\theta_2 - \theta_1)$ in the small angle approximation is

$$\text{V.23)}\quad (\ddot{\theta}_2 - \ddot{\theta}_1) + \frac{1 + R_2 C K_V K_D}{(R_1+R_2)C}(\dot{\theta}_2 - \dot{\theta}_1) + \frac{K_V K_D}{(R_1+R_2)C}(\theta_2 - \theta_1) = \frac{1}{(R_1+R_2)C}(\Omega - \omega_1) + \dot{\Omega} - \dot{\omega}_1$$

The exact equation for $(\theta_2 - \theta_1)$ gives the same lock range as before since the D.C. conditions are not affected by the resistor R_2. The interesting results are in the damping constant and damping ratio. From Eq. (V.23), the natural frequency is

$$\text{V.24)}\quad \omega_o = \sqrt{\frac{K_D K_V}{(R_1+R_2)C}}$$

The damping constant is given by

$$\text{V.25)}\quad \gamma = \frac{1 + R_2 C K_V K_D}{(R_1+R_2)C}$$

For large $K_V K_D$, even a small R_2 will make $R_2 C K_V K_D \gg 1$. Assuming $R_2 \ll R_1$, Eqs. (V.24) and (V.25) become

$$\text{V.26)}\quad \text{a)}\quad \omega_o \cong \sqrt{\frac{K_D K_V}{R_1 C}}$$

$$\text{b)}\quad \gamma \cong \frac{R_2}{R_1} K_V K_D = R_2 C \omega_o^2$$

Thus, the damping ratio is

$$\text{V.27)}\quad \frac{\gamma}{\omega_o} = R_2 C \omega_o$$

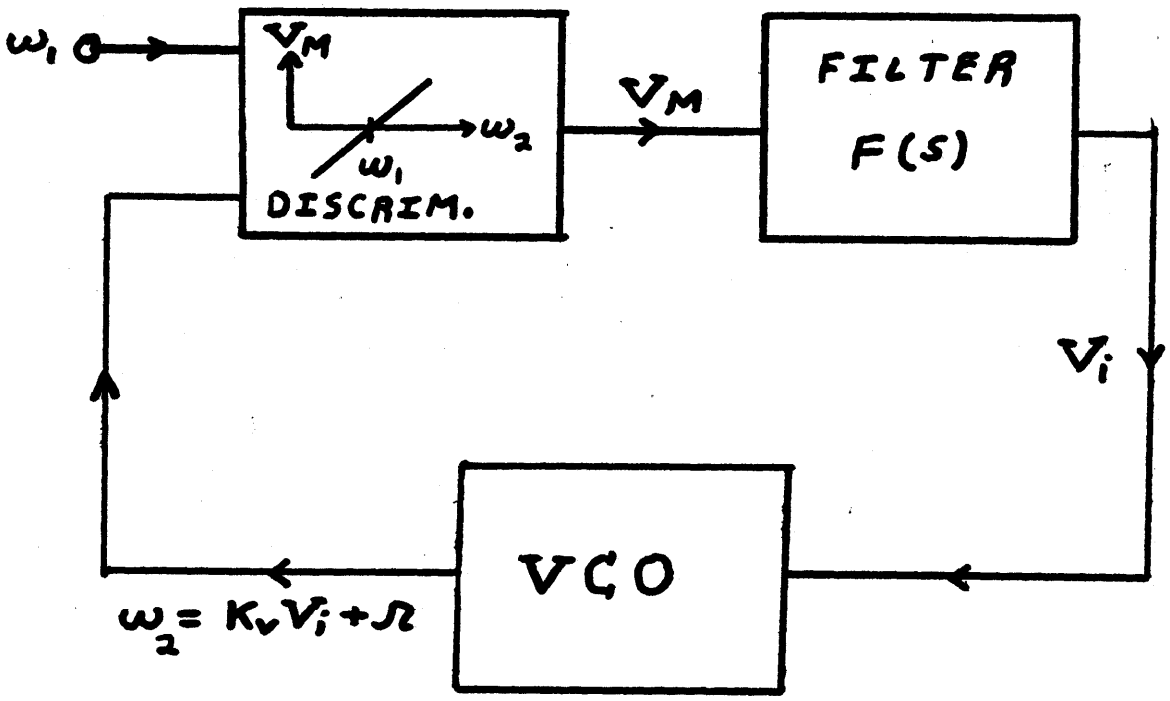

$$V_M = -K_\omega (\omega_2 - \omega_1)$$

DISCRIMINATOR GENERATED BY ARBITRARY METHOD

Figure 5.3. Frequency-Locked Loop Block Diagram

For large gains, the natural frequency ω_o will be large, so it is easy to obtain damping ratios >1. The lock range and damping may be controlled independently using the lead lag filter. This type of filter may be used to obtain stability in other types of loops as will be shown below.

2. Frequency-Locked Loop

A block diagram for the frequency locked loop is shown in Fig. 5.3. The frequency discriminator may be generated in an arbitrary manner. For example, the frequency ω_1 may be a natural resonance frequency and the discriminator may be a lock-in derivative output in the linear region. The purpose of the frequency locked loop is to maintain ω_2 nearly equal to ω_1.

The discriminator output is given by assumption as

V.28) $$V_M = -K_\omega (\omega_2 - \omega_1)$$

where K_ω is a positive constant with dimensions of volts per angular frequency. ω_2, the VCO output frequency, is given by

V.29) $$\omega_2 = K_V V_i + \Omega$$

where Ω is the VCO freerunning frequency which may drift. If the VCO is a laser, then V_i will be the PZT control voltage.

For a filter with transfer function F(s), the voltages V_i and V_M are related by

V.30) $$V_i(t) = \int F(s)\, V_M(s)\, e^{jst}\, ds$$

A harmonic oscillator equation was obtained for the phase locked loop using a filter with only a single pole. This is due to the fact that the phase to frequency characteristic of the loop introduces a pole into the circuit giving a first order equation in time when F(s) = 1. For the frequency locked loop, a two pole filter is required in order to obtain the desired damped oscillator equation.

Consider the schematically represented two-pole filter of Fig. 5.4. A lead lag filter is included to adjust the damping. The transfer function is given by

V.31) $$F(s) = \frac{1 + js\tau_3}{1 + js(\tau_2 + \tau_3)} \frac{1}{1 + js\tau_1}$$

Equation (V.30) becomes

V.32) $$V_i(t) = \int \frac{(1 + js\tau_3) V_M(s)\, e^{jst}\, ds}{1 + js(\tau_1 + \tau_2 + \tau_3) + (js)^2 \tau_1 (\tau_2 + \tau_3)}$$

This immediately gives

V.33) $$\tau_1(\tau_2 + \tau_3)\ddot{V}_i + (\tau_1 + \tau_2 + \tau_3)\dot{V}_i + V_i = V_M + \tau_3 \dot{V}_M$$

Using (V.28) and (V.29), the voltage V_M is related to V_i by

V.34) $$V_M = -K_\omega K_V V_i - K_\omega(\Omega - \omega_1)$$

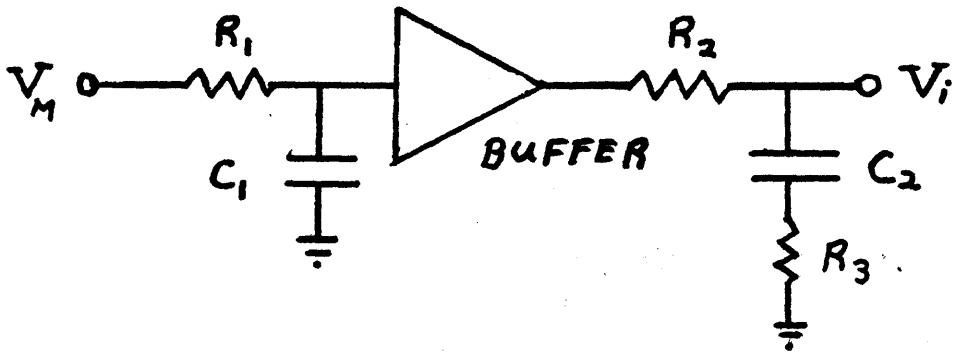

$$F(s) = \frac{1}{1+jS\tau_1} \times \frac{1+jS\tau_3}{1+jS(\tau_2+\tau_3)}$$

where $\tau_1 = R_1 C_1$; $\tau_2 = R_2 C_2$; $\tau_3 = R_3 C_2$

Figure 5.4. Two Pole Filter and Transfer Function (schematic representation)

Equations (V.33) and (V.34) allow the loop equation to be written as

V.35) $$\dddot{V}_i + \frac{\tau_1+\tau_2+\tau_3(1+K_\omega K_V)}{\tau_1(\tau_2+\tau_3)}\ddot{V}_i + \frac{1+K_\omega K_V}{\tau_1(\tau_2+\tau_3)}\dot{V}_i + \frac{K_\omega K_V}{\tau_1(\tau_2+\tau_3)}V_i =$$

$$= \frac{K_\omega(\dot{\omega}_1-\dot{\Omega})}{\tau_1(\tau_2+\tau_3)} + \frac{\tau_3 K_\omega(\ddot{\omega}_1-\ddot{\Omega})}{\tau_1(\tau_2+\tau_3)}$$

A similar equation can be written for ω_2, but this will not be done here.

In the limit that all time derivatives on the right of (V.35) may be neglected, the slowly varying solution (D.C. limit) is given by

V.36) $$V_i = \frac{K_\omega(\omega_1-\Omega)}{1+K_\omega K_V}$$

The VCO frequency ω_2 is then given by (V.29) as

V.37)

a) $$\omega_2 = \frac{K_\omega K_V(\omega_1-\Omega)}{1+K_\omega K_V} + \Omega$$

or

b) $$\omega_2 = \omega_1 + \frac{\Omega-\omega_1}{1+K_\omega K_V}$$

$K_\omega K_V$ is the total loop frequency to frequency gain and is dimensionless. (The filter gain has been included in $K_\omega K_V$.)

From (V.37b), the VCO frequency tracks the frequency ω_1

only to an accuracy of order $1/K_\omega K_V$. Thus, it is desirable to have the largest gain possible.

Equation (V.35) shows that the natural frequency of the loop is given by

V.38) $$\omega_o = \sqrt{\frac{1+K_\omega K_V}{\tau_1(\tau_2+\tau_3)}}$$

The damping constant is

V.39) $$\gamma = \frac{\tau_1+\tau_2+\tau_3(1+K_\omega K_V)}{\tau_1(\tau_2+\tau_3)}$$

In the regime where $K_\omega K_V >> 1$ and $K_\omega K_V \tau_3 >> \tau_2, \tau_1$, but $\tau_3 << \tau_2$, the natural frequency and damping constant are given by

V.40) a) $$\omega_o \cong \sqrt{\frac{K_\omega K_V}{\tau_1\tau_2}} \equiv \sqrt{\frac{G}{\tau_1\tau_2}}$$

b) $$\gamma \cong \omega_o^2 \tau_3$$

The damping ratio γ/ω_o is then

V.41) $$\frac{\gamma}{\omega_o} = \omega_o \tau_3$$

so that the loop natural frequency and damping may be controlled independently. This is the most useful regime.

If a lead-lag filter is not used, so that $\tau_3 = 0$, then it may be shown that when $\tau_1 \cong \tau_2$, the loop is unstable for large gains since $\frac{\gamma}{\omega_o} \sim \frac{2}{\sqrt{G}}$. Instead, one should take $\tau_1 << \tau_2$

so that $\frac{\alpha}{\omega_0} \sim \sqrt{\tau_2/\tau_1 G}$. The disadvantage here is that the loop damping decreases with increasing gain rather than increasing as it does in (V.41). Furthermore, the natural frequency and damping cannot be controlled independently.

In Eq. (V.40), it is desirable to have $\tau_1 << \tau_2$ to obtain a large natural frequency at reasonable gain. Clearly, a low natural frequency, even when properly damped, will result in a slow ringing if the loop is perturbed.

3. Two Loop Stabilization System

A block diagram of the basic two loop system utilized in the experiment is shown in Fig. 5.5. The purpose of the loop is to lock the laser beat frequency ω_1 as closely as possible to the VCO free running frequency Ω_2. Ω_2 is determined by the input voltage V_{input} with all loops open. The loop containing the lasers will be denoted as the 'outer' loop, while that containing the VCO will be denoted the 'inner' loop. Basically, the inner loop acts to generate a descriminator pattern $V_M(\omega_1 - \Omega_2)$. The outer loop which operates at much higher gain than the inner loop changes ω_1 to equal Ω_2 to an accuracy determined by the ratio of the gains. Since the VCO can track the laser beat note over a range of about one MHz, lock is not easily lost. Furthermore, the noise on the signal V_M is mostly second harmonic ($2\omega_1$) due to the use of a carrier suppressed

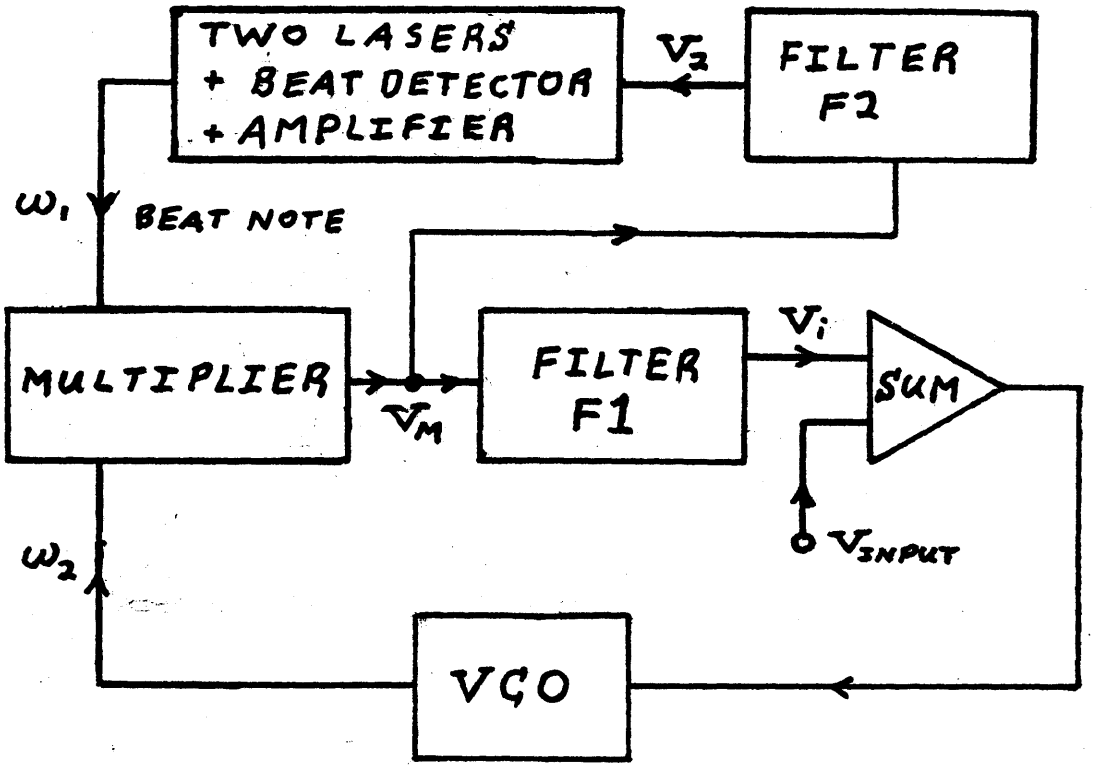

Figure 5.5. Twin Laser Beat Frequency Stabilization System-Simplified Block Diagram

multiplier. This may be compared to an ordinary frequency to voltage converter which has first harmonic noise inherent in its operation.

The system is run in a regime where the time constants of the inner loop are fast compared to those of the outer loop. Since the VCO response is virtually instantaneous, the inner loop easily tracks abrupt frequency changes of the laser. The outer loop then responds to correct the error.

A quantitative description of the loop operation will now be given. Both the filters F1 and F2 are lead lag filters of the type shown in Fig. 5.2b. The previously derived equation (V.23) for the inner phase locked loop may be immediately written down, since it is valid for arbitrary $\omega_1(t)$. This is

$$\text{V.42)}\quad (\ddot{\theta}_2-\ddot{\theta}_1)+\frac{1+R_2 C K_V K_D}{(R_1+R_2)C}(\dot{\theta}_2-\dot{\theta}_1)+\frac{K_V K_D}{(R_1+R_2)C}(\theta_2-\theta_1)=$$

$$=\frac{1}{(R_1+R_2)C}(\Omega_2-\omega_1)+\dot{\Omega}-\dot{\omega}_1$$

Equation (V.3) for V_M in the small angle $(\theta_2 - \theta_1)$ approximation is given by

$$\text{V.43)}\quad V_M \cong -K_D(\theta_2-\theta_1)$$

where a locked inner loop is assumed. Equation (V.42) may be multiplied by $(-K_D)$ to give the equation of motion for V_M.

V.44) $$\ddot{V}_M + \frac{1+R_2 C K_V K_D}{(R_1+R_2)C}\dot{V}_M + \frac{K_V K_D}{(R_1+R_2)C}V_M =$$

$$= \frac{-K_D(\Omega_2-\omega_1)}{(R_1+R_2)C} - K_D(\dot{\Omega}_2-\dot{\omega}_1)$$

The definitions of all constants are the same as for the phase-locked loop. If the rate of variation of ω_1 is small and Ω_2 is $\sim$ constant, then the D.C. solution of (V.44) obviously gives a linear discriminator pattern. For the general case, ω_1 and $\dot{\omega}_1$ must be related to V_M via the outer loop.

The filter F2 is shown in Fig. 5.6, and it has a transfer fuction given by

V.45) $$F_2(s) = \frac{1+js\tau}{1+js\tau'}$$

The voltage V_2 is then related to V_M by

V.46) $$V_2(t) = \int \frac{1+js\tau}{1+js\tau'} V_M(s) e^{jst} ds$$

Thus,

V.47) $$V_2 + \tau'\dot{V}_2 = V_M + \tau\dot{V}_M$$

ω_1 may be written in terms of V_2 and the free running beat frequency Ω_1 as

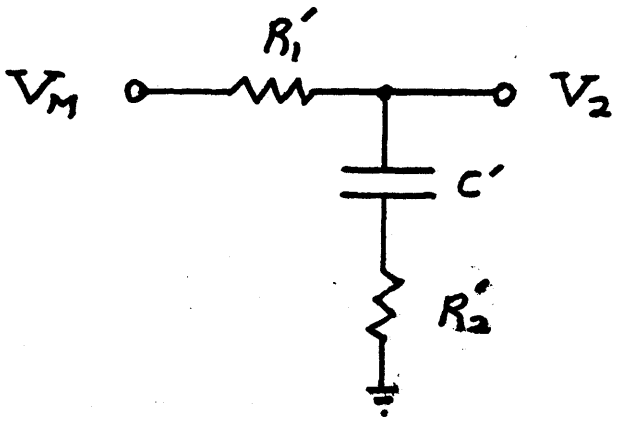

$$F_2(s) = \frac{1 + j s \tau}{1 + j s \tau'}$$

$$\tau = R_2' C'$$

$$\tau' = (R_1' + R_2') C'$$

Figure 5.6. Outer Loop Filter and Transfer Function

V.48) $$\omega_1 = -K_L V_2 + \Omega_1$$

where the constant $K_L > 0$ includes any gain present in F2. The minus sign results in ω_1 and ω_2 being pushed toward each other. This is accomplished by choice of the laser relative frequencies and an overall $\pm$ phase of F2 which is put into $-K_L$. Using (V.48) in (V.47) gives

V.49) $$(\omega_1 - \Omega_1) + \tau'(\dot{\omega}_1 - \dot{\Omega}_1) = -K_L (V_M + \tau \dot{V}_M)$$

Adding equation (V.44) to its time derivative multiplied by τ and using equation (V.49) one obtains for the loop equation:

$$\tau' \dddot{\omega}_1 + \ddot{\omega}_1 \left(1 + \frac{1 + \tau_2 K_V K_D}{\tau_1 + \tau_2} \tau' + \tau K_D K_L\right) +$$

$$+ \dot{\omega}_1 \left(\frac{1 + \tau_2 K_V K_D}{\tau_1 + \tau_2} + \tau' \frac{K_V K_D}{\tau_1 + \tau_2} + \frac{K_D K_L \tau}{\tau_1 + \tau_2} + K_D K_L\right) +$$

$$+ \omega_1 \left(\frac{K_D (K_L + K_V)}{\tau_1 + \tau_2}\right) = \frac{K_D K_L}{\tau_1 + \tau_2} (\Omega_2 + \tau \dot{\Omega}_2) +$$

$$+ \frac{K_D K_V}{\tau_1 + \tau_2} (\Omega_1 + \tau' \dot{\Omega}_1)$$

$$+ \frac{1 + \tau_2 K_V K_D}{\tau_1 + \tau_2} (\dot{\Omega}_1 + \tau' \ddot{\Omega}_1)$$

$$+ K_D K_L (\dot{\Omega}_2 + \tau \ddot{\Omega}_2)$$

$$+ \ddot{\Omega}_1 + \tau' \dddot{\Omega}_1$$

where $\tau_1 = R_1C$ and $\tau_2 = R_2C$. (inner loop time constants).

In the limit that the driving terms are slowly varying enough that the third derivative term may be neglected, this equation reduces to a harmonic oscillator equation. For suitably large gains this can be done. When the driving terms are constant or slowly varying, the equation has the D.C. solution:

V.51) $$\omega_1 = \frac{K_D K_L \Omega_2 + K_D K_V \Omega_1}{K_D (K_L + K_V)}$$

Thus,

V.52) $$\omega_1 - \Omega_2 = \frac{K_D K_V (\Omega_1 - \Omega_2)}{K_D (K_L + K_V)}$$

For large outer loop gains $K_L >> K_V$, the drift $\Omega_1 - \Omega_2$ is reduced by the factor K_V/K_L.

In the limit of large gains so that $\tau_2 K_V K_D$, $\tau K_D K_L >> 1$ (Note that $(K_V K_D)_{exp} \sim 10^7$ rad/sec and $K_L >> K_V$, the natural frequency is given by

V.53) $$\omega_o \cong \sqrt{\frac{K_L}{K_V(\tau_2\tau' + \tau\tau_1)}}$$

where it is assumed that $K_L >> K_V$ and $\tau_1 >> \tau_2$.

With the same approximations, the damping constant is given by

V.54) $$\gamma \cong \left(1 + \frac{\tau}{\tau_1}\right) \Big/ \left(\tau + \tau_2 \frac{\tau'}{\tau_1} \frac{K_V}{K_L}\right)$$

where $\frac{K_V}{K_L}\frac{\tau'}{\tau_1} << 1$ is assumed. The damping ratio is then

V.55) $$\frac{\gamma}{\omega_0} \cong \sqrt{\frac{K_V}{K_L}}\ \frac{(1+\frac{\tau}{\tau_1})\sqrt{\tau_2\tau' + \tau\tau_1}}{\tau + \tau_2\frac{\tau'}{\tau_1}\frac{K_V}{K_L}}$$

For τ such that $\tau\tau_1 \quad \tau_2\tau'$, and $\frac{\tau'}{\tau_1}\ \frac{K_V}{K_L}\ \tau_2 << \tau$, (V.55) becomes

V.56) $$\frac{\gamma}{\omega_0} \cong \sqrt{\frac{K_V}{K_L}}\ \frac{\sqrt{\tau_2\tau'}}{\tau}$$

Experimentally, $\tau_2 \sim 10^{-3}$ sec, $\tau' \sim 10^{-1}$ sec, and $\tau_1 \sim 10^{-2}$ sec. The gain ratio K_V/K_L is $\sim 10^{-3}$, so the above approximations are easily met with 10^{-5} sec $\lesssim \tau \lesssim 10^{-2}$ sec. For a damping ratio $\gtrsim$ 1, τ must be $\lesssim 10^{-3}$ sec. The loop does in fact behave as predicted by (V.56). Increasing τ using the outer loop damping potentiometer leads to oscillation.

The actual system block diagram is shown in Fig.5.7. In order to allow frequency modulation of the laser difference frequency, laser L2 and the VCO are synchronously modulated sinusoidally. From Eq. (V.50), one can easily find the equation of motion for $(\omega_1 - \Omega_2)$. The driving terms for the new equation depend only on $(\Omega_1 - \Omega_2)$ and its time derivatives. Thus, if Ω_1 and Ω_2 are modulated synchronously so that

V.57) a) $\Omega_1 \equiv \Omega_1^{(0)} + \Delta \sin\delta t$

b) $\Omega_2 \equiv \Omega_2^{(0)} + \Delta \sin\delta t$

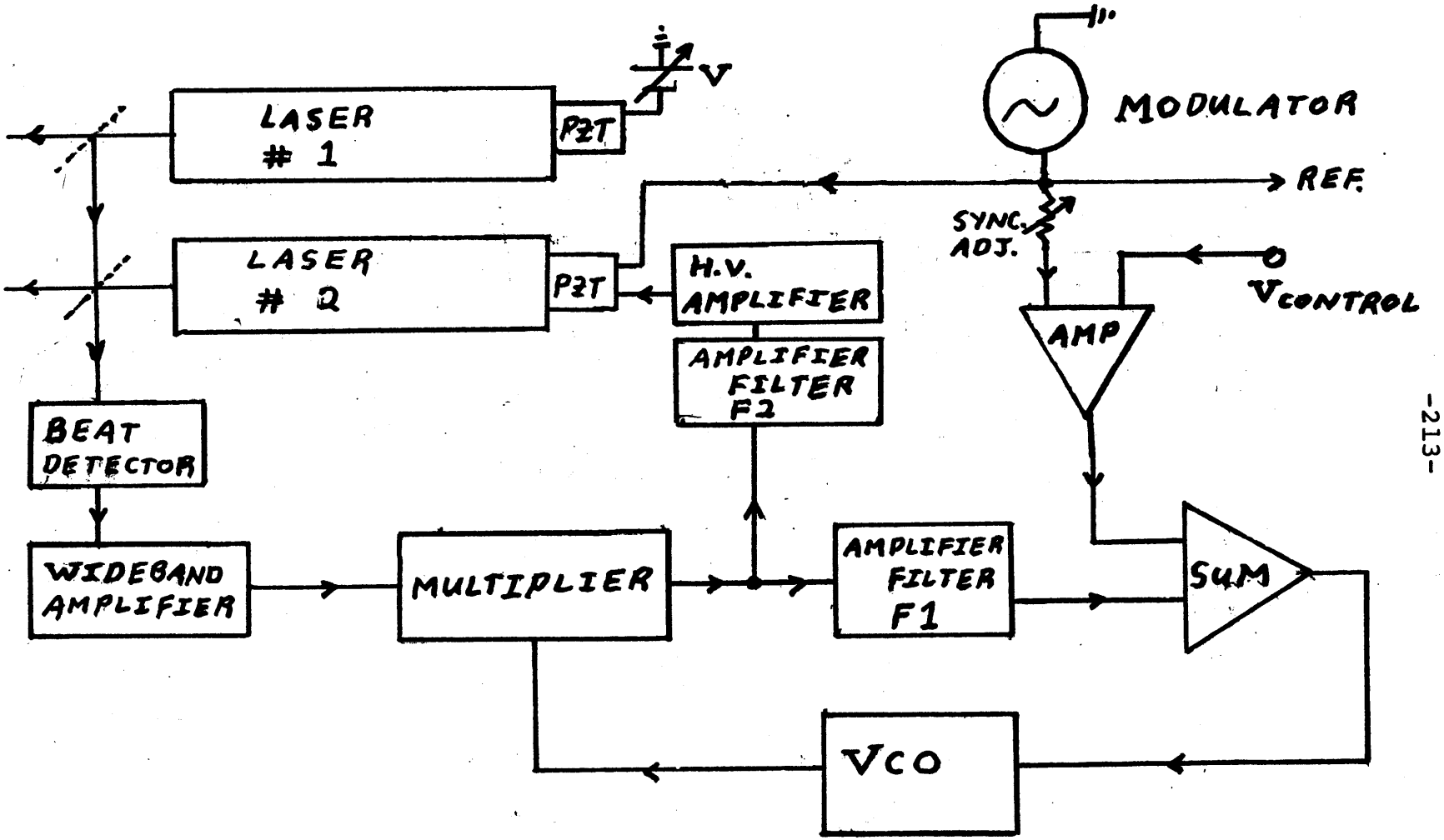

Figure 5.7. Twin Laser Beat Frequency Stabilization System - Diagram Showing Sweep and Modulation Components

then

V.58) $$\Omega_1 - \Omega_2 = \Omega_1^{(0)} - \Omega_2^{(0)}$$

An error signal is produced only if the right hand side of (V.58) varies.

The VCO centerline frequency $\Omega_2^{(0)}$ is controlled by an input voltage from the online computer. An error voltage is generated which acts on the piezoelectric transducer of laser L2 to keep the beat frequency $\omega_1 \cong \Omega_2$. Fig.4.8 shows the frequency spectrum of the locked laser beatnote when no frequency modulation is present. This should be compared to the free running spectrum as shown in Chapter IV. In practice, the outer loop time constant was $\sim$.1 sec, since the extra resolution attainable with .01 sec time constant was unnecessary in the present experiment. In this case, the jitter was a few kHz, well below the 70 kHz p-p frequency modulation which was utilized to obtain the derivative spectra.

Appendix 5.1 shows the actual circuit diagrams utilized in the locking system.

CHAPTER VI

N_2O HYPERFINE STRUCTURE

1. Data and Qualitative Structure

The copropagating wave spectrometer described above was utilized to study the N_2O hyperfine spectra for a number of ro-vibrational transitions. As stated in Chapter II, the strong wave-weak-wave technique causes the lineshape to be assymmetric with respect to zero beat frequency. The beat frequency cannot be swept through zero in the locked state so the lineshapes were obtained by sweeping the weak laser from $\sim$1000 kHz $\rightarrow$ 50 kHz with respect to the strong laser starting at either high or low relative frequency.

During the initial experiments, a telescope (x7) was used to reduce the intensity of the lasers in an attempt to obtain very narrow linewidths. Fig. 6.1 shows the result of a free running sweep with equal (full) power for both lasers (400 mw). The fluorescence cell pressure was $\sim$1μ. As can be seen from the figure, the weak crossing resonances (small bumps) are not saturating, compared to the central resonance at zero beat frequency. This central resonance arises from crossing resonances between M degenerate $\Delta F = -1$ transitions and is uninteresting. In order to improve the relative intensity of the weak resonances,

Figure 6.1. Free Running Sweep of Laser 2 with Respect to Laser 1; P(3); Left 2/3 mtorr; Right 1/2 mtorr.

the power of one of the lasers was reduced. However, the power could not be lowered significantly without reducing the overall signal to an unusable level. Due to the fixed volume viewed by the fluorescence detector, the pressure could not be lowered without considerable loss in signal.

In the next experiments, the telescope was removed in order to enhance the weak resonances. It was clear from the outset that the lineshape would be smeared together by power broadening if equal laser powers were used. This was indeed the case. Instead, one of the lasers was attenuated and the pair of copropagating waves was multiply passed through the fluorescence cell (3 passes). The laser intensity is attenuated only due to passing through the A.R. coated NaCl windows, since the N_2O absorption is $\sim 10^{-6}$/cm mTorr. The cell diameter was sufficiently large (3") that the beams from alternate passes did not overlap in space. A pressure of $\sim$ 4μ was used to increase the signal size. (Note that the mean free path at this pressure was $\lesssim$1 cm while the beam spacings were > 2cm.) Fig. 6.2 shows the improvement in the relative size of the weak signal as one of the lasers is attenuated (P(3)). Each of the lineshapes is the result of an average of 20 sweeps corresponding to a total integration time of 1 1/2 hrs. This was necessary since the total signal after lock-in detection was only a few microvolts, giving a single sweep signal to noise ratio of only $\sim$3:1. (The detector noise prior to lock-in

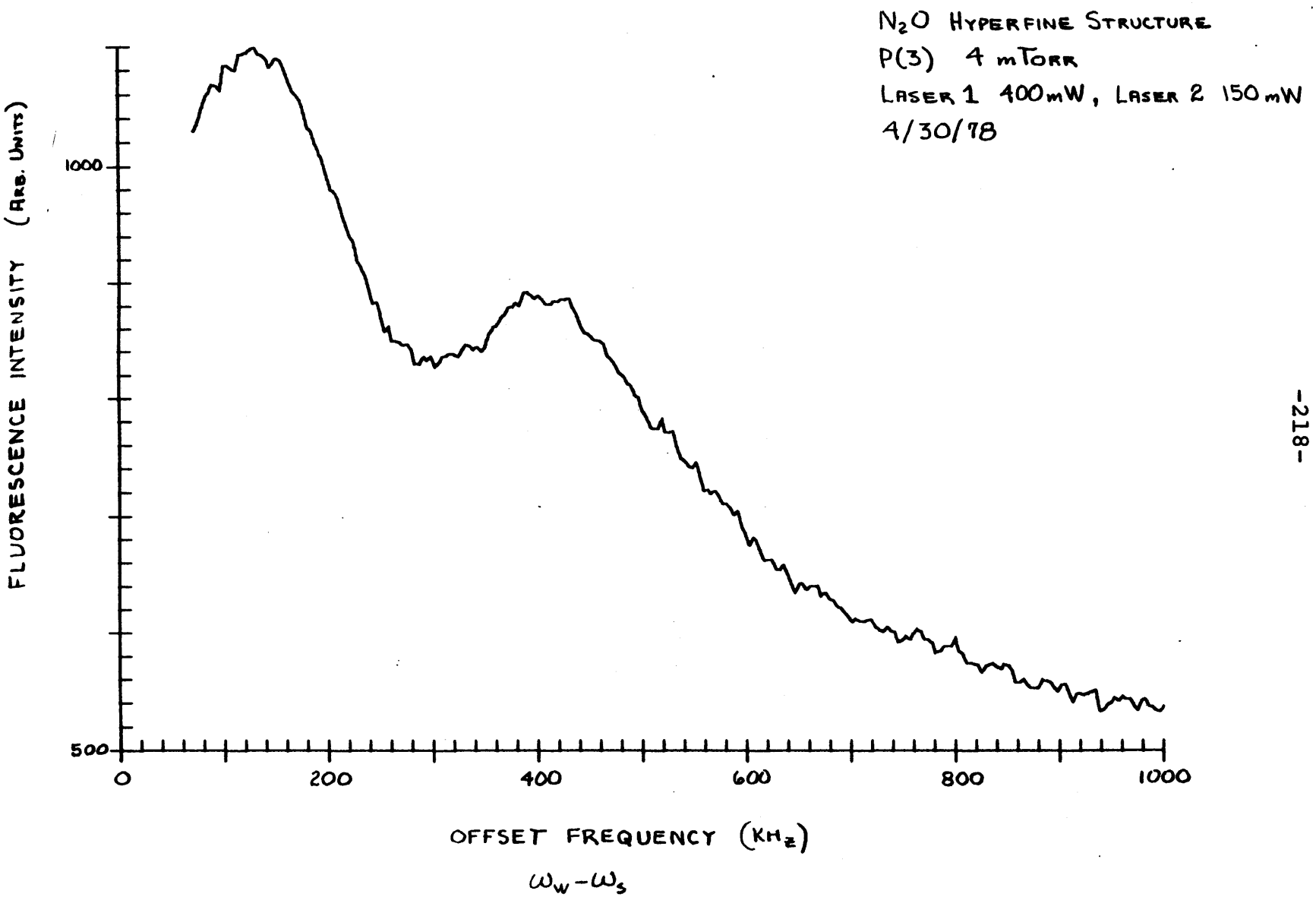

Figure 6.2a (a-d) Strong-Wave-Weak-Wave Lineshapes for P(3) as Weak-Wave Intensity is Reduced. (Note: ω_w = weak laser frequency, etc.) See Fig. 6.3, 6.4 for Laser 2 power = 20 mW.

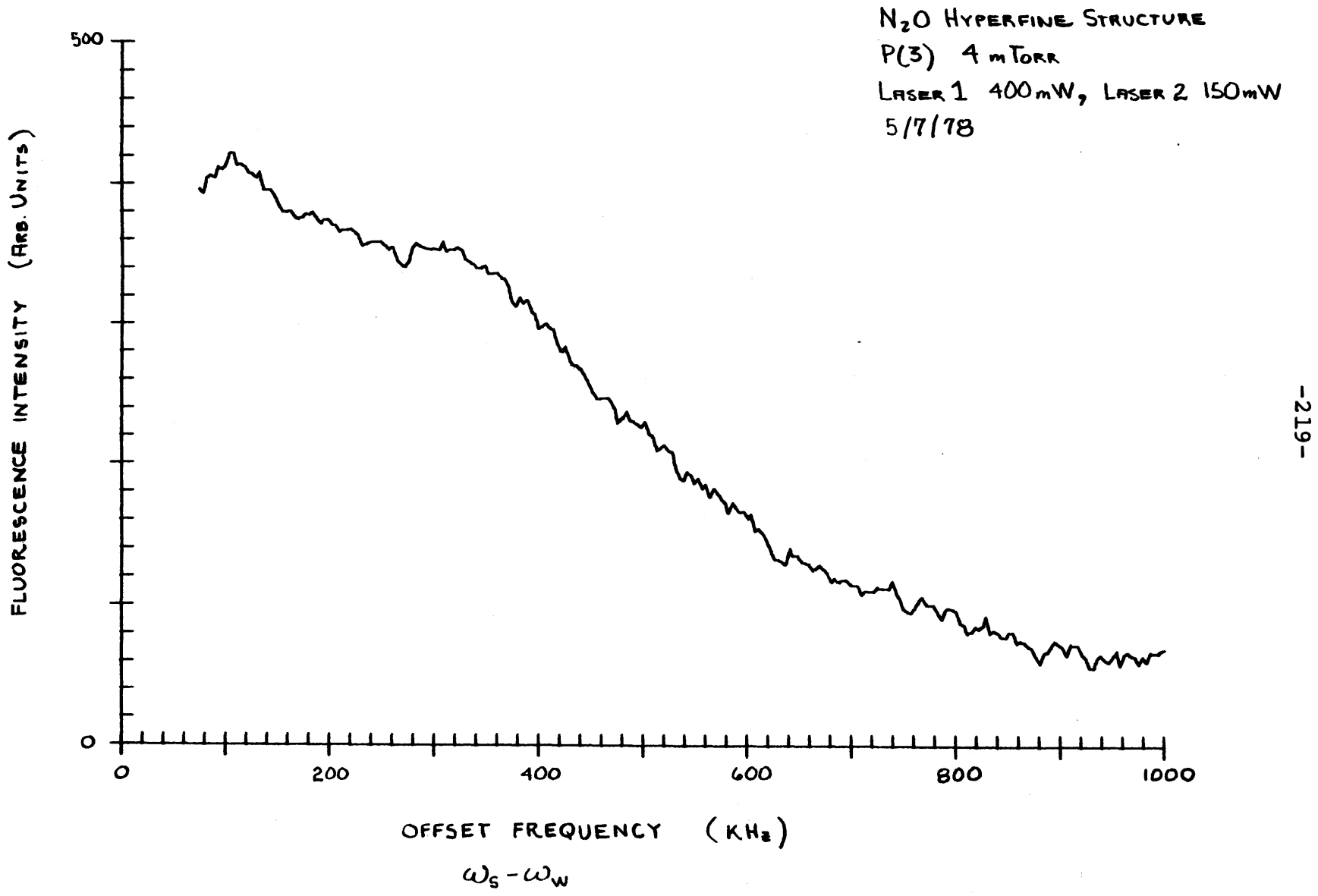
N_2O Hyperfine Structure
P(3) 4 mTorr
Laser 1 400mW, Laser 2 150mW
5/7/78
500
0
Fluorescence Intensity (Arb. Units)
0
200
400
600
800
1000
Offset Frequency (KHz)
$\omega_s - \omega_w$

Figure 6.2b

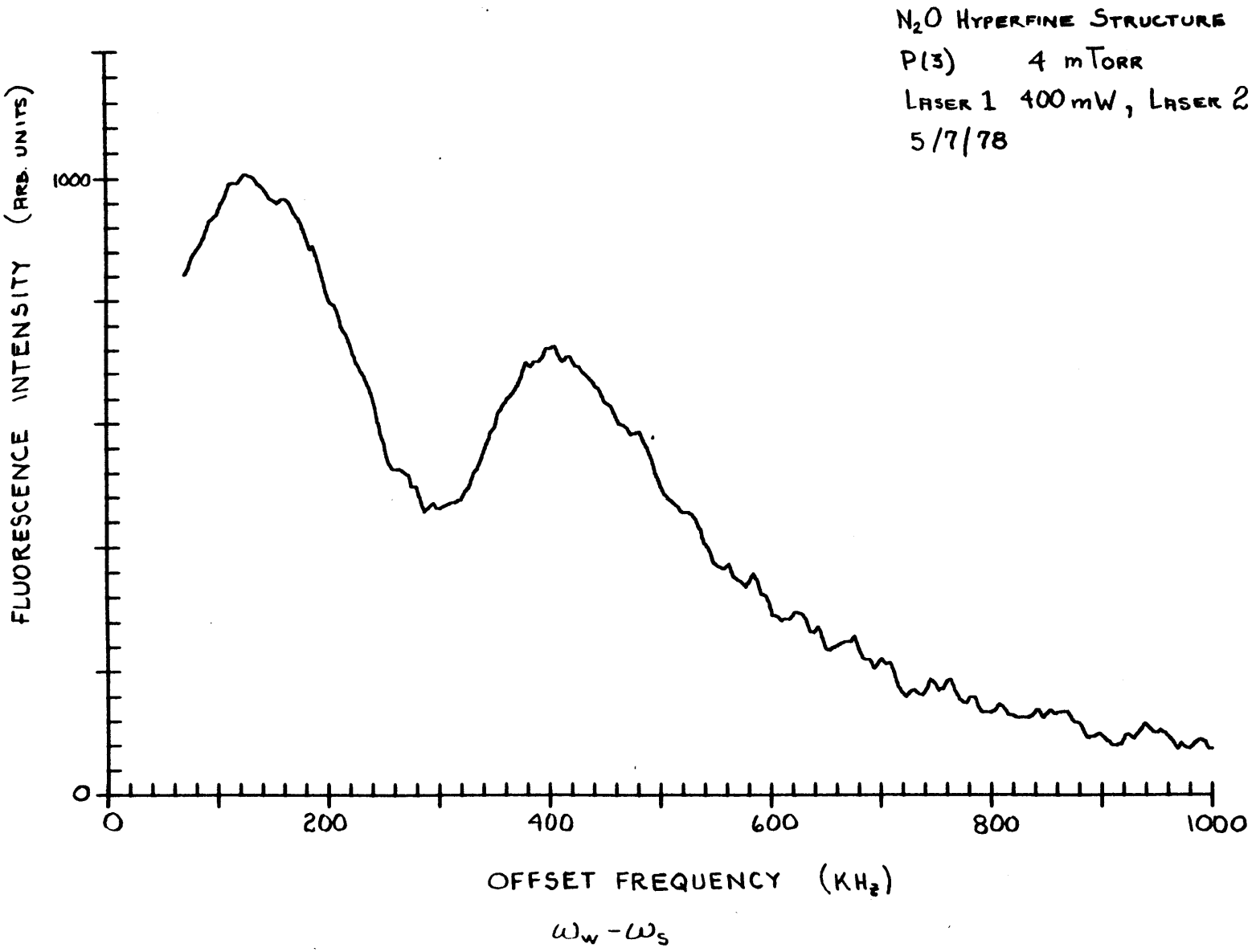
N_2O Hyperfine Structure
P(3) 4 mTorr
Laser 1 400 mW, Laser 2 50 mW
5/7/78
FLUORESCENCE INTENSITY (ARB. UNITS)
1000
0
0
200
400
600
800
1000
OFFSET FREQUENCY (KH_z)
$\omega_w - \omega_s$

Figure 6.2c

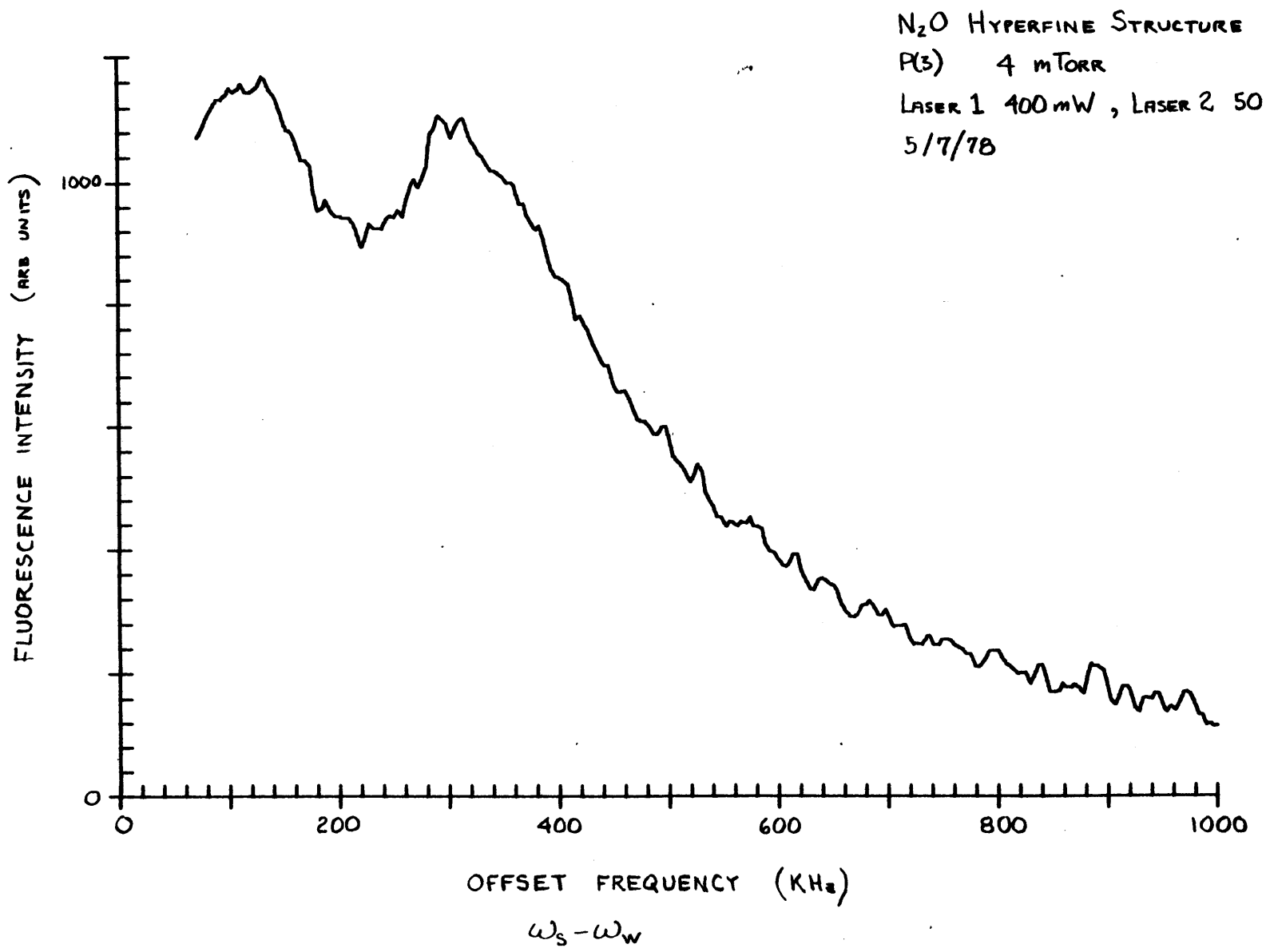
N_2O Hyperfine Structure
P(3) 4 mTorr
Laser 1 400 mW , Laser 2 50 mW
5/7/78
FLUORESCENCE INTENSITY (ARB UNITS)
1000
0
0
200
400
600
800
1000
OFFSET FREQUENCY (KH_z)
$\omega_s - \omega_w$

Figure 6.2d

detection was ∿50 - 80 μv).

The above technique was used to obtain the lineshape for 5 rotational vibrational transitions in N_2O. Figs. 6.3 → 6.12 show the data obtained. From a qualitative analysis of the lineshapes important information may be obtained immediately.

Consider the lineshapes for P(3). The side with the weak laser at high frequency relative to the strong laser has the larger splitting. This requires that the outer N nucleus coupling constant (eqQ) must be negative as shown in Fig. 6.13. The inner N nucleus coupling does not alter this result, provided that its coupling is smaller than that of the outer N nucleus. This is most easily understood by considering the perturbation limit where the levels may be labelled approximately by F and F_1. Here $F_1 = J + I_1$ and $F = F + I_2$, where I_1, I_2 are the spins of the outer and inner N nuclei respectively. The strong transitions require $\Delta F = \Delta F_1 = \Delta J$. Only strong transitions can give significant crossing resonance signals with weak transitions since the resonance requires that the weak laser interact with the strong transition. The important weak transitions with the largest splittings require $\Delta F = \Delta F_1 = 0$. (The $\Delta F = 0$, $\Delta F_1 = \Delta J$ transitions give splittings primarily due to the inner nucleus coupling). An examination of the level structure for the ground state shown in Fig. 1.2 shows that transitions with $\Delta F = \Delta F_1$ give roughly the same frequencies as the unperturbed levels.

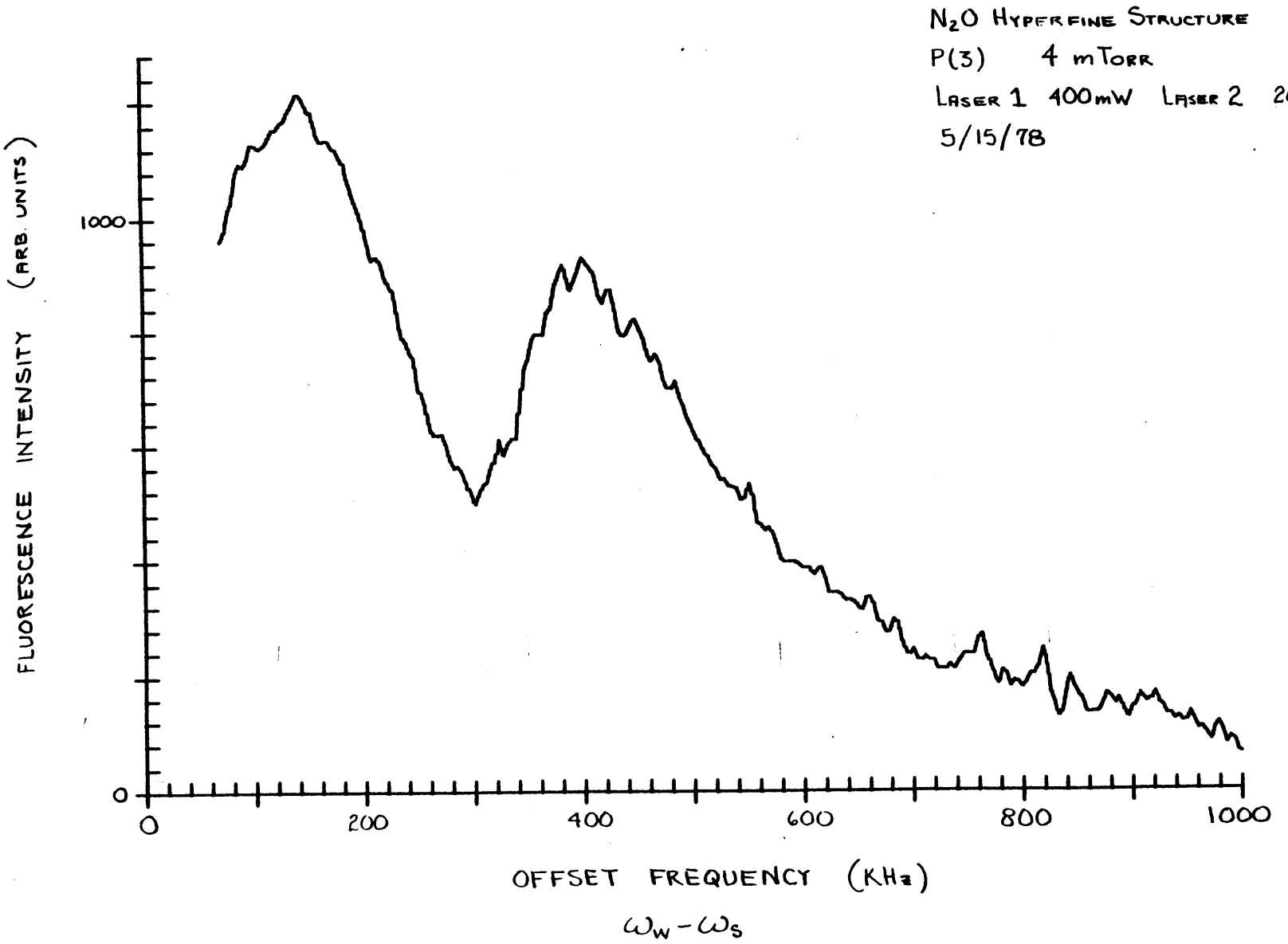
N_2O Hyperfine Structure
P(3) 4 mTorr
Laser 1 400mW Laser 2 20 mW
5/15/78
FLUORESCENCE INTENSITY (ARB. UNITS)
1000
0
0
200
400
600
800
1000
OFFSET FREQUENCY (KHz)
$\omega_W - \omega_S$

Figure 6.3.

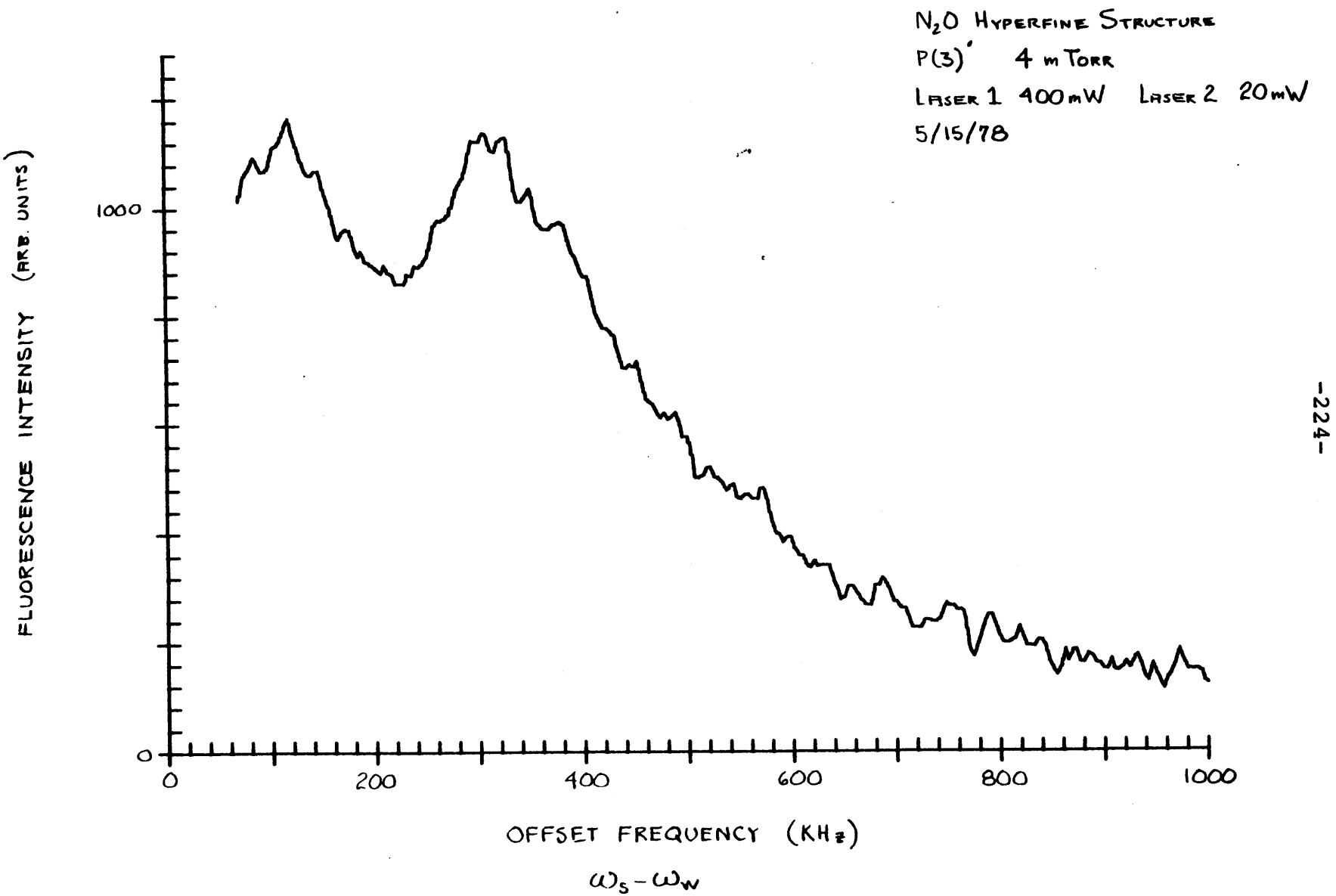
N_2O Hyperfine Structure
P(3)' 4 m Torr
Laser 1 400 mW Laser 2 20 mW
5/15/78
Fluorescence Intensity (arb. units)
1000
0
0
200
400
600
800
1000
Offset Frequency (KHz)
$\omega_s - \omega_w$

Figure 6.4.

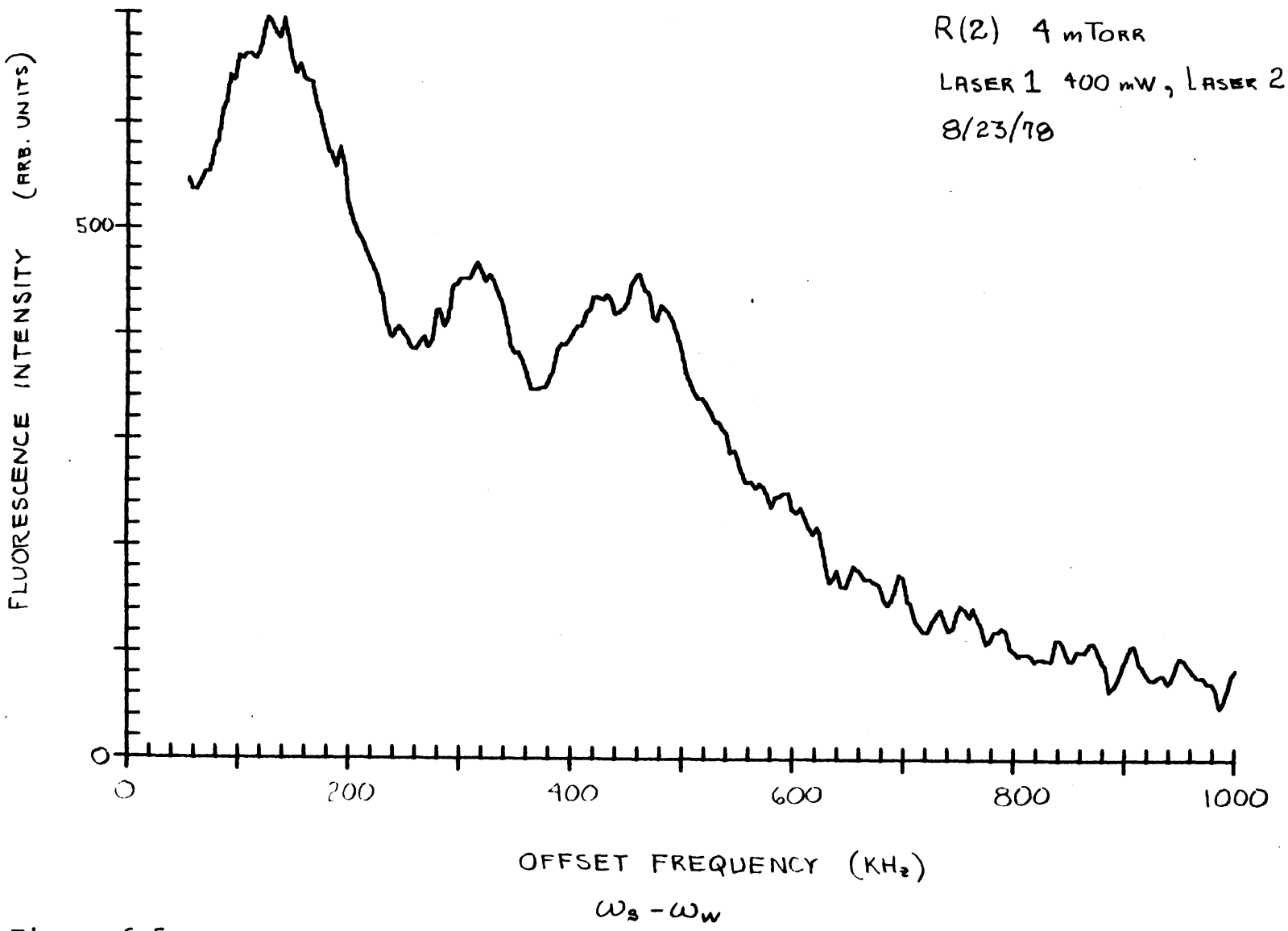
N_2O Hyperfine Structure
R(2) 4 mTorr
Laser 1 400 mW, Laser 2 20mW
8/23/78
Fluorescence Intensity (arb. units)
500
0
0
200
400
600
800
1000
Offset Frequency (KH_z)
$\omega_s - \omega_w$

Figure 6.5.

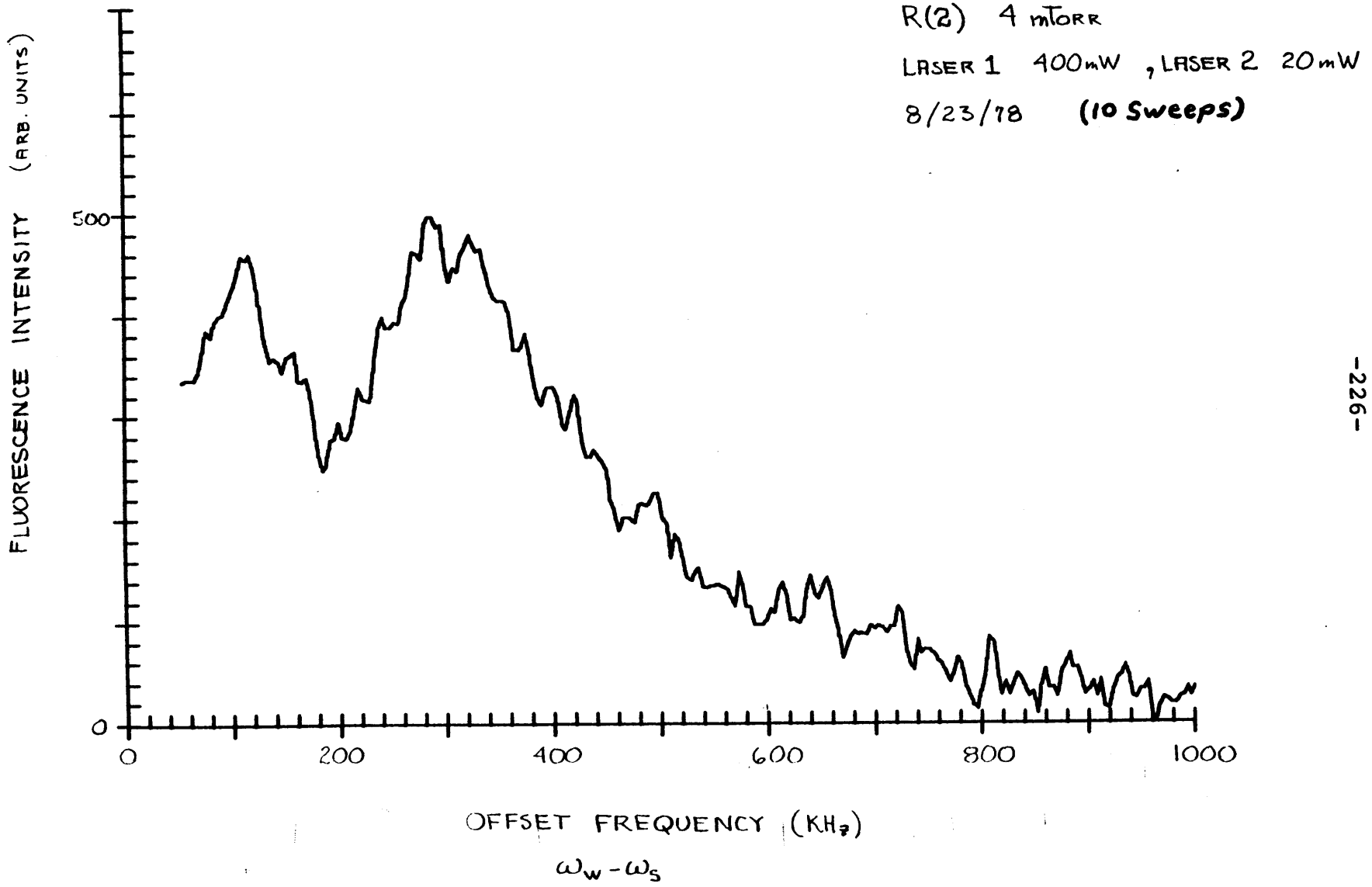
N_2O Hyperfine Structure
R(2) 4 mTorr
Laser 1 400mW , Laser 2 20mW
8/23/78 (10 Sweeps)
Fluorescence Intensity (arb. units)
500
0
0
200
400
600
800
1000
Offset Frequency (KHz)
$\omega_w - \omega_s$

Figure 6.6.

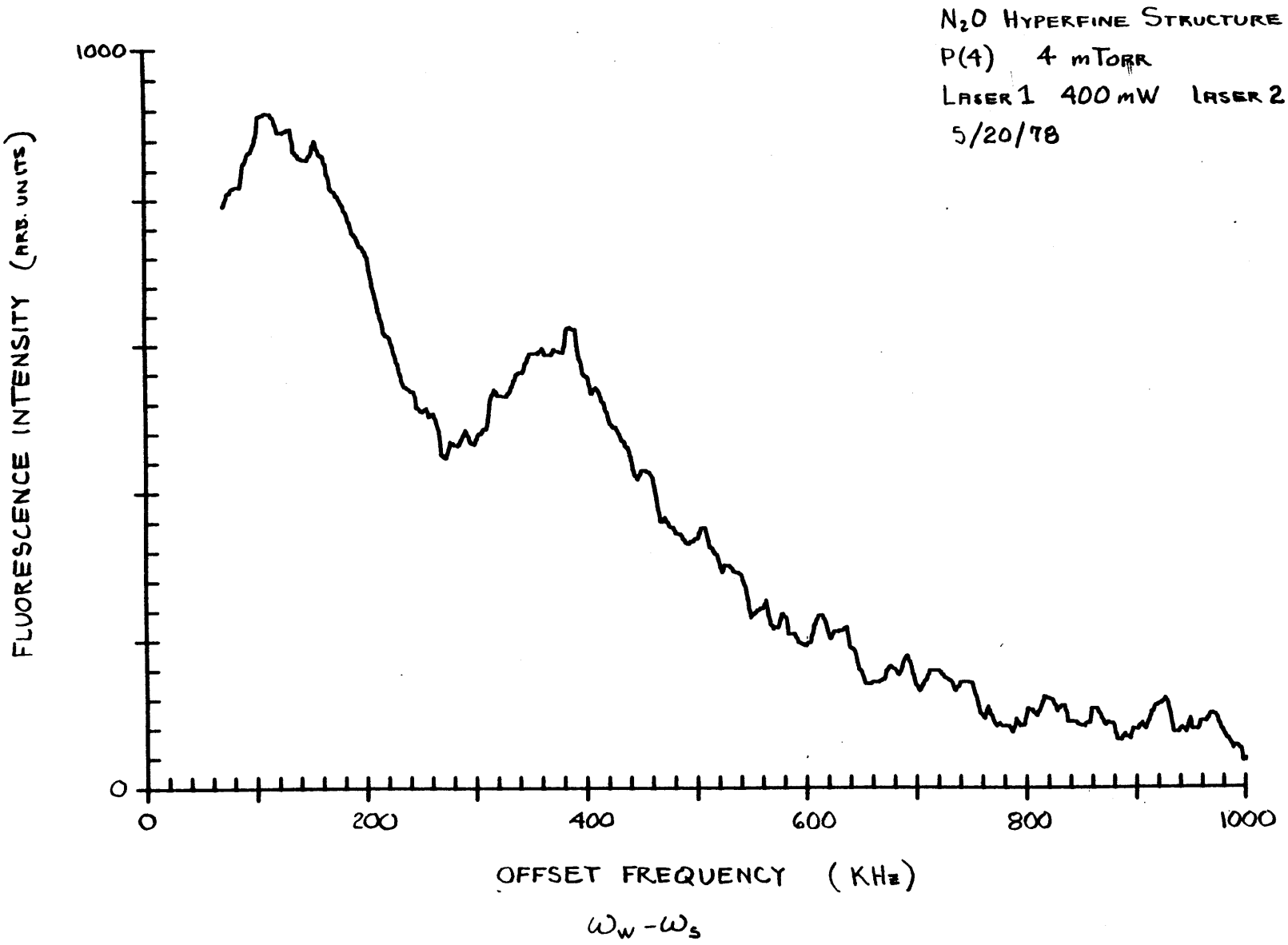
N_2O Hyperfine Structure
P(4) 4 mTorr
Laser 1 400 mW Laser 2 25mW
5/20/78
1000
0
Fluorescence Intensity (arb. units)
0
200
400
600
800
1000
Offset Frequency (KHz)
$\omega_w - \omega_s$

Figure 6.7.

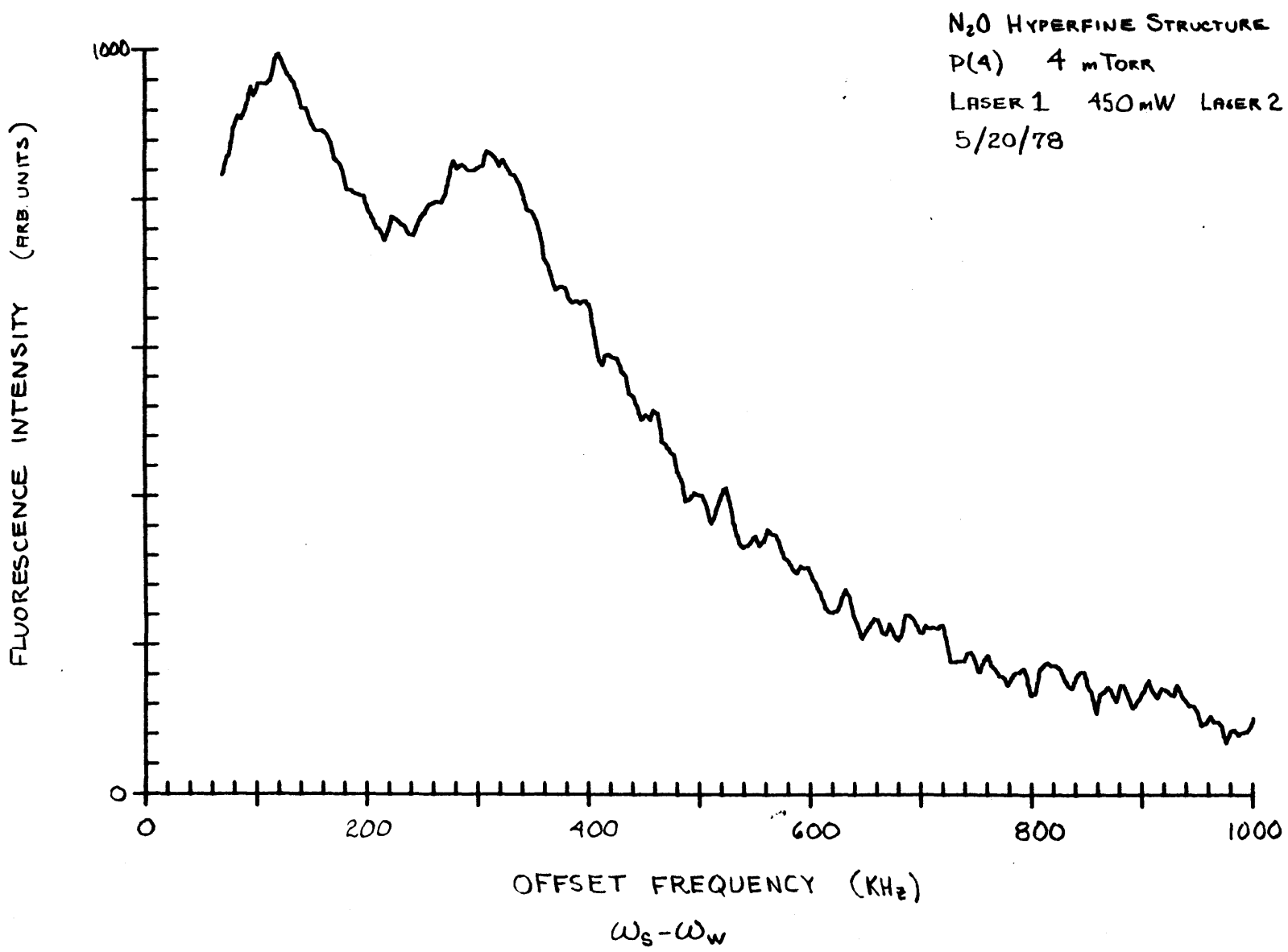
N_2O Hyperfine Structure
P(4) 4 mTorr
Laser 1 450mW Laser 2 24mW
5/20/78
Fluorescence Intensity (arb. units)
1000
0
0
200
400
600
800
1000
Offset Frequency (KH_z)
$\omega_s - \omega_w$

Figure 6.8.

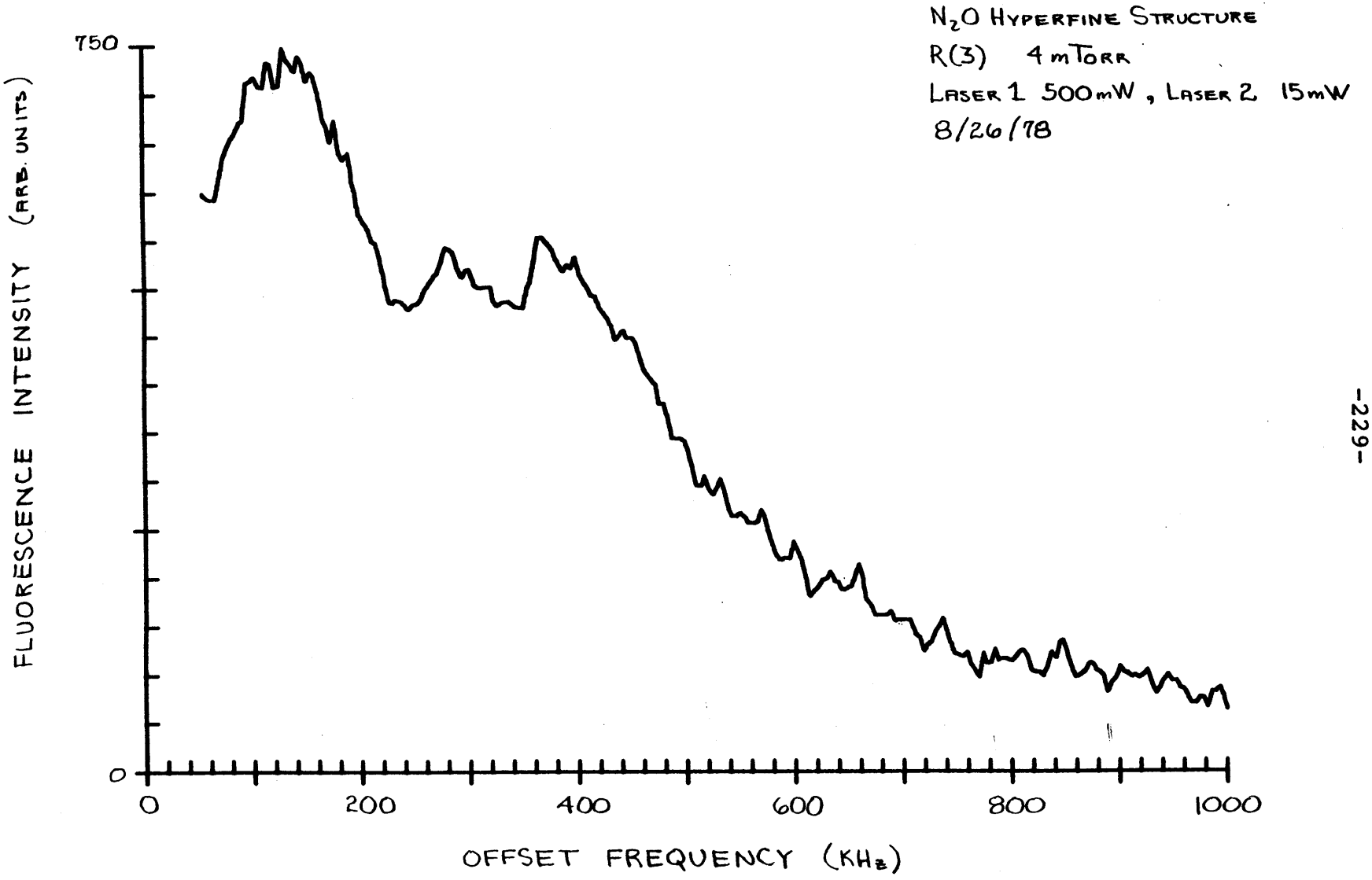
N_2O Hyperfine Structure
R(3) 4 mTorr
Laser 1 500mW, Laser 2. 15mW
8/26/78
750
0
Fluorescence Intensity (arb. units)
0
200
400
600
800
1000
Offset Frequency (KH_z)
$\omega_s - \omega_w$

Figure 6.9.

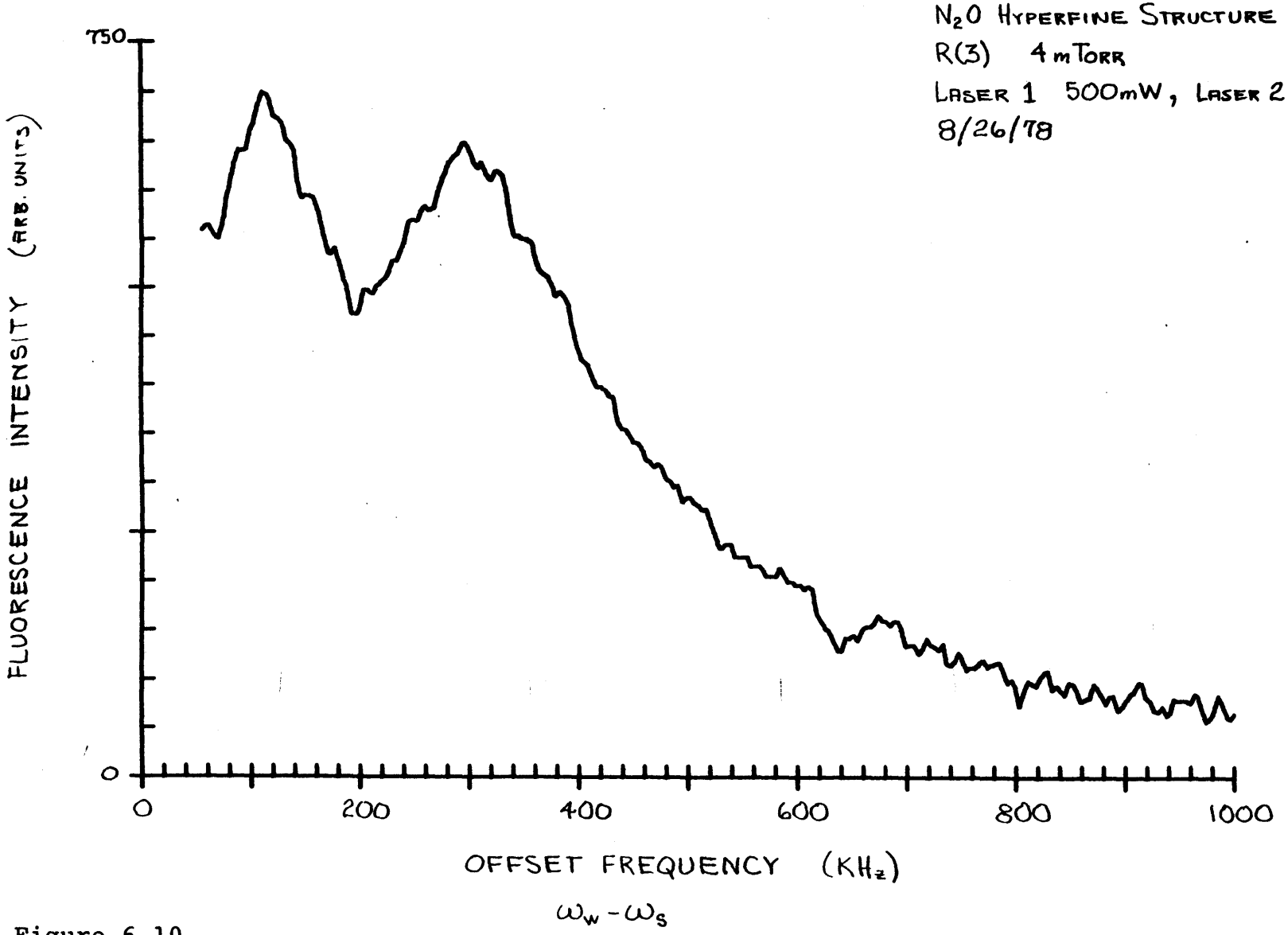
N_2O Hyperfine Structure
R(3) 4 mTorr
Laser 1 500mW, Laser 2 15mW
8/26/78
750
0
FLUORESCENCE INTENSITY (ARB. UNITS)
0
200
400
600
800
1000
OFFSET FREQUENCY (KHz)
$\omega_w - \omega_s$

Figure 6.10.

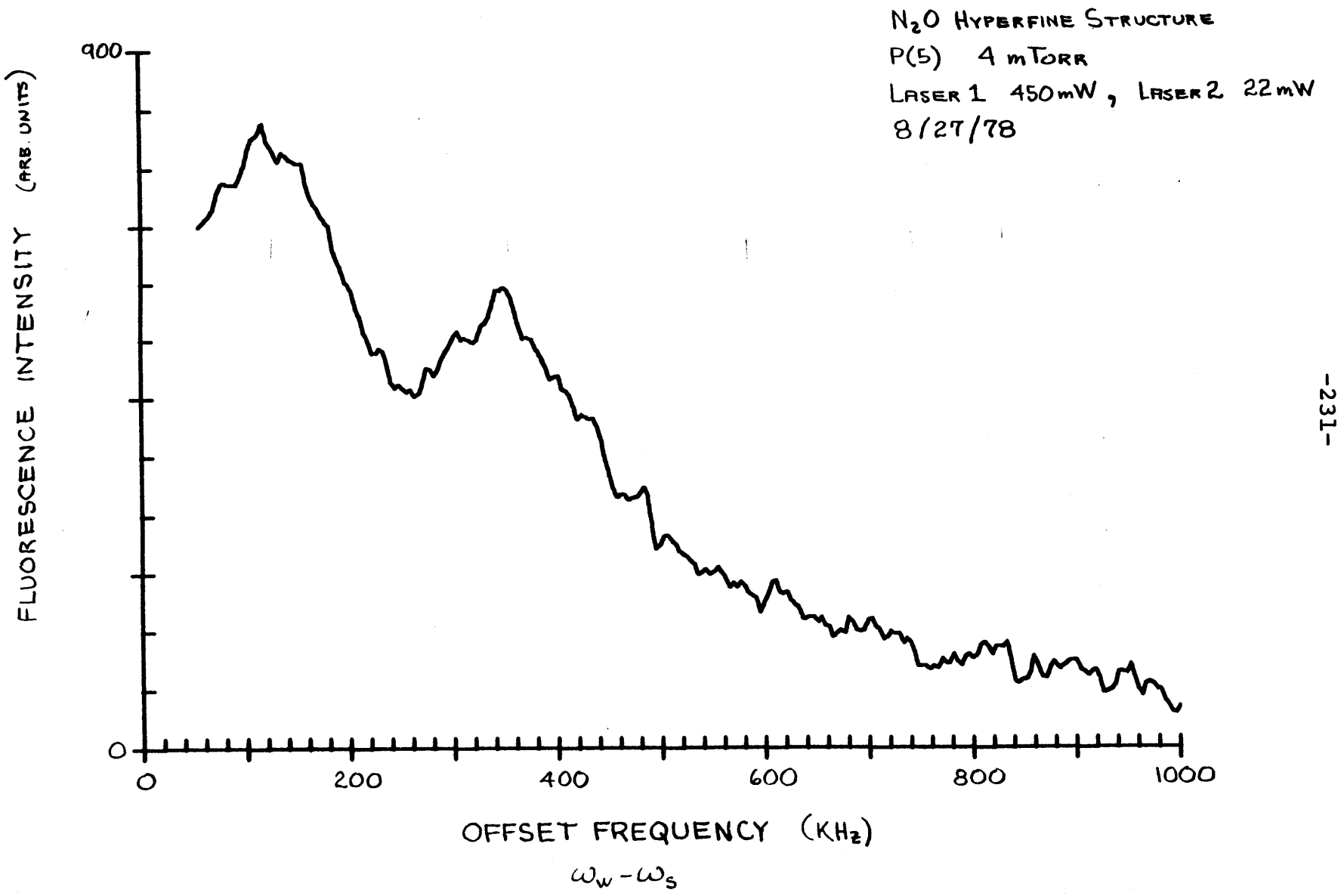
N_2O Hyperfine Structure
P(5) 4 mTorr
Laser 1 450mW, Laser 2 22mW
8/27/78
900
0
Fluorescence Intensity (arb. units)
0
200
400
600
800
1000
Offset Frequency (KH_z)
$\omega_w - \omega_s$

Figure 6.11.

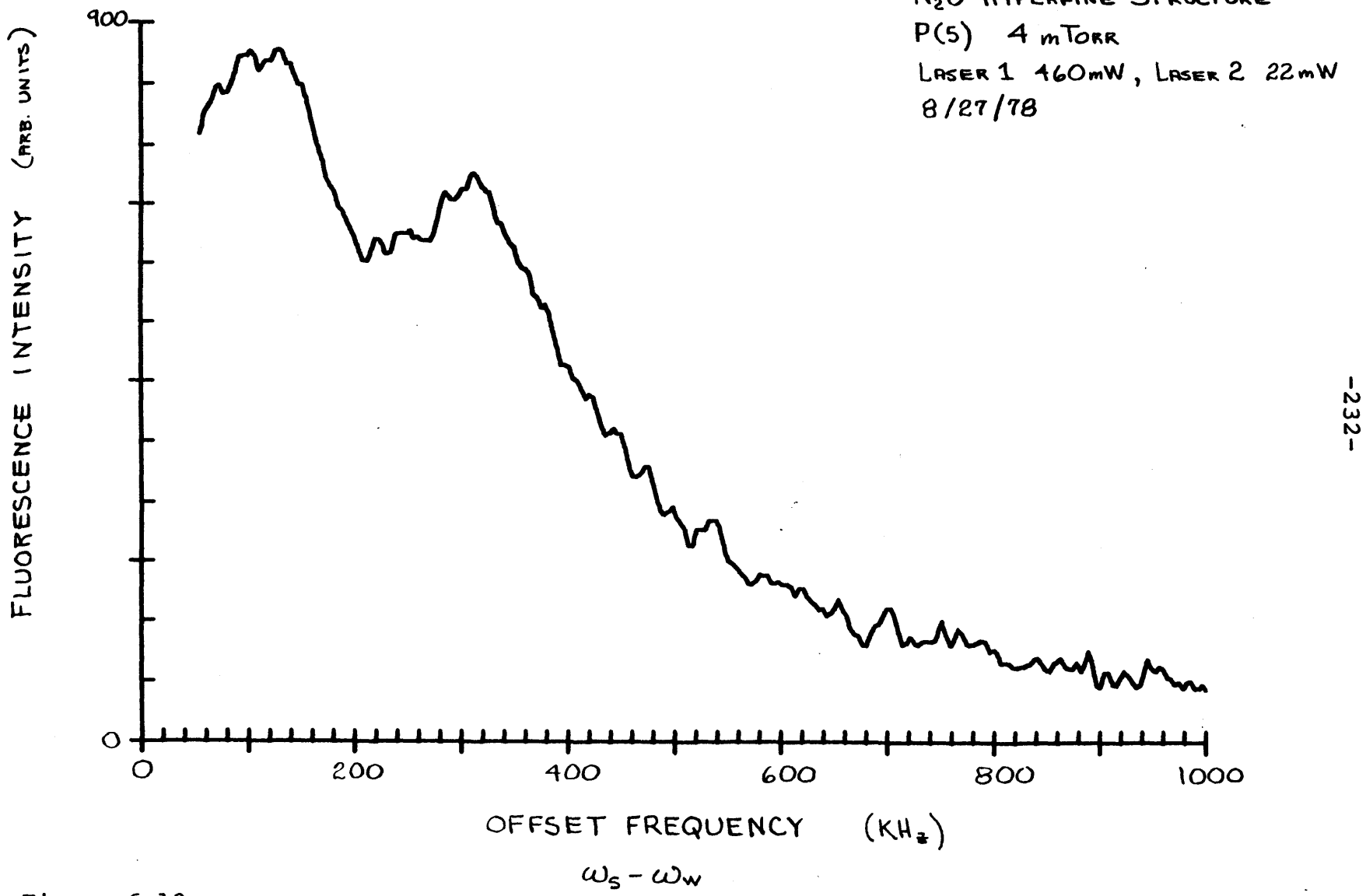
N_2O Hyperfine Structure
P(5) 4 mTorr
Laser 1 460mW, Laser 2 22mW
8/27/78
900
0
FLUORESCENCE INTENSITY (ARB. UNITS)
0
200
400
600
800
1000
OFFSET FREQUENCY (KHz)
$\omega_s - \omega_w$

Figure 6.12.

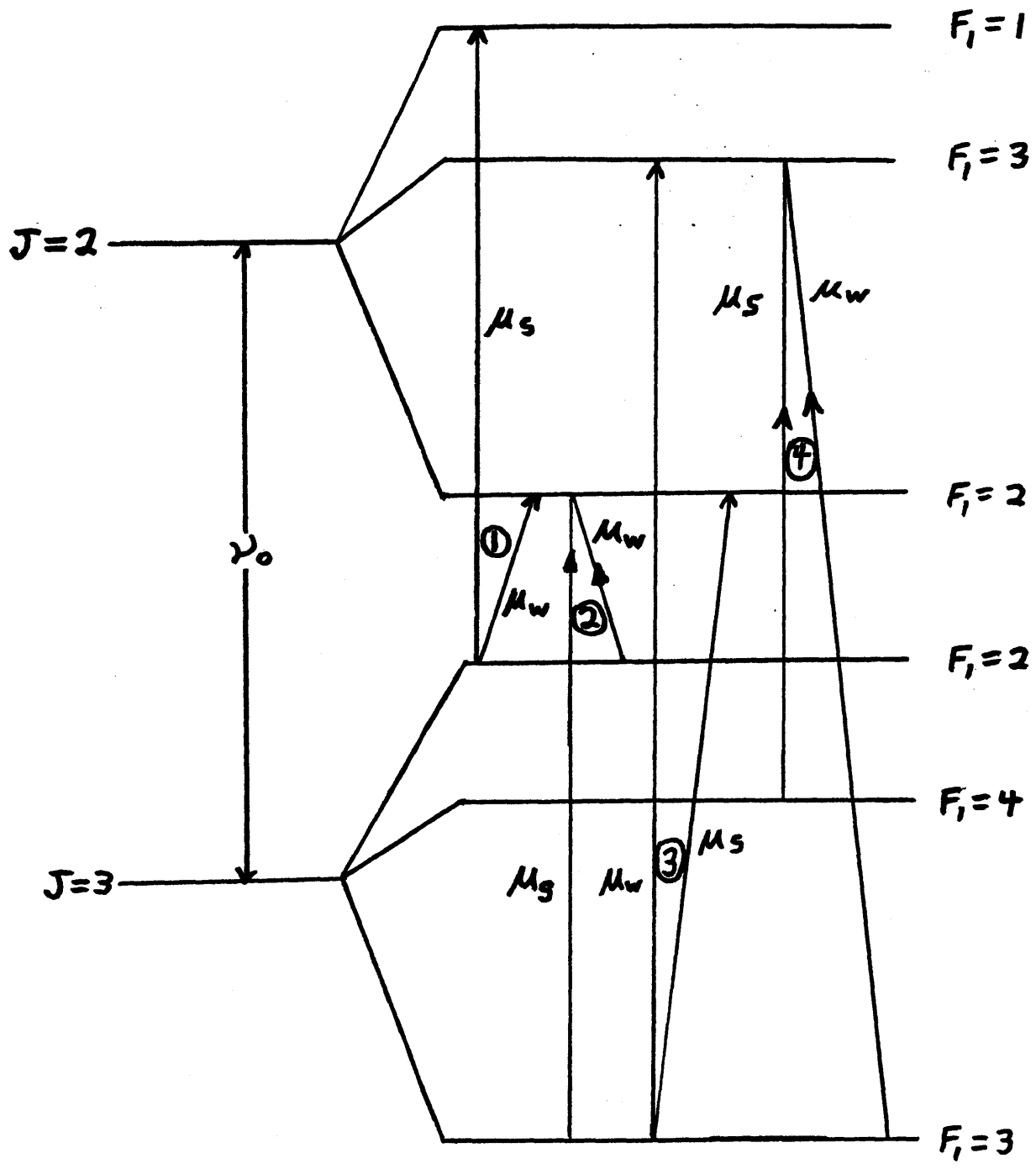

Figure 6.13. Simplified P(3) Energy Level Diagram for eqQ < 0 (μ_s = strong transition, μ_w = weak transition) Transitions 1 and 2 contribute when $\omega_w > \omega_s$, 3 and 4 contribute when $\omega_w < \omega_s$

The most important qualitative result is the demonstration of the vibrational effect on the outer nucleus coupling constant. The vibrational effect is manifested in the dramatic difference between the spectra of R(2) and P(3) shown in Figs. 6.3 and 6.5. If the upper and lower vibrational levels have identical coupling constants (eqQ) then the corresponding R and P branch splittings would be identical, except for the obvious interchange of the $\omega_w > \omega_s$ and $\omega_w < \omega_s$ spectra. One can assume that the γ_{ij} for the two vibrationally excited states are roughly equal, since the γ_{ij} are due to the collision broadening of similar levels. For identical upper-lower level coupling constants, the transition matrix elements between two given levels (labelled by their hyperfine splittings) would be independent of their corresponding vibrational states. Hence, the R and P branch patterns would be identical as stated. The difference between Fig. 6.3 and 6.5 may be understood as follows. Suppose that the lower level outer nucleus coupling constant is larger than the upper level constant. The coupling energy may be written in the form $H_Q = (eqQ)g(F_1 J, I_1)$. For lower J, the g function always gives larger splittings. In the P branch, the lower level has the larger J and the larger $|eqQ|$, while the upper level has the smaller J and the smaller $|eqQ|$. The net effect is to give similar splittings as shown by the appearance of the single large peak in Fig. 6.3. For the R branch, the lower level has the lower J and the larger coupling

constant, giving a particularly large splitting, while the upper level has the larger J and the smaller coupling constant giving a particularly small splitting. Thus, the two component structure of the outer peak is resolved in Fig. 6.5. There are, of course, a number of similar frequency transitions contributing to each component due to the effect of the inner N nucleus.

The behavior of P(4) and R(3) is similar to that described above, except that the splittings are smaller due to the increased J values.

2. Detailed Lineshape Analysis

The quantitative analysis of the N_2O hyperfine spectra requires the implementation of a complex computer program which sums up the contributions from the various crossing resonances. Since there are 9 levels to chose from (neglecting M degeneracy!), the number of ways to select 3 level crossing resonances is 729 each for inverted and noninverted $\underline{V}$ configurations. Including M degeneracy means that thousands of transitions must be considered. Fortunately, the selection rules eliminate a large number of the 729 resonances and in addition, many of the transitions are exceedingly weak and may be neglected. With some reasonable approximations, the sums over the M degenerate levels may be done in closed form and the lineshape calculation may be reduced to a tractable length for a moderately fast computer.

The analysis begins with the strong-wave-weak-wave lineshape for a single transition given by Eq. (II.37). Since the exact lineshape is cumbersome in form, the following approximate shape is used

VI.1) $$I \propto \frac{\alpha^2 S}{\sqrt{1+S}} \frac{Q}{\left(\frac{\Delta}{\delta}\right)^2 + \frac{Q^2}{4}} \; ; \; Q = 1+\sqrt{1+S}$$

This use of this lineshape requires the assumption that all the γ's are equal as stated in Chapter II. Since the γ will be a fitting parameter and the rate equation result ($\gamma_{23} \rightarrow \infty$) gives only a factor of two change as the width, with no change in the relative intensities, the choice of the γ's should not be overly critical. Note that the size of γ is collision dominated and both vibrational levels are roughly equivalent, i.e. there are many J levels to which an interacting molecule can relax. Furthermore, the extra S dependence contained in Eq. (II.37) does little to alter the relative intensities, and the Lorentzian squared term (which remains after subtracting out all Lorentzian terms) is small. The important aspect of Eq. (VI.1) is that it contains the effect that for large S, $I \propto \alpha^2$. In the actual fitting procedure $S = S_o \mu_{12}^2$ where μ_{12}^2 is the square of the electric dipole matrix for $\mu_o = 1$. S_o is taken as a fitting parameter.

A considerable reduction in the required computer time can

be obtained by replacing the M degeneracy sums of Eq. (VI.1) by an approximate closed form expression. Noting that $\alpha^2 \propto \mu_{13}^2$, the weak saturation limit S << 1 allows the sums to be done in closed form as computed in Chapter II. For arbitrary S, the extra S dependence (other than $\alpha^2 S$) of Eq. (VI.1) is modelled by replacing S by $\bar{S}$, where

VI.2) $$\bar{S} = S_o \overline{\mu_{12}^2}$$

and

VI.3) $$\overline{\mu_{12}^2} = |\langle 1||\mu||2\rangle|^2 \frac{1}{2F+1} \sum_{M=-F}^{F} \frac{\mu_{12}^2(M)}{|\langle 1||\mu||2\rangle|^2}$$

The sum depends only on Clebsch-Gordon coefficients and for the strong wave $\vec{\mu} \equiv \mu_z \hat{e}_z$. In this form, the sum of the M contributions for a particular crossing resonance depends only on the reduced matrix elements of the coupled transitions (for $\mu_o = 1$). Using the R-P symmetries described in Chapter II, the path is now cleared for a computer fit to the data.

3. Least Squares Fit

A derivative technique is used experimentally to eliminate the Doppler broadened background and to further enhance the narrow weak crossing resonances with respect to the broad central

(zero beat frequency) resonance. Thus, the basic form for the contribution of a single crossing resonance which has been summed over M degeneracy is taken to be

VI.4) $$I = C_1 \mu_{12}^2 \mu_{13}^2 f_{123} \frac{S_o^{3/2}}{\sqrt{1+\bar{S}}} \frac{\bar{Q}\left(\frac{\Delta}{\gamma}\right)}{\left[\left(\frac{\Delta}{\gamma}\right)^2 + \frac{\bar{Q}^2}{4}\right]^2} ; \quad \bar{Q} = 1+\sqrt{1+\bar{S}}$$

where C_1 is an overall scale factor (same for all transitions) and f_{123} is the weighting function obtained by doing the appropriate Clebsch-Gordon M sums as in Chapter II. S_o is a constant which is the same for all transitions. An extra factor of $\sqrt{S_o}$ is added to eliminate the variation in the amplitude of (VI.4) as S_o is changed. Thus, only the relative intensities, determined by $\bar{S}$, μ_{12}^2, μ_{13}^2, are affected by changing S_o. The μ_{ij} are <u>reduced</u> matrix elements (with $\mu_o = 1$ as μ_o is contained in S_o) since the M sums have been done. Δ is given by

VI.5)

a) $\Delta = \Omega_2 - \Omega_1 - \omega_{32}$; V configuration

b) $\Delta = \Omega_2 - \Omega_1 - \omega_{23}$; inverted V configuration

1 = common level

The least squares fitting technique requires the derivatives of (VI.4) with respect to the fitting parameters. As will be seen below, only first derivatives are needed. A seven parameter fit is required. These are the upper and lower level, inner and outer

N nucleus generalized coupling a(J) and γ, S_o, C_1. Note that the coupling constant dependence is contained in $\omega_{32}(\omega_{23})$ and in the reduced matrix elements. In order to perform the differentiation, the derivatives of I with respect to C_1, $\bar{S}$, γ, $\bar{\mu}_{13}^2$ and ω_{32} are calculated first. Then the chain rule is utilized to generate the required parameter derivatives. The derivatives of $\omega_{32}(\omega_{23})$ and the μ_{ij}^2 with respect to the coupling constants are calculated numerically. In addition, the sign change $\omega_{32} \to \omega_{23}$ for inverted V is taken into account by incorporating an overall minus sign into the lower vibrational level eigenvalues and their parameter derivatives.

The least squares fit requires the minimization of χ^2 defined by

VI.6) $$\chi^2 = \sum_i \frac{1}{\sigma_i^2} [y_i - y(x_i)]^2$$

$y(x_i)$ is the theoretical lineshape and y_i is the experimental value at $x = x_i$. σ_i is the estimated uncertainty in the value of y_i.

For a particular set of parameters near the minimum, $y(x_i)$ may be written as $y_o(x_i)$, and χ^2 may be expanded in a Taylor series about the given point in parameter space. Hence.

VI.7) $$\chi^2 \cong \chi_o^2 + \sum_j \frac{\partial \chi_o^2}{\partial a^j} \delta a^j + \frac{1}{2} \sum_{jk} \frac{\partial^2 \chi_o^2}{\partial a^j \partial a^k} \delta a^j \delta a^k$$

where $\psi_0 = \psi(y_0)$

The condition that χ^2 be minimized requires that a^K be such that

VI.8) $$\frac{\partial \psi^2}{\partial a^K} = 0$$

From (VI.7), this requires (using $\partial a^j / \partial a^K = \delta^j_K$)

VI.9) $$\frac{\partial \psi_0^2}{\partial a^K} + \sum_j \frac{\partial^2 \psi_0^2}{\partial a^j \partial a^K} \delta a^j = 0$$

Eq. (VI.9) may be written in matrix form as

VI.10) $$\beta = \alpha \, \delta a$$

where $$\beta_K \equiv -\frac{1}{2} \frac{\partial \psi_0^2}{\partial a^K} \quad , \quad \alpha_{ij} \equiv \frac{1}{2} \frac{\partial^2 \psi_0^2}{\partial a^i \partial a^j}$$

(The 1/2 factor is for later convenience.) Matrix inversion then yields δa. This procedure will converge rapidly if the starting point is near the minimum. For points far from the minimum, the second derivatives can cause the search to end at a maximum since $\partial \chi^2 / \partial a^K$ will still be zero. This problem may be remedied by using a gradient search initially. Basically, $\delta \vec{a}$ is taken parallel to minus the gradient which is the direction of steepest descent of χ^2. By starting with the gradient search, the parabolic expansion is used only near a minimum. This allows

a simplification in the form of the α_{ij}. One can evaluate α and β as follows: The β_K are given by

VI.11) $$\beta_k = -\frac{1}{2}\frac{\partial \chi_o^2}{\partial a^k} = \sum_i \frac{1}{\sigma_i^2}(y_i - y_o(x_i))\frac{\partial y_o(x_i)}{\partial a^k}$$

and the α_{jK} are given by

VI.12) $$\alpha_{jk} = \sum_i \frac{1}{\sigma_i^2}\left[\frac{\partial y_o(x_i)}{\partial a^j}\frac{\partial y_o(x_i)}{\partial a^k} - (y_i - y_o(x_i))\frac{\partial^2 y_o(x_i)}{\partial a^j \partial a^k}\right]$$

$$= \frac{1}{2}\frac{\partial^2 \chi_o^2}{\partial a^j \partial a^k}$$

In the linear approximation of y_o, the 2nd derivative term vanishes. Furthermore, near the minimum, $(y_1 - y_o(x_i))$ is small on the average. Thus, α_{jK} is approximated by

VI.13) $$\alpha_{jk} \cong \sum_i \frac{1}{\sigma_i^2}\frac{\partial y_o(x_i)}{\partial a^j}\frac{\partial y_o(x_i)}{\partial a^k}$$

This eliminates the need for second derivatives. The actual fitting technique utilized is a variation of a general fitting program called CURFIT as described in Bevington[1]. This ingeneous program allows one to interpolate between a gradient search and a parabolic fit as required.

It can be shown that the path directions for the gradient search and parabolic expansion are nearly perpendicular to each other so that the optimum path lies between the two extremes.[1]

The CURFIT program takes this fact into account by defining a new matrix α' which is given by

VI.14) $$\alpha'_{jk} = \alpha_{jk}(1 + \lambda\delta_{jk})$$

where λ is a parameter ≥ 0. When λ is large, the diagonal elements of α' dominate, and the matrix equation (VI.10) reduces to

VI.15) $$\beta_j \cong \lambda \alpha_{jj} \delta a_j$$

This yields δa_j which are proportional to the negative gradient components β_j. The program acts like a gradient search with the characteristic length of a_j (for which χ^2 varies significantly) given by $\alpha_{ij}^{-1/2}$ (see Bevington[1] p.217 f.) For large λ, the step size is small.

In actual operation, an initial value of λ is chosen (usually 1). The program decreases λ by a given factor if $\chi^2(a^j + \delta a^j)$ is less than $\chi^2(a^j)$ and increases λ by the same factor if χ^2 has not decreased. As the program begins to home in on the minimum, λ is continually decreased until it is $<< 1$. The parabolic fit is attained to some predetermined accuracy $\Delta\chi^2/\chi^2$. The parameter uncertainties are given by

VI.16) $$\sigma_j = \sqrt{\alpha^{-1}_{jj}}$$

which is the characteristic length in a_j for significant ($\Delta\chi^2 = 1$)

variation of χ^2. The matrix α^{-1} is the inverse matrix of α.

4. Program Operation

The lineshape calculation starts by determining upper and lower vibrational level eigenvalues and eigenfunctions for the initial set of coupling parameters, using the techniques described in Chapter I. The squared (μ_{ij}^2) reduced transition matrix is then calculated using the basis set reduced transition matrix. Following this, each parameter is incremented by 1% (one at a time) and the new eigenvalues and transition matrix are calculated. The approximate derivatives of the eigenvalues and the squared transition matrix are then easily calculated. An overall minus sign is incorporated into the lower level eigenvalues and their derivatives as stated above. Finally, a minimum μ^2 is given and all matrix elements which fall below the minimum are replaced by zero. This is utilized to eliminate unnecessary algebra in the main calculator block. Using the PDP 1145 at the Bates Accelerator facility, the entire set of results described above is calculated nearly instantaneously.

The lineshape and its derivatives are calculated in parallel to reduce computer time. This requires the arrays $y_K(I)$ where $K = 1, 7$ and I is the index labelling the points to be calculated ($I = 1, 255$). Out of the nine upper and nine lower levels, an appropriate set of three levels corresponding to a V or inverted V

configuration is chosen. A check of the transition matrix is made to ensure that the matrix elements for both transitions do not vanish. The total angular momenta of the levels are determined from a previously generated table and used to calculate the weighting function f_{123} of Eq. (VI.4). The value of the function (VI.4) and its derivatives is then summed into each point of the arrays $y_K(I)$.

With the lineshape calculated, the results for χ^2 and its derivatives are easily determined. The new parameters are quickly calculated as described above, and a new lineshape is determined. If χ^2 has decreased, λ is decreased and another new set of parameters is calculated. If χ^2 has increased, λ is increased and the old set of parameters is recalculated. Increasing λ reduces the step size, as well as increasing the percentage of gradient search. For sufficiently large λ, χ^2 decreases and the overall procedure is iterated.

A brief description of each subprogram is given in Table VI.1. The actual Fortran program is given in Appendix 6.1. Figures 6.14-6.23 show the fits obtained. For low J transitions, the fits are quite good. The error bars on the data are of the size required to reduce $\chi^2 \sim 1$ in order to obtain the correct parameter errors. At higher J, the fitting becomes difficult, due to the fact that the $\Delta F = 0$ transitions become very weak. This causes the power broadening of the strong wave interacting with weak transition

TABLE VI.1

CURVE FITTING PROGRAM LIST

1) MAIN HYPFIT

Master program - Reads in data and input files; generates angular momentum tables; controls calculation and fit programs

2) SUBROUTINE FUNCT

Calls ENPAR 1 to calculate eigenvalues, transition matrix, and derivatives of these with respect to generalized coupling constants; Selects 3 levels for resonance (V or inverted V); Calculates weighting function and average μ_{12}^2 ; Calls CALC 1 to calculate contribution of resonance to lineshape and lineshape parameter derivatives.

3) SUBROUTINE ENPAR 1

Calculates eigenvalues, transition matrix and derivatives of these with respect to generalized coupling constants using EIGEN. Eliminates small transition matrix elements.

4) SUBROUTINE EIGEN

Calculates eigenvalues and eigenfunctions given J and coupling constants.

5) SUBROUTINE CALC 1

Calculator block for lineshape and parameter derivatives

6) SUBROUTINE JETFIT

Least squares fitting program analagous to CURFIT described in text; Controlled by HYPFIT.

7) SUBROUTINE MATINV

Called by JETFIT to invert modified curvature matrix α'

8) CHISQE

Calculates χ^2. Called by HYPFIT and JETFIT

Table VI.1 (continued)

9) JETPLO

Prepares theoretical and experimental data for plotting program.

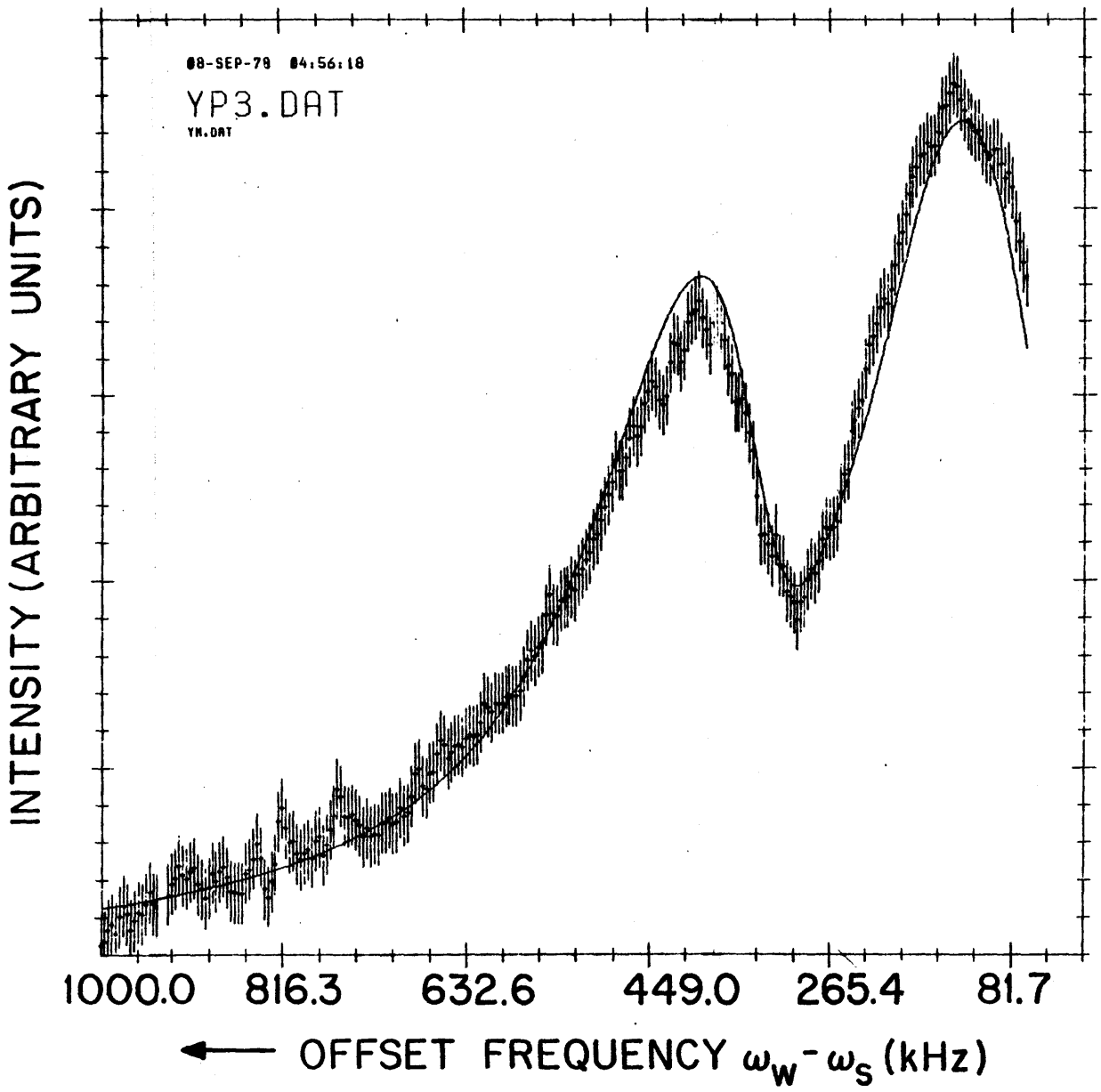
08-SEP-79 04:56:18
YP3.DAT
YM.DAT
INTENSITY (ARBITRARY UNITS)
1000.0
816.3
632.6
449.0
265.4
81.7
OFFSET FREQUENCY $\omega_W - \omega_S$ (kHz)

Figure 6.14.

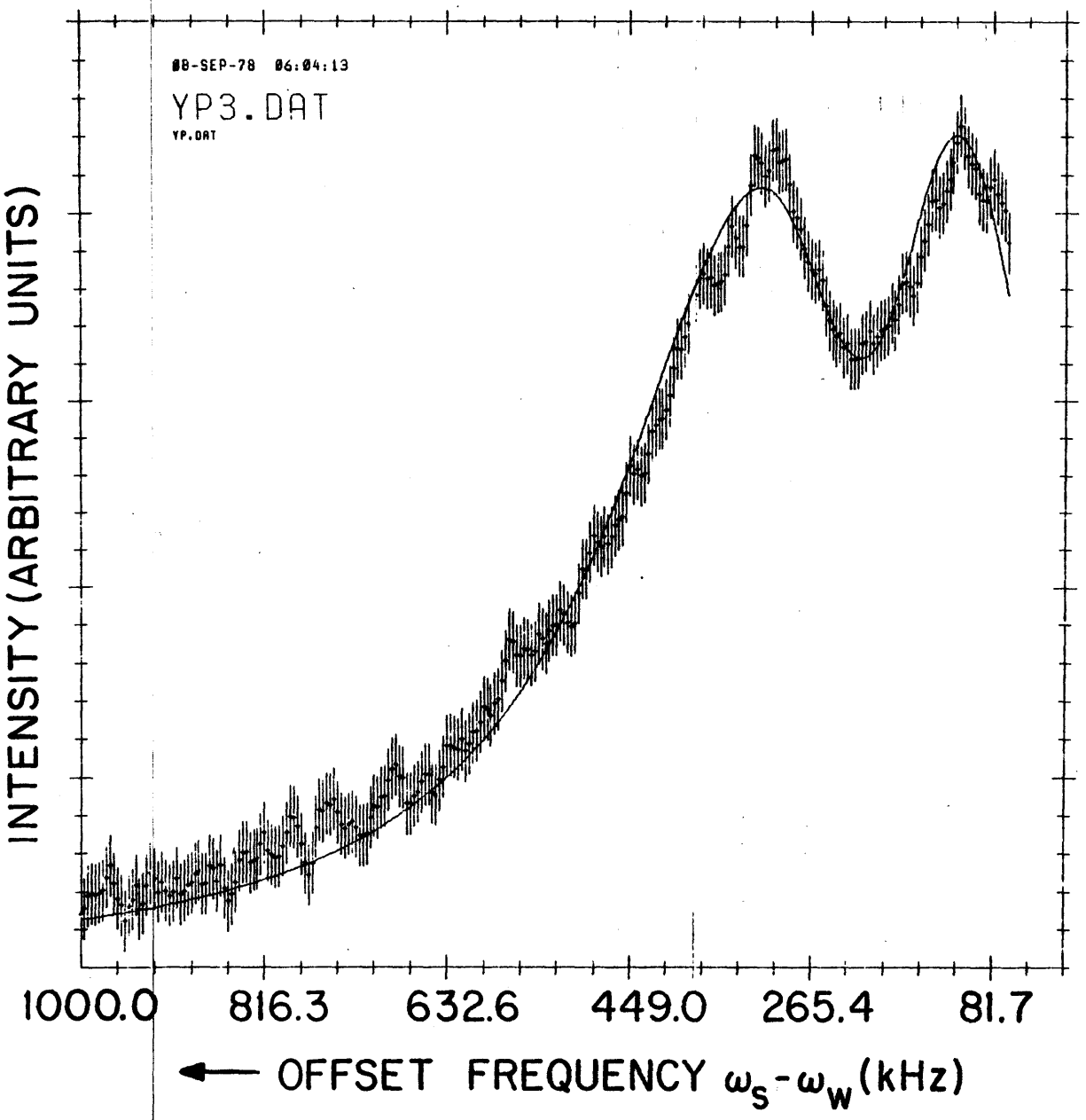
08-SEP-78 06:04:13
YP3.DAT
YP.DAT
INTENSITY (ARBITRARY UNITS)
1000.0
816.3
632.6
449.0
265.4
81.7
← OFFSET FREQUENCY $\omega_s - \omega_w$ (kHz)

Figure 6.15.

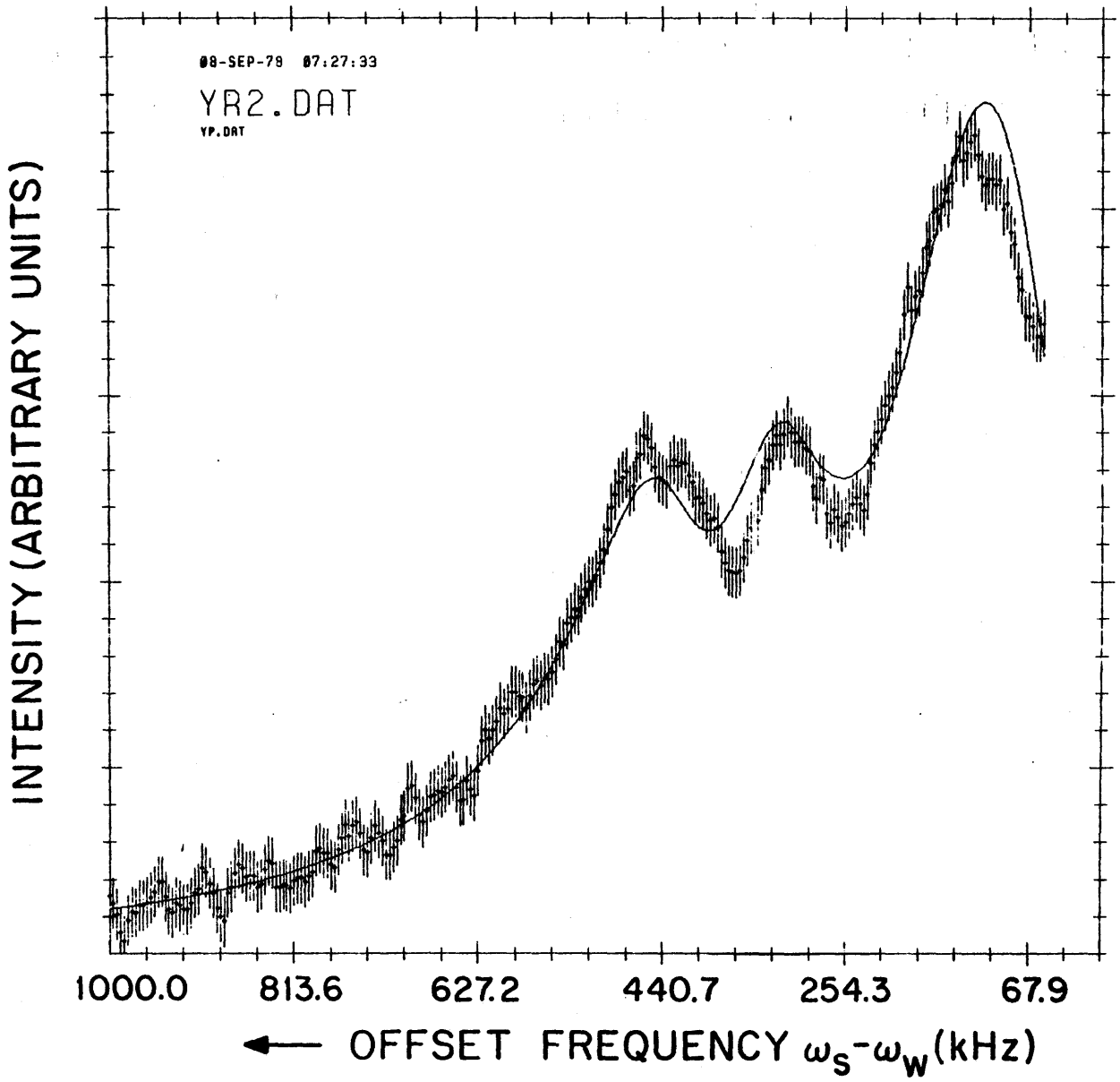
08-SEP-79 07:27:33
YR2.DAT
YP.DAT
INTENSITY (ARBITRARY UNITS)
1000.0
813.6
627.2
440.7
254.3
67.9
OFFSET FREQUENCY $\omega_S-\omega_W$(kHz)

Figure 6.16.

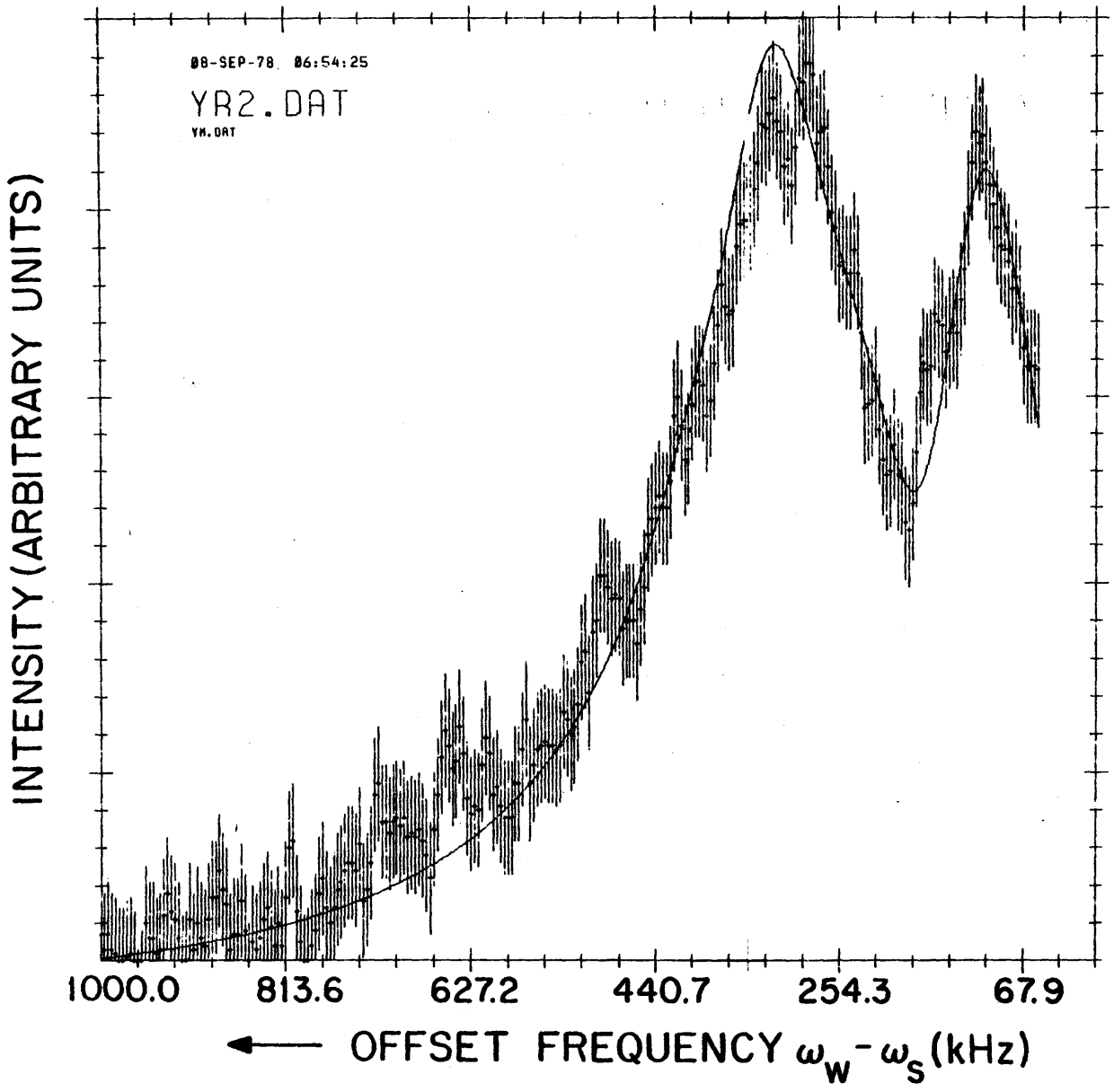
08-SEP-78 06:54:25
YR2.DAT
YM.DAT
INTENSITY (ARBITRARY UNITS)
1000.0
813.6
627.2
440.7
254.3
67.9
OFFSET FREQUENCY $\omega_W - \omega_S$ (kHz)

Figure 6.17.

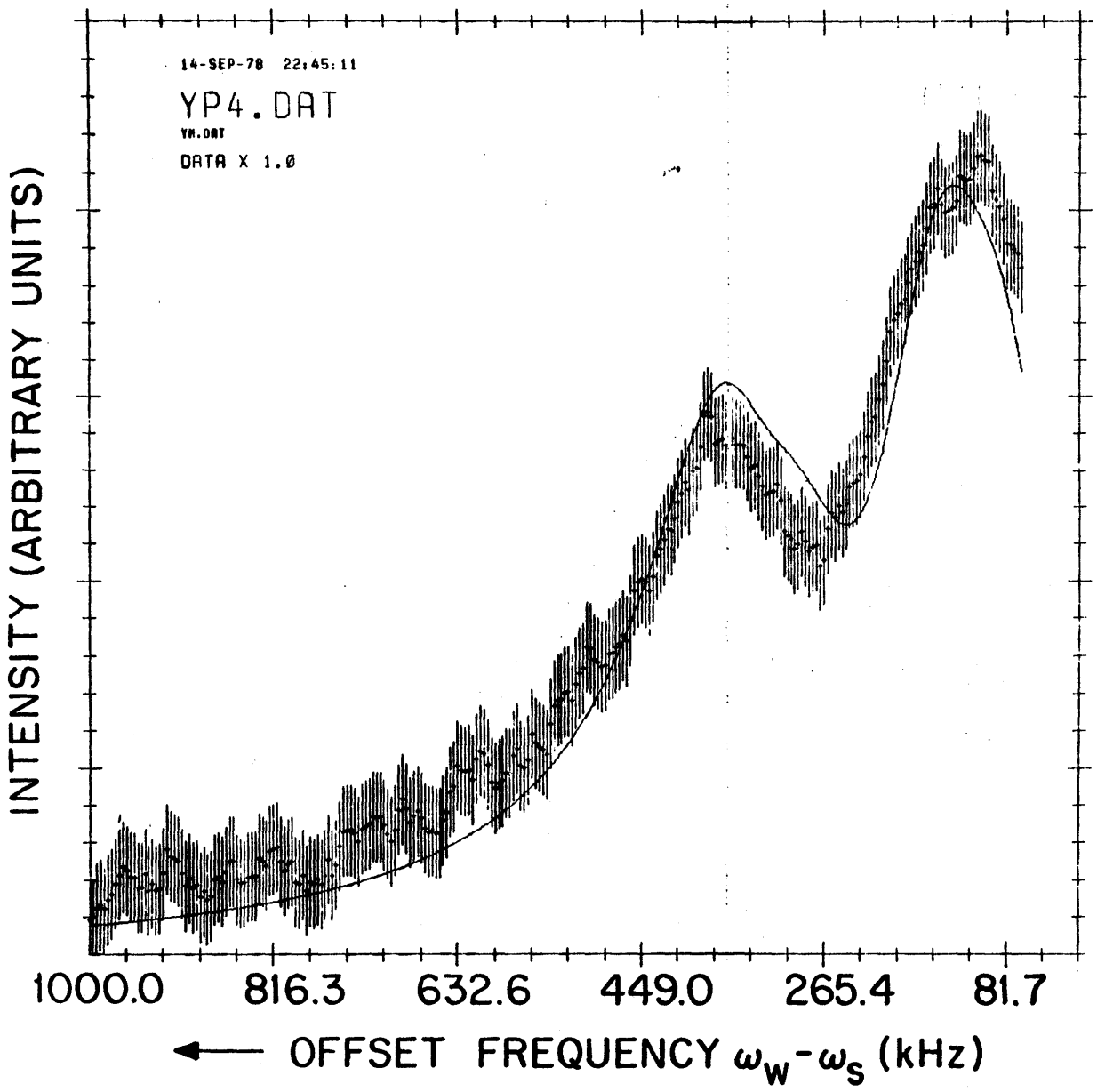
14-SEP-78 22:45:11
YP4.DAT
YN.DAT
DATA X 1.0
INTENSITY (ARBITRARY UNITS)
1000.0
816.3
632.6
449.0
265.4
81.7
OFFSET FREQUENCY $\omega_W - \omega_S$ (kHz)

Figure 6.18.

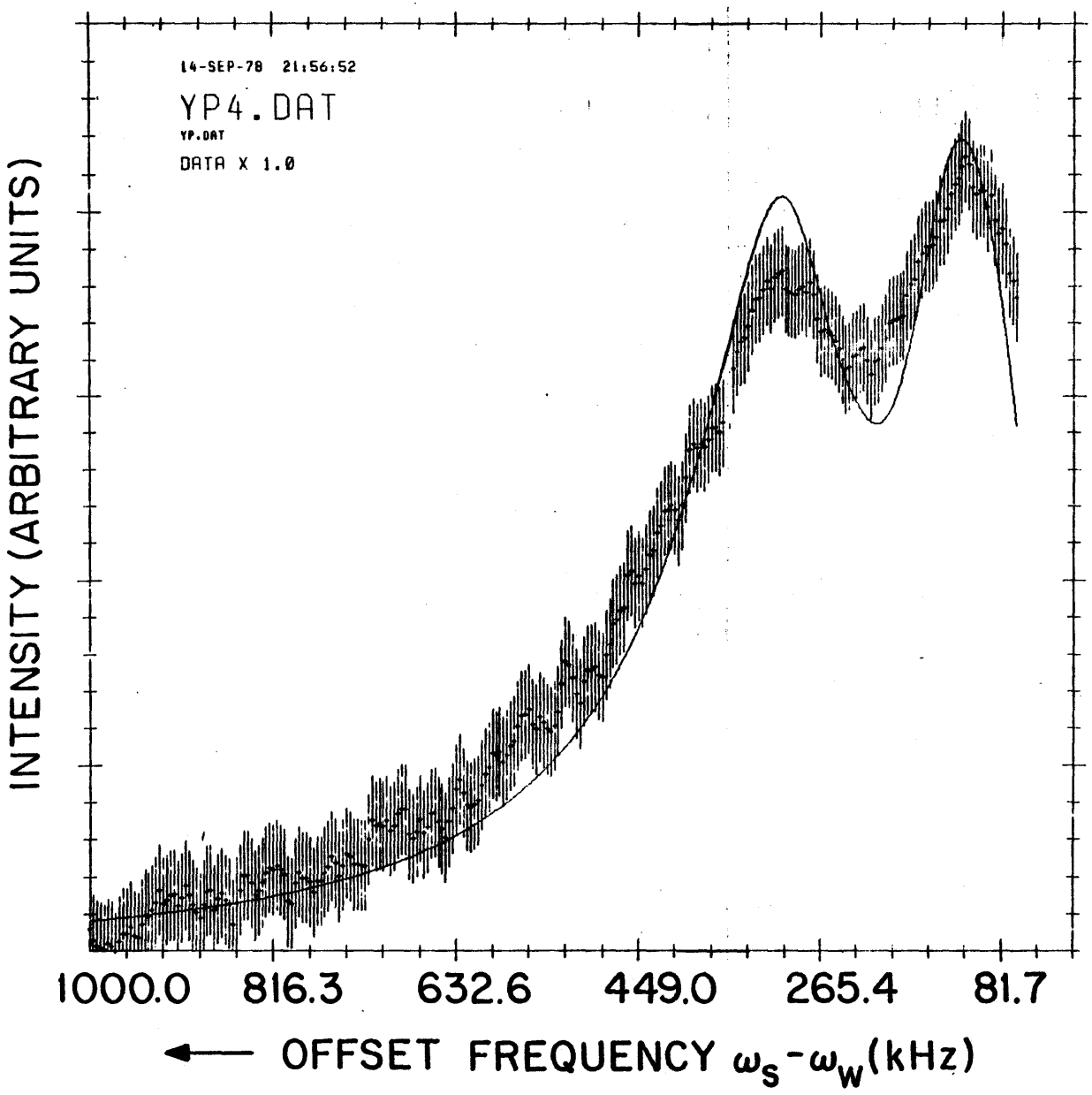
14-SEP-78 21:56:52
YP4.DAT
YP.DAT
DATA X 1.0
INTENSITY (ARBITRARY UNITS)
1000.0
816.3
632.6
449.0
265.4
81.7
OFFSET FREQUENCY $\omega_s - \omega_w$(kHz)

Figure 6.19.

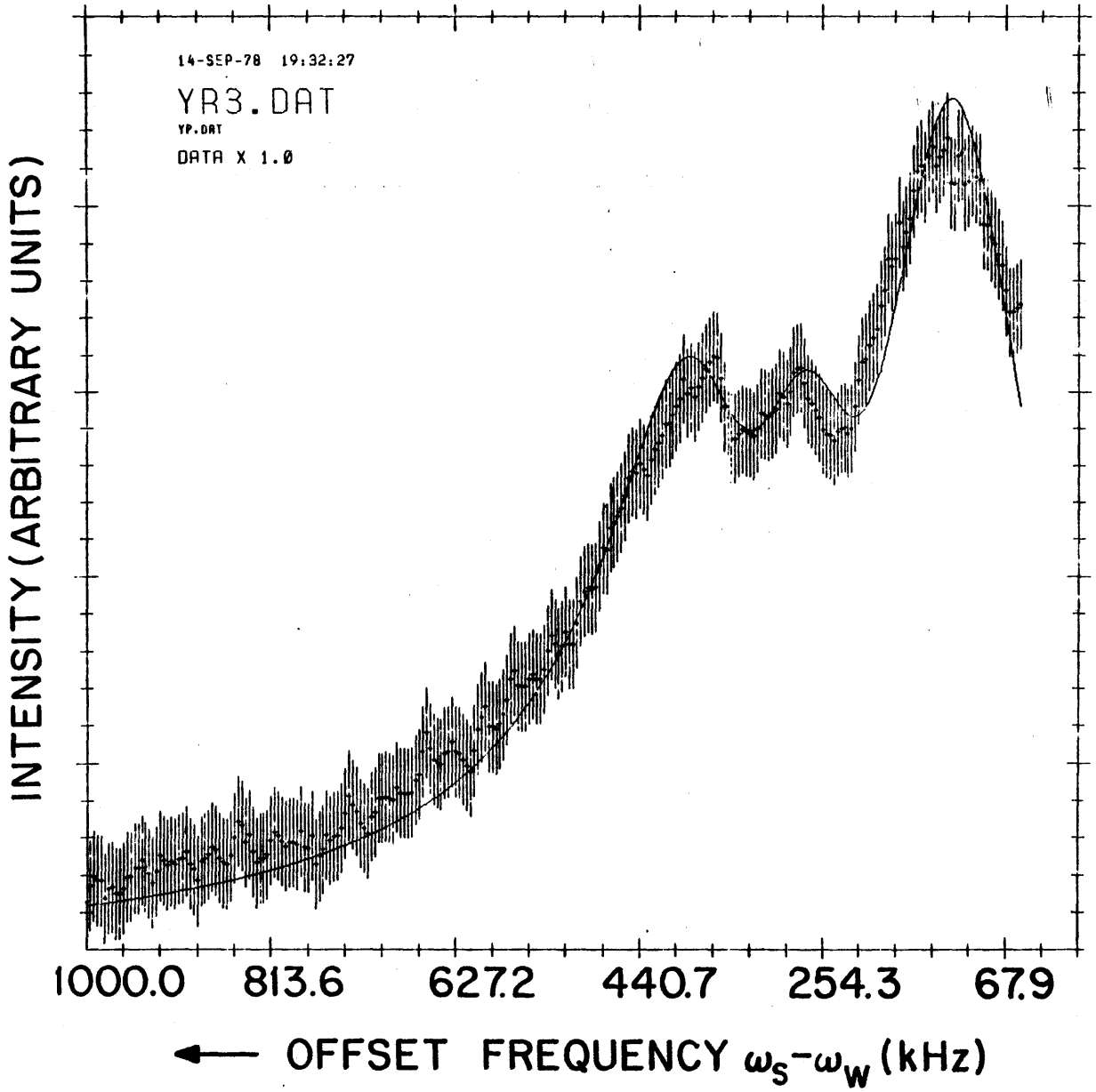
14-SEP-78 19:32:27
YR3.DAT
YP.DAT
DATA X 1.0
INTENSITY (ARBITRARY UNITS)
1000.0
813.6
627.2
440.7
254.3
67.9
OFFSET FREQUENCY $\omega_S - \omega_W$ (kHz)

Figure 6.20.

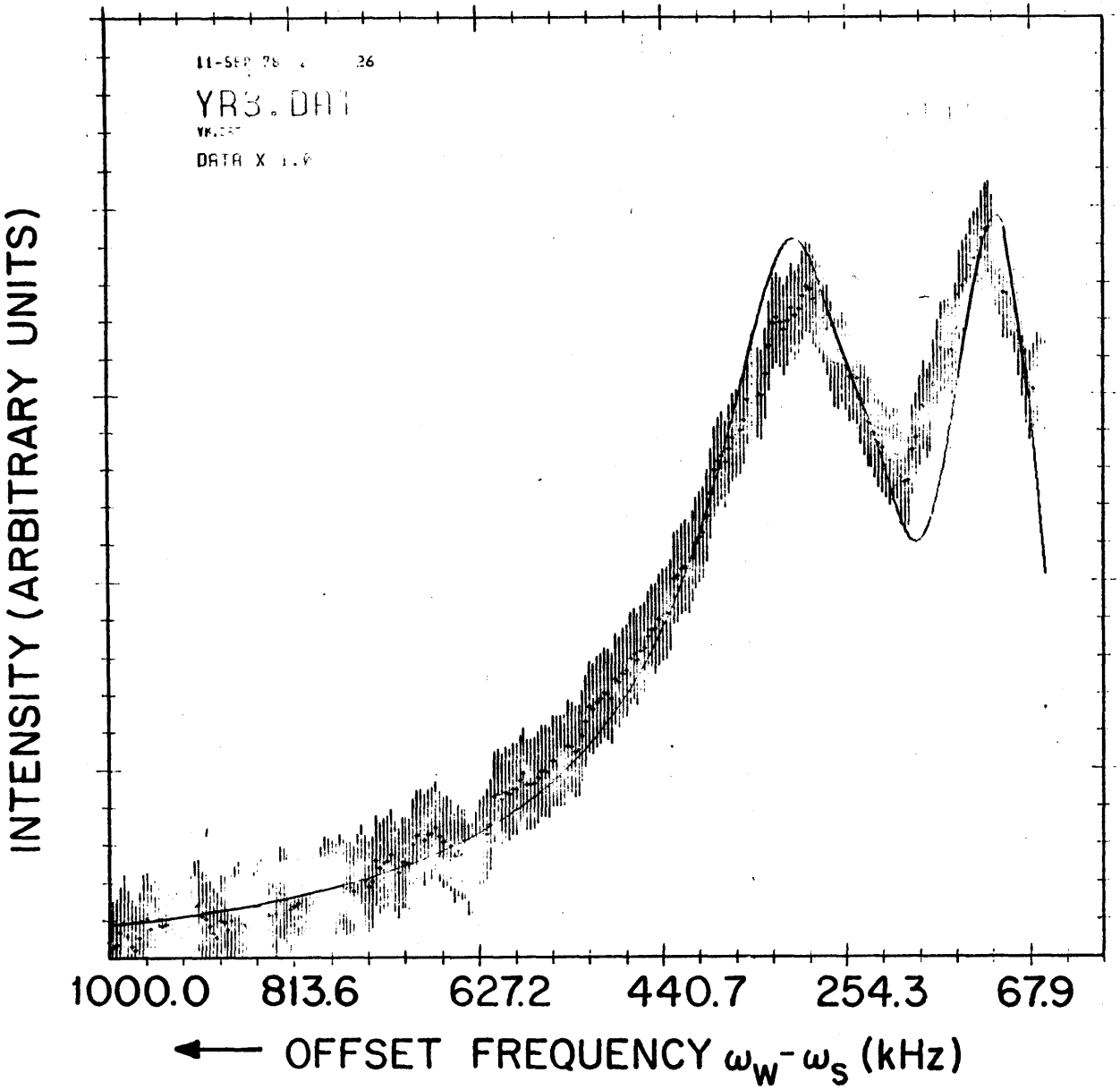
YR3.DAT
INTENSITY (ARBITRARY UNITS)
1000.0
813.6
627.2
440.7
254.3
67.9
OFFSET FREQUENCY $\omega_W - \omega_S$ (kHz)

Figure 6.21.

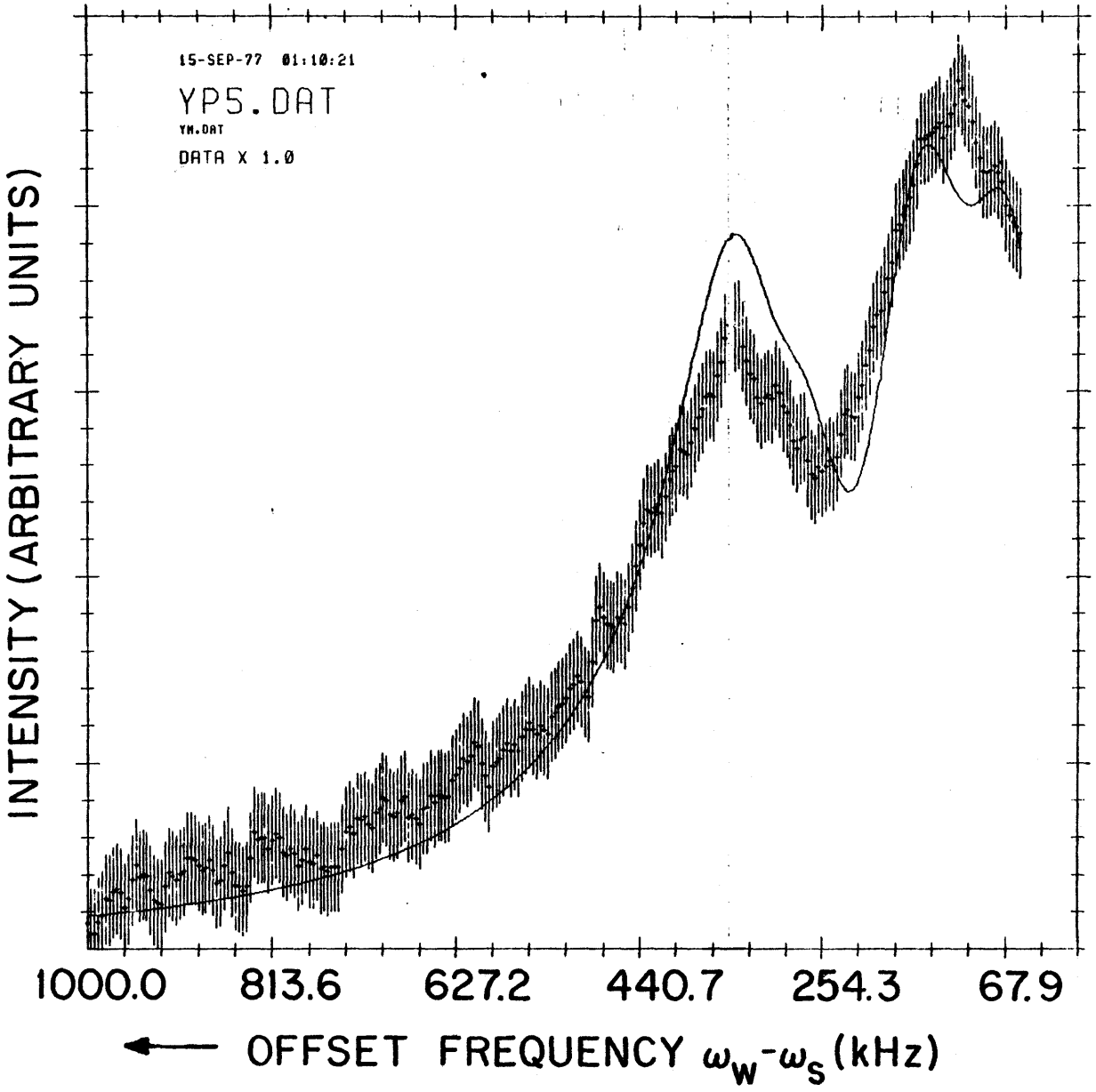
15-SEP-77 01:10:21
YP5.DAT
YM.DAT
DATA X 1.0
INTENSITY (ARBITRARY UNITS)
1000.0
813.6
627.2
440.7
254.3
67.9
OFFSET FREQUENCY $\omega_W - \omega_S$ (kHz)

Figure 6.22.

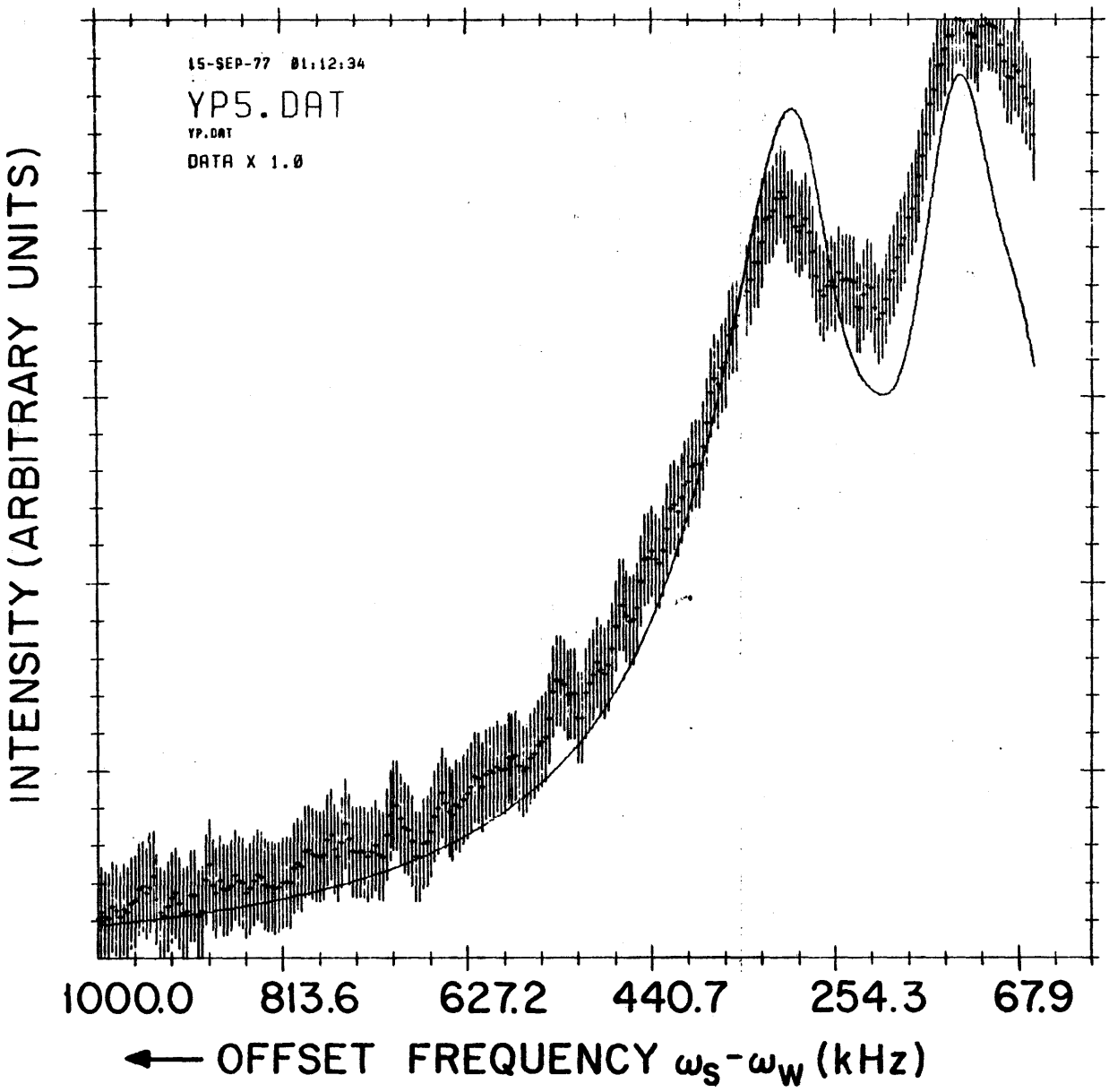
15-SEP-77 01:12:34
YP5.DAT
YP.DAT
DATA X 1.0
INTENSITY (ARBITRARY UNITS)
1000.0
813.6
627.2
440.7
254.3
67.9
← OFFSET FREQUENCY $\omega_S - \omega_W$ (kHz)

Figure 6.23.

to be so small, that it does not entirely dominate the power broadening of the weak wave interacting with strong transition. Since this latter contribution has been neglected, the theoretical lineshape is not sufficiently broadened. It should be pointed out that the results for the strong-wave weak-wave lineshape developed in Chapter II are valid, not only when the weak wave is weakly saturating, but also in the regime where the weak wave is less strongly saturating than the strong wave. i.e. $S_w > 1$, $S_s >> 1$, but $S_w/S_s << 1$, using obvious notation. This last condition may be derived by developing a perturbation expansion in $\varepsilon = \alpha^2/\beta^2$, using the notation of Chapter II. The same expansion equations will then be obtained, but they are valid only near resonance. This is due to the fact that, so long as the strong and weak waves interact with the common level, the rapid transitions induced by the strong wave cause the weak wave to interact with atoms of the common level for the short time $\sim 1/\beta$. The 'effective' weak wave saturation parameter is then of order $\varepsilon = \alpha^2/\beta^2$. Off resonance, however, the weak wave is not weakened in its effect and an incorrect Doppler broadened background is obtained. Since the contribution near resonance is the required result, the lineshape (VI.4) will be reasonably accurate, in the extended regime described.

The experiment was performed in a regime where the weak wave interacting with a strong transition was not quite weakly

saturating, but the strong wave intensity was sufficiently large that $S_s >> S_s$, as long as J was not too large. For R(2) and P(3), the S_s was a few times larger than S_w, and the program could compensate for the error incurred. At $J \sim 5$, this condition breaks down, so the P(5) fits were poor.

The effect of a 5% variation in the outer nucleus coupling constants for R(3) is shown in Fig. 6.24. The purpose of the figure is to demonstrate the sensitivity of the theoretical lineshape to the coupling constants.

Having obtained the raw data in the form of the generalized coupling constants a(J) given in Table VI.2, the results for the coupling constants of the two vibrational levels will be calculated in the following chapter.

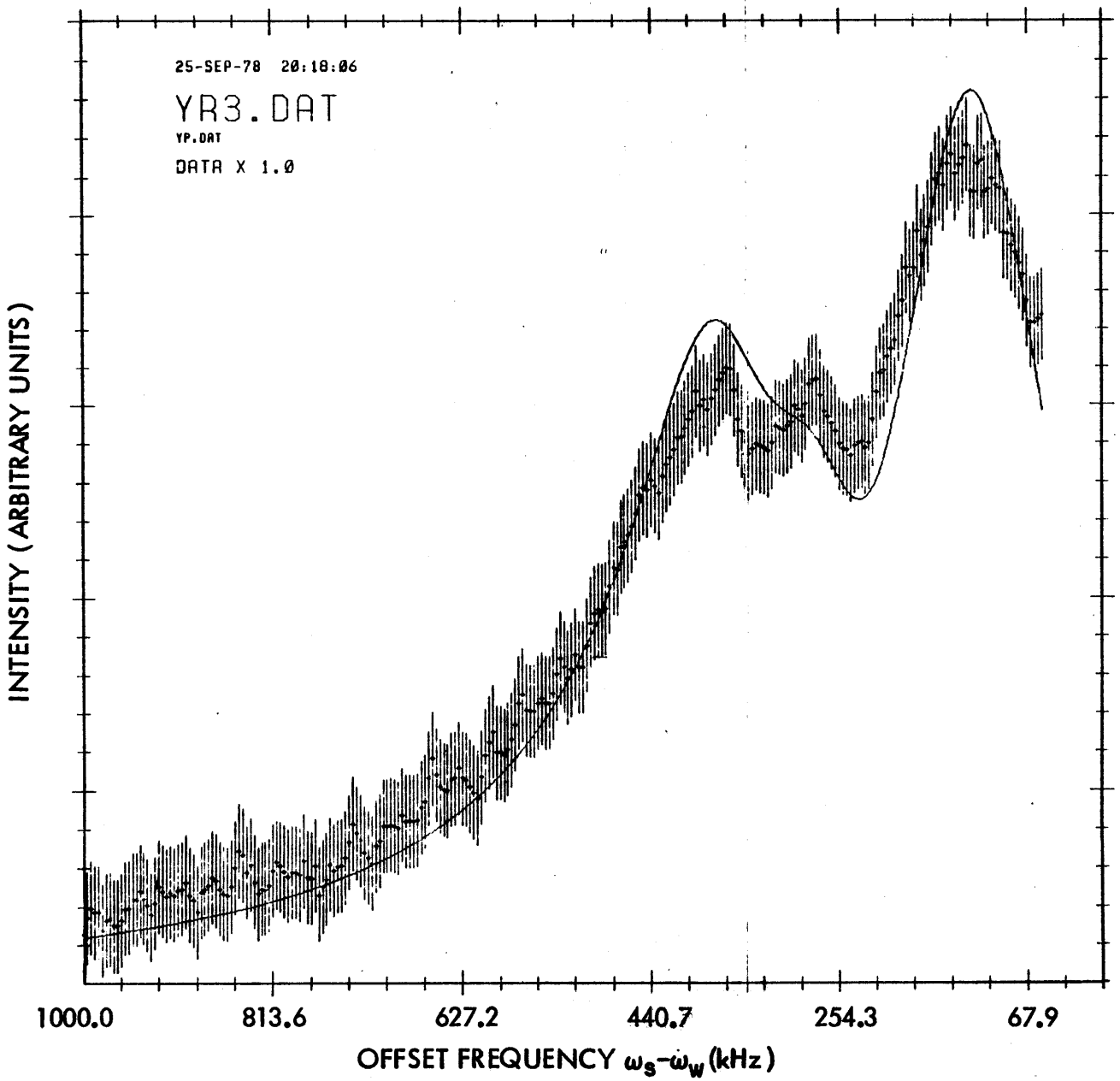

Figure 6.24. Effect of Varying $\alpha(J)$ on R(3) ($\alpha 1$: 132 → 128; $\alpha 3$: 100 → 106)

TABLE VI.2

$N_2^{14}O$ Generalized Coupling Constants a(J) in kHz

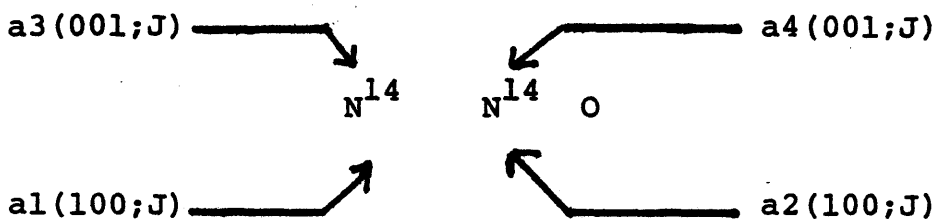

DEFINITION OF COUPLING CONSTANTS

SHOWING NUCLEUS AND VIBRATIONAL STATE

Line ; Figure		a1(J)	a2(J)	a3(J)	a4(J)
P(5)	VI.22,23	148.0±.3	16.0±.6	100.0±.4	66.0±.5
P(4)	VI.18	145.0±.5	25.1±.7	93.5±.7	60.7±.8
P(4)	VI.19	145.0±	27.3±	94.0±	65.0±
R(3)	VI.21	139.0±.5	22.0±.9	109.0±.5	42.0±.6
R(3)	VI.20	132.0±.6	16.8±1.0	100.0±.6	45.4±.6
R(2)	VI.16	114.0±	21.0±	92.2±	34.0±
R(2)	VI.17	116.0±1.1	13.6±2.1	100.0±1.0	49.6±1.2
P(3)	VI.14	142.0±.5	27.0±.6	83.7±.6	57.9±.7
P(3)	VI.15	134.0±.4	9.6±1.4	77.6±.6	60.9±1.0

References

1. P. R. Bevington, Data Reduction and Error Analysis for the Physical Sciences, McGraw Hill, New York (1969).

CHAPTER VII

RESULTS AND CONCLUSIONS

1. Determination of Coupling Constants (eqQ)

The coupling constants eqQ will be determined from their relationship to the generalized constants a(J) of Table VI.2. This relation depends on the molecular model. For the simplest model, the rigid rotor-harmonic oscillator approximation is assumed. (see Chapter I) The (100) and (001) vibrational states have no vibrational angular momentum, so K = 0. From Eq. (I.53), one has for these states

VII.1) $$a(J) = \frac{-eqQ}{2} \frac{J}{2J+3}$$

Inverting Eq. (VII.1) yields

VII.2) $$-eqQ = 2\,a(J)\,\frac{2J+3}{J}$$

In this approximation, the eqQ for each N nucleus depends only on the vibrational state and is independent of J. With Eq. (VII.2), one can calculate the eqQ using each of the lines listed in Table VI.2. The results are given in Table VII.1. Since the entrees in the separate columns of Table VII.1 should be identical for all the lines, the values are averaged. The

TABLE VII.1

Nuclear Electric Quadrupole Coupling Constants $N_2^{14}O$

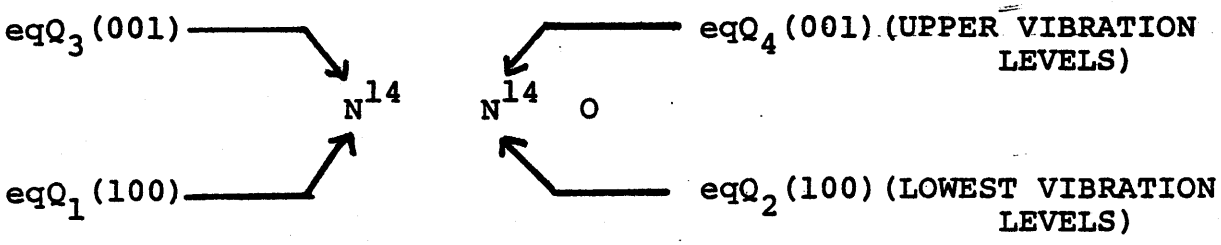

DEFINITION OF COUPLING CONSTANTS

SHOWING NUCLEUS AND VIBRATIONAL STATE

LINE	$-eqQ_1$ (kHz)	$-eqQ_2$ (kHz)	$-eqQ_3$ (kHz)	$-eqQ_4$ (kHz)
P(5)	769.6	83.2	550.0	363.0
P(4)	797.5	138.1	561.0	364.2
	797.5	150.2	564.0	390.0
R(3)	834.0	132.0	599.5	231.0
	792.0	100.8	550.0	249.7
R(2)	798.0	147.0	553.2	204.0
	812.0	95.2	600.0	297.6
P(3)	852.0	162.0	585.9	405.3
	804.0	57.6	543.2	426.3
AVERAGE:	806.3	118.5	567.4	325.7
	±23.7	±35.3	±22.7	±81.9

average eqQ and root mean square deviation from the mean are given at the end of each column in Table VII.1.

There are a number of contributions to the uncertainty in the coupling constants. The most important is the approximate nature of the fitting function. Power broadening due to the weak wave has been neglected. In addition, Lorentzian derivatives have been used for the various crossing resonance lineshapes. Experimentally, a finite frequency modulation of one of the lasers has been utilized to obtain a lock-in 'derivative' lineshape. A distortion from a true Lorentzian derivative occurs as shown in Chapter IV. The frequency modulation amplitude ω_1 was fixed at $\sim$35kHz so that the narrow resonances (HWHM $\sim$50 kHz) would be enhanced. As shown in Fig. 4.13, the maximum derivative point is shifted by about 15-20% of the 50 kHz width. Thus, there is only about 10 kHz error in the location of the narrow hyperfine peaks which occur $\sim$400 kHz from zero beat frequency. The fitting function errors are partially eliminated by allowing both the saturation parameter scale factor S_o and the collision broadening parameter γ to be determined by the fitting procedure. An estimate of the error due to the fitting function is best obtained by considering the variation in the coupling constants derived from the various lines, as given by the root mean square deviation. Nonlinearity of the frequency sweeping circuits is much less than 1% and does not contribute significant error.

The statistical error due to noise in the data is given by the uncertainties in the generalized coupling constants of Table VI.2. These fractional errors are small compared to the root mean square deviations given in Table VII.1. Since the statistical error due to the noise in the experimental data is small compared to the (rms) systematic error due to the approximate fitting function, the (rms) deviations will be taken as the estimators of the total error. The results for the eqQ of the two nitrogen nuclei are given in Table VII.2.

The outer N nucleus produces hyperfine structure which is well resolved. Thus, an accurate determination of its coupling constant is possible, as demonstrated by the small (rms) deviations shown in Table VII.2. However, the central N nucleus produces structure which is unresolved. Its coupling is not so accurately determined and the fractional uncertainty is about 25%.

There is a steady decrease in the outer N nucleus coupling as the vibrational energy is increased. This trend is consistent with the qualitative difference between the R- and P- branch spectra as explained in Chapter VI. The sign of the outer N nucleus coupling constants is also consistent with the qualitative requirements. For the inner N nucleus, however, there appears to be an initial decrease of the coupling in changing from the ground state to the (100) vibrational state, followed

TABLE VII.2

Vibrational Dependence of $N_2^{14}O$ Nuclear Electric Quadrupole Coupling Constants

DEFINITION OF COUPLING CONSTANTS

	VIBRATIONAL STATE		
$eqQ(N^{14})$	000	100	001
OUTER (kHz)	-1020 [1]	-806.3 ± 23.7	-567.4 ± 22.7
INNER (kHz)	-270 [1]	-118.5 ± 35.3	-325.7 ± 81.9

by an increase for the (001) vibrational state. As pointed out by Townes and Schawlow[2] the innter N nucleus in N_2O is double bonded to both the outer nitrogen and the oxygen. The symmetrically located valence electrons result in a very small electric field gradient (q) at the central nitrogen. Since the electric quadrupole coupling is proportional to q, it is also small. In this case, the distortion of the electron distribution about the inner N nucleus due to the neighboring ions ($\bar{N} = \overset{+}{N} = 0$) is probably responsible for most of the observed coupling. The (100) vibration is nearly symmetrical. For this state, the increase in the bond lengths tends to reduce the distortion, thus decreasing the coupling. The asymmetric vibration of the (001) state, however, tends to increase the distortion of the electron distribution at the central N nucleus. As a result, the coupling tends to increase.

There is experimental evidence which seems to contradict this picture of the vibrational effects on the inner nucleus coupling. Figure 6.5 for R(2) shows the outermost peak to be broader than the central peak. This could be due to the intersection of the various Lorentzian derivative contributions, but then the theoretical curve should show the same effect. Figure 6.16 shows that these two peaks are predicated to have equal widths. The outer peak arises from the (100) level splittings, for which the outer N nucleus coupling is largest

and J = 2. If the inner N nucleus coupling for the (100) state were larger than that of the (001) state, the various contributions to the outer peak would be split more than that of the central peak, and the R(2) data would be explained. However, it has not been possible to obtain good fits to any of the individual spectra with this assumption.

Using the coupling constants given in Table VII.2, the energy levels for P(3) and R(2) are calculated and shown in Figures 7.1 and 7.2 respectively. These may be compared to Figure 1.2 which shows the energy levels based on the ground state coupling constants.

2. Suggestions for Further Study

The resolution obtainable thus far has been limited primarily by power broadening. Significant improvement can be realized by using a telescopic beam expander in order to reduce the intensity, while maintaining full laser power. However, lower intensities require lower pressures for saturation, causing a reduction in the fluorescence signal. Longer integration times can be utilized to solve this problem. However, the total power and absolute frequency must then be maintained constant over correspondingly longer periods. This is best accomplished by introducing a servo system to control the absolute frequency (and hence the power) of one of the lasers, by locking to a

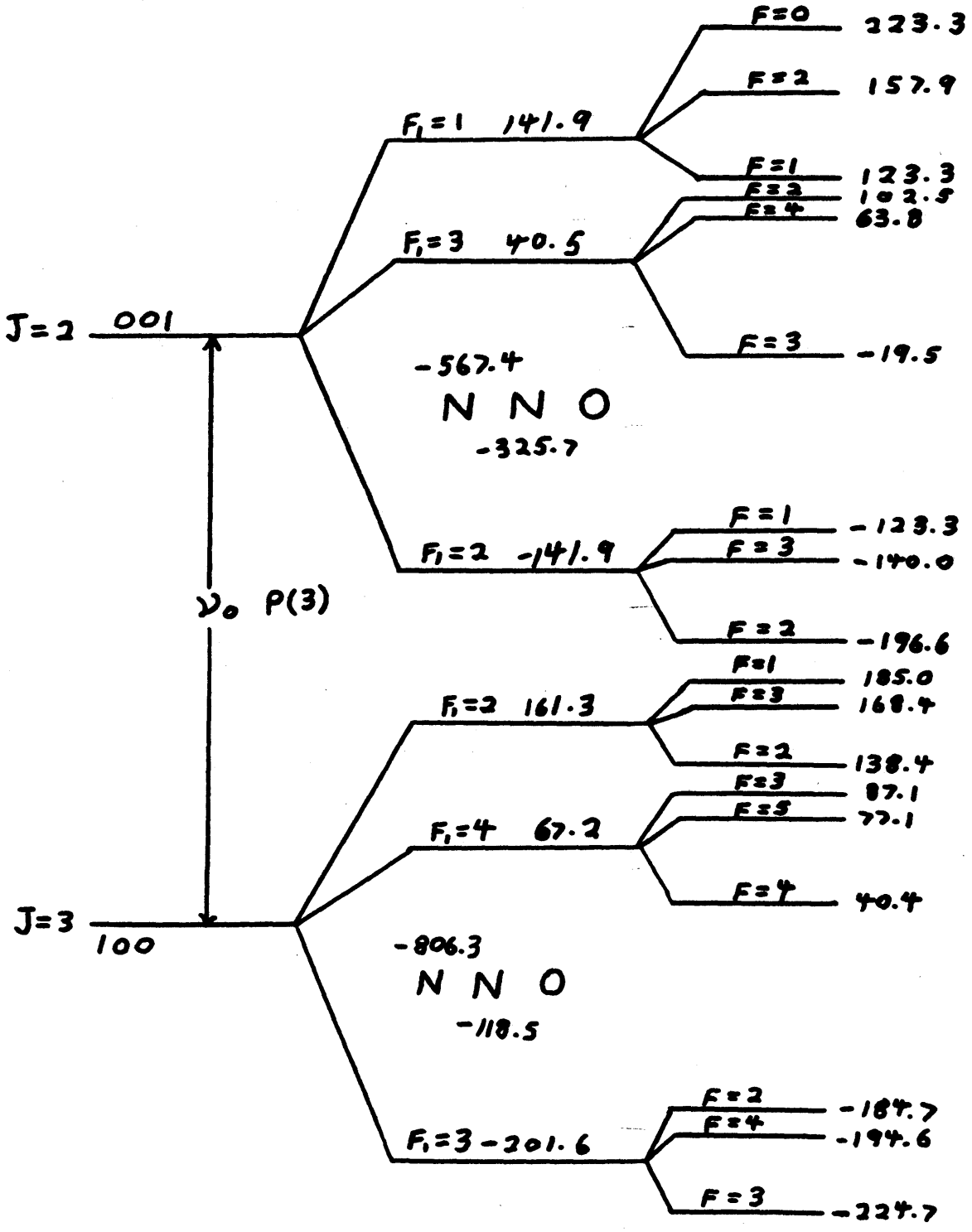

Figure 7.1 $N_2^{14}O$ Hyperfine Structure P(3): Excited Vibrational States (Splittings in kHz)

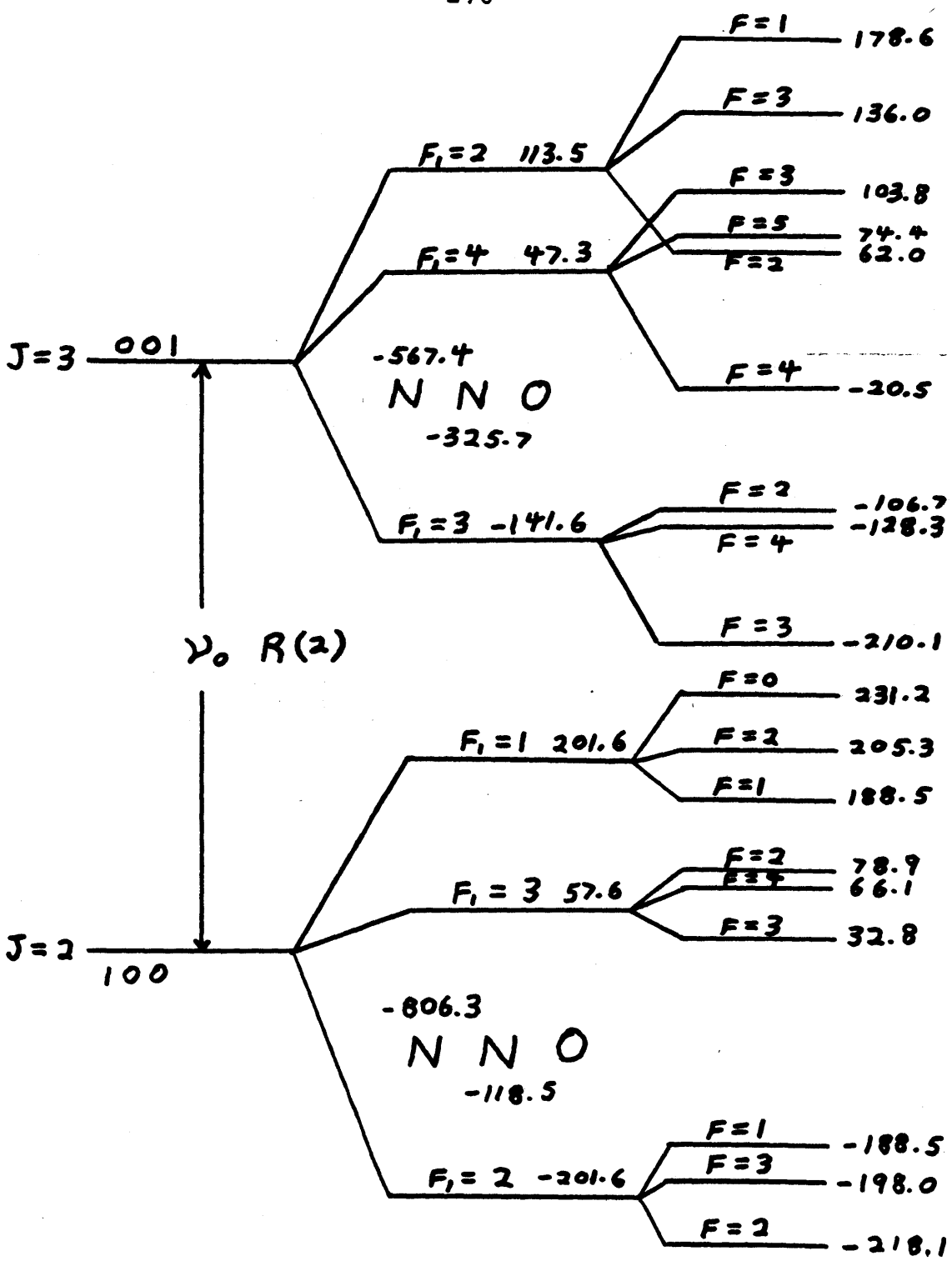

Figure 7.2 $N_2^{14}O$ Hyperfine Structure R(2): Excited Vibrational States (Splittings in kHz)

saturation resonance in an external cell. The existing servo system can be used to control the offset frequency of the two laser system. With a spectrometer of this type, a resolution of ∿10 kHz should be readily obtainable.

Magnetic hyperfine structure will contribute significantly to the $\vec{I}\cdot\vec{J}$ coupling for large J ∿ 50-100. In the high J region, the $\Delta F \neq \Delta J$ transitions are strongly suppressed and the techniques used to study the spectra at lower values of J are not applicable. The molecular g factor[1] (Paschen-Bach region) and electric quadrupole coupling constants (determined at low J) are known. Thus, the magnetic $\vec{I}\cdot\vec{J}$ coupling constants can be determined by observing the Zeeman spectra at high J and studying th the transition from the weak magnetic field to Paschen-Bach region. The theoretical problem is simplified at high J, since only $\Delta F = \Delta J$ transitions need be considered, and the experiment may be done with both laser fields weakly saturating (i.e. with a telescope.

References

1. A. G. Smith, H. Ring, W. V. Smith, and W. Gordy, Phys. Rev. 73, 633 (1948); D. K. Coles, E. S. Elyash, and J. G. Gorman, Phys. Rev. 72, 971 (1947).

2. C. H. Townes and A. L. Schawlow, Microwave Spectroscopy, Dover Publications, Inc., New York (1975).

3. M. J. Kelly, J. E. Thomas, J.-P. Monchalin, N. A. Kurnit, and A. Javan, Phys. Rev. Lett. 37, 686 (1976).

APPENDIX I.1

WIGNER-ECKART THEOREM

The operator T_K^q is defined to be a tensor operator with respect to an angular momentum $\vec{J}$ if the following commutation relationships are satisfied:

a) $[J_\pm, T_K^q] = T_K^{q\pm1}\sqrt{(K\mp q)(K\pm q+1)}$

b) $[J_z, T_K^q] = T_K^q\, q$

where $J_\pm = J_x \pm i J_y \;;\; \hbar = 1$

For operators T_K^q satisfying (a, b), the Wigner-Eckart Theorem is stated as

c) $\langle \alpha' j' m' | T_K^q | \alpha j m \rangle = \langle j, K; m, q | j, K; j', m' \rangle \times \langle \alpha' j' \| T_K \| \alpha j \rangle$

where the first bracket on the right is a Clebsch-Gordon coefficient and the second bracket is a reduced matrix element, independent of spatial orientation (q, m, m'). α pertains to all other quantum numbers not explicitly represented.

APPENDIX I.2

Direction Cosine Matrix Elements - Symmetric Rotor Basis

$$\langle J, K\pm1, M\pm1 | \Phi_{xx} | JKM \rangle = (\mp)_K \frac{i}{4} \frac{[(J\mp M)(J\pm M+1)(J\mp K)(J\pm K+1)]^{\frac{1}{2}}}{J(J+1)}$$

$$\langle J, K\pm1, M\pm1 | \Phi_{yx} | JKM \rangle = (\mp)_M (\pm)_K \frac{1}{4} \frac{[(J\mp M)(J\pm M+1)(J\mp K)(J\pm K+1)]^{\frac{1}{2}}}{J(J+1)}$$

$$\langle J, K\pm1, M | \Phi_{zx} | JKM \rangle = (\mp)_K \frac{i}{2} \frac{M[(J\mp K)(J\pm K+1)]^{\frac{1}{2}}}{J(J+1)}$$

$$\langle J, K\pm1, M\pm1 | \Phi_{xy} | JKM \rangle = \frac{1}{4} \frac{[(J\mp M)(J\pm M+1)(J\mp K)(J\pm K+1)]^{\frac{1}{2}}}{J(J+1)}$$

$$\langle J, K\pm1, M\pm1 | \Phi_{yy} | JKM \rangle = (\mp)_M \frac{i}{4} \frac{[(J\mp M)(J\pm M+1)(J\mp K)(J\pm K+1)]^{\frac{1}{2}}}{J(J+1)}$$

$$\langle J, K\pm1, M | \Phi_{zy} | JKM \rangle = \frac{1}{2} \frac{M[(J\mp K)(J\pm K+1)]^{\frac{1}{2}}}{J(J+1)}$$

$$\langle J, K, M\pm1 | \Phi_{xz} | JKM \rangle = \frac{1}{2} \frac{K[(J\mp M)(J\pm M+1)]^{\frac{1}{2}}}{J(J+1)}$$

$$\langle J, K, M\pm1 | \Phi_{yz} | JKM \rangle = (\mp)_M \frac{i}{2} \frac{K[(J\mp M)(J\pm M+1)]^{\frac{1}{2}}}{J(J+1)}$$

$$\langle JKM | \Phi_{zz} | JKM \rangle = \frac{KM}{J(J+1)}$$

$$\langle JKM|\Phi_{xx}|J+1,K\pm1,M\pm1\rangle = (\pm)_M \frac{i}{4} \frac{[(J\pm M+1)(J\pm M+2)(J\pm K+1)(J\pm K+2)]^{\frac{1}{2}}}{(J+1)[(2J+1)(2J+3)]^{1/2}}$$

$$\langle JKM|\Phi_{yx}|J+1,K\pm1,M\pm1\rangle = -\frac{1}{4} \frac{[(J\pm M+1)(J\pm M+2)(J\pm K+1)(J\pm K+2)]^{\frac{1}{2}}}{(J+1)[(2J+1)(2J+3)]^{1/2}}$$

$$\langle JKM|\Phi_{zx}|J+1,K\pm1,M\rangle = -\frac{i}{2} \frac{[(J+1)^2-M^2]^{\frac{1}{2}}[(J\pm K+1)(J\pm K+2)]^{\frac{1}{2}}}{(J+1)[(2J+1)(2J+3)]^{1/2}}$$

$$\langle JKM|\Phi_{xy}|J+1,K\pm1,M\pm1\rangle = (\mp)_M(\mp)_K \frac{1}{4} \frac{[(J\pm M+1)(J\pm M+2)(J\pm K+1)(J\pm K+2)]^{\frac{1}{2}}}{(J+1)[(2J+1)(2J+3)]^{1/2}}$$

$$\langle JKM|\Phi_{yy}|J+1,K\pm1,M\pm1\rangle = (\pm)_K \frac{i}{4} \frac{[(J\pm M+1)(J\pm M+2)(J\pm K+1)(J\pm K+2)]^{\frac{1}{2}}}{(J+1)[(2J+1)(2J+3)]^{1/2}}$$

$$\langle JKM|\Phi_{zy}|J+1,K\pm1,M\rangle = (\mp)_K \frac{1}{2} \frac{[(J+1)^2-M^2]^{\frac{1}{2}}[(J\pm K+1)(J\pm K+2)]^{\frac{1}{2}}}{(J+1)[(2J+1)(2J+3)]^{1/2}}$$

$$\langle JKM|\Phi_{xz}|J+1,K,M\pm1\rangle = (\mp)_M \frac{1}{2} \frac{[(J\pm M+1)(J\pm M+2)]^{1/2}[(J+1)^2-K^2]^{\frac{1}{2}}}{(J+1)[(2J+1)(2J+3)]^{1/2}}$$

$$\langle JKM|\Phi_{yz}|J+1,K,M\pm1\rangle = -\frac{i}{2} \frac{[(J\pm M+1)(J\pm M+2)]^{1/2}[(J+1)^2-K^2]^{\frac{1}{2}}}{(J+1)[(2J+1)(2J+3)]^{1/2}}$$

$$\langle JKM|\Phi_{zz}|J+1,K,M\rangle = \frac{[(J+1)^2-M^2]^{1/2}[(J+1)^2-K^2]^{\frac{1}{2}}}{(J+1)[(2J+1)(2J+3)]^{1/2}}$$

Appendix I.2 (continued)

$$\langle JKM|Q_{xx}|J-1,K\pm1,M\pm1\rangle = (\pm)_M \frac{i}{4} \frac{[(J\mp M-1)(J\mp M)(J\mp K-1)(J\mp K)]^{\frac{1}{2}}}{J(4J^2-1)^{1/2}}$$

$$\langle JKM|Q_{yx}|J-1,K\pm1,M\pm1\rangle = -\frac{1}{4} \frac{[(J\mp M-1)(J\mp M)(J\mp K-1)(J\mp K)]^{\frac{1}{2}}}{J(4J^2-1)^{1/2}}$$

$$\langle JKM|Q_{zx}|J-1,K\pm1,M\rangle = \frac{i}{2} \frac{[(J^2-M^2)(J\mp K-1)(J\mp K)]^{\frac{1}{2}}}{J(4J^2-1)^{1/2}}$$

$$\langle JKM|Q_{xy}|J-1,K\pm1,M\pm1\rangle = (\pm)_M(\pm)_K \frac{1}{4} \frac{[(J\mp M-1)(J\mp M)(J\mp K-1)(J\mp K)]^{1/2}}{J(4J^2-1)^{1/2}}$$

$$\langle JKM|Q_{yy}|J-1,K\pm1,M\pm1\rangle = (\pm)_K \frac{i}{4} \frac{[(J\mp M-1)(J\mp M)(J\mp K-1)(J\mp K)]^{1/2}}{J(4J^2-1)^{1/2}}$$

$$\langle JKM|Q_{zy}|J-1,K\pm1,M\rangle = (\pm)_K \frac{1}{2} \frac{[(J^2-M^2)(J\mp K-1)(J\mp K)]^{\frac{1}{2}}}{J(4J^2-1)^{1/2}}$$

$$\langle JKM|Q_{xz}|J-1,K,M\pm1\rangle = (\pm)_M \frac{1}{2} \frac{[(J\mp M-1)(J\mp M)(J^2-K^2)]^{\frac{1}{2}}}{J(4J^2-1)^{1/2}}$$

$$\langle JKM|Q_{yz}|J-1,K,M\pm1\rangle = \frac{i}{2} \frac{[(J\mp M-1)(J\mp M)(J^2-K^2)]^{\frac{1}{2}}}{J(4J^2-1)^{1/2}}$$

$$\langle JKM|Q_{zz}|J-1,K,M\rangle = \frac{[(J^2-M^2)(J^2-K^2)]^{\frac{1}{2}}}{J(4J^2-1)^{1/2}}$$

APPENDIX I.3

SUMMARY : TWO COUPLED NUCLEI HYPERFINE STRUCTURE

I. 1) $H = H_1 + H_2$; $H_1 = H_1(\vec{I}_1 \cdot \vec{J})$; $H_2 = H_2(\vec{I}_2 \cdot \vec{J})$; $I_1 = I_2 = 1$; $\vec{F}_i = \vec{J} + \vec{I}_i$

2) $|W; FM\rangle = \sum_{F_i} a(F_i) |F_i; FM\rangle$; $H|W; FM\rangle = W|W; FM\rangle$

3) $\sum_{F_i'} [\delta_{F_i F_i'}(W_i(F_i) - W) + A(F_i, F_i')]\, a(F_i') = 0$

4) $A_F(F_i; F_i') = \sum_{F_2} C_F(F_i'; F_2)\, C_F(F_i; F_2)\, W_2(F_2)$; $|F_i; FM\rangle = \sum_{F_2} C_F(F_i, F_2) |F_2; FM\rangle$

II. 1) $\underline{F = J+2}$; $W = W_1(J+1) + W_2(J+1)$; $|W; FM\rangle = |J+1; J+2, M\rangle$

2) $\underline{F = J-2}$; $W = W_1(J-1) + W_2(J-1)$; $|W; FM\rangle = |J-1; J-2, M\rangle$

3) $\underline{F = J+1}$; $|W; FM\rangle = a(J)|J; J+1, M\rangle + a(J+1)|J+1; J+1, M\rangle$

$$\begin{vmatrix} W_1(J) - W + A(J,J) & A(J, J+1) \\ A(J+1, J) & W_1(J+1) - W + A(J+1, J+1) \end{vmatrix} = 0$$

a) $A(J,J) = \frac{1}{(J+1)^2} W_2(J) + \frac{J(J+2)}{(J+1)^2} W_2(J+1)$ c) $A(J, J+1) = A(J+1, J) = \frac{\sqrt{J(J+2)}}{(J+1)^2} (W_2(J) - W_2(J+1))$

b) $A(J+1, J+1) = \frac{1}{(J+1)^2} [J(J+2) W_2(J) + W_2(J+1)]$

4) $\underline{F = J-1}$; $|W; FM\rangle = a(J)|J; J-1, M\rangle + a(J-1)|J-1; J-1, M\rangle$

$$\begin{vmatrix} W_1(J) - W + A(J,J) & A(J, J-1) \\ A(J-1, J) & W_1(J-1) - W + A(J-1, J-1) \end{vmatrix} = 0$$

a) $A(J,J) = \frac{1}{J^2} W_2(J) + \frac{J^2-1}{J^2} W_2(J-1)$ c) $A(J, J-1) = A(J-1, J) = \frac{\sqrt{J^2-1}}{J^2} (W_2(J-1) - W_2(J))$

b) $A(J-1, J-1) = \frac{1}{J^2} W_2(J-1) + \frac{J^2-1}{J^2} W_2(J)$

5) $\underline{F=J}$; $|W;FM\rangle = a(J-1)|J-1;J,M\rangle + a(J)|J;J,M\rangle + a(J+1)|J+1;J,M\rangle$

$$\begin{vmatrix} W_1(J-1)-W+A(J-1,J-1) & A(J-1,J) & A(J-1,J+1) \\ A(J,J-1) & W_1(J)-W+A(J,J) & A(J,J+1) \\ A(J+1,J-1) & A(J+1,J) & W_1(J+1)-W+A(J+1,J+1) \end{vmatrix} = 0$$

a) $A(J-1,J-1) = \frac{1}{J^2(2J+1)^2} W_2(J-1) + \frac{1}{J^2} \frac{2J-1}{2J+1} W_2(J) + \frac{(2J-1)(2J+3)}{(2J+1)^2} W_2(J+1)$

b) $A(J-1,J) = A(J,J-1) = \sqrt{\frac{2J-1}{2J+1}} \left[\frac{W_2(J-1)}{J^2(2J+1)} + \frac{J^2+J-1}{J^2(J+1)} W_2(J) - \frac{2J+3}{(J+1)(2J+1)} W_2(J+1) \right]$

c) $A(J-1,J+1) = A(J+1,J-1) = \frac{\sqrt{(2J+3)(2J-1)}}{2J+1} \left[\frac{W_2(J-1)}{J(2J+1)} - \frac{W_2(J)}{J(J+1)} + \frac{W_2(J+1)}{(J+1)(2J+1)} \right]$

d) $A(J,J) = \frac{1}{J^2} \frac{2J-1}{2J+1} W_2(J-1) + \frac{(J^2+J-1)^2}{J^2(J+1)^2} W_2(J) + \frac{1}{(J+1)^2} \frac{2J+3}{2J+1} W_2(J+1)$

e) $A(J,J+1) = A(J+1,J) = \sqrt{\frac{2J+3}{2J+1}} \left[\frac{2J-1}{J(2J+1)} W_2(J-1) - \frac{J^2+J-1}{J(J+1)^2} W_2(J) - \frac{W_2(J+1)}{(J+1)^2(2J+1)} \right]$

5) $A(J+1,J+1) = \frac{(2J-1)(2J+3)}{(2J+1)^2} W_2(J-1) + \frac{2J+3}{(J+1)^2(2J+1)} W_2(J) + \frac{W_2(J+1)}{(J+1)^2(2J+1)^2}$

APPENDIX I.4

PROGRAM FOR CALCULATION OF ELECTRIC DIPOLE REDUCED MATRIX FOR $|J,F_1;F,M\rangle$ BASIS

```
CLASER FOCAL

01.01 C CALCULATE REDUCED MATRIX (J-1,K2;N1/U1/J,K1;N)
01.05 A ! "J GREATER THAN OR EQUAL TO  3",J
01.10 F K1=J-1,J+1;DO 1.20
01.15 Q
01.20 F N=K1-1,K1+1;DO 1.30
01.30 F K2=J-2,J;DO 1.40
01.40 F N1=K2-1,K2+1;DO 2.0

02.50 S Y1=FABS(N1-N)-1
02.60 S Y2=FABS(K2-K1)-1
02.70 IF (Y1)2.80,2.81,2.86
02.80 S M=N;G 2.84
02.81 S M=0;G 2.84
02.84 IF (Y2)2.85,2.85,2.86
02.85 D 3.0
02.86 S SUM=0;S M=0

03.10 S J2=J-1
03.12 S SUM=0
03.15 F M1=-1,1;DO 4.0
03.17 S J1=N;S J3=N1;S M3=M;S M4=0;DO 10.0
03.18 S SUM=SUM/CG
03.20 DO 20.0

04.10 F M2=-1,1;DO 5.0
```

Appendix I.4 (continued)

```
05.20 S J1=J; S J3=K1; S M3=M-M2; S M4=M1; DO 10.0
05.25 S U=CG
05.30 S J1=K1; S M4=M2; S J3=N; S M3=M; DO 10.0
05.32 S U=U*CG
05.35 S J1=J2; S M4=M1; S J3=K2; S M3=M-M2; DO 10.0
05.37 S U=U*CG
05.40 S J1=K2; S M4=M2; S J3=N1; S M3=M; DO 10.0
05.42 S U=U*CG
05.45 IF (U) 5.50, 5.60, 5.50
05.50 S X1=FSQT((J↑2-(M-M2-M1)↑2)/((2*J-1)*(2*J+1)))
05.55 S U=U*X1
05.60 S SUM=SUM+U

10.05 C CALCULATE (J1, 1;M3-M4, M4/J1, 1; J3, M3)
10.10 S I=J3-J1
10.12 S X2=FABS(M3)
10.14 S X3=J3-X2
10.16 IF (X3) 10.17, 10.20, 10.20
10.17 S CG=0; G 10.90
10.20 IF (I) 10.30, 10.35, 10.40
10.30 IF (M4) 10.45, 10.50, 10.55
10.35 IF (M4) 10.60, 10.65, 10.70
10.40 IF (M4) 10.75, 10.80, 10.85
10.45 S CG=FSQT((J1+M3)*(J1+M3+1)/(2*J1*(2*J1+1))); G 10.90
10.50 S CG=-FSQT((J1↑2-M3↑2)/(J1*(2*J1+1))); G 10.90
10.55 S CG=FSQT((J1-M3)*(J1-M3+1)/(2*J1*(2*J1+1))); G 10.90
10.60 S CG=FSQT((J1+M3+1)*(J1-M3)/(2*J1*(J1+1))); G 10.90
10.65 S CG=M3/(FSQT(J1*(J1+1))); G 10.90
10.70 S CG=-FSQT((J1-M3+1)*(J1+M3)/(2*J1*(J1+1))); G 10.90
10.75 S CG=FSQT((J1-M3)*(J1-M3+1)/(2*(2*J1+1)*(J1+1))); G 10.90
10.80 S CG=FSQT(((J1+1)↑2-M3↑2)/((2*J1+1)*(J1+1))); G 10.90
10.85 S CG=FSQT((J1+M3)*(J1+M3+1)/(2*(2*J1+1)*(J1+1))); G 10.90
10.90 S Z1=1

20.10 T ! "(", %2.0, J2, K2, N1, M, "/U10/", J, K1, N, M, ")", " = ", %5.3, SUM

31.99 C END PROGRAM
```

Appendix I.4 (continued)

P(J) Reduced Electric Dipole Matrix for $|J, F_1; F, M\rangle$ States: $\langle J'; F_1'; F' || \mu || J, F_1, F \rangle$

Note: M indicates is the value which maximizes the Clebsch-Gordon Coefficient.

J GREATER THAN OR EQUAL TO 3:3

J'	F1'	F'		J	F1	F		
(2	1	0	0/U10/	3	2	1	0)	= -0.7746
(2	1	1	1/U10/	3	2	1	1)	= -0.3873
(2	1	2	0/U10/	3	2	1	0)	= -0.0775
(2	2	1	1/U10/	3	2	1	1)	= -0.2236
(2	2	2	0/U10/	3	2	1	0)	= -0.1000
(2	3	2	0/U10/	3	2	1	0)	= -0.0338
(2	1	1	0/U10/	3	2	2	0)	= -0.6708
(2	1	2	2/U10/	3	2	2	2)	= -0.3000
(2	2	1	0/U10/	3	2	2	0)	= 0.1291
(2	2	2	2/U10/	3	2	2	2)	= -0.2152
(2	2	3	0/U10/	3	2	2	0)	= -0.0361
(2	3	2	2/U10/	3	2	2	2)	= 0.0146
(2	3	3	0/U10/	3	2	2	0)	= -0.0348
(2	1	2	0/U10/	3	2	3	0)	= -0.7099
(2	2	2	0/U10/	3	2	3	0)	= 0.1013
(2	2	3	3/U10/	3	2	3	3)	= -0.2434
(2	3	2	0/U10/	3	2	3	0)	= -0.0025
(2	3	3	3/U10/	3	2	3	3)	= 0.0123
(2	3	4	0/U10/	3	2	3	0)	= -0.0369
(2	2	1	0/U10/	3	3	2	0)	= -0.7303
(2	2	2	2/U10/	3	3	2	2)	= -0.2434
(2	2	3	0/U10/	3	3	2	0)	= -0.0348
(2	3	2	2/U10/	3	3	2	2)	= -0.2057
(2	3	3	0/U10/	3	3	2	0)	= -0.0615
(2	2	2	0/U10/	3	3	3	0)	= -0.6835
(2	2	3	3/U10/	3	3	3	3)	= -0.2057
(2	3	2	0/U10/	3	3	3	0)	= 0.0727
(2	3	3	3/U10/	3	3	3	3)	= -0.2000
(2	3	4	0/U10/	3	3	3	0)	= -0.0546
(2	2	3	0/U10/	3	3	4	0)	= -0.6999
(2	3	3	0/U10/	3	3	4	0)	= 0.0619
(2	3	4	4/U10/	3	3	4	4)	= -0.2113
(2	3	2	0/U10/	3	4	3	0)	= -0.7423
(2	3	3	3/U10/	3	4	3	3)	= -0.1856
(2	3	4	0/U10/	3	4	3	0)	= -0.0206
(2	3	3	0/U10/	3	4	4	0)	= -0.7187
(2	3	4	4/U10/	3	4	4	4)	= -0.1637
(2	3	4	0/U10/	3	4	5	0)	= -0.7238*

Appendix I.4 (continued)

J GREATER THAN OR EQUAL TO 3:4

	J'	F,'	F'		J	F,	F			
(	3	2	1	0/U10/	4	3	2	0)	=	-0.7559
(	3	2	2	2/U10/	4	3	2	2)	=	-0.2520
(	3	2	3	0/U10/	4	3	2	0)	=	-0.0360
(	3	3	2	2/U10/	4	3	2	2)	=	-0.1782
(	3	3	3	0/U10/	4	3	2	0)	=	-0.0532
(	3	4	3	0/U10/	4	3	2	0)	=	-0.0201
(	3	2	2	0/U10/	4	3	3	0)	=	-0.7127
(	3	2	3	3/U10/	4	3	3	3)	=	-0.2130
(	3	3	2	0/U10/	4	3	3	0)	=	0.0630
(	3	3	3	3/U10/	4	3	3	3)	=	-0.1732
(	3	3	4	0/U10/	4	3	3	0)	=	-0.0473
(	3	4	3	3/U10/	4	3	3	3)	=	0.0060
(	3	4	4	0/U10/	4	3	3	0)	=	-0.0203
(	3	2	3	0/U10/	4	3	4	0)	=	-0.7244
(	3	3	3	0/U10/	4	3	4	0)	=	0.0536
(	3	3	4	4/U10/	4	3	4	4)	=	-0.1830
(	3	4	3	0/U10/	4	3	4	0)	=	-0.0008
(	3	4	4	4/U10/	4	3	4	4)	=	0.0053
(	3	4	5	0/U10/	4	3	4	0)	=	-0.0210
(	3	3	2	0/U10/	4	4	3	0)	=	-0.7319
(	3	3	3	3/U10/	4	4	3	3)	=	-0.1830
(	3	3	4	0/U10/	4	4	3	0)	=	-0.0203
(	3	4	3	3/U10/	4	4	3	3)	=	-0.1614
(	3	4	4	0/U10/	4	4	3	0)	=	-0.0368
(	3	3	3	0/U10/	4	4	4	0)	=	-0.7087
(	3	3	4	4/U10/	4	4	4	4)	=	-0.1614
(	3	4	3	0/U10/	4	4	4	0)	=	0.0417
(	3	4	4	4/U10/	4	4	4	4)	=	-0.1583
(	3	4	5	0/U10/	4	4	4	0)	=	-0.0333
(	3	3	4	0/U10/	4	4	5	0)	=	-0.7136
(	3	4	4	0/U10/	4	4	5	0)	=	0.0369
(	3	4	5	5/U10/	4	4	5	5)	=	-0.1633
(	3	4	3	0/U10/	4	5	4	0)	=	-0.7370
(	3	4	4	4/U10/	4	5	4	4)	=	-0.1474
(	3	4	5	0/U10/	4	5	4	0)	=	-0.0134
(	3	4	4	0/U10/	4	5	5	0)	=	-0.7221
(	3	4	5	5/U10/	4	5	5	5)	=	-0.1333
(	3	4	5	0/U10/	4	5	6	0)	=	-0.7248*

Appendix I.4 (continued)

J GREATER THAN OR EQUAL TO 3: 5

	J'	F1'	F'		J	F1	F			
(	4	3	2	0/U10/	5	4	3	0)	=	-0.7454
(	4	3	3	3/U10/	5	4	3	3)	=	-0.1863
(	4	3	4	0/U10/	5	4	3	0)	=	-0.0207
(	4	4	3	3/U10/	5	4	3	3)	=	-0.1443
(	4	4	4	0/U10/	5	4	3	0)	=	-0.0329
(	4	5	4	0/U10/	5	4	3	0)	=	-0.0132
(	4	3	3	0/U10/	5	4	4	0)	=	-0.7217
(	4	3	4	4/U10/	5	4	4	4)	=	-0.1643
(	4	4	3	0/U10/	5	4	4	0)	=	0.0373
(	4	4	4	4/U10/	5	4	4	4)	=	-0.1416
(	4	4	5	0/U10/	5	4	4	0)	=	-0.0298
(	4	5	4	4/U10/	5	4	4	4)	=	0.0030
(	4	5	5	0/U10/	5	4	4	0)	=	-0.0133
(	4	3	4	0/U10/	5	4	5	0)	=	-0.7267
(	4	4	4	0/U10/	5	4	5	0)	=	0.0330
(	4	4	5	5/U10/	5	4	5	5)	=	-0.1461
(	4	5	4	0/U10/	5	4	5	0)	=	-0.0003
(	4	5	5	5/U10/	5	4	5	5)	=	0.0027
(	4	5	6	0/U10/	5	4	5	0)	=	-0.0136
(	4	4	3	0/U10/	5	5	4	0)	=	-0.7303
(	4	4	4	4/U10/	5	5	4	4)	=	-0.1461
(	4	4	5	0/U10/	5	5	4	0)	=	-0.0133
(	4	5	4	4/U10/	5	5	4	4)	=	-0.1321
(	4	5	5	0/U10/	5	5	4	0)	=	-0.0244
(	4	4	4	0/U10/	5	5	5	0)	=	-0.7156
(	4	4	5	5/U10/	5	5	5	5)	=	-0.1321
(	4	5	4	0/U10/	5	5	5	0)	=	0.0270
(	4	5	5	5/U10/	5	5	5	5)	=	-0.1304
(	4	5	6	0/U10/	5	5	5	0)	=	-0.0225
(	4	4	5	0/U10/	5	5	6	0)	=	-0.7131
(	4	5	5	0/U10/	5	5	6	0)	=	0.0244
(	4	5	6	6/U10/	5	5	6	6)	=	-0.1330
(	4	5	4	0/U10/	5	6	5	0)	=	-0.7329
(	4	5	5	5/U10/	5	6	5	5)	=	-0.1222
(	4	5	6	0/U10/	5	6	5	0)	=	-0.0094
(	4	5	5	0/U10/	5	6	6	0)	=	-0.7227
(	4	5	6	6/U10/	5	6	6	6)	=	-0.1124
(	4	5	6	0/U10/	5	6	7	0)	=	-0.7242*

Appendix I.4 (continued)

J GREATER THAN OR EQUAL TO 3:20

J	K	F		J	K	F		
(19	18	17	0/U10/	20	19	18	0)	= -0.7161
(19	18	18	18/U10/	20	19	18	18)	= -0.0377
(19	18	19	0/U10/	20	19	18	0)	= -0.0010
(19	19	18	18/U10/	20	19	18	18)	= -0.0358
(19	19	19	0/U10/	20	19	18	0)	= -0.0018
(19	20	19	0/U10/	20	19	18	0)	= -0.0009
(19	18	18	0/U10/	20	19	19	0)	= -0.7151
(19	18	19	19/U10/	20	19	19	19)	= -0.0367
(19	19	18	0/U10/	20	19	19	0)	= 0.0019
(19	19	19	19/U10/	20	19	19	19)	= -0.0357
(19	19	20	0/U10/	20	19	19	0)	= -0.0018
(19	20	19	19/U10/	20	19	19	19)	= 0.0001
(19	20	20	0/U10/	20	19	19	0)	= -0.0009
(19	18	19	0/U10/	20	19	20	0)	= -0.7152
(19	19	19	0/U10/	20	19	20	0)	= 0.0018
(19	19	20	20/U10/	20	19	20	20)	= -0.0358
(19	20	19	0/U10/	20	19	20	0)	= -0.0000
(19	20	20	20/U10/	20	19	20	20)	= 0.0001
(19	20	21	0/U10/	20	19	20	0)	= -0.0009
(19	19	18	0/U10/	20	20	19	0)	= -0.7152
(19	19	19	19/U10/	20	20	19	19)	= -0.0358
(19	19	20	0/U10/	20	20	19	0)	= -0.0009
(19	20	19	19/U10/	20	20	19	19)	= -0.0349
(19	20	20	0/U10/	20	20	19	0)	= -0.0017
(19	19	19	0/U10/	20	20	20	0)	= -0.7143
(19	19	20	20/U10/	20	20	20	20)	= -0.0349
(19	20	19	0/U10/	20	20	20	0)	= 0.0018
(19	20	20	20/U10/	20	20	20	20)	= -0.0348
(19	20	21	0/U10/	20	20	20	0)	= -0.0017
(19	19	20	0/U10/	20	20	21	0)	= -0.7144
(19	20	20	0/U10/	20	20	21	0)	= 0.0017
(19	20	21	21/U10/	20	20	21	21)	= -0.0349
(19	20	19	0/U10/	20	21	20	0)	= -0.7153
(19	20	20	20/U10/	20	21	20	20)	= -0.0341
(19	20	21	0/U10/	20	21	20	0)	= -0.0008
(19	20	20	0/U10/	20	21	21	0)	= -0.7145
(19	20	21	21/U10/	20	21	21	21)	= -0.0333
(19	20	21	0/U10/	20	21	22	0)	= -0.7145*

APPENDIX I.5A

Eigenstates and Eigenvalues for J = 3 ($I_1 = I_2 = 1$)

BASIS	L'	L1'	L2'	L3'	L4'	L5'	L6'	L7'	L8'	L9'
J = 3	F_1	J-1	J-1	J-1	J	J	J	J+1	J+1	J+1
EIGENSTATE	F	J-2	J-1	J	J-1	J	J+1	J	J+1	J+2
L1=1	W= 258.000	1.000	0.000	0.000	0.000	0.000	0.000	0.000	0.000	0.000
L1=2	W=-218.457	0.000	-.103	0.000	0.995	0.000	0.000	0.000	0.000	0.000
L1=3	W= 221.001	0.000	0.000	0.996	0.000	-.038	0.000	0.080	0.000	0.000
L1=4	W= 153.957	0.000	0.995	0.000	0.103	0.000	0.000	0.000	0.000	0.000
L1=5	W= 130.986	0.000	0.000	0.077	0.000	-.077	0.000	-.994	0.000	0.000
L1=6	W= 24.929	0.000	0.000	0.000	0.000	0.000	0.083	0.000	-.997	0.000
L1=7	W=-308.987	0.000	0.000	0.044	0.000	0.996	0.000	-.073	0.000	0.000
L1=8	W=-239.929	0.000	0.000	0.000	0.000	0.000	0.997	0.000	0.083	0.000
L1=9	W= 107.500	0.000	0.000	0.000	0.000	0.000	0.000	0.000	0.000	1.000

NOTE: W (kHz) ; $-eqQ_1 = 1020$; $-eqQ_2 = 270$

$N_2O = \underset{1}{N}\,\underset{2}{N}\,O$

APPENDIX I.5B

Eigenstates and Eigenvalues for J = 2 ($I_1 = I_2 = 1$)

J = 2

EIGENSTATE		BASIS L'	L1'	L2'	L3'	L4'	L5'	L6'	L7'	L8'	L9'
L1=1	W= 322.490	1.000	0.000	0.000	0.000	0.000	0.000	0.000	0.000	0.000
L1=2	W=-228.836	0.000	-.129	0.000	0.992	0.000	0.000	0.000	0.000	0.000
L1=3	W= 264.676	0.000	0.000	0.993	0.000	-.038	0.000	0.109	0.000	0.000
L1=4	W= 228.836	0.000	0.992	0.000	0.129	0.000	0.000	0.000	0.000	0.000
L1=5	W= 122.651	0.000	0.000	0.104	0.000	-.116	0.000	-.988	0.000	0.000
L1=6	W= 17.826	0.000	0.000	0.000	0.000	0.000	0.103	0.000	-.995	0.000
L1=7	W=-295.187	0.000	0.000	0.050	0.000	0.993	0.000	-.111	0.000	0.000
L1=8	W=-248.176	0.000	0.000	0.000	0.000	0.000	0.995	0.000	0.103	0.000
L1=9	W= 92.140	0.000	0.000	0.000	0.000	0.000	0.000	0.000	0.000	1.000

APPENDIX I.5C

Square of P-Branch Transition Reduced Matrix Elements

$$|\langle J=2, L' \| \mu \| J=3, L \rangle|^2$$

LOWER LEVEL J = 3 \ UPPER LEVEL J = 2, L'	L1	L2	L3	L4	L5	L6	L7	L8	L9
L1=1	0.6000	0.0295	0.0059	0.1705	0.0014	0.0000	0.0099	0.0000	0.0000
L1=2	0.0000	0.5512	0.0003	0.0007	0.0540	0.0030	0.0375	0.0010	0.0000
L1=3	0.0000	0.0000	0.5102	0.0000	0.0006	0.0009	0.0097	0.0542	0.0013
L1=4	0.0000	0.0192	0.0830	0.4288	0.0000	0.0010	0.0633	0.0086	0.0000
L1=5	0.0000	0.0000	0.0005	0.0000	0.5416	0.0400	0.0006	0.0003	0.0005
L1=6	0.0000	0.0000	0.0000	0.0000	0.0000	0.5234	0.0000	0.0003	0.0212
L1=7	0.0000	0.0000	0.0001	0.0000	0.0024	0.0262	0.4790	0.0546	0.0030
L1=8	0.0000	0.0000	0.0000	0.0000	0.0000	0.0055	0.0000	0.4810	0.0502
L1=9	0.0000	0.0000	0.0000	0.0000	0.0000	0.0000	0.0000	0.0000	0.5239

APPENDIX II.1

CLEBSCH-GORDON SUMS (eq. II.42) FOR IMPORTANT P-BRANCH 3-LEVEL RESONANCES

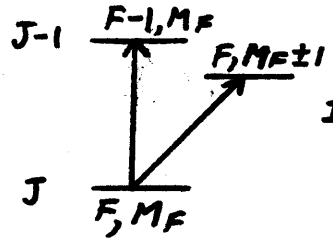

$$I = |\langle F-1||M||F\rangle|^2 |\langle F||M||F\rangle|^2 \frac{(2F-1)(4F+1)}{30F}$$

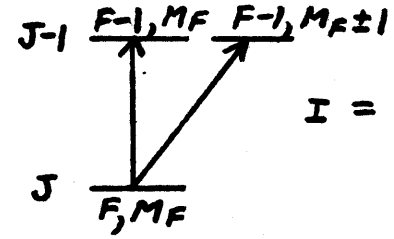

$$I = |\langle F-1||M||F\rangle|^4 \frac{(F-1)(2F-1)(6F+1)}{30F(2F+1)}$$

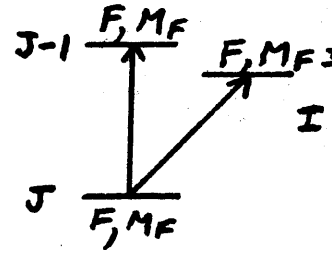

$$I = |\langle F||M||F\rangle|^2 |\langle F||\tilde{M}||F\rangle|^2 \frac{(2F+1)(2F^2+2F+1)}{30F(F+1)}$$

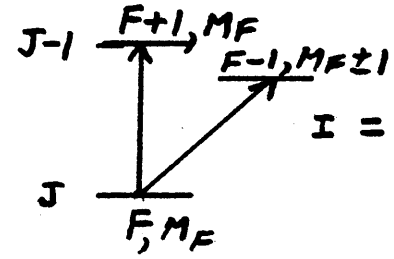

$$I = |\langle F+1||M||F\rangle|^2 |\langle F-1||M||F\rangle|^2 \frac{12F^2+7F-4}{30(2F+1)}$$

NOTE: ALL ADDITIONAL QUANTUM NUMBERS SUPPRESSED IN REDUCED MATRIX ELEMENTS

Appendix II.1 (continued)

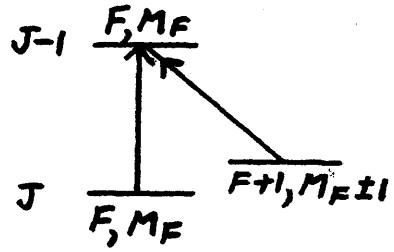

$$I = |\langle F||M||F\rangle|^2 |\langle F||M||F+1\rangle|^2 \frac{(2F+1)(4F+3)}{30(F+1)}$$

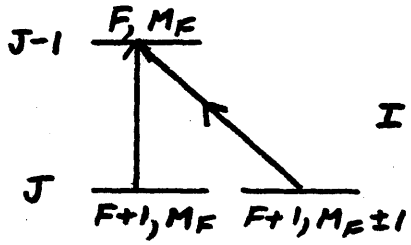

$$I = |\langle F||M||F+1\rangle|^4 \frac{(2F+1)(F+2)(6F+5)}{30(F+1)(2F+3)}$$

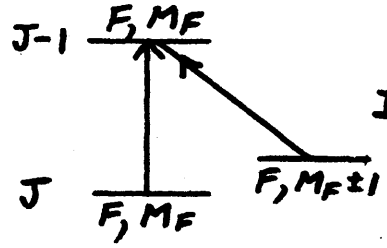

$$I = |\langle F||M||F\rangle|^2 |\langle F||\vec{M}||F\rangle|^2 \frac{(2F+1)(2F^2+2F+1)}{30F(F+1)}$$

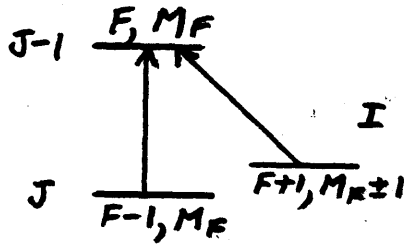

$$I = |\langle F||M||F-1\rangle|^2 |\langle F||M||F+1\rangle|^2 \frac{(2F+1)(12F^2+12F+1)}{30(2F-1)(2F+3)}$$

APPENDIX IV.1

DATA TAKING PROGRAM

(North Star BASIC)

```
  1 REM LOC         NAME
  2 REM 12        COMMAND
  4 REM 200       DATA IN
  5 REM 300      NEW SWEEP
  6 REM 400      END SWEEP
  7 REM 500        PRINT
  8 REM 600      NORMALIZE
  9 REM 700          PLOT
 10 REM 900         DELAY
 11 REM 1000    READ FROM DISC
 12 REM COMMAND
 13 REM
 14      DIM A(256), S(256), D1(256), F$(8)
 15      PRINT "MASTER CONTROL"
 20      PRINT "COMMANDS:"
 22      PRINT "1 NEW DATA RUN (ACCUMULATED ARRAY ZEROED)"
 24      PRINT "2 RESUME DATA RUN (DON'T ZERO ACCUMULATED)"
 26      PRINT "3 PRINT ACCUMULATED"
 28      PRINT "4 PLOT ACCUMULATED"
 29      PRINT "5 READ FROM DISC"
 30      PRINT "TYPE COMMAND NUMBER"\ INPUT Q
 32 IF Q = 0 THEN 15
 34 IF Q = 1 THEN 50
 36 IF Q = 2 THEN 52
 38 IF Q = 3 THEN 54
 39 IF Q = 4 THEN 56
 40 IF Q = 5 THEN 58 ELSE 15
 45 REM
 50    GOSUB 100\GOTO 15
 52    GOSUB 130\GOTO 15
 54    GOSUB 500\GOTO 15
 56    GOSUB 700\GOTO 15
 58    GOSUB 1000\GOTO 15
 97 REM
 98 REM  SWEEP
 99 REM
100 N1 = 0
120 FOR I = 0 TO 225\A(I) = 0 \NEXT I
130 GOSUB 300
140 FOR I = 0 TO 255\S(I) = 0\NEXT I
150 FOR F = 0 TO 255\GOSUB\200 NEXT F
```

Appendix IV.1 (continued)

```
160 GOSUB 400
170 PRINT "TYPE 1 TO EXIT TO COMMAND ELSE SWEEP"
180 INPUT Q\IF Q< >L THEN 130
190 RETURN
191 REM
192 REM DATA IN
193 REM
200 OUT 62, 0\OUT 63, F
210 D=350\GOSUB 900
220 OUT 59, 1\S(F)=INP(59)*256 + INP(58)
230 RETURN
231 REM
299 REM NEW SWEEP
300 FOR F=255 to 0 STEP -1\OUT 63, F\NEXT F
310 PRINT\PRINT "TYPE RETURN TO START SWEEP"
320 INPUT Q
330 RETURN
331 REM
398 REM END SWEEP
399 REM
400 PRINT PRINT "END OF SWEEP. TYPE L TO ADD IT",
401 PRINT "TO ACCUMULATED DATA"
410 INPUT Q
420 IF Q=1 THEN 430 ELSE 450
430 FOR I=0 to 255\A(I)=A(I) + S(I)\NEXT I
440 N1=N1 + 1
445 PRINT "NUMBER OF SWEEPS EQUALS  ", N1
450 RETURN
451 REM
498 REM PRINT
499 REM
500 PRINT "TYPE FILE NAME TO BE USED"
502 INPUT F$
504 OPEN #0, F$
509 FOR P=0 TO 16
510 FOR L=0 TO 14
520 I = 15*P + L
530 PRINT I, A(I)
535 WRITE #0, I, A(I)
540 NEXT L
550 INPUT Q
560 NEXT P
565 CLOSE #0
570 RETURN
```

```
 598  REM NORMALIZE
 599  REM
 600  M1=0\M2 = 1E12
 610  FOR I1=0 TO 255
 620  IF A(I1)>M1 THEN M1=A(I1)
 630  IF A(I1)<M2 THEN M2=A(I1)
 640  NEXT I1
 660  FOR I1=0 TO 255
 670  D1(I1) = (A(I1)-M2)*(255/(M1-M2))
 680  NEXT I1
 690  RETURN
 691  REM
 698  REM PLOT
 699  REM
 700  FOR F=255 TO 0 STEP -1\OUT 63, F\NEXT F
 710  PRINT\PRINT "TYPE RETURN WHEN READY TO PLOT"
 720  INPUT Q
 730  GOSUB 600
 740  FOR I1=0 TO 255
 750  OUT 63, I1\OUT 61, D1(I1)
 755  FOR L1=0 TO 50\NEXT L1
 760  NEXT I1
 770  RETURN
 771  REM
 898  REM DELAY
 899  REM
 900  FOR I3=0 TO D\NEXT I3
 910  RETURN
1000  PRINT "TYPE FILE NAME TO BE READ"
1005  INPUT F$
1010  OPEN #0, F$
1020  FOR I=0 TO 254
1030  READ 0 , I, A(I)
1035  NEXT I
1037  CLOSE #0
1040  RETURN
```

APPENDIX V.1

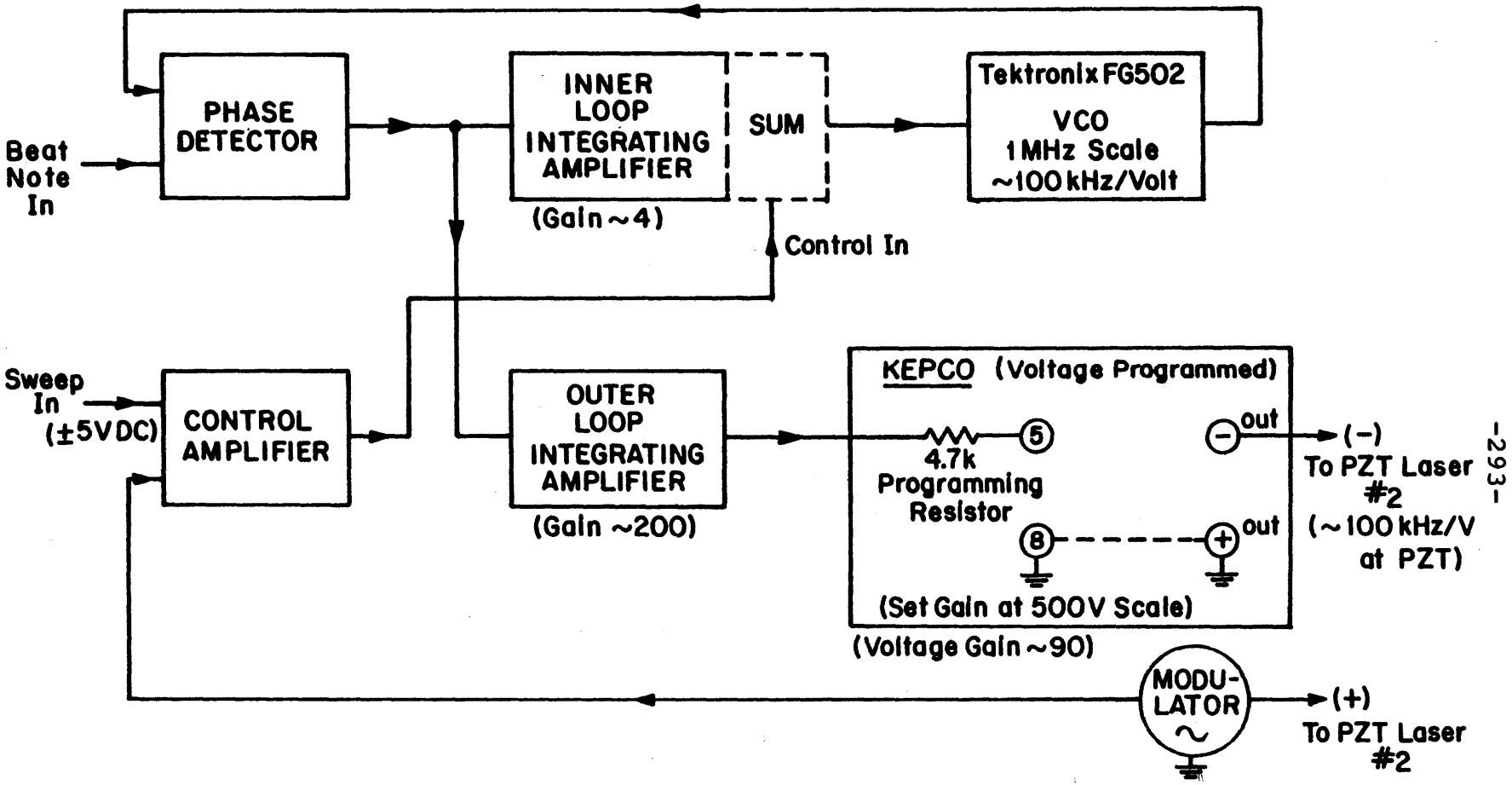
Beat Note In
PHASE DETECTOR
INNER LOOP INTEGRATING AMPLIFIER
(Gain ~4)
SUM
Control In
Tektronix FG502
VCO
1 MHz Scale
~100 kHz/Volt
Sweep In (±5VDC)
CONTROL AMPLIFIER
OUTER LOOP INTEGRATING AMPLIFIER
(Gain ~200)
KEPCO (Voltage Programmed)
5
4.7k Programming Resistor
8
out
out
(Set Gain at 500V Scale)
(Voltage Gain ~90)
(-) To PZT Laser #2 (~100 kHz/V at PZT)
MODU-LATOR
(+) To PZT Laser #2

Appendix V.1 (continued)

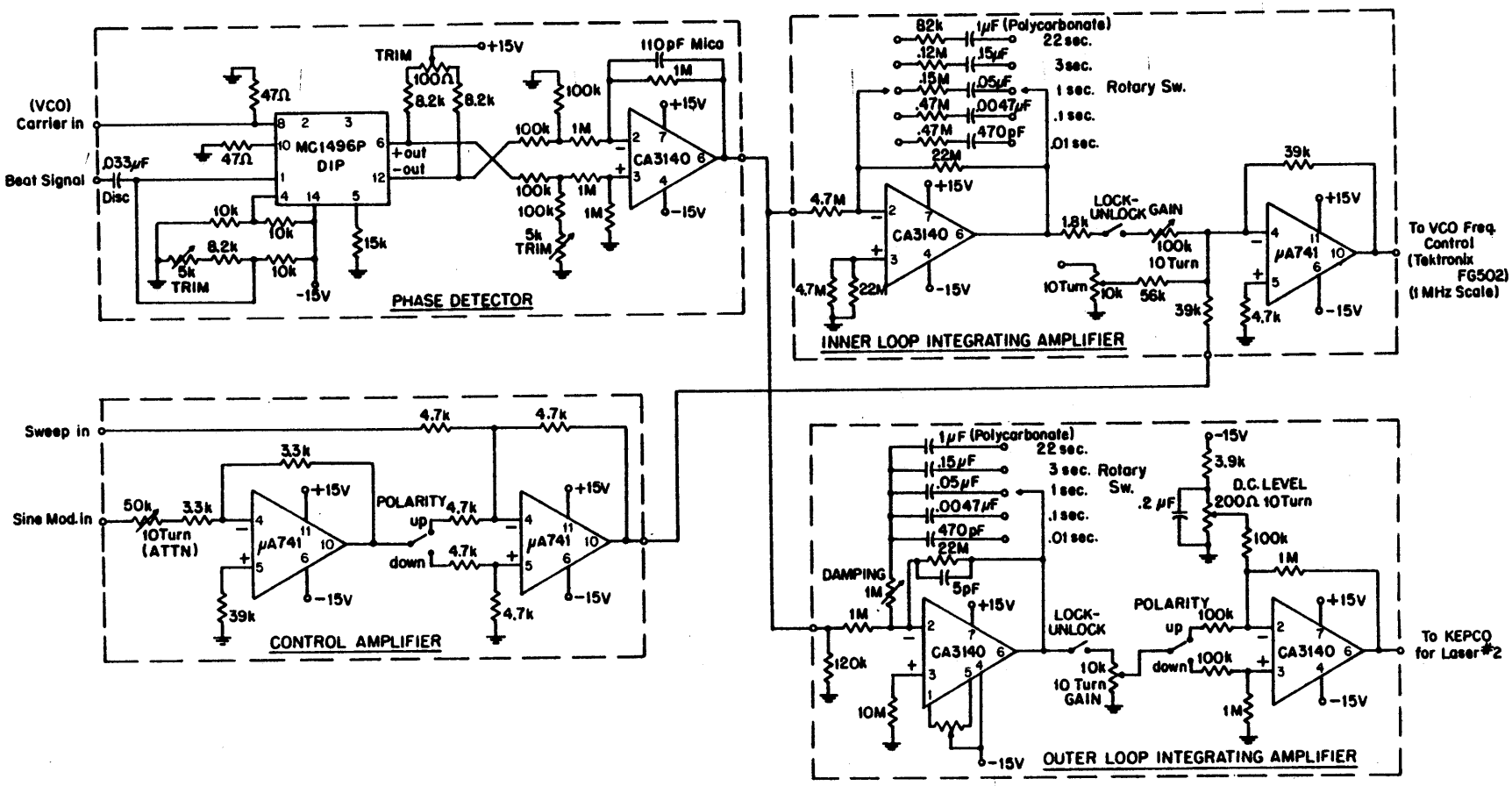

Appendix V.1 (continued)

Notes 1) $\tau_{\text{inner loop}} = .01$ sec
$\tau_{\text{outer loop}} = .1$ sec
} Rotary Switch Settings

2) VCO INPUT .5 v p.-p.
Beat Signal 1.5-2 v p.-p.

Laser Frequencies

3) Polarity Switches: Both Up $\nu_2 < \nu_1$

Both Down $\nu_2 > \nu_1$

4) PZT Polarities:

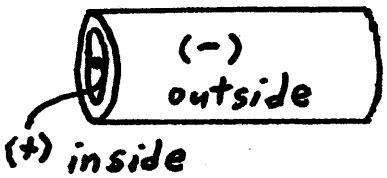

PZT 5H
2" Cylinder
(Clevite Corp.)

5) Sine Mod. in (ATTN) adjusted to give minimum error signal at outer loop Amp. input after ν_1, ν_2 set with correct relative positions (corresponding to polarities above) with outer loop unlocked.

6) D.C. level adj. for inner loop not used

7) Zener diodes across Kepco outputs to limit maximum voltage to ∿350 V - prevents PZT damage.

APPENDIX VI.1

```
C       MAIN HYPFIT
C
        BYTE INFIL1(24),INFIL2(24)
        COMMON /F1/W(2,9),DW(2,9,4),T2(9,9),DT2(9,9,4)
     &  /F2/LL,M1,M2,M3,M4,U2,U3,FJ,U22,L2,L3
     &  /F3/YM(255,7),YP(255,7)/F4/N1(9),N2(9)/F5/U(9,9)/F6/JI,UTOL,I3
     &  /F7/AD(7)/F8/X(255)/F9/YMEXP(255),YPEXP(255)/F10/A1(7)
     &  /F11/SIGMAA(7),FLAMDA,CHISQ,CHISQ1,WM(3),WP(3),II
C
C       INPUT PARAMETERS
C

        WM(1)=1.
        WM(2)=0.
        WM(3)=1.
        WP(1)=0.
        WP(2)=1.
        WP(3)=1.
        CALL ASSIGN(6,'HYPFIT.OUT',0)
        CALL ASSIGN(5,'HYPFIT.DAT',0)
        READ(5,10)INFIL1
        READ(5,10)INFIL2
10      FORMAT(24A1)
        READ(5,15)(AD(I),I=1,7),JI,TOL,ITMAX,Z,SIG,X1,FLAMDA,II,UTOL,I3
15      FORMAT(7F,I,F,I,F,F,F,F,I,F,I)
        CALL CLOSE(5)
        CALL ASSIGN(5,INFIL2,24)
                DO 30 L1=1,9
30      READ(5,25)(U(L1,L2),L2=1,9)
25      FORMAT(9F)
        CALL CLOSE(5)
        CALL ASSIGN(5,INFIL1,24)
                DO 45 I=1,255
45      READ(5,50)YMEXP(I)
                DO 60 I=1,255
60      READ(5,50)YPEXP(I)
50      FORMAT(F10.2)
        CALL CLOSE(5)
                DO 80 I=1,255
        YMEXP(I)=YMEXP(I)-Z
80      YPEXP(I)=YPEXP(I)-Z
C
        I=0
                DO 110 K1=JI-1,JI+1
                DO 110 N11=K1-1,K1+1
        I=I+1
        N1(I)=N11
110     N2(I)=N11+I3
                DO 120 I=1,255
120     X(I)=1000.-(1000.-X1)*(I-1)/254.
        IT=0
        WRITE(6,125)(I,I=1,7)
125     FORMAT(' ',2X,'CHISQ',4X,'FLAMDA',2X,7(2X,'PARAM',I1,3X)//)
C
C       CALC INITIAL CHISQ AND DERIV:HAS INITIAL AD(7)
C
                DO 210 J1=1,7
210     A1(J1)=AD(J1)
        CALL FUNCT
        CALL CHISQE
        D=(WM(II)+WP(II))*255.-7.
        CHISQR=CHISQ/(D*SIG*SIG)
        WRITE(6,330)CHISQR,FLAMDA,(A1(I),I=1,7)
220     IT=IT+1
        IF(IT.GT.ITMAX) GOTO 430
        CALL JETFIT
        CHISQR=CHISQ/(D*SIG*SIG)
                DO 225 I=1,7
225     SIGMAA(I)=SIG*SIGMAA(I)
        WRITE(6,330)CHISQR,FLAMDA,(A1(I),I=1,7)
        WRITE(6,332)(SIGMAA(I),I=1,7)
330     FORMAT(' ',E9.3,2X,E7.1,7(1X,E10.3))
332     FORMAT(' ',18X,7(1X,E10.3))
        IF((CHISQ1-CHISQ)/CHISQ1.GT.TOL) GOTO 220
430     WRITE(6,435)
435     FORMAT(' ', 'I',2X,'YMEXP(I)',2X,'YM(I)',2X,'YPEXP(I)',
     &  2X,'YP(I)')
                DO 450 I=1,255
        YM(I,7)=A1(7)*YM(I,7)
450     YP(I,7)=A1(7)*YP(I,7)
        WRITE(6,460)(I,YMEXP(I),YM(I,7),YPEXP(I),YP(I,7),I=1,255)
460     FORMAT(' ', 255(' ', I3,2X,4(F8.2,2X)/))
C       CALL JETSTO(YMEXP,SIG,YM(1,7),'YM.DAT',255,X1)
C       CALL JETSTO(YPEXP,SIG,YP(1,7),'YP.DAT',255,X1)
        WRITE(4,500)
500     FORMAT(' ','HYPFIT IS FINISHED')
        END
```

Appendix VI.1 (continued)

```
      FUNCTION
      SUBROUTINE FUNCT
      REAL*4 N
      COMMON/F2/LL,M1,M2,M3,M4,U2,U3,FJ,U22,L2,L3
     &/F3/YM(255,7),YP(255,7)/F7/AD(7)/F6/JI,UTOL,I3
     &/F4/N1(9),N2(9)/F1/W(2,9),DW(2,9,4),T2(9,9),DT2(9,9,4)
C
C
      CALL ENPAR1
            DO 5 K=1,7
            DO 5 I=1,255
      YM(I,K)=0
5     YP(I,K)=0
      I4=I3+2
            DO 160 L1=1,9
            DO 160 L2=1,9
            DO 160 L3=1,9
            DO 160 L4=1,2
      GOTO(6,7),L4
C     SELECT 3 LEVEL RES
6     LL=2
      M1=L1
      M3=L1
      M2=L2
      M4=L3
      U3=T2(M3,M4)
      U2=T2(M1,M2)
      IF(U3*U2.EQ.0.) GOTO 160
      I=-I3*(N2(L2)+N2(L3)-2*N1(L1))+3
      N=FLOAT(N1(L1))
      GOTO(8,160,9),I4
C
C     SELECT 3 LEVEL RES INV V
C
7     LL=1
      M2=L1
      M4=L1
      M1=L2
      M3=L3
      U3=T2(M3,M4)
      U2=T2(M1,M2)
      IF(U3*U2.EQ.0) GOTO 160
      I=-I3*(2*N2(L1)-N1(L2)-N1(L3))+3
      N=FLOAT(N2(L1))
      GOTO(9,160,8),I4
8     GOTO(10,20,30,160,160),I
9     GOTO(110,120,130,160,160),I
10    FJ=(2.*N-1.)*(N-1.)*(6.*N+1.)/(30.*N*(2.*N+1.))
      U22=U2*(2.*N-1.)/((2.*N+1.)*3.)
      GOTO 150
20    FJ=(2.*N-1.)*(4.*N+1.)/(30.*N)
      U22=U2/3.
      GOTO 150
30    IF(N2(L2)-N1(L1).EQ.0) GOTO 40
      FJ=(12.*N*N+7.*N-4.)/(30.*(2.*N+1.))
      U22=U2/3.
      GOTO 150
40    FJ=(2.*N+1.)*(2.*N*N+2.*N+1.)/(30.*N*(N+1.))
      U22=U2/3.
      GOTO 150
110   FJ=(N+2.)*(2.*N+1.)*(6.*N+5.)/(30.*(N+1.)*(2.*N+3.))
      U22=U2*(2.*N+1.)/((2.*N+3.)*3.)
      GOTO 150
120   FJ=(2.*N+1.)*(4.*N+3.)/(30.*(N+1.))
      U22=U2/3.
      GOTO 150
130   IF(N2(L1)-N1(L2).EQ.0) GOTO 140
      FJ=(2.*N+1.)*(12.*N*N+12.*N+1.)/(30.*(2.*N-1.)*(2.*N+3.))
      U22=U2/3.
      GOTO 150
140   FJ=(2.*N+1)*(2.*N*N+2.*N+1.)/(30.*N*(N+1.))
      U22=U2/3.
150   CALL CALC1
160   CONTINUE
            DO 200 K=1,6
            DO 200 I=1,255
      YM(I,K)=AD(7)*YM(I,K)
200   YP(I,K)=AD(7)*YP(I,K)
      RETURN
      END
```

Appendix VI.1 (continued)

```
      SUBROUTINE ENPAR1
      REAL*4 J
      DIMENSION W11(2,9),B(2,9,9),B11(9,9)
      COMMON/F5/U(9,9)/F1/W(2,9),DW(2,9,4),T2(9,9),DT2(9,9,4)
     &  /F6/JI,UTOL,I3/F7/AD(7)
C
C     CALCULATE DERIV OF EIGENVALUES WRT PARAM
C
            DO 5 L=1,2
            DO 5 L1=1,9
            DO 3 K=1,4
3     DW(L,L1,K)=0.
            DO 5 L2=1,9
5     B(L,L1,L2)=0.
      L=1
      J=FLOAT(JI)
      A1=AD(1)
      A2=AD(2)
      CALL EIGEN(J,L,A1,A2,B)
      L=2
      J=FLOAT(JI+I3)
      A1=AD(3)
      A2=AD(4)
      CALL EIGEN(J,L,A1,A2,B)
            DO 10 L1=1,9
            DO 10 L2=1,9
      T2(L1,L2)=0.
            DO 10 K=1,4
10    DT2(L1,L2,K)=0.
            DO 25 L1=1,9
            DO 25 L2=1,9
            DO 20 M1=1,9
            DO 20 M2=1,9
20    T2(L1,L2)=T2(L1,L2)+B(1,L1,M1)*U(M1,M2)*B(2,L2,M2)
25    T2(L1,L2)=T2(L1,L2)*T2(L1,L2)
            DO 30 L=1,2
            DO 30 L1=1,9
30    W11(L,L1)=W(L,L1)
            DO 35 L1=1,9
            DO 35 L2=1,9
35    B11(L1,L2)=B(1,L1,L2)
      L=1
      J=FLOAT(JI)
      A1=1.01*AD(1)
      A2=AD(2)
      CALL EIGEN(J,L,A1,A2,B)
            DO 40 L1=1,9
40    DW(1,L1,1)=(-W(1,L1)+W11(1,L1))/(.01*AD(1))
            DO 45 L1=1,9
            DO 45 L2=1,9
            DO 42 M1=1,9
            DO 42 M2=1,9
42    DT2(L1,L2,1)=DT2(L1,L2,1)+B(1,L1,M1)*U(M1,M2)*B(2,L2,M2)
45    DT2(L1,L2,1)=(DT2(L1,L2,1)*DT2(L1,L2,1)-T2(L1,L2))/(.01*AD(1))
      L=1
      J=FLOAT(JI)
      A1=AD(1)
      A2=1.01*AD(2)
      CALL EIGEN(J,L,A1,A2,B)
            DO 50 L1=1,9
50    DW(1,L1,2)=(-W(1,L1)+W11(1,L1))/(.01*AD(2))
            DO 55 L1=1,9
            DO 55 L2=1,9
            DO 52 M1=1,9
            DO 52 M2=1,9
52    DT2(L1,L2,2)=DT2(L1,L2,2)+B(1,L1,M1)*U(M1,M2)*B(2,L2,M2)
55    DT2(L1,L2,2)=(DT2(L1,L2,2)*DT2(L1,L2,2)-T2(L1,L2))/(.01*AD(2))
      L=2
      J=FLOAT(JI+I3)
      A1=1.01*AD(3)
      A2=AD(4)
      CALL EIGEN(J,L,A1,A2,B)
            DO 60 L1=1,9
60    DW(2,L1,3)=(W(2,L1)-W11(2,L1))/(.01*AD(3))
            DO 65 L1=1,9
            DO 65 L2=1,9
            DO 62 M1=1,9
            DO 62 M2=1,9
62    DT2(L1,L2,3)=DT2(L1,L2,3)+B11(L1,M1)*U(M1,M2)*B(2,L2,M2)
65    DT2(L1,L2,3)=(DT2(L1,L2,3)*DT2(L1,L2,3)-T2(L1,L2))/(.01*AD(3))
      L=2
      J=FLOAT(JI+I3)
      A1=AD(3)
      A2=1.01*AD(4)
      CALL EIGEN(J,L,A1,A2,B)
            DO 70 L1=1,9
70    DW(2,L1,4)=(W(2,L1)-W11(2,L1))/(.01*AD(4))
            DO 75 L1=1,9
            DO 75 L2=1,9
            DO 72 M1=1,9
            DO 72 M2=1,9
72    DT2(L1,L2,4)=DT2(L1,L2,4)+B11(L1,M1)*U(M1,M2)*B(2,L2,M2)
75    DT2(L1,L2,4)=(DT2(L1,L2,4)*DT2(L1,L2,4)-T2(L1,L2))/(.01*AD(4))
            DO 80 L1=1,9
      W(1,L1)=W11(1,L1)
80    W(2,L1)=W11(2,L1)
            DO 100 L1=1,9
            DO 100 L2=1,9
      IF(T2(L1,L2).GT.UTOL) GOTO 100
      T2(L1,L2)=0.
100   CONTINUE
      RETURN
      END
```

Appendix VI.1 (continued)

```
      SUBROUTINE EIGEN(J,L,A1,A2,B)
      REAL*4 J
      DIMENSION W1(3),A(3,3),B(2,9,9)
      COMMON/F1/W(2,9),DW(2,9,4),T2(9,9)
      W1(1)=A1*(J+1.)*(2.*J+3.)/(2.*J*(2.*J-1.))
      W1(2)=-A1*(2.*J+3.)/(2.*J)
      W1(3)=A1/2.
      A(1,1)=W1(1)+A2*(J*J-1.)*(4.*J*J-9.)/(2.*J*J*(4.*J*J-1.))
      A(1,2)=-A2*SQRT((2.*J-1.)/(2.*J+1.))
     &*3.*(J-1.)*(2.*J+3.)/(2.*J*J*(2.*J-1.))
      A(1,3)=A2*SQRT((2.*J-1.)*(2.*J+3.))*6./(2.*J*(4.*J*J-1.))
      A(2,2)=W1(2)-A2*(2.*J+3.)*(J*J+J-3.)/(2.*J*J*(J+1.))
      A(2,3)=A2*SQRT((2.*J+3.)/(2.*J+1.))*3.*(J+2.)/(2.*J*(J+1.))
      A(3,3)=W1(3)+A2*(J+2.)*(2.*J+5.)/(2.*(J+1.)*(2.*J+1.))
      C=-F(A,0.)
      X=A(1,1)
10    X0=X
      X=X+F(A,X)/F1(A,X)
      IF(ABS(X-X0).GT..001) GOTO 10
      W(L,3)=X
      AL=-A(1,1)-A(2,2)-A(3,3)+X
      BE=-C/X
      Q=SQRT(AL*AL-4.*BE)
      W(L,5)=(Q-AL)/2.
      W(L,7)=(-Q-AL)/2.
            DO 20 K=1,3
      AP=W(L,2*K+1)-A(1,1)+A(1,2)*A(1,3)/A(2,3)
      AP=AP/(A(1,2)+A(1,3)*(W(L,2*K+1)-A(2,2))/A(2,3))
      B1=-A(1,2)/A(2,3)-AP*(A(2,2)-W(L,2*K+1))/A(2,3)

      B(L,2*K+1,3)=1./SQRT(1.+AP*AP+B1*B1)
      B(L,2*K+1,5)=AP*B(L,2*K+1,3)
20    B(L,2*K+1,7)=B1*B(L,2*K+1,3)
      A(1,1)=W1(2)+A2*(2.*J+3.)*(J*J+J-3.)/(2.*J*J*(2.*J-1.))
      A(1,2)=A2*SQRT(J*J-1.)*3.*(2.*J+3.)/(2.*J*J*(2.*J-1.))
      A(2,2)=W1(1)-A2*(J+1.)*(4.*J*J-9.)/(2.*J*J*(2.*J-1.))
      BE=A(1,1)*A(2,2)-A(1,2)*A(1,2)
      AL=A(1,1)+A(2,2)
      Q=SQRT(AL*AL-4.*BE)
      W(L,4)=(AL+Q)/2.
      W(L,2)=(AL-Q)/2.
            DO 30 K=1,2
      AP=(W(L,2*K)-A(1,1))/A(1,2)
      B(L,2*K,4)=1./SQRT(1.+AP*AP)
30    B(L,2*K,2)=AP*B(L,2*K,4)
      A(1,1)=W1(2)+A2*(J*J+J-3.)/(2.*J*(J+1.))
      A(1,2)=-A2*SQRT(J*(J+2.))*3./(2.*J*(J+1.))
      A(2,2)=W1(3)-A2*(2.*J+5)/(2.*(J+1.))
      BE=A(1,1)*A(2,2)-A(1,2)*A(1,2)
      AL=A(1,1)+A(2,2)
      Q=SQRT(AL*AL-4.*BE)
      W(L,6)=(AL+Q)/2.
      W(L,8)=(AL-Q)/2.
            DO 40 K=3,4
      AP=(W(L,2*K)-A(1,1))/A(1,2)
      B(L,2*K,6)=1./SQRT(1.+AP*AP)
40    B(L,2*K,8)=AP*B(L,2*K,6)
      W(L,9)=(A1+A2)/2.
      B(L,9,9)=1.
      W(L,1)=W(L,9)*(J+1.)*(2.*J+3.)/(J*(2.*J-1.))
      B(L,1,1)=1.
      RETURN
      END
```

Appendix VI.1 (continued)

```
      FUNCTION F(A,X)
      DIMENSION A(3,3)
      F=((A(1,1)-X)*(A(2,2)-X)-A(1,2)*A(1,2))*(A(3,3)-X)
      F=F-A(2,3)*A(2,3)*(A(1,1)-X)-A(1,3)*A(1,3)
     &*(A(2,2)-X)+2.*A(1,2)*A(1,3)*A(2,3)
      RETURN
      END


      FUNCTION F1(A,X)
      DIMENSION A(3,3)
      F1=(A(2,2)-X)*(A(3,3)-X)
     &+(A(1,1)-X)*(A(3,3)-X)+(A(2,2)-X)*(A(1,1)-X)
      F1=F1-A(2,3)*A(2,3)-A(1,3)*A(1,3)-A(1,2)*A(1,2)
      RETURN
      END
```

Appendix VI.1 (continued)

```
      SUBROUTINE CALC1
      DIMENSION DT22(4),DT33(4)
      COMMON/F1/W(2,9),DW(2,9,4),T2(9,9),DT2(9,9,4)
     &  /F2/LL,M1,M2,M3,M4,U2,U3,FJ,U22,L2,L3
     &  /F3/YM(255,7),YP(255,7)/F7/AD(7)/F8/X(255)
C
C     CALCULATE CONTRIBUTION FOR ALL X(I) OF SINGLE RES
C
C     CALC ALL QUANTITIES FIXED FOR GIVEN RES
C
C     SCALE AT END OF FUNCT
C
      W0=W(LL,L3)-W(LL,L2)
      BETA=AD(6)*U22
      VJ=SQRT(1.+BETA)
      QJ=1.+VJ
      AJ=((SQRT(AD(5)))**3)*AD(6)*U2*QJ/VJ
      AJ=AJ*U3*FJ*SQRT(AD(6))
      BJ=-1./(2.*(1.+BETA)*QJ)
      EJ=QJ*AD(5)/(2.*VJ)
      QJ=QJ*QJ/2.
      Q4=QJ*AD(5)/2.
      VJ=3./(2.*AD(6))
      BET=3./(2.*AD(5))
            DO 10 K=1,4
      DT22(K)=DT2(M1,M2,K)/U2
10    DT33(K)=DT2(M3,M4,K)/U3
C
C     CALC LINESHAPE AND DERIV ALL X(I) GIV RES
C
            DO 100 I=1,255
      DM=X(I)-W0
      DP=X(I)+W0
      TM=DM*DM+Q4
      TP=DP*DP+Q4
      AJM=AJ/(TM*TM)
      AJP=AJ/(TP*TP)
      YJM=DM*AJM
      YJP=DP*AJP
      FJM=BJ-EJ/TM
      FJP=BJ-EJ/TP
C
      YM(I,5)=YM(I,5)+YJM*(BET-QJ/TM)
      YP(I,5)=YP(I,5)+YJP*(BET-QJ/TP)
      YM(I,6)=YM(I,6)+YJM*(VJ+U22*FJM)
      YP(I,6)=YP(I,6)+YJP*(VJ+U22*FJP)
      YM(I,7)=YM(I,7)+YJM
      YP(I,7)=YP(I,7)+YJP
            DO 90 K=2*LL-1,2*LL
      YM(I,K)=YM(I,K)+AJM*(4.*DM*DM/TM-1.)*(DW(LL,L3,K)-
     &  DW(LL,L2,K))
90    YP(I,K)=YP(I,K)-AJP*(4.*DP*DP/TP-1.)*(DW(LL,L3,K)-
     &  DW(LL,L2,K))
            DO 95 K=1,4
      YM(I,K)=YM(I,K)+YJM*(DT33(K)+(1.+FJM*BETA)*DT22(K))
95    YP(I,K)=YP(I,K)+YJP*(DT33(K)+(1.+FJP*BETA)*DT22(K))
100   CONTINUE
      RETURN
      END
```

Appendix VI.1 (continued)

```
      SUBROUTINE JETFIT
      REAL*8 ARRAY(7,7)
      DIMENSION BETA(7),ALPHA(7,7),B1(7)
      COMMON /F7/AD(7)/F10/A1(7)/F9/YMEXP(255),YPEXP(255)
     & /F3/YM(255,7),YP(255,7)/F11/SIGMAA(7),FLAMDA,CHISQ,CHISQ1
     & ,WM(3),WP(3),II
C
C     EVALUATE ALPHA AND BETA MATRICES
C
31            DO 34 J1=1,7
      BETA(J1)=0.
              DO 34 K1=1,J1
34    ALPHA(J1,K1)=0.
41            DO 50 I=1,255
              DO 46 J1=1,7
      BETA(J1)=BETA(J1)+(YMEXP(I)-A1(7)*YM(I,7))*YM(I,J1)*WM(II)
     & +(YPEXP(I)-A1(7)*YP(I,7))*YP(I,J1)*WP(II)
              DO 46 K1=1,J1
46    ALPHA(J1,K1)=ALPHA(J1,K1)+(YM(I,J1)*YM(I,K1))*WM(II)
     & +YP(I,J1)*YP(I,K1)*WP(II)
50    CONTINUE
51            DO 53 J1=1,7
              DO 53 K1=1,J1
53    ALPHA(K1,J1)=ALPHA(J1,K1)
C
C     EVALUATE CHISQ AT STARTING POINT
C
      CHISQ1=CHISQ
C
C     INVERT MODIFIED CURVATURE MATRIX TO FIND NEW PARAMETERS
C
71            DO 74 J1=1,7
              DO 73 K1=1,7
73    ARRAY(J1,K1)=ALPHA(J1,K1)/SQRT(ALPHA(J1,J1)*ALPHA(K1,K1))
74    ARRAY(J1,J1)=1.+FLAMDA
80    CALL JETINV(ARRAY,7,DET)
81            DO 84 J1=1,7
      B1(J1)=A1(J1)
              DO 84 K1=1,7
84    B1(J1)=B1(J1)+BETA(K1)*ARRAY(J1,K1)/SQRT(ALPHA(J1,J1)*
     & ALPHA(K1,K1))
C
C     IF CHISQ INCR,INCR FLAMDA AND TRY AGAIN
C
              DO 86 J1=1,7
86    AD(J1)=B1(J1)
      CALL FUNCT
      CALL CHISQE
      IF(CHISQ1-CHISQ) 95,101,101
95    FLAMDA=2.*FLAMDA
      GOTO 71
C
C     EVALUATE PARAMETERS AND UNCERTAINTIES
C
101           DO 103 J1=1,7
      A1(J1)=B1(J1)
103   SIGMAA(J1)=SQRT(ARRAY(J1,J1)/ALPHA(J1,J1))
      FLAMDA=FLAMDA/2.
110   RETURN
      END
```

Appendix VI.1 (continued)

```
C  SUBROUTINE MATINV
C
C  PURPOSE
C     INVERT A SYMMETRIC MATRIX AND CALCULATE ITS DETERMINANT
C
C  USAGE
C     CALL MATINV (ARRAY, NORDER, DET)
C
C  DESCRIPTION OF PARAMETERS
C     ARRAY  - INPUT MATRIX WHICH IS REPLACED BY ITS INVERSE
C     NORDER - DEGREE OF MATRIX (ORDER OF DETERMINANT)
C     DET    - DETERMINANT OF INPUT MATRIX
C
C  SUBROUTINES AND FUNCTION SUBPROGRAMS REQUIRED
C     NONE
C
C  COMMENTS
C     DIMENSION STATEMENT VALID FOR NORDER UP TO 10
C
      SUBROUTINE MATINV (ARRAY,NORDER,DET)
        DOUBLE PRECISION ARRAY,AMAX,SAVE
      DIMENSION  ARRAY(10,10),IK(10),JK(10)
 10   DET = 1.
 11   DO 100 K=1, NORDER
C
C  FIND LARGEST ELEMENT ARRAY(I,J) IN REST OF MATRIX
C
      AMAX = 0.0
 21   DO 30 I=K, NORDER
      DO 30 J=K, NORDER
 23   IF ( DABS(AMAX) -  DABS(ARRAY(I,J))) 24,24,30
 24   AMAX = ARRAY(I,J)
      IK(K) =I
      JK(K) =J
 30   CONTINUE
C
C  INTERCHANGE ROWS AND COLUMNS TO PUT AMAX IN ARRAY(K,K)
C
 31   IF (AMAX) 41,32,41
 32   DET = 0.0
      GO TO 140
 41   I = IK(K)
      IF (I-K) 21,51,43
 43   DO 50 J=1,NORDER
      SAVE = ARRAY(K,J)
      ARRAY(K,J) = ARRAY(I,J)
 50   ARRAY(I,J) = -SAVE
 51   J = JK(K)
      IF (J-K) 21,61,53
 53   DO 60 I=1, NORDER
      SAVE = ARRAY(I,K)
      ARRAY(I,K) = ARRAY(I,J)
 60   ARRAY(I,J) = -SAVE
C
C  ACCUMULATE ELEMENTS OF INVERSE MATRIX
C
 61   DO 70 I=1, NORDER
      IF (I-K) 63,70,63
 63   ARRAY (I,K) = -ARRAY(I,K) / AMAX
 70   CONTINUE
 71   DO 80 I=1, NORDER
      DO 80 J=1, NORDER
      IF (I-K) 74,80,74
 74   IF (J-K) 75, 80, 75
 75   ARRAY(I,J) = ARRAY(I,J) + ARRAY(I,K)*ARRAY(K,J)
 80   CONTINUE
 81   DO 90 J=1, NORDER
      IF (J-K) 83, 90, 83
 83   ARRAY(K,J) = ARRAY(K,J) / AMAX
 90   CONTINUE
      ARRAY(K,K) = 1.0/ AMAX
100   DET = DET * AMAX
C
C  RESTORE ORDERING OF MATRIX
C
101   DO 130 L=1, NORDER
      K = NORDER - L + 1
      J = IK(K)
      IF ( J-K) 111, 111, 105
105   DO 110 I=1, NORDER
      SAVE = ARRAY(I,K)
      ARRAY(I,K) = -ARRAY(I,J)
110   ARRAY(I,J) = SAVE
111   I = JK(K)
      IF ( I-K) 130, 130, 113
113   DO 120 J=1, NORDER
      SAVE = ARRAY(K,J)
      ARRAY(K,J) = -ARRAY(I,J)
120   ARRAY(I,J) = SAVE
130   CONTINUE
140   RETURN
      END
```

Appendix VI.1 (continued)

```
      SUBROUTINE CHISQE
      COMMON /F3/YM(255,7),YP(255,7)/F9/YMEXP(255),YPEXP(255)
     &/F7/AD(7)/F11/SIGMAA(7),FLAMDA,CHISQ,CHISQ1,WM(3),WP(3),II
      CHISQ=0
            DO 10 I=1,255
      CHISQ=CHISQ+(AD(7)*YM(I,7)-YMEXP(I))*(AD(7)*YM(I,7)-YMEXP(I))
     &*WM(II)
10    CHISQ=CHISQ+(AD(7)*YP(I,7)-YPEXP(I))*(AD(7)*YP(I,7)-YPEXP(I))
     &*WP(II)
      RETURN
      END
```

Appendix VI.1 (continued)

```
C       MAIN JETPLO
        DIMENSION YMEXP(255),YM(255),YPEXP(255),YP(255),AD(7)
        BYTE IFLAG(24),INFIL1(24),INFIL2(24)
        CALL ASSIGN(5,'HYPFIT.DAT',0)
        READ(5,10)INFIL1
        READ(5,10)INFIL2
        READ(5,15)(AD(I),I=1,7),JI,TOL,ITMAX,Z,SIG,X1,FLAMDA,II,UTOL,I3
15      FORMAT(7F,I,F,I,F,F,F,F,I,F,I)
        CALL CLOSE(5)
        CALL ASSIGN(5,'HYPFIT.OUT',0)
5       READ(5,10)IFLAG
10      FORMAT(24A1)
        IF(IFLAG(2).EQ.'I')GO TO 50!READ DATA
        GO TO 5!SEARCH FOR FLAG
50      READ(5,100)(I,YMEXP(I),YM(I),YPEXP(I),YP(I),I=1,255)
100     FORMAT(X,255(X,I3,2X,4(F8.2,2X)/))
        CALL CLOSE(5)
        CALL JETSTO(YMEXP,SIG,YM(1),'YM.DAT',255,X1,INFIL1)
        CALL JETSTO(YPEXP,SIG,YP(1),'YP.DAT',255,X1,INFIL1)
        WRITE(4,500)
500     FORMAT(' ','JETPLO IS FINISHED')
        END


        SUBROUTINE JETSTO(Y,SIGMAY,YFIT,OFILE,NPTS,EFIRST,INFIL1)
        DIMENSION Y(256),YFIT(256),PARAM(128)
        REAL*4 INFIL1(6)
        DIMENSION SIGMYY(256),OFILE(6)
                DO 10 I=1,128
10              PARAM(I)=0.0
                DO 12 I=1,6
12      PARAM(4+I)=INFIL1(I)
        CALL ASSIGN(1,OFILE,6)
        DELCH=-(1000.-EFIRST)/254.
        NWORDS=(NPTS+127)/128
        NSTORE=NWORDS*128
        NFITS=1
        NBLKS=NWORDS*(NFITS+2)+1
        DEFINE FILE 1(NBLKS,256,U,IDUM)
        PARAM(1)=1000.
        PARAM(2)=DELCH
        PARAM(3)=NPTS
        PARAM(4)=NFITS
                DO 11 I=1,NPTS
11              SIGMYY(I)=SIGMAY
        CALL STORE(PARAM,128,1)
        CALL STORE(Y,NSTORE,2)
        NB2=2+NWORDS
        CALL STORE(SIGMYY,NSTORE,NB2)
        NB3=NB2+NWORDS
        CALL STORE(YFIT,NSTORE,NB3)
        CALL CLOSE(1)
        RETURN
        END
```